UNIVERSITY OF GAZİANTEP
GRADUATE SCHOOL OF
NATURAL & APPLIED SCIENCES

DESIGN AND CONSTRUCTION OF A COMPACT HIGH ENERGY RATE FORMING (HERF) HAMMER

Ph.D THESIS
IN
MECHANICAL ENGINEERING

BY
ERDOĞAN KANCA
AUGUST 2009

Design and Construction of a Compact High Energy Rate Forming (HERF) Hammer

Ph.D Thesis
in
Mechanical Engineering
University of Gaziantep

Supervisor
Prof. Dr. Ömer EYERCİOĞLU

by
Erdoğan KANCA
August 2009

T.C.
UNIVERSITY OF GAZİANTEP
GRADUATE SCHOOL OF NATURAL & APPLIED SCIENCES
(MECHANICAL ENGINEERING)

Name of the thesis: Design and construction of a compact High Energy Rate Forming (HERF) Hammer.

Name of the student: Erdoğan KANCA
Exam date : 10.08.2009

Approval of the Graduate School of Natural and Applied Sciences

(Prof. Dr. Ramazan KOÇ)

I certify that this thesis satisfies all the requirements as a thesis for the degree of Doctor of Philosophy.

(Prof. Dr. Sedat BAYSEÇ)
Head of Department

This is to certify that we have read this thesis and that in our opinion it is fully adequate, in scope and quality, as a thesis for the degree of Doctor of Philosophy.

(Prof. Dr Ömer EYERCİOĞLU)
Supervisor

Examining Committee Members

Title and Name-surname	signature
Prof. Dr. İ. Hüseyin FİLİZ (Chairman)	______________________
Prof. Dr. M. Kemal APALAK	______________________
Prof. Dr. İ. Halil GÜZELBEY	______________________
Prof. Dr. Ömer EYERCİOĞLU (Supervisor)	______________________
Asst. Prof. Dr. Necip Fazıl YILMAZ	______________________

To my wife and son

Ayşegül and Mehmet Kadir

ABSTRACT

DESIGN AND CONSTRUCTION OF A COMPACT HIGH ENERGY RATE FORMING (HERF) HAMMER

KANCA Erdoğan
Ph.D. in Mechanical Eng.
Supervisor: Prof. Dr. Ömer EYERCİOĞLU
August 2009, 181 pages

High speed forming is receiving increasing attention due to high rate of production, smaller-size equipment, improved quality of the products and economic reasons. It is also preferred to manufacture parts which cannot be produced by other methods because of size and material characteristics. However, high speed forming requires specially designed equipment and techniques. **High Energy Rate Forming (HERF)** hammers operate at forming speeds between 5 and 22 m/s.

The aim of this study is to design and construct a compact prototype HERF hammer which uses two-cylinder internal combustion to produce forming energy and a mechanical re-cocking mechanism. Therefore, it can be considered as a new type of HERF hammer in the literature. It's a compact prototype having a capacity of 100 J and 12 m/s forming speed. The performance characteristics of the HERF hammer were compared with conventional hydraulic and mechanical presses. For this purpose, forging and blanking operations were carried out on three different materials (aluminum, St37 and AISI 304) using these presses.

The results of open die cylindrical forging operations show that the barreling effect is reduced by increasing punch speed. The blanking load and energy values for all of the materials under investigation were significantly reduced at HERF hammers. From the microstructural analyses of the blanked surfaces, formation of adiabatic shear band was observed at higher strain rates. The surface quality of the blanks are also much better at HERF hammers showing less dishing and lower surface roughness. The corrosion test results indicate that the resistance to corrosion of the blank surfaces increased with increasing punch speed.

Key Words: HERF; Forging, Blanking; Piercing, Adiabatic Shear, Barreling

ÖZ

KOMPAKT BİR YÜKSEK ENERJİLİ ŞEKİLLENDİRME (YEŞ) ÇEKİCİNİN TASARIM VE İMALATI

KANCA Erdoğan
Doktora Tezi, Mak. Müh. Bölümü
Tez Yöneticisi: Prof. Dr. Ömer EYERCİOĞLU
Ağustos 2009, 181 sayfa

Yüksek hızla şekillendirmeye; yüksek üretim oranı, boyutlarının küçüklüğü, ürünlerinin kaliteli oluşu ve ekonomikliğinden dolayı ilgi artmaktadır. Yüksek hızla şekillendirmenin bir başka tercih sebebi ise, boyut ve malzeme karakteristiğinden dolayı başka şekillendirme yöntemleriyle imal edilemeyen parçaları şekillendirebilmesidir. **Yüksek Enerjili Şekillendirme (YEŞ)** çekiçleri, 5 ile 22 m/s hız aralığında çalışmaktadırlar.

Bu çalışmanın amacı kompakt bir YEŞ çekicinin prototip olarak tasarlanıp, imalatının yapılmasıdır. Tasarlanan çekiç şekillendirme enerjisini iki zamanlı içten yanmalı motorla sağlamakta ve işlemin tetiklenmesini de mekanik olarak yapmaktadır. Bundan dolayı, imal edilen çekiç, literatürde yeni bir tip YEŞ olarak kabul edilebilir. Kompakt olan prototip, 100 J kapasitesinde ve 12 m/s şekillendirme hızındadır. YEŞ çekicin performans özellikleri hidrolik ve mekanik preslerle kıyaslanmıştır. Bu amaçla alüminyum, St 37 ve AISI 304 kullanılarak dövme ve kesme işlemleri yapılmıştır.

Açık kalıpta yapılan silindirik dövme işlemleri sonucunda, dövme hızının artması ile malzemelerin fıçılaşmasının azaldığı görülmüştür. Bu tez kapsamında çalışılan tüm malzemelerin, kesme yük ve enerjilerinin, YEŞ çekiçleri ile kayda değer oranda azaldıkları görülmüştür. Mikro yapı analizlerinden, yüksek gerinim oranlarında, kesme yüzeylerinde adiyabatik kesme bantlarının oluştuğu gözlemlenmiştir. YEŞ çekiçleri ile kesilmiş malzemelerin, hidrolik ve konvansiyonel mekanik preslerle kesilenlere oranla, yüzeylerinde daha az tabaklanma ve yüzey pürüzlülüğü oluştuğu belirlenmiştir. Korozyon test sonuçları, zımbalama hızının artması ile kesme yüzeylerinin korozyon direncinin arttığını göstermiştir.

Anahtar Kelimeler: YEŞ, Dövme. Kesme, Adiyabatik Kesme, Fıçılaşma

ACKNOWLEDGEMENTS

I owe special thanks to my supervisor, Prof. Dr. Ömer Eyercioğlu, for his help and endless encouragement throughout this study.

Deep appreciation and thanks are due to Prof. Dr. İ. Hüseyin Filiz, Prof. Dr. M. Kemal Apalak and Asst. Prof. Dr. Necip Fazıl Yılmaz for serving on the committee and their valuable suggestions and comments.

I would like to thank Assoc. Prof Dr. İ. Hakkı Karahan, Asst. Prof. Dr. Erdoğan Özbay, Süleyman Başaran, Kürşad Göv, Asst. Prof. Dr. Murat Eskil, Ali Kılıç for their contributions.

Thanks are also due to Turgut Kaya, İsmail Hakkı Özaktaş, Mikail Kalkan, Abdi Küçükoğlu, Çavuş Güneş, Mehmet Taşdemir, Fatih Özkan, Oğuz Sarıdağ, Musta Turgut Aygördü for their assistance with laboratory work.

Finally, I would like to thank my wife and son (Ayşegül and Mehmet Kadir) for their continuous support and encouragement.

CONTENTS

ABSTRACT I
ÖZ II
ACKNOWLEDGEMENTS III
TABLE OF CONTENTS IV
LIST OF TABLES X
LIST OF FIGURES XII
LIST OF SYMBOLS XVIII

CHAPTER 1 INTRODUCTION 1

1.1 INTRODUCTION 1

1.2 RESERCH OBJECTIVES 3

1.3 ORGANIZATION OF THE THESIS 3

CHAPTER 2 LITERATURE REVIEW 5

2.1 INTRODUCTION 5

2.2 HIGH ENERGY RATE FORMING HAMMER 5
  2.2.1 Definitions 5
  2.2.2 History of High Energy Rate Forming Machines 6
  2.2.3 High Energy Rate Forming Machines Energy Releasing Methods 6
  2.2.4 Application Area of HERF Hammers 8
    2.2.4.1 Forging Applications by Using HERF Hammers 8
    2.2.4.2 Adiabatic Shear Band Formation in the HERF Hammers Application.. 14

CHAPTER 3 FUNDAMENTALS OF METAL WORKING 22

3.1 INTRODUCTION 22

3.2 CLASIFICATION OF METAL WORKING 22

3.3 MECHANICAL BEHAVIOUR OF METAL WORKING PROCESSES....24
3.3.1 Flow Stress 25
3.3.1.1 Flow Stress Dependence on Strain 25
3.3.1.2 Flow Stress Dependence on Strain Rate 28
3.3.1.3 Flow Stress Dependence on Temperature 29
3.3.1.4 Flow Stress Dependence on Combined Temperature and Strain-Rate ..30
3.3.2 Friction and Lubrication 32

3.4 FORGING PROCESS 34
3.4.1 Classification of Forging Process According to Die Type 34
3.4.1.1 Open Die Forging 34
3.4.1.2 Close Die Forging 35
3.4.1.3 Net Shape (Precision) Forging 36
3.4.2 Classification of Forging Process According to Temperature 37
3.4.2.1 Hot Forging 37
3.4.2.2 Cold Forging 38
3.4.2.3 Warm Forging 39
3.4.3 Classification of Forging Machines 40
3.4.3.1 Force Restricted (Hydraulic Presses) Machines 42
3.4.3.2 Stroke Restricted (Mechanical Presses) Machines 44
3.4.3.3 Energy Restricted Machines 47
3.4.3.3.1 Screw Presses 47
3.4.3.3.2 Hammers 48
3.4.3.3.2.1 Gravity Drop Hammers 49
3.4.3.3.2.2 Board Drop Hammers 49
3.4.3.3.2.3 Air-lift Gravity Drop Hammers 50
3.4.3.3.2.4 Electro-hydraulic Gravity-Drop Hammers. 50
3.4.3.3.2.5 Power Drop Hammers 51
3.4.3.3.2.6 Counter Blow Hammer 52
3.4.3.3.3 High Energy Rate Forming Hammers 52
3.4.4 Determination of Load and Energy 53

3.5 HIGH ENERGY RATE FORMING (HERF) HAMMER 54
3.5.1 Classification of HERF Hammers 56

3.5.1.1 Pneumatic-Hydraulic HERF Hammer 57
3.5.1.2 Pneumatic-Mechanic HERF Hammer 58
3.5.1.3 Hydraulic-Hydraulic HERF Hammer 58
3.5.1.4 Combustion-Pneumatic HERF Hammer 58
3.5.1.4.1 Petro-Forge 59
3.5.1.4.2 Advantages of Combustion-Pneumatic HERF Hammer 61
3.5.2 Economics of HERF Hammer 62
3.5.3 Metallurgical Effect of HERF Hammer 64

3.6 SHEET METAL CUTTING 64
3.6.1 Cutting Processes 66
3.6.2 Blanking Processes 67
3.6.3 Piercing Processes 68
3.6.4 Optimum Clearance 69
3.6.5 Quality of Sheared Edges 73
3.6.6 Cutting Forces 74

CHAPTER 4 DESIGN AND CONSTRUCTION OF HIGH ENERGY RATE FORMING (HERF) HAMMER 76

4.1 INTRODUCTION 76

4.2 PARTS OF HERF HAMMER 77
4.2.1 Frame 77
4.2.2 Power Unit 78
4.2.3 Injection Unit 79
4.2.4 Ignition Unit 80
4.2.5 Re-cocking Mechanism 81
4.2.5.1 AC Servo Motor, Driver Unit and Energy Flywheel 81
4.2.5.2 Trigger Mechanism 82
4.2.5.3 Locking Mechanism 83
4.2.5.4 Chain-gear Mechanism 83
4.2.5.5 Motion Flywheel and Compression Car 84
4.2.5.6 Release Cam and Spring Locking Mechanism 85

4.3 DETERMINATION OF THE GENERATED FORMING ENERGY 86
4.3.1 Otto Cycle 86
4.3.2 Theoretical Determination of the Generated Forming Energy 90
4.3.3 Energy Losses 94
4.3.4 Factors Affecting Generated Forging Energy 96
4.3.4.1 Compression Rate 96
4.3.4.2 Temperature 97
4.3.4.3 Injection Time 98
4.3.4.4 Fuel Rate 98

4.4 MEASURMENT UNIT 99
4.4.1 Magnetic Ruler 99
4.4.2 Loadcell 100

CHAPTER 5 EXPERIMENTAL STUDY 101

5.1 INTRODUCTION 101

5.2 MATERIALS 101
5.2.1 AISI 304 Stainless Steel 101
5.2.2 St 37 Mild Steel 103
5.2.3 Aluminum 103

5.3 EQUIPMENT 104
5.3.1 Machines 104
5.3.1.1 Hydraulic Press (HP) 104
5.3.1.2 Conventional Mechanical Press (CP) 105
5.3.1.3 High Energy Rate Forming (HERF) Hammer 106
5.3.1.4 Laser Cutting Machine (LCM) 107
5.3.2 Dies 108
5.3.2.1 Forging Die 108
5.3.2.2 Blanking Die 109

5.4 EXPERIMENTAL PROCEDURES 110
5.4.1 Load and Energy Measurements 110

5.4.2 Metallographic Examinations..111
5.4.3 Surface Roughness Measurements on the Sheared Surfaces 111
5.4.4 Corrosion Tests on the Sheared Surfaces 112
5.4.5 SEM Observations..113

CHAPTER 6 RESULTS AND DISCUSSIONS 115

6.1 INTRODUCTION 115

6.2 LOAD AND ENERGY 115

6.2.1 Forging Load and Energy..115
6.2.1.1 Load and Energy Comparison According to Forging Speed 115
6.2.1.2 Amount of Barreling in Forging...118
6.2.1.3 Friction Measurement..122
6.2.2 Blanking Load and Energy...125
6.2.2.1 Effect of Blanking Speed on Aluminum 125
6.2.2.2 Effect of Blanking Speed on Mild Steel...131
6.2.2.3 Effect of Blanking Speed on Stainless Steel 136
6.2.2.4 Effect of Blanking Speed on the Load and Energy 140
6.2.2.5 A proposed Die Clearance Selection Diagram for the HERF Hammer142
6.2.3 Micro-structures of the Blanked Surfaces 144
6.2.3. Explanation of Blanking Load and Energy Reduction in HERF Hammer 149

6.3 SHEAR SURFACE QUALITY 151

6.3.1 Shear Surface Geometry..151
6.3.2 Surface Roughness 156
6.3.2.1 Effects of High Speed Blanking on the Shear Surface Roughness of St 37 Mild Steel..156
6.3.2.2 Effects of High Speed Blanking on the Shear Surface Roughness of AISI 304 Stainless Steel 158

6.4 CORROSION BEHAVIOUR..160

6.4.1 Effects of High Speed Blanking on the Shear Surface Corrosion of St 37 Mild Steel...160

6.4.2 Effects of high speed blanking on the shear surface corrosion of AISI 304 164

CHAPTER 7 CONCLUSIONS AND FUTURE STUDIES 171

7.1 INTRODUCTION 171

7.2 CONCLUSIONS 171

7.2.1 The HERF Hammer 171

7.2.2 Forging using the HERF Hammer 172

7.2.3 Blanking using the HERF Hammer 172

7.3 FUTURE STUDIES 174

REFERENCES 175

LIST OF TABLES

Table 3.1 Strength Strain-hardening Material coefficient, K (MPa) exponent, *n* 28

Table 3.2 Typical values of the strain-rate exponent, m, at room temperature **(Groover, 1996)** 29

Table 3.3 Strain-rate Sensitivity and Coefficient of Friction in Cold, Warm, and Hot Working 31

Table 3.4 Typical characteristics of hot, warm and cold forging processes **(Sheljaskov, 1994)** 40

Table 3.5 Typical Values of Velocity for Different Forging Equipment **(Semiatin,1988).** 53

Table 3.6 Shear strengths of various steels and nonferrous metals at room temperature 75

Table 4.1 Technical specifications of used engine 91

Table 4.2 Technical specifications of used gasoline 92

Table 5.1 Chemical composition of AISI 304 stainless steel 102

Table 5.2 Chemical composition of St37 mild steel 103

Table 5.3 Mechanical properties of St37 mild steel 103

Table 5.4 Chemical composition of aluminum 103

Table 5.5 Mechanical properties of aluminum 104

Table 5.6 Mechanical and thermal properties of the specifications of the die material SAE 4140 108

Table 6.1 Maximum load and energy of forging processes 118

Table 6.2 Geometric values obtained from forging at different speeds 121

Table 6. 3Geometric values of before and after ring compression test 122

Table 6.4 Maximum load and energy of blanking processes 128

Table 6.5 Maximum load and energy of blanking processes 133

Table 6.6 Maximum load and energy of blanking processes 138

Table 6.7 Maximum load and energy of blanking processes 142

Table 6. 8 Geometric values of 5mm Aluminum at different blanked speed........... 152

Table 6.9 Geometric values of 3.5mm St37 mild steel at different blanked speed.. 153

Table 6.10 Geometric values of 2mm AISI 304stainless steel at different blanked speed 155

Table 6.11 The corrosion potential of all blanks 161

Table 6.12 Open circuit potentials in 0.5 mol/dm^3 in de-aerated sulphuric acid solution vs. SCE 165

LIST OF FIGURES

Figure 2.1 High energy rate forming energy releasing by explosive forming **(Tobias, 1985)** 6

Figure 2.2 Electro hydraulic working energy releasing method **(Tobias, 1985)** 7

Figure 2.3 Magnetic forming energy releasing method **(Tobias, 1985)** 7

Figure 2.4 Bulk forming energy releasing method **(Tobias, 1985)** 8

Figure 3.1 Main classifications of manufacturing processes **(Groover, 1996)** 23

Figure 3.2 Classification of metal working processes **(Groover, 1996)** 23

Figure 3.3 Systematic approaches to metal working **(Lange, 1985)** 24

Figure 3.4 Mathematical approximations of the true stress–strain curve 26

Figure 3.5 True stress-strain curve plotted on log-log scale **(Groover, 1996)** 27

Figure 3.6 Effect of strain-rate on flow stress at an elevated work temperature plotted on log-log coordinates **(Groover, 1996)** 29

Figure 3.7 (a) Tensile strengths decrease with increasing temperature, (b) Decrease of the strain-hardening exponent of aluminum with increasing temperature **(Carrecker and Hibbard, 1957).** 30

Figure 3.8 Effect of temperature on flow stress for typical metal 31

Figure 3.9 (a) Solid cylindrical billet upset between two flat dies. (b) Uniform deformation (c) Deformation with friction 33

Figure 3.10 Open-die forging 35

Figure 3.11 Closed-die forging 36

Figure 3.12 Schematic Drawing of Hydraulic Press 43

Figure 3.13 Drive shafts a) crankshaft, b) eccentric shaft 45

Figure 3.14 Schematic Drawing of Mechanical Press 45

Figure 3.15 Crank press drive layout 46

Figure 3.16 Schematic Drawing of Screw Press 47

Figure 3.17 Schematic Drawing of Board Drop Hammers 50

Figure 3.18 Schematic Power Drop Hammers 51

Figure 3.19 Schematic view of Vertical Counter-Blow Hammer 52

Figure 3.20Pneumatic-Hydraulic HERF hammers working principles **(Tobias, 1985)** 58

Figure 3.21 Petro-Forge HERF hammers working principles **(Chan et al, 1966)** 59

Figure 3.22 Cost comparison between conventional forming and High Energy Rate Forming 63

Figure 3.23 (a) Schematic illustration of shearing with a punch and die, indicating some of the process variables Characteristic features of (b) a punched hole and (c) the slug, note that the scales of the two figures are different **(Altan et al, 1973)**...... 65

Figure 3.24 Basic shearing operations 66

Figure 3.25 Bar cropping.. 66

Figure 3.26 Schematic diagram of punching forces vs. punch penetration from Ref **(Hambli, 2001)**. 1: Elastic stage, 2: elastoplastic stage, 3: elastoplastic stage in which damage occurs, 4: initiation and propagation of cracks leading to final rupture 67

Figure 3.27 Simple blanking with a punch and die **(Brokken, 1998)** 68

Figure 3.28 Secondary crack formation during blanking process**(Tekiner, 2006)**.... 70

Figure 3.29 Illustration of crack propagation angle and diagonal angle 71

Figure 3.30 Ranges of punch-to-die clearance per side recommended by one manufacturer for piercing and blanking of various metals up to 3.18 mm thick **(Semiatin, 1988).** 72

Figure 3.31 Cutting surfaces at the different clearances 73

Figure 4.1Frame of the hammer…………………………………………………..77

Figure 4.2 The used internal combustion engine.. 78

Figure 4.3 Different views of injection unit and pump location 79

Figure 4.4The working principle of injection mechanism 80

Figure 4.5 Ignition unit.. 80

Figure 4.6 a) AC servo motor driver unit b) Main flywheel and AC servo motor..... 81

Figure 4.7 Trigger arm and its latch 82

Figure 4.8 Functioning principle of trigger mechanism... 82

Figure 4.9 Locking mechanism 83

Figure 4.10 Chain-gear-mechanisms 83

Figure 4.11 Different views of compression car 84

Figure 4.12 Schematic view of the compression car 84

Figure 4.13 a) Freilassen cam mechanism b) Spring locking mechanism 85

Figure 4.14 Schematic views of release cam and spring locking mechanism 86

Figure 4.15 Pressure–volume and temperature–entropy diagrams for an air standard Otto cycle 87

Figure 4.16 Combustion chamber and Displacement volume 88

Figure 4.17 Tap dead center and Bottom dead center 88

Figure 4.18 Diagram of working principle 91

Figure 4.19 Alternative measure of P2 by using Motor meter 92

Figure 4.20 Experimental arrangement 94

Figure 4.21 Motion of the ram and anvil for workpiece during an impact 95

Figure 4.22 P_2 with respect to piston velocity 96

Figure 4.23 P_2 with respect to Thermal efficiency 97

Figure 4.24 Ram velocities with respect to injection time 98

Figure 4.25 Specifically-designed magnetic piece and velocity measurement schedule 99

Figure 4.26 Stroke-time graph output of used software. 100

Figure 4.27 (a) Loadcell mounting, (b) Load time curve 100

Figure 5.1 Stress-strain curve of AISI 304 depending on strain rate 102

Figure 5.2 Stress-strain curve of AISI 304 depending on temperature 102

Figure 5.3 Hydraulic press used for experimental studies 105

Figure 5.4 Eccentric press used for experimental studies 106

Figure 5.5 Schematic view of magnetic ruler, loadcell and data-logger 107

Figure 5.6 Laser cutting machine used for experimental studies 108

Figure 5.7 Forging dies and the billets 109

Figure 5.8 Photo of the blanking die set and the sheet. 109

Figure 5.9 Schematic view of the blanking die, sheet metal and the punch 109

Figure 5.10 The load-stroke diagram and the surface obtained in blanking operation 110

Figure 5.11 A sample ring specimen 111

Figure 5.12 The surface roughness measuring unit. 112

Figure 5.13 The Corrosion test equipment 113

Figure 5.14 SEM machine used for experiments 114

Figure 6.1 Load-stroke curves of the aluminum depending on the forging speed ... 116

Figure 6.2 Load-stroke curves of the mild steel depending on the forging speed ... 117

Figure 6.3 Load-stroke curves of the stainless steel depending on the forging speed 117

Figure 6.4 Main stages at the closed die forging operations 118

Figure 6.5 Schematic view of load-stroke curve of different forging speed 119

Figure 6.6 Dimensions of workpiece with barreling 120

Figure 6.7 Before and after open die forging views 121

Figure 6. 8 Views of before and after ring compression test 122

Figure 6. 9 The standard a ring compression test friction coefficient chart 123

Figure 6.10 Comparison of ideal and measured forging loads for aluminum on HERF hammer 124

Figure 6.11 Comparison of ideal and measured forging loads for aluminum on HP 124

Figure 6.12 Load-stroke curves of aluminum for different clearances at HP 125

Figure 6.13 Load-stroke curves of aluminum depending on the clearances at CP .. 126

Figure 6.14 General load-stroke diagram obtained in our HERF hammer 127

Figure 6.15 Load-stroke curves of aluminum depending on the clearances at HERF 128

Figure 6.16 Comparison of the ideal die clearances with respect to the blanking speed 129

Figure 6.17 Effects of the blanking speed on the die clearance per side for the first group (soft) materials. 130

Figure 6.18 Load-stroke curves of mild steel material depending on the die clearances at HP 131

Figure 6.19 Load-stroke curves of mild steel material depending on the clearances 132

Figure 6.20 Load-stroke curves of mild steel material depending on the clearances at HERF 133

Figure 6.21 Comparison of the ideal die clearances with respect to the blanking speed at mild steel 134

Figure 6.22 Effects of the blanking speed on the die clearance per site at the second group (medium-hard) materials. 135

Figure 6.23 Load-stroke curves of stainless steel depending on the die clearances. 136

Figure 6.24 Load-stroke curve variation of stainless steel depending on the die clearances at CP 137

Figure 6.25 Load-stroke curve variation of stainless steel depending on the die clearances at HERF 137

Figure 6.26 Comparison of the ideal die clearances relies on the blanking speed at SS 138

Figure 6.27 Effects of the blanking speed on the die clearance per side for the third group (hard) materials. 139

Figure 6.28 The load stroke diagram of St 37 with thickness values of 3.5, 5, and 6 mm according to HP 140

Figure 6.29 The load stroke diagram of St 37 with thickness values of 3.5, 5, and 6 mm according to CP 141

Figure 6.30 The load stroke graphics of St 37 with thickness values of 3.5, 5, and 6 mm according to HERF 141

Figure 6.31 Die clearances selection diagram for the HERF hammer 143

Figure 6.32 Micro-structure of blanking and piercing part of 3.5mm St37 at 145

Figure 6.33 Micro-structure of blanking and piercing part of 3.5mm St37 146

Figure 6.34 Micro-structure of blanking and piercing part of 3.5mm St37 147

Figure 6.35 Micro-structure of blanking and piercing part of 5mm St37 148

Figure 6. 36 a) Adiabatic shear band Ref (Bronkhorst, 2006) b) adiabatic shear band result of the HERF hammer c) non-adiabatic shear band result of the CP..............150

Figure 6.37 Shear and fracture surfaces of the aluminum materials according to the press type and die clearances...151

Figure 6. 38 Shear and fracture surfaces of the mild steel material according to the press type and die clearances...153

Figure 6. 39 Shear and fracture surfaces of the stainless steel materials according to the press type and die clearances..154

Figure 6. 40 Views of St 37 blanked material with thickness values of 3.5, 5, and 6 mm at HP, CP, and HERF hammers 155

Figure 6. 41 Relationship among the three different types of cutting machines with using four different die clearances a) cutting surface b) fracture surface 156

Figure 6. 42 SEM views the shear and fracture region of the St 37 blanks obtained from machines with different punching speeds...157

Figure 6. 43 Surface roughness (Ra) for different cutting conditions.....................158

Figure 6. 44 SEM views of the blanks cut by a)CP b)LCM c)HERF 159

Figure 6. 45 Potential corrosion graphics of the blanks produced in different clearances for a) Hydraulic b) Conventional c) HERF 162

Figure 6. 46 The comparison of the blanks with the best corrosion rate for each shearing technique...163

Figure 6. 47 SEM views of the shear and fracture surface of the blanks after corrosion test for a) Hydraulic b) Conventional c) HERF 164

Figure 6. 48 Potentiodynamic polarization curves of specimens at different blanking speeds. 166

Figure 6. 49 Cyclic voltammograms of HERF cutting (frame cycle line), laser cutting (diagonal cross line), and conventional cutting (solid black line) AISI 304 steels..167

Figure 6. 50 SEM micrographs of the samples before corrosion test a) CP b)LCM c)HERF..168

Figure 6. 51 Corrosion micrographs of specimens before corrosion test, a) CP b) LCM c) HERF. 169

LIST OF SYMBOLS

$\boldsymbol{\alpha}$	Crank angle
$\boldsymbol{\beta}$	Direction of crack propagation
$\boldsymbol{\theta_d}$	Diagonal angle
μ	Coefficient of friction between the workpiece and the die
$\boldsymbol{\acute{\eta}}$	Mechanical and electrical losses
ε	Effective strain
$\dot{\varepsilon}$	Effective Strain-rate
$\boldsymbol{\sigma}$	The flow stress
$\boldsymbol{\acute{\eta}_i}$	The impact efficiency
A	Surface area
A	Strength coefficient, combining the effects of the *K* and *C* values
Ab	Area of the annular under the face of the piston
AC	Alternative Current
Ac	Seal area of the piston
AISI	American Iron and Steel Institute
BDC	Bottom Dead Center
C	Strength constant
Cl	Clearance
CP	Conventional Mechanical Press
CR	Compression Ratio
CV	Cyclic Voltammograms
$\mathbf{C_{vo}}$	Specific heat coefficient at constant volume
$\mathbf{D_a}$	Diameter of surface of workpiece that contacts the upper die after the forging operation
$\mathbf{D_b}$	Diameter of the central point of the workpiece after the forging operation
$\mathbf{D_c}$	Diameter of surface of workpiece that contacts the lower die after the forging operation
$\mathbf{D_m}$	Die diameter
$\mathbf{d_o}$	Diameter before forging
$\mathbf{D_p}$	Punch diameter

DCP	Direction of Crack Propagation
E	Total Energy
$\mathbf{E_a}$	Energy for spring back of the anvil
$\mathbf{E_{ar}}$	Energy to overcome the air drag
$\mathbf{E_{cor}}$	The corrosion potential
$\mathbf{E_d}$	Energy used for deformation
$\mathbf{E_{e1}}$	Energy used for elastic deformation of the dies and the machine
$\mathbf{E_f}$	Energy used for friction in die and machine guides
$\mathbf{E_m}$	Energy used for spring back of the moving parts
EDM	Electro-Discharge Machining
F	Force
h	Height of the workpiece
HERF	High Energy Rate Forming
$\mathbf{h_o}$	Height of cylinder before forging
HP	Hydraulic Press
HV	Hardness Vickers
HVF	High Velocity Forming
ICE	Internal Combustion Engine
k	Coefficient of gas constant
K	Strength Coefficient
l	Length of the connecting rod
L	Load on the press
l	Length or perimeter of the cut (mm).
LCM	Laser Cutting Machine
$\mathbf{L_{sh}}$	Average cutting force (in N), with angular shear,
m	Strain-rate sensitivity exponent
$\mathbf{m_a}$	Amount of air mass,
$\mathbf{m_f}$	Amount of fluid
n	Corrected coefficient of k in practice
n	Strain Hardening exponent
OCP	Open Circuit Potential
P	Pressure
P	Power
$\mathbf{P_t}$	Gauze electrode for polarization and corrosion measurements

Q	Energy produced in internal combustion engine
r	Crank radius
r	Radius of the workpiece
R_a	The average surface roughness values
SAE	American Automotive Engineering
SCE	Saturated Calomel Electrode
SCS	Shear Compression Specimens
SEM	Scanning Electron Microscopy
SS	Stainless Steel
T	Temperature
T	Tangential force
t	Sheet thickness (mm)
TDC	Top Dead Center
TEM	Transmission Electron Microscope
U_p	Punch penetration corresponding to the first crack initiation within the sheet
V	Volume of workpiece
V_c	Combustion chamber volume
V_d	Displacement volume
$\dot{V}$	Volumetric flow rate of hydraulic fluid
v	Ram impact velocity
W	Work done
WE	Working Electrodes
Y	Tensile yield strength

CHAPTER 1

INTRODUCTION

1.1 INTRODUCTION

While forging may be one of the most ancient of metal working techniques, it remains today one of the most important manufacturing processes embracing primary process such as the reduction in size of large cast ingots (approximately 1m diameter), to the net-shape microforming of electronic components (<1mm) **(Hartley and Pillinger, 2006).** The energy that promotes deformation is applied by a hammer, press, up-setter or ring roller, either alone or in combination. The shape is imparted by tools that contact the workpiece and by careful control of the deformation process **(Aktakka, 2006).**

Today, forging is used in different industries for manufacturing of variety parts such as; balls for rolling bearing, small bolts, pins as well as gears, cam and crankshafts, shafts, axles, holding hooks, flanges, hand tools aircraft landing structures, turbine blades, some medical instrument components such as surgery blades etc. As in metal forming there are different classifications for forging such as in terms of temperature (hot, warm, and cold), die (open and closed die), and shape (compact shapes, disc shapes, and long shapes) **(Cora, 2004)**.

Selection of equipment to produce forging depends, ideally on the type of work metal and on the design of forging. In practice, however, selection of the size and type of equipment usually depends primarily on cost and production quantity. Conventional forging presses such as mechanical presses are usually large in size but they have a low production and a high cost rate. For production whereby these types of presses are used, this causes workpiece to be moved to different sections and thus get out of the production band. Getting out of the production band, which leads to time and energy losses, increases the cost per unit. Because of the shortcomings of conventional presses, in the 1960's several forming related to the plastic deformation process were developed which had the characteristic feature of involving the conversion at very high rate of some form of energy into forming work-hence these processes are known as High Energy Rate Forming (HERF) **(Davies and Austin, 1970).** There are certain advantages of using HERF hammers. The products manufactured by conventional methods can be manufactured at high speed forming in same cost, with higher quality and they do not need finishing process **(Davies and Austin, 1970), (Yaldız et al, 2007).**

High-energy-rate forming equipments are based upon three methods of releasing energy: (1) chemical (high explosives, propellants, gas mixtures), (2) electrical (exploding wires, spark discharges, magnetic fields), and (3) mechanical (pneumatic-mechanical presses). High energy-rate forming is applied to sheet metal in draw – forming, bulging, sizing, punching, swaging, flanging, heading, powder compaction, cutting, welding, and surface hardening. The materials that are fabricated by HERF include magnesium, aluminum, beryllium, titanium, zirconium, carbon and alloy steels, stainless steels, super alloys, the refractory metals, and composites.

There are three basic types of HERF hammer, namely, ram-and-inner-frame machines, two-ram machines, and controlled-energy-flow (counterblow) machines. In all three types, the energy is derived from high-pressure gas (usually nitrogen) that is stored within the machine and released to accelerate the platens. The machines are designed to minimize shock transmission to the floor. Therefore, a special foundation is not needed, and the machine can be placed directly on the factory floor. There is dearth of research in literature related to the effect of high energy rate forging speed on the behavior of forged materials.

1.2 RESERCH OBJECTIVES

The objectives of this thesis can be listed as follows:

- To design and construct a compact prototype High Energy Rate Forming (HERF) hammer which uses two-cylinder internal combustion engine (burning compressed air-fuel mixture) to produce forming energy and a mechanical re-cocking mechanism.

- To compare the performance characteristics of the HERF hammer with conventional hydraulic and mechanical presses, forging and blanking operations to be carried out on three different materials (aluminum, mild steel St37 and stainless steel AISI 304).

1.3 ORGANIZATION OF THE THESIS

This thesis is comprised of seven chapters. Chapter 2 covers a literature review and Chapter 3 provides the general background information about load, stress, energy determination in forging, high energy rate forming machines, economics of high energy rate forming machine, and their metallurgical effects.

Chapter 4 covers design and construction of the prototype high energy rate forming machine. Frame, power unit, injection unit, ignition unit, re-cocking mechanism and working principles of the constructed proto-type HERF hammer are explained in detail in this chapter.

In Chapter 5, experimental work is presented. In order to compare the performance of the designed and constructed HERF hammer with those of the Conventional and Hydraulic presses, open die forging and blanking operation are performed on the three different types of materials.

In Chapter 6, the load and energy measurements in the forging and blanking processes are described. Initially, aluminum, mild steel (St37) and stainless steel (AISI304) are forged with the hydraulic, conventional and high energy rate forming machines. The load-stroke behaviors of the materials are compared depending on the forging press types. Later, aluminum, mild steel, and stainless steel are also blanked at five different clearances with the hydraulic, conventional and high energy rate forming machines. Load-stroke curves of each material depending on both die clearances and blanking speed are plotted and results are discussed. A summary of results achieved so far and conclusions are presented in Chapter 7, Moreover recommendations for future studies are also given in Chapter 7.

CHAPTER 2

LITERATURE REVIEW

2.1 INTRODUCTION

The following literature review focuses on the definition and properties of high energy rate forming. Brief information about the history of high energy rate forming hammer is presented. Forging and blanking applications and their characteristic behaviors under the high energy rate forming are discussed in detail.

2.2 HIGH ENERGY RATE FORMING HAMMER

2.2.1 Definitions

In the 1960's several forming related to the plastic deformation process were developed which had the characteristic feature of involving the conversion at very high rate of some form of energy into forming work hence, these processes are known as High Energy Rate Forming (HERF) **(Davies and Austin, 1970).** The high energy rate forming (HERF) processes, sometimes called high-velocity forming (HVF) processes; develop high rates of energy transfer to the workpiece by an increase in magnitude of the velocity component of the forming operation itself. A HERF processes is any process which operates at forming speed of range 6-24 m/s (**Semiatin, 1988**).

2.2.2 History of High Energy Rate Forming Machines

The first HERF hammer was developed by the Convair Division of the General Dynamics Corporation, and it was marketed under the name of Dynapak. The machine was launched with a great deal of the publicity as a “revolutionary concept of metal forming” and as a result, in rapid succession other HERF hammers appeared in the USA for example, the Clearing Hermes Machine, the Verson Hammer, The Ken-O-Matic etc. Almost all industrialized countries followed suit and produced their own models, for instance, The CEFF Machine (West German and USA), The Krupp Hammer (West German), The Hi-Formac (Japanese) as well as copies of the original Dynapak, built in British. Hungarian and Russian research establishment; all actuated with compressed air or nitrogen heaving a maximum impact velocity of 18-25 m/s and primarily intended for single blow hot forging operation **(Tobias, 1985).**

2.2.3 High Energy Rate Forming Machines Energy Releasing Methods

High energy rate forming equipment is based on upon four methods of releasing energy **(Tobias, 1985).** The first and the most typical method of these is explosive forming. The energy of an explosive charge, triggered by a detonator, is transmitted through a medium (water or sand) to impinge on a sheet/plate or tube, to accelerate this into a die as demonstrated in Figure 2.1.

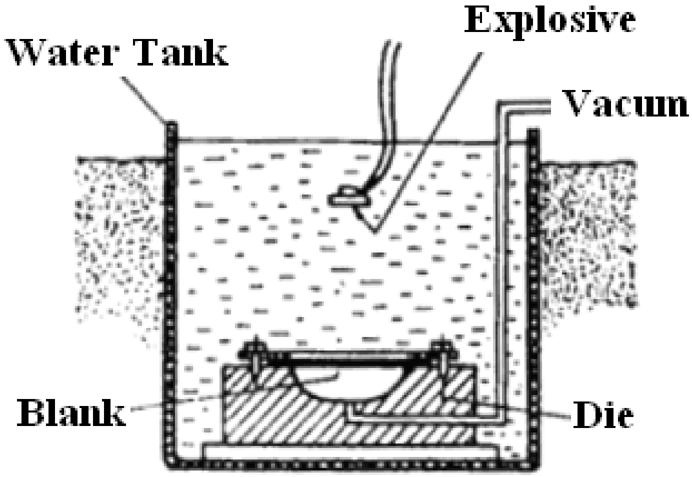

Figure 2.1 High energy rate forming energy releasing by explosive forming **(Tobias, 1985)**

In the second method, electrical energy stored in a capacitance can be used in an analogues manner; by discharging it through a thin wire, or electrodes submersed in a fluid medium, a high intensity shock wave is generated which can be utilized similarly, the process being called Electro hydraulic forming **(Wick, 1960)**. Electro hydraulic working energy releasing is illustrated in Figure 2.2

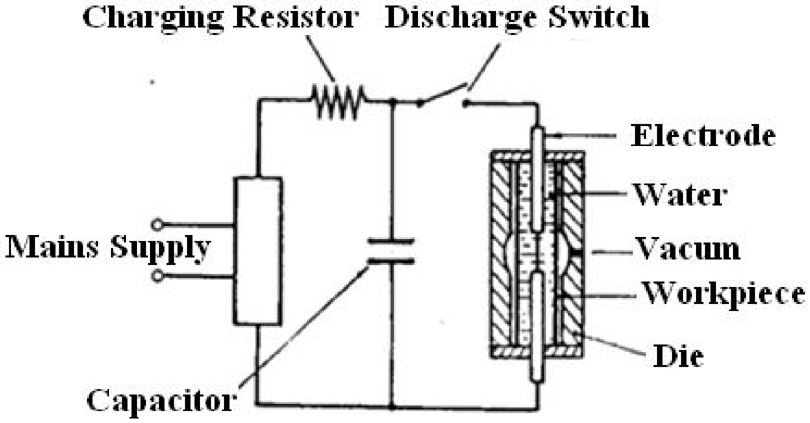
Charging Resistor
Discharge Switch
Electrode
Water
Mains Supply
Vacum
Workpiece
Die
Capacitor

Figure 2.2 Electro hydraulic working energy releasing method **(Tobias, 1985)**

The third method is the magnetic forming. In this method, electrical energy is used by discharging it through a magnetic coil. The magnetic field generated induces a current in a nearby conductor (the workpiece) and this produces a second magnetic field. The two magnetic fields repel each other and the workpiece is accelerated into a die. The working principle of this process is presented in Figure 2.3.

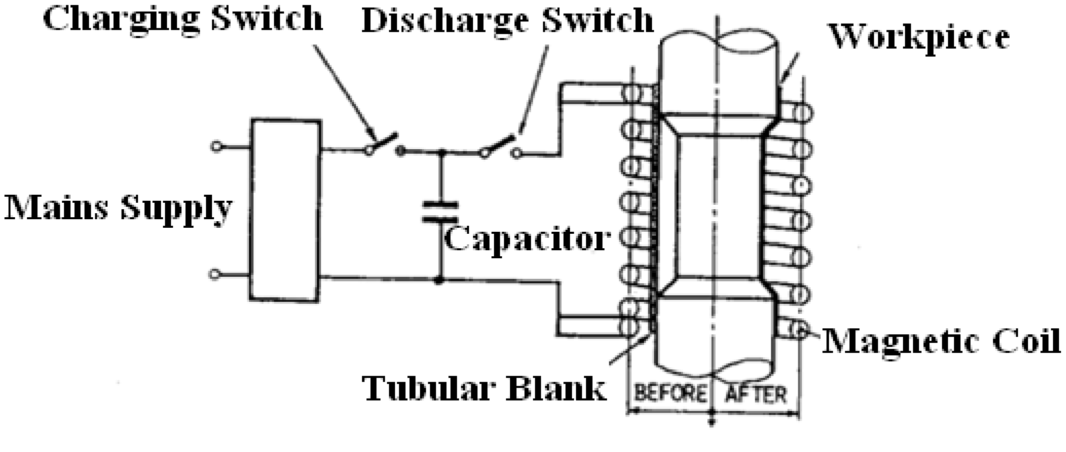
Charging Switch
Discharge Switch
Workpiece
Mains Supply
Capacitor
Magnetic Coil
Tubular Blank
BEFORE
AFTER

Figure 2.3 Magnetic forming energy releasing method **(Davies and Austin, 1970)**

The last method is the bulk forming. Bulk forming is the forming of billets with dies, high speed hammers were developed which used the energy contained in compressed gas (usually nitrogen or air), acting on a piston which accelerated a die to impinge another, to form a hot or cold billet. This method is schematically illustrated in Figure 2.4.

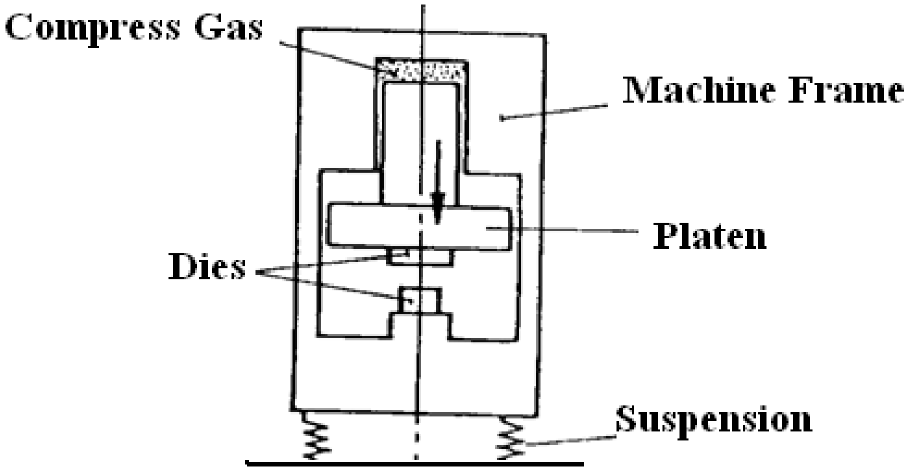

Figure 2.4 Bulk forming energy releasing method **(Tobias, 1985)**

2.2.4 Application Area of HERF Hammers

High energy rate forming is applied to bulk deformation in forging and sheet metal in draw forming, blanking, punching, swaging, flanging, heading, powder compacting, cutting, welding, and surface hardening. The materials fabricated by HERF include magnesium, aluminium, beryllium, titanium, zirconium, carbon and alloy steel, stainless steel, super alloy, the refractory metals and composites (**Semiatin, 1988)**.

2.2.4.1 Forging Applications by Using HERF Hammers

Forging is a process of forming metal parts by the use of heat and pressure. Forging develops a grain structure in the metal, which makes it stronger in the direction that it has been stretched. Forging is done in special moulds called “dies” and when the dies are properly designed to take advantage of the grain structure introduce by the forging process, the resulting parts are stronger along the important directions than those manufactured by CNC machine.

Die loads taking barrelling into consideration in addition to the inertial forces during the high speed cold forging of the sintered preform under axial symmetry and plain strain conditions was determined via the energy analysis method by **Singh and Jha (2001).** When determining the die loads, appropriate interfacial friction law and yield criterion for the previous sintered material were used. **Singh and Jha (2001)** concluded that the interfacial friction between the workpiece and die is quite different from sliding friction in machine parts and is a function of both pressure and adhesion. They also concluded that the effect of inertial force on die load is not negligible during high speed sinter forging and must be considered while calculating the die loads.

Hallström (2000) determined the best average friction factor on the tool/workpiece interface to obtain the most realistic filling when simulating material flow in forging. Experimental comparisons of the simulations are also performed. Experimental processes were performed by a counter blow hammer. That was a five step hammer where each blow delivers a maximum energy of 200 kJ. **Hallström (2000)** concluded that the best conformity between simulation and experiment is established when friction factor, m= 0.2 for the upper tool and m=1.0 for the lower tool is used.

The numerical simulations of the high-velocity impact forging processes were described by **Yoo and Yang (1997).** In that study, the explicit time integration finite element method was used to compute the deformation of the workpiece and the dies. In order to consider the effects of strain hardening, strain rate hardening and thermal softening, which are frequently observed in high-velocity deformation phenomena, the Johnson-Cook yield surface model was applied. Through the copper blow test simulation, the developed program was verified and applied to simulations of high-velocity multi-blow forging processes. Two types of workpiece configurations, cylinder and block, were used for high-velocity multi-blow forging simulations. **Yoo and Yang (1997)** found that the change of the blow efficiencies and the clash load generated by the blow operations could be efficiently analyzed.

Berg et al (1995) studied on the open-loop problem of selecting a nominal ram velocity profile to produce a desired microstructure, given a specified die and preform geometry and forging temperature. Two approaches for doing so are applied to a simple, but representative problem. The first is based on classical numerical optimization techniques. The second is based on inverse neural networks and offers potential savings in critical computations. Simulation studies for the two methods show good results.

Hamouda (2002) stated that determination of stress–strain properties of material and formulation of suitable constitutive laws is very important on the study of: (i) the elastic–plastic response and collapse mode of structures and (ii) high speed metal cutting and metal forming processes. **Hamouda (2002)** defined reasons of the energy losses in an existing ballistic rig. The effect of energy losses due to impact into the study of dynamic flow stress of a material is also examined by **Hamouda (2002).** He presented that loss of kinetic energy varying from 1 to 20% of the initial energy and total energy loss was found around 7%. In that article, the effects of friction, inertia, and temperature rise during the dynamic compression tests are also presented and discussed.

The design of the first industrial rocket engine and its propelled forge hammer were described by **Bodurov and Penchev (2005).** The new technological capabilities of the industrial rocket engine propelled hammers like a “sticking impact”, dynamic regulation of the deformation process parameters, and minimization of the manufacturing drain were also discussed. They concluded that the industrial rocket engine propelled hammer show that the designed new industrial rocket engine can be successfully used for making means of production and especially for propelling of forging hammers.

Yaldız et al (2007) stated high speed forging is an important production method that requires specially designed high energy rate forming machines. Most of the high energy rates forging machines are devices that consist of a system in which energy is stored and a differential piston mechanism is used to release the energy at high rate. They adapted an accelerator on the conventional press in order to eliminate the usage of specially designed high energy rate forming machines and to obtain high speed forming benefits. They also affirmed that the designed energy accelerator can be incorporated into mechanical press to convert the low speed operation into high-speed operation of a hammer. By adapting the accelerator on the conventional press, speeds of conventional presses improved from 1.5 m/s to the 10 m/s. They investigated that products manufactured by utilizing the pneumatic accelerator have higher surface quality then the surfaces of products produced in conventional presses and they do not need finishing process.

Deformation of metals through the high energy rate forming machines can be quite effective in increasing the forming limits of the metal sheets as well as effectively treating some other common metal forming problems, such as wrinkling and distortion **(Seth et al, 2005).**

High velocity formability of cold rolled sheet steel as developed in impact with a curved punch were examined by the **Seth et al. (2005).** To study forming over large areas, they launched a steel sheet sample electromagnetically at a shaped punch at velocities of 50-220 m/s, using a flat spiral electromagnetic coil and an aluminum driver sheet. They estimated the impact velocity with the help of high speed camera, and observed that the impact velocity of the samples increase nearly linearly with the energy of launch. The failure strains of all the steels were dramatically increased beyond those obtained in tensile tests as expected from the forming limit diagram. The forming limits of steels with both very low and high quasi-static ductility were similar to those in high velocity forming. They also stated that formability seemed to depend largely on local boundary conditions as dictated by the punch/tool geometry used. The strain distribution obtained depended on shape of the punch used for impact. Thus it appears that in high velocity impact, the quasi-static ductility of the material is not of primary importance to the materials formability. At high velocities, high strains to failure can be obtained with steels having very low quasi-static ductility.

Gupta et al. (2007) presented the collapse behavior of the hemi-spherical and shallow-spherical shells and their modes of the deformation under impact loading. Aluminum spherical shells of various radii and thicknesses were made by spinning. These spinning aluminum samples subjected to the impact loading under a drop hammer and the load histories were obtained in all the cases. They were also performed the three dimensional numerical simulations of the all tested specimen geometries by using LS-DYNA. They concluded that the impact mean collapse load and hence the energy absorbed during deformation were found to be higher than their corresponding static values, and are found to be depended on both thicknesses and radius of the shell.

Mamalis et al. (1998) employed the explosive and electromagnetic high energy rate compaction forming ‘powder-in-tube’ techniques for near net-shape manufacturing of axisymmetric silver/superconducting Yttrium-Barium-Copper-Oxygen (YBCO) ceramic. They considered the isodynamic compaction in which the impulse-form pressure is applied over the whole outer surface of the metal tube containing the powder to be compacted. The integrity of the components and the effect of the compaction processes on the superconducting properties were examined. At the end of the study, it was observed that both explosive and electromagnetic compaction of YBCO superconducting powders are potential techniques for the manufacture of high integrity superconducting components. The electromagnetic compaction technique has particular potential for the net shape manufacture of metal sheathed conductors used typically in long conductor applications. They also concluded that manufacture by means of explosive technology may offer economic benefits compared with electromagnetic compaction since the specific costs for the latter with larger equipment are much higher than the related cost of explosive processing with the same energy level.

Rusinek et al. (2009) presented on the experimental and numerical analysis of the failure process of mild steel sheets subjected to normal impact by hemi-spherical projectiles. They performed experiments by using direct impact technique based on Hopkinson tube as a force measurement device. The test covered a wide range of impact velocities. Both lubricated and dry conditions between specimen and projectile have been applied. Different failure models for each case were found. At the end of the research, petalling was observed at the lubricated condition whereas for dry condition a radial neck along with a whole enlargement reduced the formation of petalling. They also simulated the perforation process by the application of 3D analysis using ABAQUS/Explicit FE code.

Plastic deformation of quench and tempered AISI 4340 steels under ballistic impact was investigated by **(Odeshi et al, 2006).** The plastic deformation was characterized by formation of adiabatic shear bands, which initiate the failure process. Whereas white etching bands are formed in steel samples tempered at 300 and 400 ^{o}C, adiabatic shear bands of the deformed type are developed in samples tempered at temperatures above 500 ^{o}C. Fracture in the samples occurred by crack initiation and propagation along the shear bands. The cracks were initiated by nucleation of micro-voids, which coalesce, grow and develop into cracks. The white etching bands formed in samples tempered at 300 and 400 ^{o}C exhibit higher cracking tendencies than the deformed bands observed in samples tempered at higher temperatures.

Dabboussi and Nemes (2005) proposed a procedure for determining the Johnson–Cook constitutive and, simplified, failure model parameters for three materials with specific importance in the aerospace industry, aluminum 6061-T6, titanium Ti-6Al-4V and austenitic, nitrogen-strengthened, stainless steel (Nitronic 33). Quasi-static and split Hopkinson pressure bar (SHPB) shear punch experiments were used to assess the materials' ductility, while the quasi-static and SHPB compression experiments were used to determine the materials' response. They also simulated the laboratory results coupled with ABAQUS/Explicit which was a tool for determination and validation of the models' parameters for each material. While the use of the Johnson–Cook model with the proposed simplified failure model proved adequate for aluminum and titanium, the same conclusion cannot be done for nitronic partly due to the intrinsic characteristics of this material and the multiplicative form of the Johnson–Cook model.

The response of AISI 4340 steel to rapid deformation at high strain rates were investigated by **(Odeshi et al, 2005).** Deformation was governed by two simultaneously occurring processes of strain hardening and thermal softening due to conversion of the large fraction of deformation energy into heat. At the onset of plastic deformation, strain hardening dominates the deformation process, during which deformation will be homogeneous. The flow stress depends on the impact velocity which determines the strain rates. As deformation proceeds, adiabatic heating occurs along narrow bands and thermal softening begins to dominate the deformation process. Flow stress subsequently decreases with increasing strain. A critical strain is eventually reached, whereby mechanical instability occasioned by stress collapse occurs resulting in strain localization along narrow bands. The time as well as the critical strain for the onset of stress collapse decrease with increasing strain rate. The time and critical strain for the commencement of adiabatic shearing is lower in steel samples tempered at 425 ^{o}C than for those tempered at 315 ^{o}C, an effect which can be attributed to increased perturbation caused by segregation in the microstructure of the steel samples that were tempered at 425 ^{o}C. Multiple shear bands were found to simultaneously initiate and propagate in the samples tempered at 425 ^{o}C. One of such multiple bands appears as distinct white etching ASB while the rest are essentially deformed bands which have features similar to the bulk material but with fine carbides and highly deformed and aligned martensite laths. They also concluded that the type of shear bands formed during adiabatic shearing is a direct consequence the intensity of accompanying fragmentation and dissolution, which eventually determine the size of the micro-constituents of adiabatic shear band and resolvability using optical microscopy.

The large-strain constitutive behavior of cold-rolled 1018 steel has been characterized at strain rates ranging from $1\text{x}10^{-3}$ to $5\text{x}10^{4}\text{s}^{-1}$ use the newly developed shear compression specimens (SCS). From that study, the following conclusions were drawn. The technique based on the SCS yields results that are quite comparable to those obtained using other techniques, such as uniaxial compression or torsion tests. Moreover, a wide range of strain rates is conveniently explored in a seamless manner using single specimen geometry and loading technique.

2.2.4.2 Adiabatic Shear Band Formation in the HERF Hammers Application

Adiabatic shear banding is a catastrophic failure mechanism that may develop in certain ductile materials which are subjected to dynamic loading **(Batra and Lear, 2005).** The phenomenon itself consists of a narrow band of sheared material, in which the local temperature may reach a significant fraction of the melting temperature, as a result of thermo mechanical coupling effects. Shear band formation is a complex function of strain, strain rate and temperature. Shear bands have been observed in many practical applications involving high-speed deformation, including machining, ballistic penetration, and high speed forming. Hence, many investigations into adiabatic shear band formation have been published over the past 20 years or so. An early and well accepted analysis of adiabatic shear banding formation relies on the competition between strain-rate hardening and thermal softening, so that when the latter overcomes the former, the material can no longer harden and fails by shear localization.

Adiabatic shear bands are areas of intensive shear deformation in which plastic work can cause temperature to rise significantly and thus soften the material and allow for greater deformation and further heating. This kind of deformation is usually referred to as adiabatic, because there is no sufficient time for the heat to be conducted away before thermal softening occurs. Once localization has taken place, the strain and the temperature are locally very large without contributing much to the overall deformation of the object, and the highly localized strains can precipitate a shear fracture. This phenomenon has been known to be crucial in situations such as high-speed impact, crash, penetration, metal forming, machining and manufacturing **(Lee et al, 2000).**

Guohe et al (2009) built an adiabatic shear critical condition in high speed cutting by linear perturbation analysis and the effects of the material characteristics and they quantitatively investigated the deformation conditions on the onset of adiabatic shear in high-speed cutting. They conclusions that the adiabatic shear in high-speed machining are likely to form under the conditions of smaller strain hardening index, smaller strain rate hardening index, larger thermal softening index, larger viscosity, larger strain, larger strain rate, larger compression stress, lower initialization temperature, smaller density and smaller thermal capacity. They also concluded that the effect of thermal conductivity on the onset of adiabatic shear can be neglected.

The effects of adiabatic shear bands on the required energy in shearing a steel rod was studied by the **Stock and Wingrove (1971).** Stock and Wingrove also used a drop weight punch to shear normalized low carbon steel and quenched and tempered high carbon steel rods. For quasi-static shearing of the rods, the change in energy before and after impact was compared with the energy required. The energy required to shear the high carbon steel was less than that required for quasi-static shearing at higher strain rates. At high strain rates, transformed bands were present along the fracture surface of the high carbon steel sheared. The energy required to shear the high carbon steel was lowered at the formation of transformed adiabatic shear bands **(Souther, 2003)**

Many of experimental methods generated adiabatic shear bands. One type of testing equipment used to produce adiabatic shear bands is the split-Hopkinson bar. This testing method allows the geometry of the test specimen to vary while controlling the strain rate. To produce adiabatic shear bands, there are numerous types of test specimen geometries when dynamically loaded in a split-Hopkinson bar.

To study the effects of temperature on adiabatic shear band formation, **Lee and Lin (1998)** used cylindrical Ti-6A1-4V specimens in a split-Hopkinson compression bar. The cylindrical specimens were dynamically loaded at temperatures ranging from 25 °C to 1100 °C at a strain rate of 2.5×10^{-3} sec^{-1}. Transformed bands were produced between 500 °C and 1100 °C. The hardness and thickness of the transformed bands differed as the temperature varied. At 500 °C, the hardness within the band was 450 Hv, whereas at 1100°C the hardness of the band dropped to 395 Hv. The thickness of the transformed band increased from 14.7 microns at 500 °C to 45 µm at 1100 °C.

A controlled-penetration specimen which was impacted by an air-gun projectile to produce adiabatic shear bands in AISI 4140 steel was used by **Chou et al. (1991).** An indentor fired upon by the air-gun projectile penetrated the steel specimen. Penetration of the indentor produced transformed bands within the steel. The test specimen allowed for the depth of penetration to be controlled. At the end of the study, it was concluded that the length of the shear band was proportional to the flow stress and depth of penetration.

Adiabatic shear bands on the surface of low carbon steels using a prismatic test specimen loaded in a split-Hopkinson compression bar was generated by **Clous et al. (2000).** The prismatic specimen allowed the temperature within the bands to be measured during formation. A fast infrared detector array was used to measure the maximum temperature experienced in the band during formation. It was measured that the maximum temperature was 850 °C in the shear band.

Meyers et al. (2003) studied the adiabatic shear banding and micro-structural changes of the 304L stainless steel due to shear localization by using the hat-shaped specimen. Using a split-Hopkinson compression bar, deformed shear bands were generated within the stainless steel. The microstructure outside the deformed band displayed individual grains that had been deformed by stacking faults, twining or a martensitic phase transformation. The presence of martensite laths were observed at twinband intersections within individual grains. The martensite laths were generated by a strain induced phase transformation caused by intense plastic deformation.

Souther (2003) developed three novel test specimens for high strain rate loading in a split-Hopkinson compression bar. Effects of intense shear deformation at high strain rates such as the formation of adiabatic shear bands, profuse twinning, strain induced phase transformations and the refinement of grain structure were observed without having to cut, section, or destroy the test specimens. The region of shear localization and adiabatic shear band formation within each specimen was known prior to testing. After testing, grains containing a laminar structure were observed in the four comers of the 304 stainless steel specimen. The laminar-structures were believed to be either dislocations and stacking faults or excessive twinning. When consecutively tested and rotated seven times, the number of laminar-structured grains within the four comers increased. A number of grains also displayed intersecting stacking faults or twins after the seventh test.

Klepaczko and Klosak (1999) studied critical impact velocity (CIV) concept in shear. They stated that deformations trapping due to thermoplastic instability caused by the propagation of plastic waves are the main physical reasons for CIV in shear. They offered a simple analytical approach on how to estimate the value of CIV. They performed a numerical study of impact shearing of a layer with a small geometric imperfection by the FE code ABAQUS, and available experimental results verified for VAR 4340 steel, N 50 HRC, obtained by direct impact on modified double shear (MDS) specimen. In particular, the numerical study was focused on the effect of the imposed velocity on the spatial deformation of the layer. Seventeen velocities were assumed in FE calculations from quasi-static to 160 m/s. Two modes of shear deformation of the layer were found: in the first mode all plastic deformation concentrates in the middle of the layer and in the second near the surface where the shear velocity is imposed. CIV could be defined as a transition between those two modes. It was shown that impact velocities higher than CIV lead to a substantial reduction in the total energy of strain localization.

The critical impact velocities existence in tension and shear was confirmed by **Klepaczko (2005)** theoretically, experimentally and numerically. Klepaczko showed that physical parameters, including thermodynamic constants, as well as material behavior in elastic and plastic ranges are involved in estimation of the CIV. Values of the CIV, both in tension and shear, can be understood as material constants. The

CIV in tension imposes very strict limits on impact tensile testing of materials. This limitation is observed because well before occurrence of the CIV at much lower velocities the strain gradients along specimen obscure the assumption of the uniformity of the strain along specimen. The CIV in tension is the upper limit of tension impact testing. Theoretical analysis of the CIV in tension has been improved by introduction of complete thermal coupling in the form of adiabatic heating. A complete analysis of the CIV in shear with thermal coupling was also performed by **Klepaczko (2005)** that is the adiabatic process of deformation superimposed on trapping of plastic shear waves was considered. He found that a unique superposition of plastic shear waves and adiabatic softening triggered this phenomenon. It was concluded that the CIV in shear was lower than that in tension.

Phenomenological plastic flow stress models are used extensively in the simulation of large deformations of metals at high strain-rates and high temperatures. Several such models exist and it is difficult to determine the applicability of any single model to the particular problem at hand. Ideally, the models are based on the underlying (subgrid) physics and therefore do not need to be recalibrated for every regime of application. **Banerjee (2005)** compared the Johnson-Cook, Steinberg-Cochran-Guinan-Lund, Zerilli-Armstrong, Mechanical Threshold Stress, and Preston-Tonks-Wallace plasticity models. He used copper as the comparison material. Firstly, he determined the parameters for the specific heat model, the equation of state, shear modulus models, and melt temperature models. He identified the applicability range of each models, then compared the flow stresses predicted by the five flow stress models with experimental data for annealed copper and quantified modeling errors. He concluded that the all the models are quite accurate at low temperatures; however, at high temperatures and under high-strain-rate conditions, their accuracy can vary significantly.

Chen et al. (2000) studied the initiation and development of shear bands in high-speed impact/contact problem. The deformable material is and modeled to be strain hardening, strain rate hardening, and thermal softening with the flow stress specified by the Johnson-Cook relation and the Gruneisen state equation. They assumed that deformation was to be adiabatic and thus the effect of heat conduction in that research was ignored. They simulated numerically a cylindrical rod impacting with a flat rigid surface at normal incidence is performed by using the large-scale crash analysis program, LS-DYNA. For comparison, they also simulated the plane strain compression and the plane strain impact problems. The formation of shear bands was observed in both plane strain and axisymmetric impact problems for steel. At higher impact speed, the deformations were found to be more localized along a curve path. They also investigated the effects of thermal softening, strain rate, plastic strain, and friction (between the impact/contact objects) on the deformation localization. They found that the impact speed, the geometry constrains, and the thermal softening characteristics had significant effects on shear localization. Among those, the thermal softening characteristics are the dominant factor on the formation of shear band.

To determine the influence of shock-prestraining on the shear behavior of ferrite, 1018 steel specimens were subjected to forced shear experiments in a split-Hopkinson pressure bar (SHPB) at room temperature and a strain rate of 3800 s^{-1} by **Dougherty et al. (2007)**. Shock-loading was performed below (12.5 GPa) and above (14 GPa) the pressure-induced epsilon phase transition occurring at 13 GPa. They investigated that twinning and microbanding were occurred only in the shock-prestrained specimens. Quasi-static compression tests showed an increase in yield and compressive strengths with increased peak shock stress. SHPB tests produced shear localization in all specimens, with shear banding occurring only in the shock-prestrained specimens.

The spatial distribution of shear bands in 304L stainless steel through the radial collapse of a thick-walled cylinder under high-strain-rate deformation ($\sim 10^4$ s^{-1}) was investigated by **Xue et al. (2004).** They also examined the shear-band initiation, propagation, and self-organization of multiple adiabatic shear bands. They also investigated the effect of grain size on spacing of shear bands at four different grain sizes: 30, 50, 140 and 280μm. A single crystal with a similar composition was also tested. At the end of the study they stated that only a modest variation of shear-band spacing within the investigated grain size range was observed.

Dynamic recrystallization (DRX) is almost universally observed in the microstructure of adiabatic shear bands. It is usually admitted that DRX results from the large temperatures that develop in the band along with very high local strains.

Rittel et al. (2009) reported the observation of dynamically recrystallized nanograins in Ti6Al4V alloy specimens that were impact loaded to only half the failure strain at which the adiabatic shear band develops. Their observation showed that DRX not only precedes adiabatic shear failure but it is also likely to be a dominant micromechanical factor in the very generation of the band. This means that adiabatic shear failure is not only a mechanical instability but also the outcome of strong microstructural evolutions leading to localized material softening prior to any thermal softening.

Chiou et al. (2000) investigated the mechanical behavior and microstructural evolution of a Ti alloy deformed at strain rates ranging from 8×102 s^{-1} to 8×103 s^{-1} and temperatures between 25 $^{\circ}$C and 900 $^{\circ}$C. They used to a compressive split-Hopkinson pressure bar and transmission electron microscope (TEM) to evaluate test results. They indicated that the mechanical behavior and microstructural evolution of the alloy are highly sensitive to both the strain rate and the temperature conditions. The flow stress curves are found to include both a work-hardening region and a work-softening region. The strain rate sensitivity parameter, β, increases with increasing strain and strain rate, but decreases with increasing temperature. The activation energy varies inversely with the flow stress, and has a low value at high deformation strain rates or low temperatures. The microstructural observations reveal that the strengthening effect evident in the deformed alloy is a result primarily of dislocations and the formation of α phase. The dislocation density increases with increasing strain rate, but decreases with increasing temperature. Additionally, the square root of the dislocation density varies linearly with the flow stress. The maximum amount of α phase is formed at a temperature of 700 $^{\circ}$C and results in the minimum fracture strain under the current loading conditions.

Bhattacharyya et al. (2005) studied the texture of oxygen-free high conductivity copper under the strong strain rate. They deformed two shear compression specimens at widely different strain rates (0.001 s^{-1} and 7000 s^{-1}) to the same strain, and their textures were determined using orientation image microscopy. They compared the stress–strain curves and the major texture components at the two strain rate levels, they realized that increase in strain rate causes increase in strain hardening which thereby influences the texture.

There are certain advantages of using HERF. The products manufactured by conventional methods can be manufactured at high speed forming in same cost, with higher quality and they do not need finishing process **(Davies and Austin, 1970), (Yaldız et al, 2007).** It is observed that the quality of shear-fractured surface improved and the amount of distortion was reduced as a result of the use of high punch speeds **(Davies and Dhawan, 1966), (Yaldız et al, 2007)**

Marouani et al. (2009) used a rate dependent constitutive model for the blanking process investigation to improve the accuracy of the predictions. They performed the material testing and the characterization in order to fit the constitutive model parameters to the experimental data. They combined classical tensile tests and video-tensile tests to establish the sheet metal constitutive law. Then, they used their identified model for numerical simulations of various blanking tests: the clearance is ranging from 3.8% to 23%, punch velocity of 23 mm/s and 123 mm/s. They noticed that both the maximum punch force and the shape of the cut edge are affected by the strain rate (punch velocity). The maximum punch force increases for the low speed until a limited value where it becomes constant **(Stegman et al, 1997)**. Explain it by the heat inverse contribution: High strain rate generate an adiabatic behavior which leads to a softness material plasticity.

As it can be seen from the literature, the previous studies were carried out well above the speed limit of the HERF. This is because of the aim of the studies which were investigation of ballistic properties of various materials. Therefore, to find out the effects of HERF on the formed product, a compact prototype HERF hammer is required.

CHAPTER 3

FUNDAMENTALS OF METAL WORKING

3.1 INTRODUCTION

In this chapter, the classification of metal working process is given. The mechanical behavior of metal working processes is summarized in section 3.3. The fundamentals of forging and sheet metal cutting are given in section 3.4 and 3.5, respectively. The presses used in these metal working processes are also explained.

3.2 CLASIFICATION OF METAL WORKING

Manufacturing, in its broadest sense, is the process of converting raw materials into products; it encompasses the design and fabrication of goods by means of various production methods and techniques. Manufacturing represents approximately 20% to 30% of the value of all goods and services produced in industrialized countries. Generally, the higher the level of manufacturing in a country, the higher living standards in that country **(Kalpakjian and Schmind, 2006)**. Figure 3.1 shows main classifications of manufacturing processes.

Metal working includes a large group of manufacturing processes in which plastic deformation is used to change the shape of metal workpiece. Deformation results from the use of a tool, usually a die in metal forming, which applies stresses that exceed the yield strength of the metal. The metal therefore deforms to take a shape determined by the geometry of the die **(Groover, 1996).**

A more recent trend has been to classify deformation processes according to the size and shape of the workpiece. Bulk deformation is the processing of workpiece that have a relatively small surface-area-to-volume (or surface-area-to-thickness) ratio, hence the term bulk. In the bulk deformation processing, the thickness or cross-section of the workpiece change. In sheet forming, the surface-area-to-thickness ratio is relatively large. In general, the material is subjected to shape changes by various dies. Changes in thickness are usually undesirable and, in fact, can lead to failure. Figure 3.2 gives classification of metal working processes.

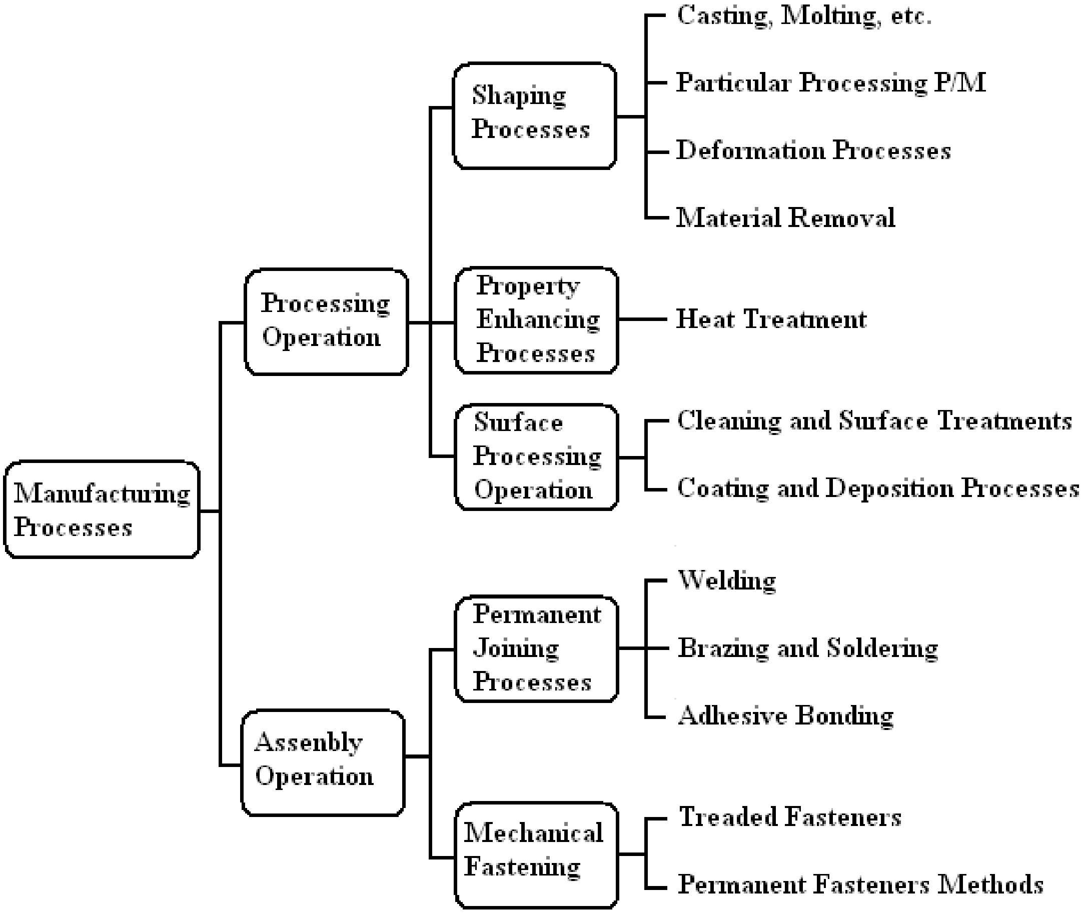
Manufacturing Processes
Processing Operation
Assenbly Operation
Shaping Processes
Property Enhancing Processes
Surface Processing Operation
Permanent Joining Processes
Mechanical Fastening
Casting, Molting, etc.
Particular Processing P/M
Deformation Processes
Material Removal
Heat Treatment
Cleaning and Surface Treatments
Coating and Deposition Processes
Welding
Brazing and Soldering
Adhesive Bonding
Treaded Fasteners
Permanent Fasteners Methods

Figure 3.1 Main classifications of manufacturing processes **(Groover, 1996)**

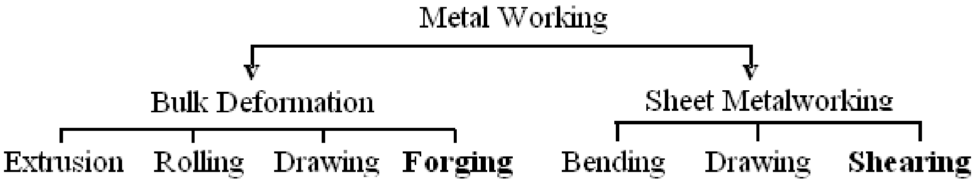
Metal Working
Bulk Deformation
Sheet Metalworking
Extrusion
Rolling
Drawing
Forging
Bending
Drawing
Shearing

Figure 3.2 Classification of metal working processes **(Groover, 1996)**

The bulk deformation processes refine the raw shapes, often adding geometric features, sometimes improving mechanical properties, and always adding commercial value. Deformation processes work by stressing the metal sufficiently to cause it to plastically flow into the desired shape.

Sheet metalworking includes cutting, bending, and drawing operations performed on relatively thin sheet of metal. Cutting is used to separate large sheets into smaller pieces, to cut out a part perimeter (blanking), or to make holes in a part (piercing). Bending and drawing are used to form sheet metal parts into their required shapes.

Desirable properties for working usually include low yield strength and high ductility. These properties are affected by temperature. Ductility is increased and yield strength is reduced when work temperature is raised. The effect of temperature gives rise to distinctions between cold working, warm working, and hot working. Strain rate and friction are additional factors that affect performance in metal working. A systematic approach that is seen in Figure 3.3 can be used to describe fully all the processes arising in metal working **(Lange, 1985)**.

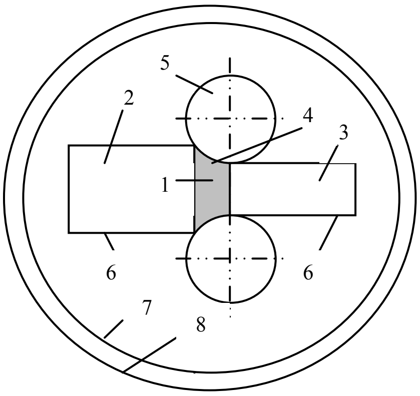

1. the plastic zone
2. characteristics of workpiece before deformation
3. characteristics of workpiece after deformation
4. the boundary area
5. the forming tool
6. surface reactions between the workpiece and surrounding atmosphere
7. the machine tool
8. the production system

Figure 3.3 Systematic approaches to metal working **(Lange, 1985)**

3.3 MECHANICAL BEHAVIOUR OF METAL WORKING PROCESSES

A metal working process is characterized mainly by geometries, velocities, and flow stress data, friction and heat transfer. The mechanical properties of a metal are strongly influenced by metallurgical factors at a microscopic level such as grain size and dislocation density. Collectively, these metallurgical properties are referred to as microstructure. When the characteristic distances, for example the average grain size are small, the material is said to have a fine microstructure. When these distances are large, the material is said to have a coarse microstructure. Finer microstructure generally corresponds to greater fracture toughness, while coarse microstructure better resists creep. For many forgings, the final microstructure is as important as the final shape.

Three parameters dominate microstructures behavior. These are the scalar rate of deformation of an infinitesimal element, or effective strain-rate,$(\dot{\varepsilon})$, effective strain, (ε), and the temperature, (T). These quantities form the thermo mechanical state together in the material at a critical point. It is often possible, at least over some range, to characterize microstructures behavior as depending on only these variables **(Berg, 1995).** In the following part of this section strain, strain rate, stress, yield stress, friction, lubrication, flow stress, deformation load and energy parameters were explained in detail.

3.3.1 Flow Stress

The flow stress (resistance to plastic deformation) of a material is the stress required to initiate or continue plastic deformation under uniaxial state of stress. The factors affecting the flow stress will be explained in detail in the following sections.

3.3.1.1 Flow Stress Dependence on Strain

With elastic deformation, the strains are proportional to the stress, so every level of stress causes some elastic deformation **(Sandor et al, 2005).** On the other hand, a definite level of stress must be applied before any plastic deformation occurs. As the stress is further increased, the amount of deformation increases, but not linearly. After plastic deformation starts, the total strain is the sum of the elastic strain (which still obeys Hooke's law) and the plastic strain. Because the elastic part of the strain is usually much less than the plastic part, it will generally be neglected and the symbol ε will signify the true plastic strain.

The strain-hardening and work-hardening terms are used interchangeably to describe the increase of the stress level necessary to continue plastic deformation. Mathematical descriptions of true stress–strain curves are needed in engineering analyses that involve plastic deformation, such as prediction of energy absorption in automobile crashes, design of dies for consist stamping parts, and analysis of the stresses around cracks **(Hosford, 2005).**

Various approximations are possible. The simplest model is one with no work-hardening. The flow stress, σ, is independent of strain, so

$$\sigma = Y, \tag{3.1}$$

where Y is the tensile yield strength (see Figure 3.4. a). For linear work-hardening (Figure 3.4b),

$$\sigma = Y + A\varepsilon. \tag{3.2}$$

It is more common for materials to work-harden with a hardening rate that decreases with strain. For many metals a log–log plot of true stress versus true strain is nearly linear **(Kalpakjian and Schmind, 2006)**.

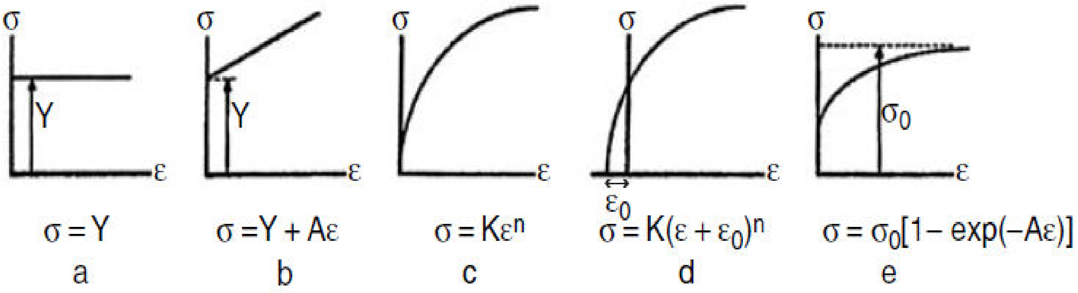

Figure 3.4 Mathematical approximations of the true stress–strain curve.

In this case, a power law,

$$\sigma = K\varepsilon^n, \tag{3.3}$$

is a reasonable approximation (Figure 3.4 c). A better fit is often obtained with

$$\sigma = K(\varepsilon + \varepsilon_0)^n. \tag{3.4}$$

(Figure 3.4 d.) This expression is useful where the material has undergone a prestrain of ε_o. Still another model is a saturation model suggested by Voce (Figure 3.4 e),

$$\sigma = \sigma_o[1 - \exp(-A\varepsilon)]. \tag{3.5}$$

Equation (3.5) predicts that the flow stress approaches an asymptote, σ_o, at high strains. This model seems to be reasonable for a number of aluminum alloys.

In plastic region, the metal's behavior is expressed by the flow curve:

$$\sigma = K * \varepsilon^n \tag{3.6}$$

Where K is the strength coefficient in (MPa); and n is the strain hardening exponent. The stress and strain in the flow curve are true stress and true strain. Figure 3.5 show the flow curve is generally valid as a relationship that defines a metal's plastic behavior in cold working.

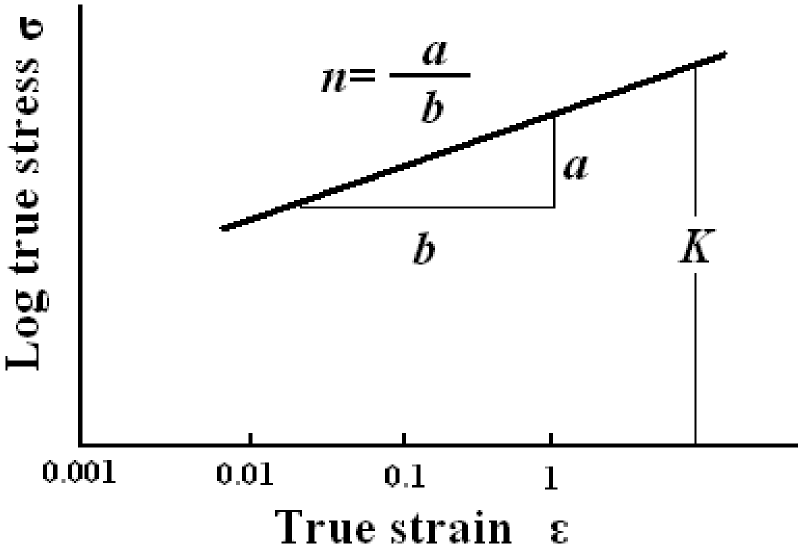

Figure 3.5 True stress-strain curve plotted on log-log scale **(Groover, 1996)**

The flow curve describes the stress-strain relationship in the region in which metal forming takes place. It indicates the flow stress of the metal, the strength property that determines the forces and power required to accomplish a particular forming operation. For most metals at room temperature, the stress-strain plot of Figure 3.5 indicates that as the metal is deformed its strength increases due to strain hardening. The stress required to continue deformation must be increased to match this increase in strength. Flow stress is defined as the instantaneous value of stress required to continue deforming the material to keep the metal “flowing”. It is the yield strength of the metal as a function of strain which can be expressed as

$$\sigma = K^n * \varepsilon^n \tag{3.7}$$

where σ, flow stress (MPa). Typical value of K and n for different metals at room temperature are listed in Table 3.1 **(Groover, 1996).**

Table 3.1 Strength Strain-hardening Material coefficient, K (MPa) exponent, *n*

Material	Strength Coefficient, K(MPa)	Strain Hardening exponent, *n*
Low-carbon steels	525 to 575	0.20 to 0.23
HSLA steels	650 to 900	0.15 to 0.18
Austenitic stainless	400 to 500	0.40 to 0.55
Copper	420 to 480	0.35 to 0.50
Aluminum alloys	400 to 550	0.20 to 0.30
70/30 brass	525 to 750	0.45 to 0.60

Note: From various sources including (**Hosford and Caddell, 1983)**

3.3.1.2 Flow Stress Dependence on Strain Rate

The effect of strain rate on strength properties is known as *strain-rate sensitivity*. Figure 3.6 shows the effect of strain-rate on flow stress at an elevated work temperature and its plotted on log-log coordinates. This relation can be formulized as follows:

$$\sigma = C * \dot{\varepsilon}^m \tag{3.8}$$

Where C is the strength constant (similar but not equal to the strength coefficient in the flow curve equation), and *m* is called the strain-rate sensitivity exponent. Slope of flow stress and strain rate gives the strain-rate sensitivity of material. When strain rate is constant to $1s^{-1}$, flow stress is defined as strength constant. Strength constant is symbolized as C. To give a sense of the effect, typical values of m for different materials are in Table 3.2 **(Groover, 1996)**.

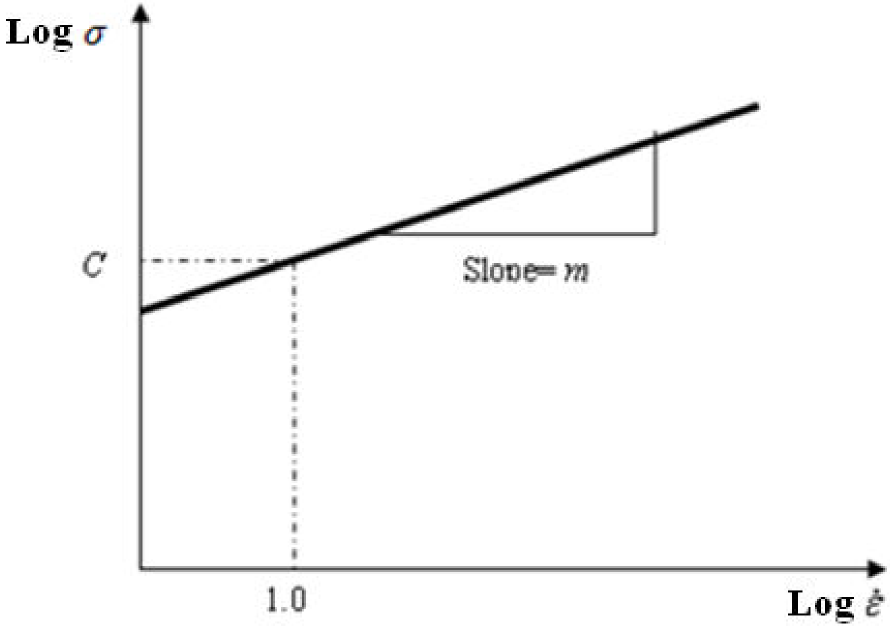

Figure 3.6 Effect of strain-rate on flow stress at an elevated work temperature plotted on log-log coordinates **(Groover, 1996)**

Table 3.2 Typical values of the strain-rate exponent, m, at room temperature **(Groover, 1996)**

Material	*m*
low-carbon steels	0.010 to 0.015
HSLA steels	0.005 to 0.010
austenitic stainless steels	−0.005 to +0.005
ferritic stainless steels	0.005 to 0.010
copper	0.005
70/30 brass	−0.005 to 0
aluminum alloys	−0.005 to +0.005
α-titanium alloys	0.01 to 0.02
zinc alloys	0.05 to 0.08

3.3.1.3 Flow Stress Dependence on Temperature

The flow curve is valid representation of stress-strain behavior of a metal during plastic deformation, particularly for cold working operation. For any metal, the value of *K* and *n* depend on temperature. Both strength and strain hardening are reduced at higher temperatures. In addition, ductility is increased at higher temperature. These property changes are important because any deformation operation can be accomplished with lower forces and power at elevated temperature.

As temperature increases, the whole level of the stress–strain curve generally drops. Figure 3.7a shows the decrease of tensile strengths of copper and aluminum. Usually the rate of work hardening also decreases at high temperatures, as shown for aluminum in Figure 3.7b.

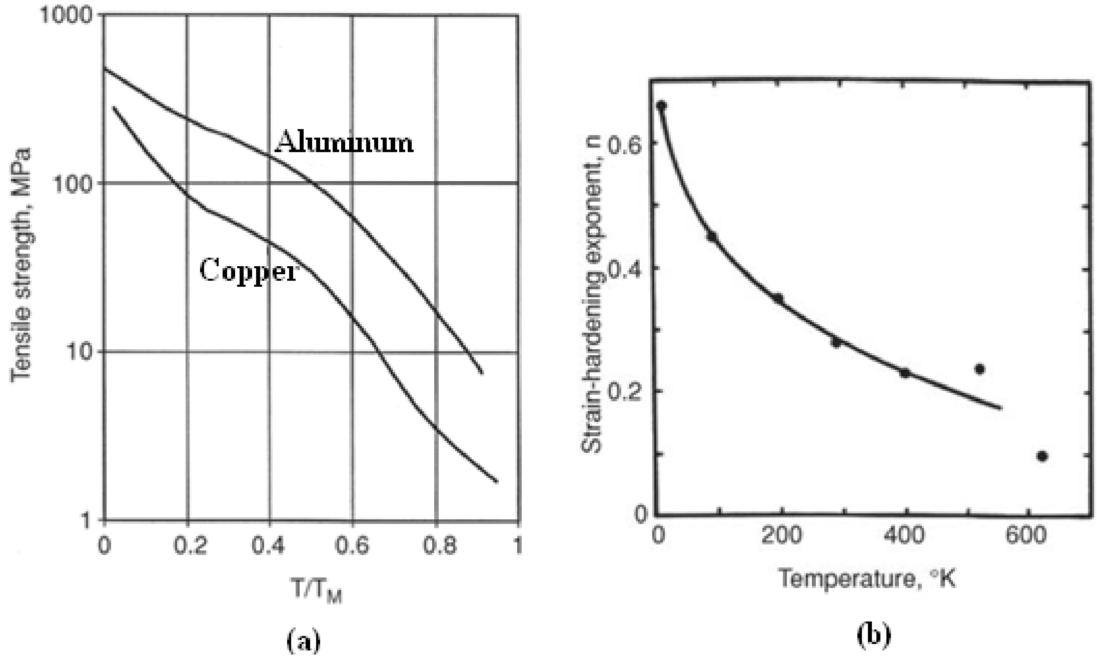

Figure 3.7 (a) Tensile strengths decrease with increasing temperature, (b) Decrease of the strain-hardening exponent of aluminum with increasing temperature **(Carrecker and Hibbard, 1957).**

3.3.1.4 Flow Stress Dependence on Combined Temperature and Strain-Rate

The effect of temperature on the parameters of Eq. 3.8 is pronounced. Increasing temperature decreases the value of C (consistent with its effect on K in the flow curve equation) and increases the value of *m*. The general result can be seen in Figure 3.8. At room temperature, the effect of strain rate is almost negligible, indicates that the flow curve is a good representation of the material behavior **(Groover, 1996).**

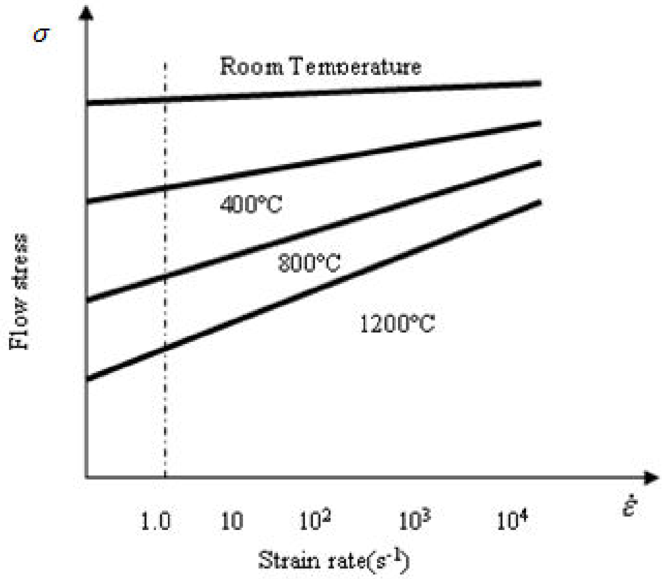

Figure 3.8 Effect of temperature on flow stress for typical metal

The effect of strain rate is important in hot working because deformation resistance of the material increases so dramatically as strain rate is increased. To give a sense of the effect, typical value of m for the three temperature ranges of metal working are given in Table 3.3.

Table 3.3 Strain-rate Sensitivity and Coefficient of Friction in Cold, Warm, and Hot Working

Category	Strain-rate Sensitivity exponent	Coefficient Of friction
Cold working	$0 \leq m \leq 0.05$	0.1
Warm working	$0.05 \leq m \leq 0.1$	0.2
Hot working	$0.05 \leq m \leq 0.4$	0.4-0.5

In cold forming, the effect of strain rate can be neglect for relatively small speeds($\dot{\varepsilon} < 10^4$). However, in hot forming, the effect of strain rate is very important and it must be taken into account. A more complete expression for flow stress as a function of both strain and strain-rate would be following:

$$\sigma = A\varepsilon^n \dot{\varepsilon}^m \tag{3.9}$$

Where, A is a strength coefficient, combining the effects of the previous K and C values. A, n, m would all be functions of temperature, and the enormous task of testing and compiling the value of these parameters for different metals and various temperatures would be forbidding.

3.3.2 Friction and Lubrication

In forging, friction greatly influences metal flow, pressure distribution, and load and energy requirements. In addition to lubrication effects, the effects of die chilling or heat transfer from the hot material to colder dies must be considered. For example, for a given lubricant, friction data obtained from hydraulic press forging cannot be used for mechanical press or hammer forging even if die and billet temperatures are comparable **(Semiatin, 1988).** In forging, the ideal lubricant is expected to:

- Reduce sliding friction between the dies and the forging in order to reduce pressure requirements, to fill the die cavity, and to control metal flow,
- Act as a parting agent and prevent local welding and subsequent damage to the die and workpiece surfaces,
- Possess insulating properties so as to reduce heat losses from the workpiece and to minimize temperature fluctuations on the die surface,
- Cover the die surface uniformly so that local lubricant breakdown and uneven metal flow are prevented,
- Be nonabrasive and noncorrosive so as to prevent erosion of the die surface, be free of residues that would accumulate in deep impressions,
- Develop a balanced gas pressure to assist quick release of the forging from the die cavity; this characteristic is particularly important in hammer forging, in which ejectors are not used,
- Be free of polluting or poisonous components and not produce smoke upon application to the dies.

No single lubricant can fulfill all of the requirements listed above; therefore, a compromise must be made for each specific application. Various types of lubricants are used, and they can be applied by swabbing or spraying. The simplest is high flash point oil swabbed onto the dies. Colloidal graphite suspensions in either oil or water are frequently used. Synthetic lubricants can be employed for light forging operations. The water-base and synthetic lubricants are extensively used primarily because of cleanliness.

Metalworking lubricants are applied to the tool-work interface in many forming operations to reduce the harmful effects of friction. Benefits obtained from the application include reduced sticking, forces, power and tool wear and better surface finish on the product **(Kalpakjian and Schmind, 2006).**

The deformation of the workpiece under frictionless conditions is shown in Figure 3.9a. Because constancy of volume is maintained, any reduction in height increases the diameter forged part. Note in Figure 3.9b that the workpiece is deformed uniformly. In actual operations, there is friction and the part develops a barrel shape shown in Figure 3.9c **(Kalpakjian and Schmind, 2006).**

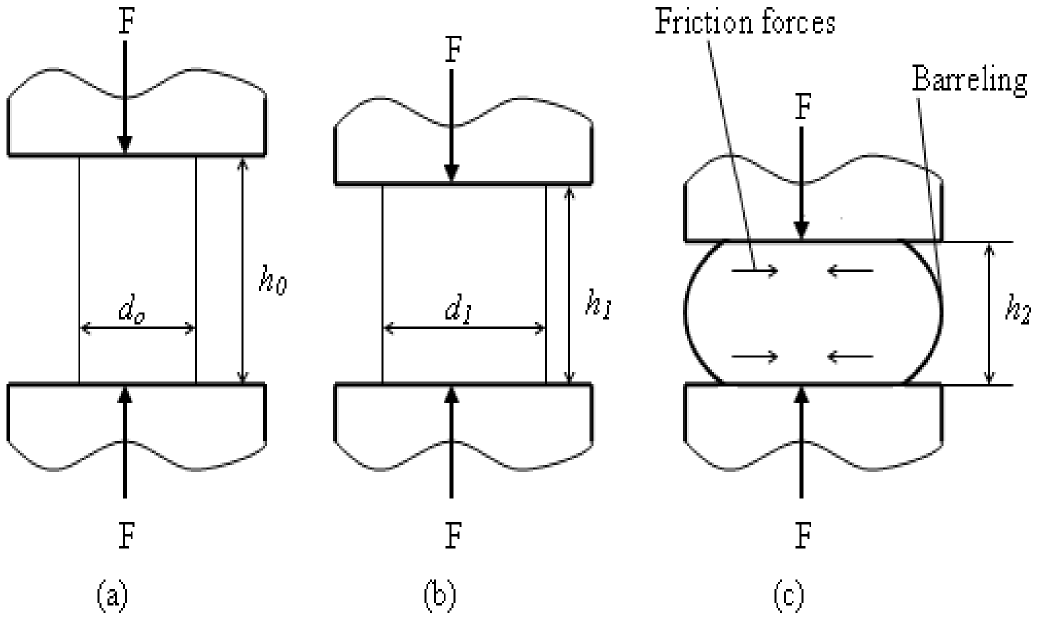

Figure 3.9 (a) Solid cylindrical billet upset between two flat dies. (b) Uniform deformation (c) Deformation with friction

Barreling is caused primarily by friction forces at the die-workpiece interfaces that oppose the outward flow of the materials at these interfaces and, thus can be minimized by using an effective lubricant. Barreling also can develop in upsetting hot workpiece between cold dies. The material at end near the die surfaces cools rapidly, while the rest of the workpiece remains relatively hot. Consequently, the material at the top and bottom of the workpiece has higher resistance to deformation than the material at its center. As a result, the central portion of the workpiece expands laterally to a greater extent than do its ends.

3.4 FORGING PROCESS

Forging is the oldest known metal working process, dating back to the days when prehistoric peoples learned to heat sponge iron and beat it with a stone to form a useful implement **(www.forging.org).** There are various classifications applied for the forging process. In general, forging processes can be classified according to:

- Type of Die Set: Open die, Close die, Net Shape (Precision) Forging
- Temperature: Cold Forging, Warm Forging, Hot Forging
- Type of Machine Used: Hydraulic Presses, Mechanical Presses, Screw Presses and Hammers, etc.

3.4.1 Classification of Forging Process According to Die Type

3.4.1.1 Open Die Forging

Open-die forging differs from impression-die in that the metal workpiece is not confined laterally by impression dies. The process is typically associated with large parts although parts weights can range from a few kilograms to 150 tons. The open-die forging process progressively works the starting stock into the desired shape, most commonly between flat-faced dies. The general shape of open die forgings is illustrated in Figure 3.10. As the stock is not contained in a closed die, a highly skilled forge operator is required in locating and positioning the workpiece on the die. Open die forgings require subsequent machining in almost all cases. Forgings are made by this process when:

- The forging is too large to be produced in closed dies,
- The required mechanical properties of the worked metal that can be developed by open-die forging cannot be obtained by other deformation processes,
- The quantity required is too small to justify the cost of closed dies,
- The delivery date is too close to permit the fabrication of dies for closed-die forging.

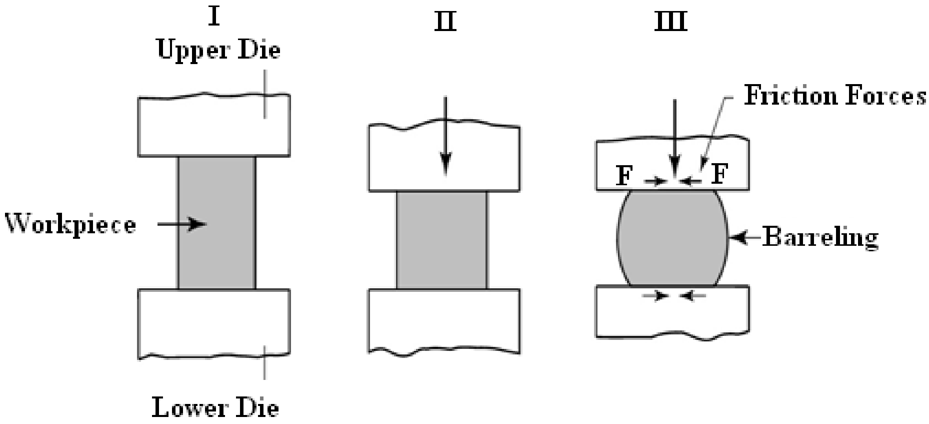

Figure 3.10 Open-die forging

3.4.1.2 Close Die Forging

Impression-die forging, often referred to as closed-die forging, accounts for the bulk of commercial forging production. It shows in Figure 3.11. As the name implies, two or more dies containing impressions of the part shape are brought together causing the workpiece to plastically deform with the metal flow restricted by the die contours. Most impression-die forging is performed at elevated temperatures and is known as hot forging. The optimum hot forging temperature depends on the material being forged. Also in the impression-die forging category are cold forging and warm forging processes.

With the use of closed dies, complex shapes and heavy reduction can be made in hot metal within closer dimensional tolerances. Closed-die forgings are usually designed to require minimal subsequent machining. Closed-die forging is adaptable to low-volume or high-volume production. In addition to producing final, or nearly final, metal shapes, closed-die forging allows control of grain flow direction, and it often improves mechanical properties in the longitudinal direction of the workpiece **(Semiatin, 1988).**

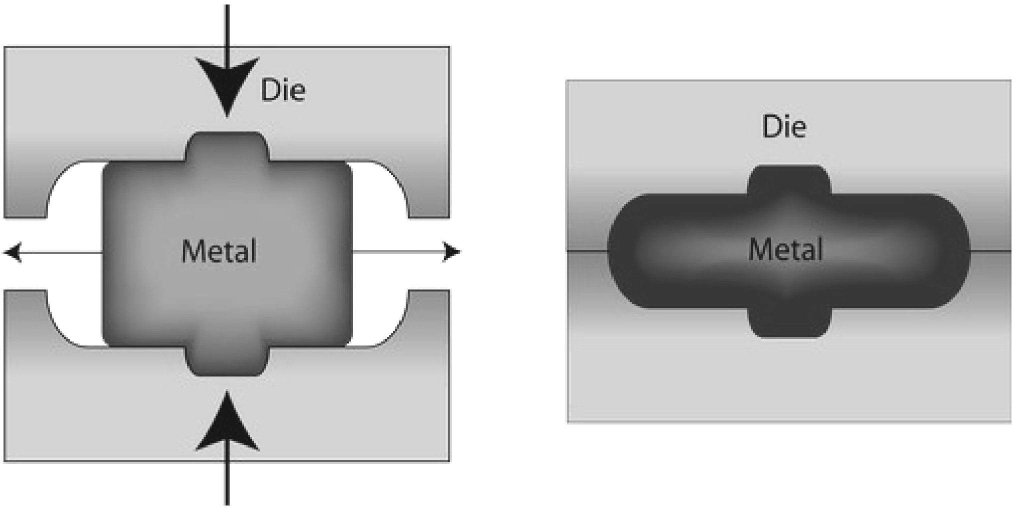

Figure 3.11 Closed-die forging

3.4.1.3 Net Shape (Precision) Forging

The term net indicates that no subsequent machining or finishing of a forged surface is required. Thus, a net shape forging requires no further work on any of the forged surfaces, although secondary operations may be required to produce minor holes, threads, and other such details. A near-net shape forging can be either one in which some but not all of the surfaces are net or one in which the surfaces require only minimal machining or finishing. Precision forging is sometimes described as close-tolerance forging to emphasize the goal of achieving, solely through the forging operation, the dimensional and surface finish tolerances required in the finished part.

Due to difficulties in achieving close tolerance and acceptable surface finish, hot forgings have traditionally been designed with a generous machining allowance, sometimes 3 mm or more. The motivation for precision forging is the elimination, or at least the reduction, of the costs associated with this machining allowance. These costs include not only the labor and indirect costs of the machining and finishing operations but also the cost of the excess raw material that is lost during machining.

The precision of a forging is defined in terms of its conformity to finished-part requirements concerning overall geometry, dimensional tolerance, and surface finish. These requirements should be derived from the performance of the part that is desired in service. The impact of the requirements on manufacturing options should also be included in the design analysis. Specifically, the application of precision forging can be enhanced by considering the capabilities of the technology during the design process **(Doege and Bohnsack, 2000).**

3.4.2 Classification of Forging Process According to Temperature

Metal forging processes use a remarkable property of metals—their ability to flow plastically in the solid state without concurrent deterioration of properties. Metal forging processes are classified according to temperature into three categories: hot forging, cold forging, and warm forging.

3.4.2.1 Hot Forging

Hot forging is the plastic deformation of metal at a temperature and strain rate such that recrystallization occurs simultaneously with deformation, thus avoiding strain hardening. For this to occur, high workpiece temperature (matching the metal's recrystallization temperature) must be attained throughout the process, so energy needed for this preheating. By hot forging, it can be produced a great variety of shapes with virtually any steel. The extensive scale formation occurs on the surface of the workpiece. Larger tolerances and allowances are needed for further machining. A form of hot forging is isothermal forging, where materials and dies are heated to the same temperature. In nearly all cases, isothermal forging is conducted on super alloys in a vacuum or highly controlled atmosphere to prevent oxidation.

Hot forging of steel parts, due to its specific severe thermal and mechanical loading, is still today one of the mass metal forming processes over 2.000.000 tons of steel parts are produced per year by hot forging in Europe alone. The tribological system in hot forging of small and medium sized steel parts includes a preheated substrate with a temperature greater than 1000 C, a graphite lubricant and plastic deformation of the hot substrate between the top or moving die, and the bottom, or stationary die. This is fixed to the die seat of the main frame in an eccentric press with a short stroke and large mechanical loads from 500 to several thousand tons. In such a system, hot work tooling has to survive the most aggressive wear situations, which finally leads to heavy damage of the tool surface due to erosion, plastic deformation, thermal and mechanical fatigue **(Navinsek et al, 2001).**

3.4.2.2 Cold Forging

The temperature of metals being cold forged may range from room temperature to several hundred degrees. The primary advantage is the material savings achieved through precision shapes that require little finishing. While cold forging usually improves mechanical properties, the improvement is not useful in many common applications and economic advantages remain the primary interest. Tool design and manufacture are critical **(Abachi, 2004).**

Cold forging steel is widely used to fabricate fasteners, such as bolt, nuts, studs, steering links, tie rods, etc. The conventional technology to manufacture high strength fasteners is through cold forming annealed steel rod into the desired geometry, followed by a quench and temper heat treatment process to achieve the targeted mechanical properties. In this case, annealing and the final heat treatment are critical to obtain the sufficient plasticity and high strength. However, annealing and the subsequent quenching and tempering not only easily cause various heat treatment defects, but also waste time for the parts to travel back and forth from process to process. Therefore, it is desirable for cold forging steel, which is used to fabricate high-strength bolts, to eliminate rod annealing and the final heat treatment (**Astakhov and Shvets, 2001), (Li and Wu, 2007).**

Cold working is the plastic deformation of metals below the recrystallization temperature. When compared to hot working, cold-working processes have certain distinct advantages:

- No heating required,
- Better surface finish obtained,

- Superior dimension control,
- Better reproducibility and interchangeability of parts,
- Improved strength properties,
- Directional properties can be imparted,
- Contamination problems minimized.

Some disadvantages associated with cold-working processes include:

- Higher forces required for deformation,
- Heavier and more powerful equipment required,
- Metal surfaces must be clean and scale-free,
- Strain hardening occurs (may require intermediate anneals),
- Imparted directional properties may be detrimental,
- May produce undesirable residual stresses.

3.4.2.3 Warm Forging

Warm forging combines the advantages of both cold and hot forging; surface quality, precision and material utilization from cold forging and, process able range of materials and shapes from hot forging side. However, the implementation of warm forging is limited by high investment costs for the rearrangement of machines and expenses for tools and development. Temperature range is usually between 600ºC and 900ºC. Ferrite brittleness and scaling factor is limiting for this working temperature range

Warm forging is known in early 70s. The growth in the automotive industry brought the cold forging application in serial mass production of a wide range of component types. This caused that some cold forging techniques have been developed to be able to get near-net and net-shape components in large batch quantities. However; the limitations in economic production of parts with complex geometry, large size and in certain alloys caused the developments and commercial usage of warm forging process.

It has some advantages compared to both hot forging and cold forging. Warm forging offers better utilization of material, improve a surface finish, and dimensional accuracy when compared with hot forging and reduced press loads when compared with cold forgings. Independent of the fact that the temperature interval of warm forging is close to hot die forging temperatures, this forming process, with regard to the used design concepts for the tool and the achievable quality of the manufactures components, is often considered an expansion of cold forging to such workpiece materials that cannot be forged at room temperature or only with difficulty **(Sheljaskov, 1994).** A comparison of the typical characteristics of hot, warm and cold forging processes is given in Table 3.4.

Table 3.4 Typical characteristics of hot, warm and cold forging processes **(Sheljaskov, 1994)**

Characteristics	**Comparison of Process**		
	Hot	**Warm**	**Cold**
Weight of the Workpiece	<60 kg	<10 kg	<2 kg
Steel Grade	Any	C desirable Other alloying elements < 10 %	Low alloyed steels (C<0.45%, other <3%)
Shape	Any without undercut	Rotationally-symmetrical without undercut	Rotationally-symmetrical without undercut
Surface Quality	Low	Medium	High
Deformation Pressure	Low	Medium	High
Energy Costs	High	Medium	Low
Tolerances	Generous	Close	Closest
Tooling Costs	Lowest	High	High

3.4.3 Classification of Forging Machines

Forging Machine can be classified according to their principle of operation. Hammers and high-energy-rate forging machines deform the workpiece by the kinetic energy of the hammer ram; they are therefore classed as energy restricted machines. The ability of mechanical presses to deform the work material is determined by the length of the press stroke and the available force at various stroke positions. Mechanical presses are therefore classified as stroke restricted machines. Hydraulic presses are termed force-restricted machines because their ability to deform the material depends on the maximum force rating of the press. Although they are similar in construction to mechanical and hydraulic presses, screw-type presses are classified as energy-restricted machines **(Semiatin, 1988).**

Press forging is similar to kneading, where a slow continuous pressure is applied to the area to be forged. The pressure will extend deep into the material and can be completed either cold or hot. Press forging is more economical than hammer forging (except when dealing with low production numbers), and closer tolerances can be obtained. A greater proportion of the work done is transmitted to the workpiece, differing from that of the hammer forging operation, where much of the work is absorbed by the machine and foundation. This method can also be used to produce larger forgings, as there is no limitation in the size of the machine**.** These are; Mechanical presses, Friction Screw Presses, Hydraulic Presses.

Hammers are energy-restricted machines since the deformation results from dissipating the kinetic energy of the ram. Hammer forging is a preferred method for individual forgings. It is the shaping of a metal or other material, by an instantaneous application of pressure to a relatively small area. A hammer or ram, delivering intermittent blows to the section to be forged, applies this pressure. These are; Board Drop Hammers, Air-Lift Gravity Drop Hammers, Power Drop Hammers, Counterblow hammers, High Energy Rate Machines.

Forging machines can be classified into three types:

- Force-restricted machines (hydraulic presses),
- Stroke-restricted machines (mechanical presses),
- Energy-restricted machines (screw presses and hammers).

3.4.3.1 Force Restricted (Hydraulic Presses) Machines

Hydraulic presses operate on the physical principle that a hydrostatic pressure is distributed evenly through a system of pipes and that a pressure p (N/m2), acting on a surface A (m^2), produces a force F (N):

$$F=p*A \tag{3.10}$$

The force acting on the slide of the press depends on the forming or blanking process performed. For this reason, the pressure p acting on the piston surface is also a function of the deformation process conducted. Its measurement may be used directly to calculate the force acting on the slide. The maximum slide force can be selected by limiting the maximum hydraulic pressure through a relief valve at any position of the slide.

The drive power P (W) of a hydraulic press depends on the volumetric flow rate of hydraulic fluid V (m^3/s) and therefore on the speed of the slide as well as on the hydraulic pressure p, the forces at the slide, and the mechanical and electrical losses η:

$$P = \frac{\dot{V} * p}{\eta} \tag{3.11}$$

In contrast to mechanical presses, there is generally no reserve of energy available in hydraulic presses. Thus, the entire power must be applied when carrying out the forming operation. For this reason, hydraulic presses require a significantly higher drive power than in mechanical presses, with comparable force capacity **(Altan, 1998).** Hydraulic presses are load-restricted machines in which hydraulic pressure moves a piston in a cylinder Figure 3.12. A chief feature is that the full press load is available at any point during the full stroke of the ram. This feature makes the hydraulic press ideally suited for extrusion-type forging operation. The ram velocity can be controlled and even varied during the stroke. The hydraulic press is a relatively slow speed machine. This results in longer contact time, which may lead to problems with heat loss from the workpiece and die deterioration. On the other hand, the slow squeezing action of a hydraulic press results in close-tolerance forgings. The initial cost of a hydraulic press is higher than that of a mechanical press of equal capacity **(Dieter, 1976).**

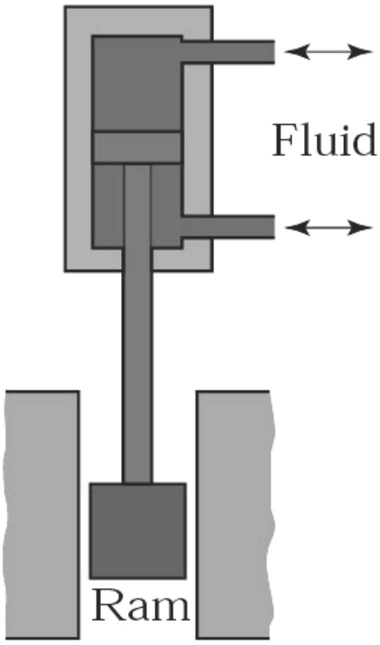

Figure 3.12 Schematic Drawing of Hydraulic Press **(Dieter, 1976)**

The principal advantages of hydraulic presses include:

- Pressure can be changed as desired at any point in the stroke by adjusting the pressure control valve,
- Deformation rate can be controlled or varied during the stroke if required. This is especially important when forging metals that are susceptible to rupture at high deformation rates,
- Split dies can be used to make parts with such features as offset flanges, projections, and back draft, which would be difficult or impossible to incorporate into hammer forgings,
- When excessive heat transfer from the hot workpiece to the dies is not a problem or can be eliminated, the gentle squeezing action of a hydraulic press results in lower maintenance costs and increased die life because of less shock as compared to other types of forging equipment,
- Maximum press force can be limited to protect tooling.

Some of the disadvantages of hydraulic presses are:

- The initial cost of a hydraulic press is higher than that of an equivalent mechanical press,
- The action of a hydraulic press is slower than that of a mechanical press,
- The slower action of a hydraulic press increases contact time between the dies and the workpiece. When forging materials at high temperatures (such as nickel-base alloys and titanium alloys), these results in shortened die life because of heat transfers from the hot work metal to the dies.

3.4.3.2 Stroke Restricted (Mechanical Presses) Machines

All mechanical presses employ flywheel energy, which is transferred to the workpiece by a network of gears, cracks, eccentrics, or levers. Driven by an electric motor and controlled by means of an air clutch, mechanical presses have a full eccentric type of drive shaft that imparts a constant-length stroke to a vertically operating ram. Various mechanisms are used to translate the rotary motion of the eccentric shaft into linear motion to move the ram shown in Figure 3.13. The ram carries the top, or moving, die, while the bottom, or stationary, die is clamped to the die seat of the main frame. The ram stroke is shorter than that of a forging hammer or a hydraulic press. Ram speed is greatest at the center of the stroke, but force is greatest at the bottom of the stroke. The capacities of these forging presses are rated on the maximum force they can apply and range from about 2.7 to 142 MN (300 to 16,000 tonf). **(Semiatin, 1988).**

Figure 3.14 also shows schematic drawing of mechanical press. Ram speed is greatest at the center of the stroke, but force is greatest at the bottom of the stroke. Because of the short stroke, mechanical presses are best suited for low-profile forgings **(Dieter,1976).**

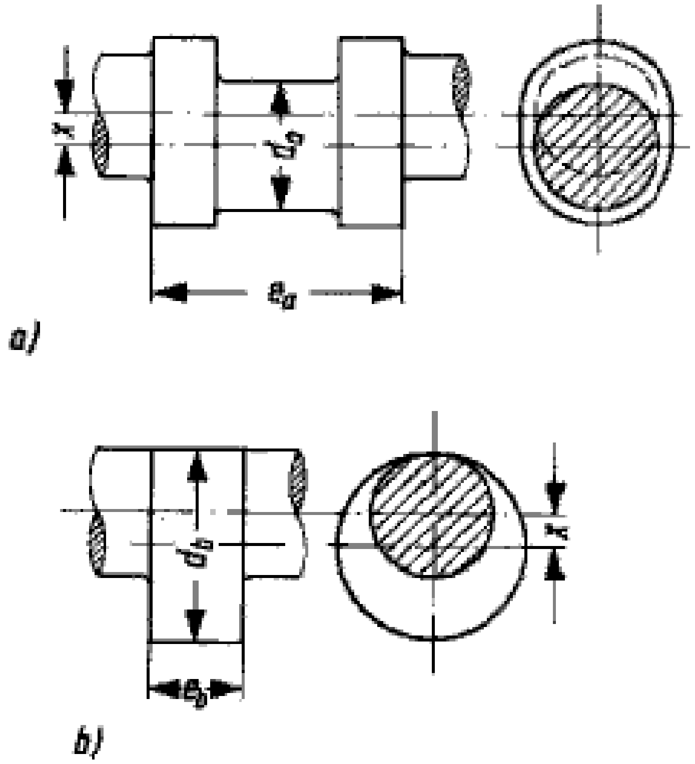
x
d_a
e_a
a)
x
d_b
e_b
b)

Figure 3.13 Drive shafts a) crankshaft, b) eccentric shaft **(Makelt, 1961)**

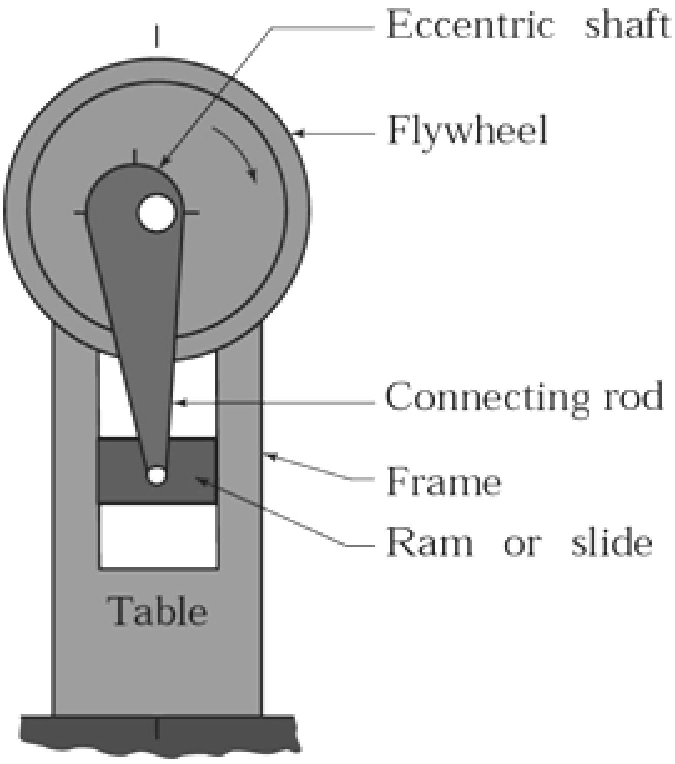
Eccentric shaft
Flywheel
Connecting rod
Frame
Ram or slide
Table

Figure 3.14 Schematic Drawing of Mechanical Press

Figure 3.15 also shows Crank press drive layout. When the work capacity is provided, and assuming that the tangential force T on the drive is always available, it can be said, on condition that r/l is very small, that:

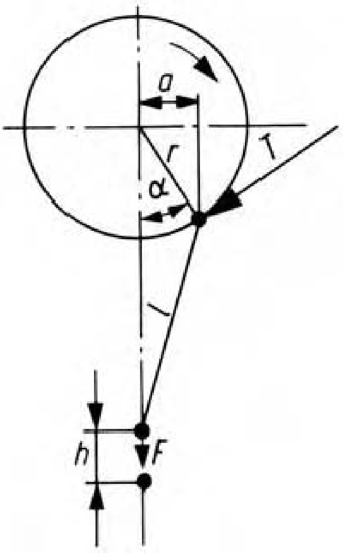

Figure 3.15 Crank press drive layout (**Makelt, 1961)**

$$\frac{T}{F} = Sin\alpha \qquad (3.12)$$

T in kN tangential force, F in kN press force, α in deg. crank angle, r in m crank radius, l in m length of the connecting rod.

$$M = F \cdot a = F \cdot r \cdot \sin \alpha \qquad (3.13)$$

For a normal crank press, a value of 0.5 is fixed for the T/F ratio. This is equal to a crank angle of 30°. Thus:

$$F_n = \frac{T}{Sin30} \qquad (3.14)$$

F in kN nominal press force. In other words, the nominal press force is available from a crank angle of 30° before BDC. The press force is smaller when $\alpha > 30°$. It reaches a minimum at $\alpha = 90°$ ($\sin 90° = 1$). The maximum is at the BDC at $\alpha = 0°$ ($\sin 0° = 0$), i.e. at the BDC the force approaches infinity. The permissible press frame load (press frame strength) is set to the nominal press force. For this reason the nominal press force must not be exceeded **(Tschaetsch, 2006).**

3.4.3.3 Energy Restricted Machines

3.4.3.3.1 Screw Presses

In a screw press, the ram is connected by a rotary joint to a spindle, which is in effect a large screw. The rotary motion of a flywheel is transformed into linear motion by the multiple threads on the spindle and its nut **(Dieter, 1976).** Figure 3.16 also shows schematic drawing of screw press. Friction screw presses are rated by spindle diameter rather than by the maximum force they can exert. Smaller machines operate at 30 to 35 strokes per minute; larger ones, at 6 to 10 strokes per minute **(Semiatin, 1988).**

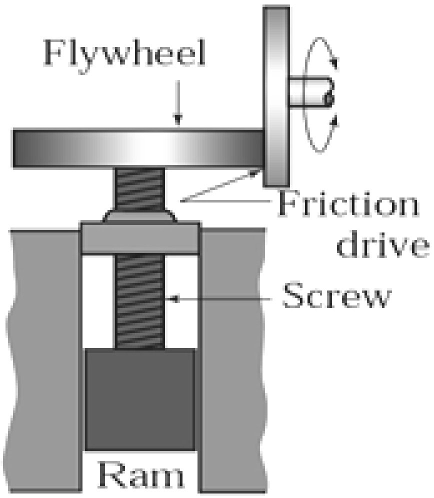

Figure 3.16 Schematic Drawing of Screw Press

Advantages of screw presses (compared to hammers and crank presses)

- Screw presses require only a small base,
- The noise level is far lower than with hammers,
- Screw presses are high-energy machines. For this reason, workpiece which require a lot of energy can be formed with them,
- The dwell periods (the time during which the workpiece is being forged) are short. This means that tool life is improved,

- The spindle thread is not self-locking. This means that a screw press can not block under stress,
- Screw presses convert their energy abruptly, similarly to hammers. Because of the lower ram impact velocity (υ = 0.7 – 1.0 m/s) the deformation resistance during hot forming is lower than with hammers (υ = 5 – 14 m/s),
- Like hammers, screw presses have no kinetically-fixed bottom dead centre. It is no longer necessary to adjust the height of the tooling. Forging can also take place in a closed die, as the excess material can be balanced out in the height of the workpiece.

3.4.3.3.2 Hammers

The hammer is the least expensive and most versatile type of equipment for generating load and energy to carry out a forming process. Hammers are primarily used for the hot forging, coining, and, to a limited extent, sheet metal forming of parts manufactured in small quantities--for example, in the aircraft industry. The hammer is an energy-restricted machine. During a working stroke, the deformation proceeds until the total kinetic energy is dissipated by plastic deformation of the material and by elastic deformation of the ram and anvil when the die faces contact each other. Therefore, the capacities of these machines should be rated in terms of energy. The practice of specifying a hammer by its ram weight, although fairly common, is not useful for the user. Ram weight can be regarded only as model or specification number.

There are basically two types of anvil hammers: gravity-drop and power-drop. In a simple gravity-drop hammer, the upper ram is positively connected to a board (board-drop hammer), a belt (belt-drop hammer), a chain (chain-drop hammer), or a piston (oil-, air-, or steam-lift drop hammer). The ram is lifted to a certain height and then dropped on the stock placed on the anvil. During the down stroke, the ram is accelerated by gravity and builds up the blow energy. The upstroke takes place immediately after the blow; the force necessary to ensure quick lift-up of the ram can be three to five times the ram weight **(Semiatin, 1988)**.

The operation principle of a power-drop hammer is similar to that of an air-drop hammer. In the down stroke, in addition to gravity, the ram is accelerated by steam, cold air, or hot air pressure. Electro-hydraulic gravity-drop hammers, introduced in the United States in recent years, are more commonly used in Europe. In this hammer, the ram is lifted with oil pressure against an air cushion. The compressed air slows the upstroke of the ram and contributes to its acceleration during the down stroke. Therefore, the electro-hydraulic hammer also has a minor power hammer action.

In hammers and presses for forging, the upper ram is accelerated downward by steam, but it can also be accelerated by cold or hot air. At the same time, the lower ram is accelerated by a steel band (for smaller capacities) or by a hydraulic coupling system (for larger capacities). The lower ram, including the die assembly, is approximately 10% heavier than the upper ram. Therefore, after the blow, the lower ram accelerates downward and pulls the upper ram back up to its starting position. The combined speed of the rams is about 7.6 m/s; both rams move with exactly one half the total closure speed. Due to the counterblow effect, relatively little energy is lost through vibration in the foundation and environment. Therefore, for comparable capacities, a counterblow hammer requires a smaller foundation than an anvil hammer.

3.4.3.3.2.1 Gravity Drop Hammers

Gravity-drop hammers consist of an anvil or base, supporting columns that contain the ram guides, and a device that returns the ram to its starting position. The energy that deforms the workpiece is derived from the downward drop of the ram; the height of the fall and the weight of the ram determine the force of the blow.

3.4.3.3.2.2 Board Drop Hammers

Board drop hammers are widely used, especially for producing forgings weighing no more than a few pounds. In board drop hammer, the ram is lifted by one or more boards keyed to it and passing between two friction rolls at the top of the hammer. Figure 3.17 also shows schematic drawing of board drop hammers. The boards are rolled upward and are than mechanically released, permitting the ram to drop from the desired height. Power for lifting the ram is supplied by one or more motors.

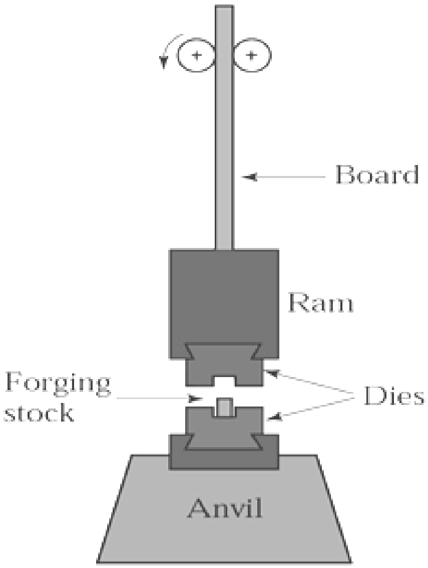

Figure 3.17 Schematic Drawing of Board Drop Hammers **(Semiatin, 1988)**

3.4.3.3.2.3 Air-lift Gravity Drop Hammers

The air-lift gravity drop hammer is similar to the board hammer in that the forging force is derived from the weight of the falling ram assembly and upper die. It differs in that the ram is raised by air or steam power. Stroke control dogs, presed on a rocker and actuated by the ram, control power to the ram cylinder. With the hammer shut down, the dogs can be reset on the rocker to adjust stroke length. A device that allows both a long stroke and a short stroke, in variable sequence, is available **(Semiatin, 1988).**

3.4.3.3.2.4 Electro-hydraulic Gravity-Drop Hammers.

In recent years, two significant innovations have been introduced in hammer design. The first is the electro-hydraulic gravity-drop hammer. In this type of hammer, the ram is lifted with oil pressure against an air cushion. The compressed air slows the upstroke of the ram and contributes to its acceleration during the down stroke blow. Therefore, the electro-hydraulic drop hammer also has a minor power hammer action. The second innovation in hammer design is the use of electronic blow-energy control. Such control allows the user to program the drop height of the ram for each individual blow. As a result, the operator can set automatically the number of blows desired in forging in each die cavity and the intensity of each individual blow. The electronic blow control increases the efficiency of the hammer operations and decreases the noise and vibration associated with unnecessarily strong hammer blows.

3.4.3.3.2.5 Power Drop Hammers

The term "power drop hammer" has come into use because "steam hammer" is no longer adequately descriptive. Many hammers of this general type are actuated by air rather than by steam. Components of a steam or air actuated power drop hammer are shown in Figure 3.18. Power drop hammers differ in principle from air lift gravity hammers in that steam under pressure of 90 to 125 psi supplements the force of gravity in the downwards stroke**(Semiatin, 1988).**

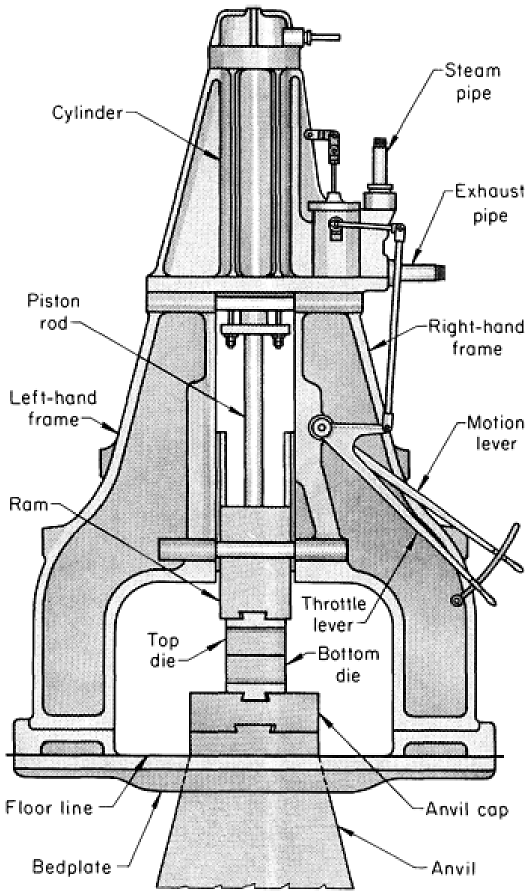
Steam pipe
Cylinder
Exhaust pipe
Piston rod
Right-hand frame
Left-hand frame
Motion lever
Ram
Throttle lever
Top die
Bottom die
Floor line
Anvil cap
Bedplate
Anvil

Figure 3.18 Schematic Power Drop Hammers

3.4.3.3.2.6 Counter Blow Hammer

The counterblow hammers, a variation of the power drop hammer. These hammers develop striking force by the movement of two rams, simultaneously approaching from opposite directions and meeting at a midway point. Components of a counter-blow hammer are shown in Figure 3.19. Some hammers are pneumatically or hydraulically actuated; others incorporate a mechanical-hydraulic or a mechanical-pneumatic system **(Semiatin, 1988).**

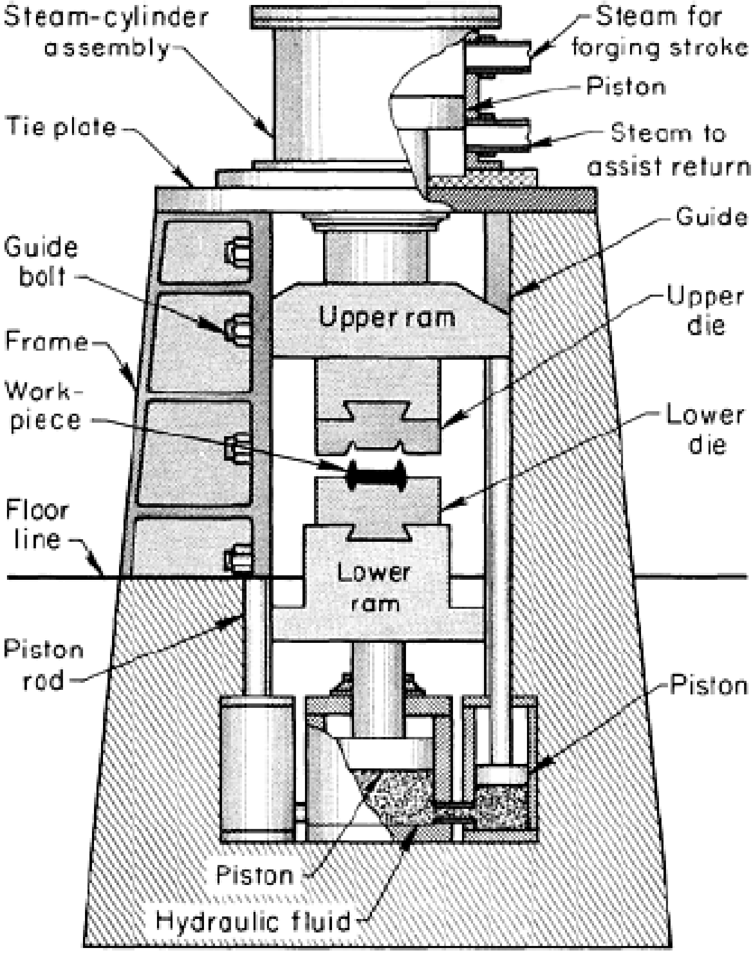
Steam-cylinder assembly
Tie plate
Guide bolt
Frame
Work-piece
Floor line
Piston rod
Steam for forging stroke
Piston
Steam to assist return
Guide
Upper ram
Upper die
Lower die
Lower ram
Piston
Piston
Hydraulic fluid

Figure 3.19 Schematic view of Vertical Counter-Blow Hammer

3.4.3.3.3 High Energy Rate Forming Hammers

High energy-rate forging is a hot or cold, closed-die forging process in which the stored energy of high-pressure gas is used to accelerate a ram to high velocities to deform the workpiece. Table 3.5 lists typical values of velocity for different forging equipment. The specific part, material, and design requirements determine the forging temperature. Refractory metals, low-carbon steels, and nickel alloys that have broad forging temperatures can be forged by HERF. Unsuitable metals include magnesium and beryllium alloy; high carbon steels; high-strength aluminum alloys; and nickel-based, heat resistant alloys. More information about these machines can be found in several publications **(Altan et al, 1973).**

Table 3.5 Typical Values of Velocity for Different Forging Equipment **(Semiatin,1988).**

Forging Machine	Velocity (m/s)	Forging Machine	Velocity (m/s)
Gravity drop hammer	3. 6-4.8	Mechanical press	0.06-1.5
Power drop hammer	3.0-9.0	Hydraulic press	0.06-0.30
HERF hammers	6.0-24.0		

3.4.4 Determination of Load and Energy

The forging force, F, in an open-die forging operation on a solid cylindrical workpiece can be estimated from the formula

$$V = A_{\circ}h_{\circ} = Ah = Const. \Rightarrow A = \frac{V}{h} \Rightarrow F = \frac{\sigma * V}{h} \qquad (3.15)$$

The work done: $W = \int_{h_f}^{h_{\circ}} F * dh = \sigma * V * \ln \frac{h_{\circ}}{h_f}$ (3.16)

If there is a friction $F = \sigma * \pi * r^2 \left(1 + \frac{2 * \mu * r}{3 * h}\right)$ (3.17)

where *V* is volume of workpiece, *A* is area end of workpiece, σ is the flow stress of the material. μ is the coefficient of friction between the workpiece and the die and *r* and *h* are radius and height of the workpiece, respectively.

3.5 HIGH ENERGY RATE FORMING (HERF) HAMMER

Conventional forging (shaping) presses are usually large in size but they have a low production and a high cost rate. For production whereby these types of presses are used this causes workpiece to be moved to different sections and thus get out of the production band. Getting out of the production band, which leads to time and energy losses, increases the cost per unit. Therefore, there is a need for **High Energy Rate Forming HERF** hammer. High-energy-rate forming equipment is based upon three methods of releasing energy:

- Chemical (high explosives, propellants, gas mixtures),
- Electrical (exploding wires, spark discharges, magnetic fields),
- Mechanical (pneumatic-mechanical presses).

The High Energy Rate Forming (HERF) processes, sometimes called High Velocity Forming (HVF) processes, develop high rates of energy transfer to the workpiece by an increase in magnitude of the velocity component of the forming operation itself. The exploitation of this high-energy-transfer concept has led to the development of new types of metalworking equipment and techniques, the most notable of which are the explosive, electro-hydraulic, magnetic, and compressed-gas forming systems. Typically, the ram velocity at impact in the HERF hammer is in the range of 6 to 24 m/s, ram velocities range from 4.5 to 9.1 m/s for a power-drop hammer and from 3.6 to 5.5 m/s for a gravity-drop hammer **(Semiatin, 1988).**

High energy-rate forming is applied to sheet metal in draw –forming, bulging, sizing, punching, swaging, flanging, heading, powder compaction, cutting, welding, and surface hardening. The materials that are fabricated by HERF include magnesium, aluminum, beryllium, titanium, zirconium, carbon and alloy steels, stainless steels, super alloys, the refractory metals, and composites.

High-energy-rate machines can be used to hot forge parts of the same general shapes as those produced with conventional hammers and presses. However, the work metal must be capable of undergoing extremely rapid deformation rates as it fills the die cavity without rupturing it. In high-energy-rate forging, the high ram velocities permit the forging of parts with thin webs, high rib height-to-width ratios, and small draft angles to profiles sufficiently accurate that machining allowance can sometimes be as little as 0.500mm. Even parts made of difficult-to-forge metals can be formed close to finished dimensions in a few blows and often without reheating

When evaluating high-energy-rate forging in relation to conventional forging, both the machine and process advantages, as a result of the high velocities, must be considered. The machine advantages are beyond dispute. For a given forming capacity, high-speed machines are much smaller than conventional forging machines, and they require much less installation/foundation and therefore a lower capital investment. These advantages arise because the principle utilized in these machines involves the conversion of the kinetic energy of a ram/platen into forming work. Kinetic energy is proportional to the square of the impact velocity; therefore, a threefold increase in impact speed produces a nine fold increase in forming energy. High-energy-rate forging machines are typically one-ninth the bulk and weight of equivalent slow-speed machines. Although the finished forging is generally made in one high-speed blow, some machines can be fired two or three times before the work metal has cooled below the forging temperature **(Wick, 1960).**

The process advantages are not as obvious as the machine advantages and depend on the particular application under consideration. In general, high-energy-rate forging offers the following advantages over conventional forging methods **(Semiatin, 1988)**:

- Complex parts can be forged in one blow from a billet or a preform,
- Many metals that have low forgeability or are difficult to forge by other methods can be successfully forged,
- Dimensional accuracy, surface detail, surface finish are improved,
- Draft allowances, both internal and external, can be reduced or, in some applications, eliminated,
- Forgings are made to size or with a minimum of machining allowance. Reduced machining lowers the induced mechanical stress and minimizes the cutting of end grain, which improves the stress-corrosion resistance of some metals, notably aluminum,

- Deep, thin sections can be forged because the rapidity of the blow provides little time for heat transfer to the die walls,
- Substantial improvement in billet quality can be achieved when cropping/shearing at high speeds,
- Severe deformation is possible, with the net result of greater grain refinement in some metals,
- Less skill is required for the operating personnel

The process, however, does have the following limitations:

- Sharp corners and small radii cannot be forged without causing undue wear,
- The process is generally limited to symmetrical parts, although some asymmetrical parts can be forged from preformed billets,
- The production rate is about the same as in hammer or hydraulic press forging, but is slower than in mechanical press forging,
- Part size is limited to about 11 to 12kg for carbon steel forgings, and to lesser weights for forgings made of stainless steel or heat-resistant alloys,
- Dies must be carefully designed and fabricated in order to withstand the high impact; compressive pre-stressing of the die inserts by a shrink ring is a common practice.

3.5.1 Classification of HERF Hammers

The characteristic feature of HERF hammers is that energy stored in some convenient form is released / discharged at a high rate and converted into forming work **(Davies and Austin, 1970).** After completion of the working stroke the power unit is re-cocked, i.e. recharged, for another cycle to commence. On the basis of this general principle of operation, the four stages of working cycle of HERF hammers are as follows:

a. The power (drive) unit in which the energy used in the forming process is either stored or generated just before the commencement of the forming stroke.

b. The release mechanism which when activated permits the ram / platen / tool assembly to commence the power stroke, in course of which the potential energy stored in the power unit is converted into kinetic energy.

c. The re-cocking mechanism for returning the ram into its original position after it is kinetic energy has been converted into forming work.

d. The machine suspension / support determining the foundation requirements, which are dependent on the overall configuration of the device.

It is convenient to divide HERF hammers into families on the basis of energy source, used for actuation and re-cocking mechanism. According to aforementioned criteria, HERF hammers can be classified as follows **(Kalpakjian and Schmind, 2006).**

3.5.1.1 Pneumatic-Hydraulic HERF Hammer

These machines are actuated by compressed air and re-cocking with hydraulic ram. It was actuated by compressed nitrogen, substituted later by compressed air for reasons of running costs. The energy contained in the compressed gas is released by a pneumatic mechanism which is an integral part of the power unit. This power unit is re-cocked by a pair of hydraulic jacks. The overall configuration of the machine falls into the category of single-acting counterblow devices.

The complete working cycle of a machine is presented in Figure 3.20, it is controlled sequentially, and there being no overlap between successive stages of the firing cycle. In principle, the firing cycle can be started with the re-cocking jacks already withdrawn to their bottom position; for safety reasons they are generally lowered as the first step. This increases the cycle time and it also has other disadvantages in hot forging. Figure 3.20 is operational cycle of these types of machines. In Figure 3.20 a, machine is at safe position and hydraulic jacks are up. In Figure 3.20 b, the machine is ready for firing and the hydraulic jacks are down. In Figure 3.20 c, the machine is triggered by injecting gas into vent space. In Figure 3.20 d, forming operation is completed and lastly in Figure 3.20 e, the machine is re-cocked with hydraulic jacks.

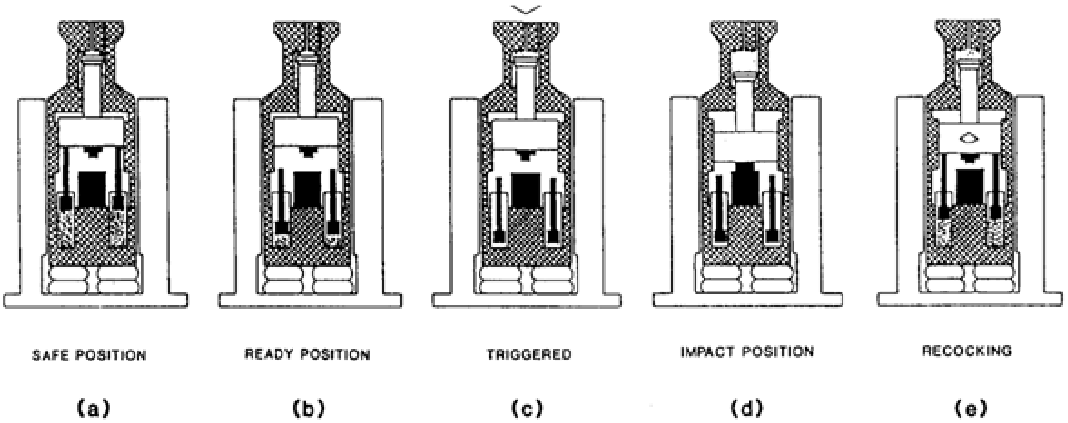

Figure 3.20 Pneumatic-Hydraulic HERF hammers working principles **(Tobias, 1985)**

3.5.1.2 Pneumatic-Mechanic HERF Hammer

These are similar to pneumatic-hydraulic HERF hammers. A variant of one of these designs uses a crank mechanism for re-cocking.

3.5.1.3 Hydraulic-Hydraulic HERF Hammer

These are the machines which the hammer is actuated hydraulically and is also re-cocked by such means.

3.5.1.4 Combustion-Pneumatic HERF Hammer

These are the machines which the hammer is actuated by combustion and are also re-cocked by back pressure. In the literature, there are three different types of combustion actuated high speed HERF hammers. These are **(Davies and Austin, 1970):**

- Petro-Forge,
- Repco High Energy Head,
- Russian Hammers.

In the concept of the thesis, a proto-type of Petro-Forge HERF hammer was designed, constructed and different kind of materials are formed by using it.

3.5.1.4.1 Petro-Forge

Petro-Forge is essentially a hybrid of a hammer and an internal combustion engine which has the following principal features **(Poullikkas, 2006).**

- Its power unit is actuated by high pressure gas generated by the combustion of a mixture of hydrocarbon fuel, generally propane or natural gas, and air,
- The piston/ram assembly is released by a pneumatic device, automatically, just before the combustion pressure reaches its peak value,
- Re-cocking, that is, the return of the piston/ram assembly is usually affected automatically as soon as the working stroke is completed, by air cushion acting on the underside of the piston (back-pressure); generally, the release and the re-cocking mechanisms are integrated with the power cylinder.

In its normal mode of operation, Petro-Forge is appropriately described as a "combustion actuated pneumatic" device. The principle of operation of the power unit with the integrated release and re-cocking mechanisms is explained with the aid of Figure 3.21 a. The unit consists of **(Davies and Austin, 1970)**, **(Poullikkas, 2006):**

- A combustion chamber,
- An expansion chamber/drive cylinder,
- Connected by a constriction known as seal.

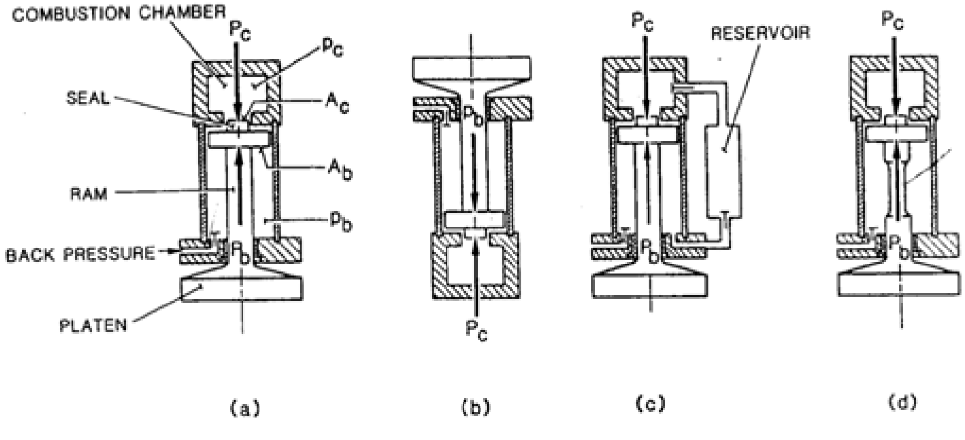

Figure 3.21 Petro-Forge HERF hammers working principles **(Chan et al, 1966)**

This seal is closed by a cylindrical p1ug projecting from the top of the piston. At the beginning of the cycle the piston/ram assembly is lifted into its top position by the back-pressure acting on the annular underside of the piston. If the back-pressure is P_b then it generates an upwards force, acting on the piston of magnitude

$$P_b = p_b * A_b \tag{3.17}$$

where A_b is the area of the annular under the face of the piston. The combustion chamber can now be filled up with a combustible fuel/air mixture to a charge pressure p_c which causes a force Pc to art on the seal/piston in the downwards direction, where A_c, is the seal area. A long as $P_b > P_c$ the piston will not move.

$$P_c = p_c * A_c \tag{3.18}$$

Some of the fuel mixture or air respectively, may leak from the combustion chamber through the seal or from the back-pressure chamber across the piston into the space on top of the piston. To prevent a pressure built-up there, which would result in premature firing, the so called vent space is connected to the atmosphere **(Davies and Austin, 1970)**, **(Poullikkas, 2006).**

Upon ignition of the fuel mixture the pressure in the combustion chamber increases n fold, where n depends on the fuel and the efficiency of the combustion process; for propane $7<n<8$ somewhat before the combustion pressure reaches its maximum level. The downwards force acting on the piston P_c overcomes the upwards force due to the back-pressure P_b the piston starts to move and the seal is opened. With this the combustion products stream into the expansion chamber to act over the whole area of the piston causing a force surge which accelerates the piston/ram assembly downwards to impinge on the workpiece and the lower die.

During the downwards stoke of the piston the back-pressure P_b is intensified and as soon as the forming operation is completed this intensified back-pressure lifts the piston/ram assembly off the workpiece and returns it to its original position, the return stroke being facilitated by the exhaust of the combustion products.

The return stroke of the piston/ram assembly is not necessarily affected by a back pressure. By inverting the power unit and making it upwards stroking, as shown in Figure 3.21 b that function can be achieved by gravity if necessary augmented by a back-pressure. Furthermore, a substantial part of the energy, lost by intensifying the back-pressure can be regained by bleeding some of it off through a non-return valve and storing it in a reservoir for use as charge pressure in the following cycle as shown in Figure 3.21 c. The back-pressure can be exhausted to the atmosphere by reducing the cross-section of the ram over part of its length see in Figure 3.21 d. This arrangement requires separate re-cocking jacks; it is wasteful on air and increases the dwell and cycle times. However, when the back-pressure chamber is small or when the energy loss incurred by the intensification of the back-pressure is undesirable and the hydraulic power for re-cocking is already available.

3.5.1.4.2 Advantages of Combustion-Pneumatic HERF Hammer

The HERF hammers discussed, work on the principle that a certain volume of gas contained in an expansion chamber (combustion chamber for Petro-Forge) at a pressure P_i is made to expand by driving a piston. The work done by the expanding gas is converted into kinetic energy of the moving mass (piston/ram/platen assembly) and this is then utilized for forming purposes **(Davies and Dhawan, 1966).**

In pneumatic-hydraulic HERF hammers at the end of the forming stroke the expanded gas is recompressed with the aid of hydraulic rams (re-cocking cycle) to prepare the machine for the next forming stroke. Thus the useful forming work and the inevitable losses are covered by a hydraulic power pack acting as the primary energy source. With combustion actuated machines, the principle of operation at the end of the forming stroke the expanded gas is discarded (open loop) by opening an exhaust valve and the piston/ram/platen assembly is returned to its original (firing) position by the back-pressure. Thus with such machines the energy is derived from two sources **(Davies and Austin, 1970)**, **(Poullikkas, 2006):**

- A low pressure air compressor supplying the air charge of the combustion chamber,
- The combustion of hydro-carbon fuel (propane). The hydro-carbon fuel acts essentially as a means for intensifying the primary power source.

Petro-forge can claim all of the machine advantages attributed to pneumatic-hydraulic HERF hammers and a good many more. The capital cost of Petro-Forge is well below that of an equivalent pneumatic-hydraulic HERF hammer because combustion actuation does not require a special and expensive high pressure compressor and/or hydraulic power-pack. Basic energy costs are about the same but maintenance costs are likely to be significantly lower.

The mechanical action of its drive unit ensures a high cycling rate, a minimal "dead time" and very short dwell re-cocking/ejection times. Re-striking of the workpiece in the same heat is feasible and bounce-free operation can be ensured. Its blow energy can be controlled within wide limits and maintained within a close tolerance. Besides the aforementioned advantages the followings can be counted as the advantages of Petro-Forge **(Poullikkas, 2006).**

- Perform better for severe coining blows than the friction screw press because of its higher stiffness. Take higher coining blows than the crank or similar press. Has a higher cycling rate than all the forming machines,
- The effects of strain rate and of component cooling have been neglected. Small compact size and consequent law capital cost. Lower installation, erection and building costs.

3.5.2 Economics of HERF Hammer

As mentioned earlier, HERF devices are only one-ninth the size and weight of conventional hammers and about two-fifths that of crank presses, and this accounts for the reduced capital investment associated with high-energy-rate forging. Furthermore, the installation costs are also lower because of the less expensive foundation requirements. Among the HERF hammers, the combustion-pneumatic machines have a lower capital cost than the pneumatic-hydraulic devices.

A cost comparison will indicate whether a HERF method or a conventional method is the most economical. For example, Figure 3.22 illustrates generalized cost-comparison curves for forming a typical part for each method. For the production of a small number of parts, the unit cost favors a HERF operation because of the generally lower initial cost of tooling, capital equipment, etc. However, as the number of parts is increased, the crossover point P is reached, and the unit cost for the conventional method becomes the lower **(Semiatin, 1988).**

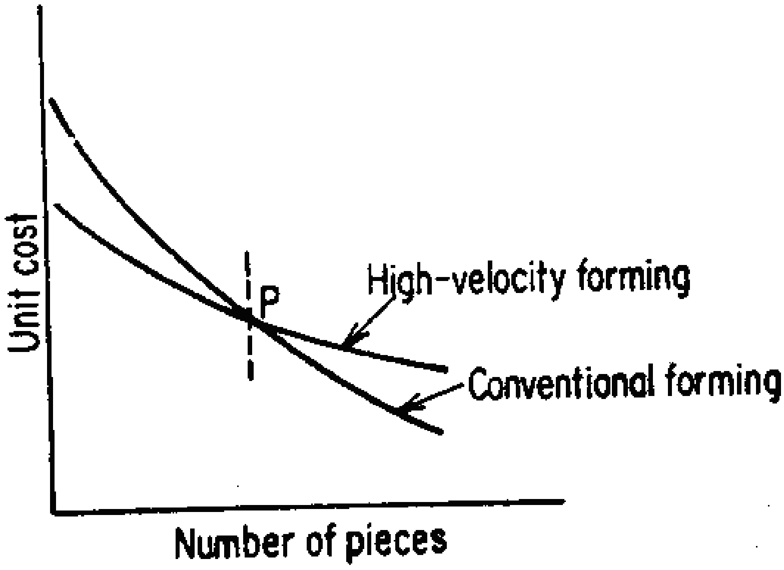

Figure 3.22 Cost comparison between conventional forming and High Energy Rate Forming

Therefore, as illustrated in Figure 3.22 in those industries having short production runs, such as the aerospace industry, many of the operations fall to the left of P; consequent HERF has been accepted more readily by the aerospace manufacturers. In industries which produce extremely large numbers of parts, such as the stamping industry, the operations fall to the right of P and, for the most part, are nor economically feasible for most HERF techniques. However, recent studies by S.A Tobas at the University of Birmingham, England, have shown that when properly designed and controlled, automated pneumatic mechanical HERF hammers can be competitive with conventional stamping and high production forging equipment. Because of these limitations, the HERF process is better suited to special, rather than general, forging operations. The cost benefits associated with its application would have to be evaluated on a case-by-case basis for each part.

3.5.3 Metallurgical Effect of HERF Hammer

There is mounting evidence that HERF has no unique effect on the metallurgical properties of the deformed material. Although is true that in the as-formed condition a high energy rate formed material can exhibit metallurgical properties that are superior to those possessed by the material prior to forming, many metals and alloys are heat-treated following forming, which generally eliminates the effects of the forming operation. In essence, the HERF techniques may produce a part more cheaply and faster but will probably not improve its service life or performance **(Kobayashi and Lee, 1973).**

In specific applications, however, HERF may produce metallurgical advantages readily produced by conventional forming, such as shock hardening, (especially surface and through hardening), rapid cold working (hardening and strengthening when subsequent heat-treatment is not used), explosive cutting or welding, and compaction of metal powders to high green densities.

3.6 SHEET METAL CUTTING

The first step in forming such a part involves cutting of the sheet into appropriate shapes by means of the physical process of shearing. A contoured part is cut between a punch and die in a press. Recent international market demands are that mechanical parts should be produced to net-shape or near net-shape with improved mechanical properties, a smooth surface finish, good dimensional accuracy and material savings, depending on service conditions **(Hambli and Guerin, 2003)**.

Shearing action has three basic stages: plastic deformation, fracture, and shear. When the metal is placed between the upper and lower blades of the shear and pressure is applied, plastic deformation first takes place. This extends into the interior of the metal from 5 to 40 per cent of its thickness. As continued pressure is applied to the cutting blade, the fracture or crack starts at the cutting edge of each blade. The fracture or crack starts at the cutting edge of each blade, the points of the greatest stress concentration. As the blade descends further, the small fractures meet and the metal is then sheared. The same shearing action takes when a punch and die are used.

The sheared edges of a blank and pierce produced in a conventional die are not smooth and vertical for the entire thickness of the part, but exhibit the characteristics represented on an exaggerated scale in Figure 3.23.

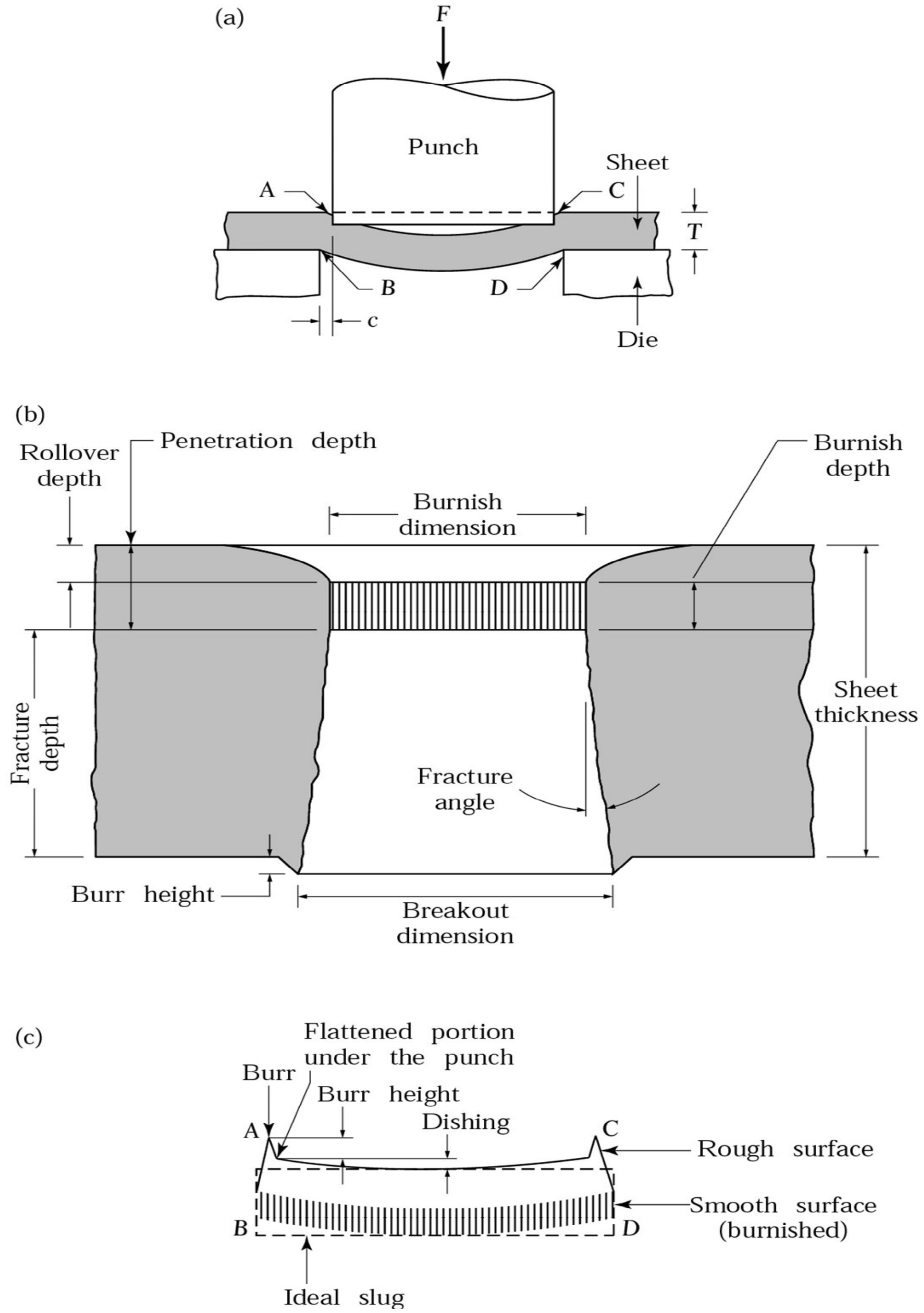
(a)
F
Punch
Sheet
A
C
T
B
D
c
Die
(b)
Rollover depth
Penetration depth
Burnish depth
Burnish dimension
Fracture depth
Sheet thickness
Fracture angle
Burr height
Breakout dimension
(c)
Flattened portion under the punch
Burr
Burr height
Dishing
A
C
Rough surface
Smooth surface (burnished)
B
D
Ideal slug

Figure 3.23 (a) Schematic illustration of shearing with a punch and die, indicating some of the process variables Characteristic features of (b) a punched hole and (c) the slug, note that the scales of the two figures are different **(Altan et al, 1973)**

Shear forming, by which parts with the desired shape are manufactured from a sheet metal especially using a punch and a die, needs this kind of standardization for compatibility and accuracy of components. However, production feasibility check, blank-layout, strip-layout, and die layout of forming by blanking or piercing have been mostly accomplished by the experience and intuitional decision of skilful engineers **(Choi and Kim, 2001).** However, the basic shearing operations are illustrated in Figure 3.24.

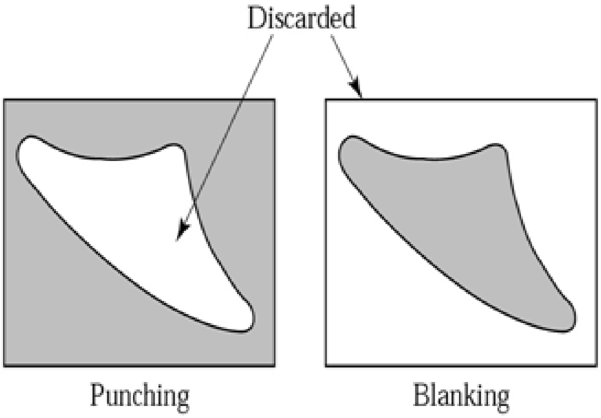
Discarded
Punching
Blanking

Figure 3.24 Basic shearing operations

3.6.1 Cutting Processes

The most widely used shearing method is the conventional shearing process shown in Figure 3.25. The shearing blade performs a linear motion, usually perpendicular to the centerline of the bar. In general such shearing tools are mounted in an eccentric press. The shearing velocity is normally less than 1 m/s **(Lange, 1985)**.

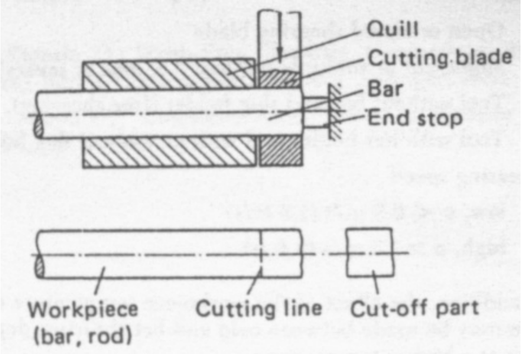
Quill
Cutting blade
Bar
End stop
Workpiece
(bar, rod)
Cutting line
Cut-off part

Figure 3.25 Bar cropping

As the process is being performed the material whose behavior is non-linear, is submitted to complex stress and strain states. Before complete rupture, the material is subjected to ductile damage and crack propagation phenomena. To describe the sheet is behavior while the process is being carried out, various parameters may be used such as the material state of hardening and damage, the metallurgical morphology, the crystallographical texture and the intragranular structures as they evolve during the procedure. The main difficulty encountered in simulating this operation is describing the behavior of the sheet continuously from the beginning of the operation up to the total rupture. In this case, choosing a behavior law is crucial, since each successive step in the whole process, as illustrated in Figure 3.26, has to be described accurately **(Hambli, 2001).**

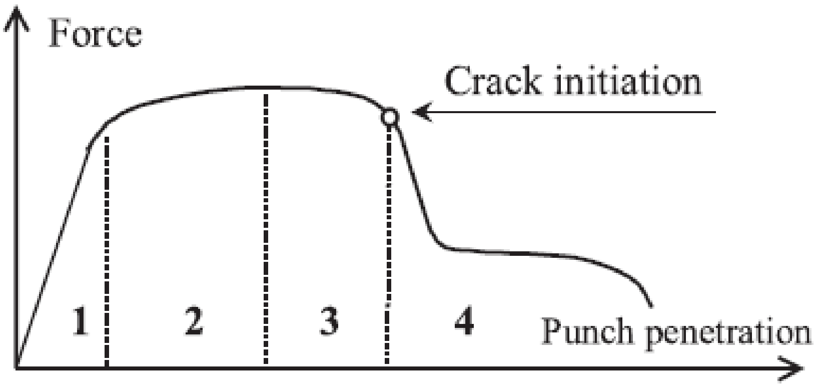

Figure 3.26 Schematic diagram of punching forces vs. punch penetration from Ref **(Hambli, 2001)**. 1: Elastic stage, 2: elastoplastic stage, 3: elastoplastic stage in which damage occurs, 4: initiation and propagation of cracks leading to final rupture

3.6.2 Blanking Processes

Blanking is an operation of cutting a flat shape from a sheet metal. The part punched out is called the blank and the remaining sheet is the scrap. In the blanking operation, the blank size is equal to the die size and the clearance is added to the punch. In sheet metal cutting with punch and die, shown in Figure 3.27, it is common for the strip to grip the punch after the cutting action is complete, i.e. at the bottom of the punch stroke. A stripping element can be built into the tool, so that when the punch withdraws the strip is pulled off the punch (**Bing and Wallbank, 2008), (Hatanaka et al, 2003) and (Hsu et al, 2008).**

Blanking is one of the most frequently used processes in sheet metal forming. However, a review of the literature on the blanking process shows that, while a large number of experimental techniques have been used to study the process from the 1950s to the present day **(Choi and Kim, 2001), (Brokken, 1998),** the amount of theoretical work done is inadequate. One reason for this may be that it is difficult to simulate the shearing process because of the narrowness of the shear band formed and the lack of an appropriate fracture criterion **(Faura et al, 1998), (Husson et al, 2008), (Shima et al, 2004).**

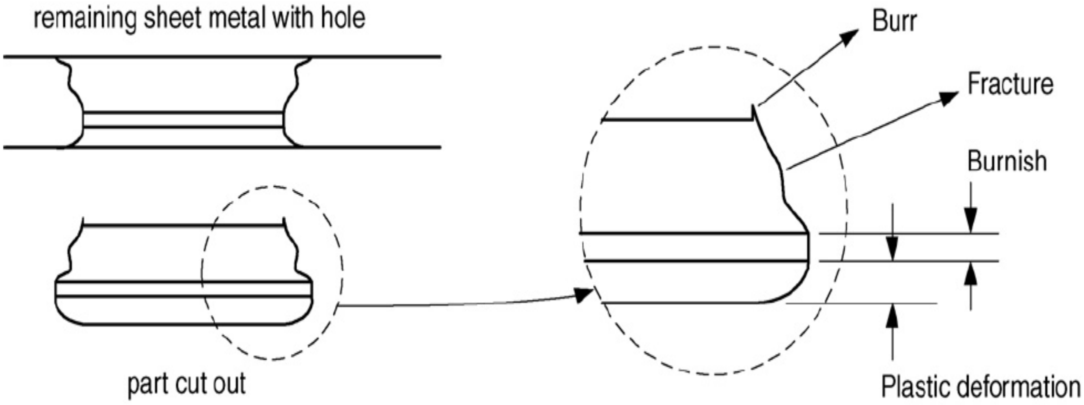

Figure 3.27 Simple blanking with a punch and die **(Brokken, 1998)**

3.6.3 Piercing Processes

Piercing is a cutting operation by which various shaped holes are made in the sheet metal. In this operation, the hole is the required operation and the material punched out is the scrap. In the piercing operation, the hole size is equal to the punch size and the clearance is added to the die **(Leea and Pourboghrat, 2005).**

Pierced holes are different from through holes that are produced by drilling or other machining methods. A properly drilled or otherwise machined through hole has a side-wall that is straight for the full thickness of the work metal, with a high degree of accuracy in size, roundness, and straightness. The sidewall of a pierced hole is generally straight and smooth for only a portion of the thickness, beginning near the punch end of the hole; the rest of the wall is broken out in an irregular cone beyond the straight portion of the hole, producing fracture, breakout, or die break. (Figure 3.23b).

The piercing operation typically begins as a cut that produces a burnished surface on the hole wall and some rollover (curved surface caused by deformation of the workpiece before cutting begins), as illustrated in Figure 3.23b. The punch completes its stroke by breaking and tearing away the metal that was not cut during the beginning of the piercing operation. The combined depth of rollover and burnish is a measure of the penetration depth of the stroke, also shown in Figure 3.23b. This is the part of the stroke during which the cutting force is exerted, before the metal fractures or breaks away (Fig. 3.23b) **(Semiatin, 1988).**

3.6.4 Optimum Clearance

Clearance, or the space between the punch and the sidewall of the die, affects the reliability of operation of piercing (and blanking) equipment, the characteristics of the cut edges, and the life of the punch and die. Published recommendations for clearances have varied widely, with most suggesting a clearance per side of 3 to 12.5% of the stock thickness for steel. Establishment of the clearance to be used for a given piercing or blanking operation is influenced by the required characteristics of the cut edge of the hole or blank and by the thickness and the properties of the work metal. Larger clearances prolong tool life. An optimal clearance can be defined as the largest clearance that will produce a hole or blank having the required characteristics of the cut edge in a given material and thickness. Because of differences in cut-edge requirements and in the effect of tool life on overall cost, clearance practices vary among plants and for different applications **(Tekiner, 2006).**

Various experimental studies **(Hambli and Guerin, 2003)** showed that the mechanical and geometrical aspect of the sheared edge during the blanking operation for a given material are affected by some parameters like the blanking clearance, the wear state of the tool, and the thickness of the sheet. In blanking processes, the clearance expressed in percent of the sheet thickness, is defined by

$$c = 100 * \frac{D_m - D_p}{2t} (\%) \tag{3.19}$$

where D_m, D_p and t are the die diameter, the punch diameter and the sheet thickness, respectively.

In the case of blanking processes, one seeks to generate cracks at the sharp edges of the punch and the die than to make, so that through the choice of the parameters of cutting, this crack is propagated as soon as possible to obtain the total rupture.

Hambli and Guerin assumed that clearance is optimum when the direction of crack propagation coincides with the line joining the points of crack initiation in the punch and die, giving cleanly blanked surfaces without secondary crack formation (Figure 3.28). In this case, the total separation of the sheet is obtained for a lower value of punch penetration. In order to obtain the optimum clearance value, the angle of the line joining the points of crack initiation in the punch and die θ_d (diagonal angle) and the angle of the Direction of Crack Propagation (DCP) β must coincide (Figure 3.29) **(Hambli and Guerin, 2003).**

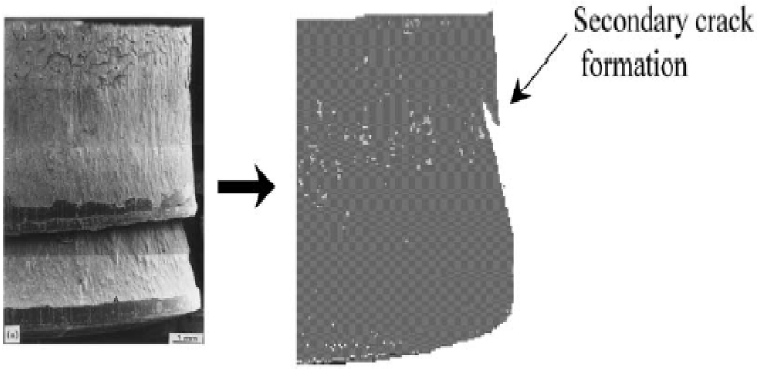

Figure 3.28 Secondary crack formation during blanking process **(Tekiner, 2006)**

The diagonal angle can be expressed by

$$\theta_d = Arc\tan\left(\frac{c}{t - U_p}\right) \tag{3.20}$$

U_p is the punch penetration corresponding to the first crack initiation within the sheet. Figure 3.30 shows the ranges of die clearance per side used by one electronics manufacturer in piercing and blanking three groups of metals up to 3.18 mm thick. The groups and the percentages of stock thickness on which these ranges of clearance were based are also listed in Figure 3.30 **(Semiatin, 1988).**

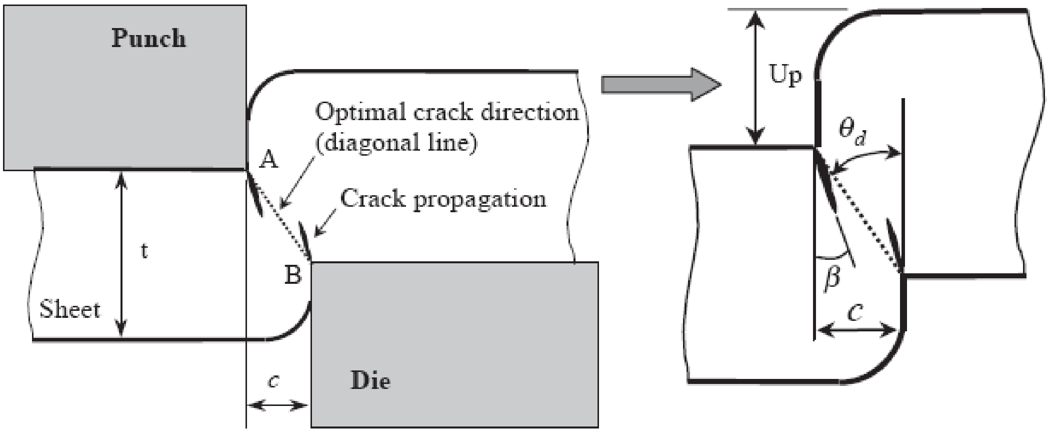
Punch
Optimal crack direction
(diagonal line)
A
Crack propagation
t
B
Sheet
c
Die
Up
θ_d
β
c

Figure 3.29 Illustration of crack propagation angle and diagonal angle

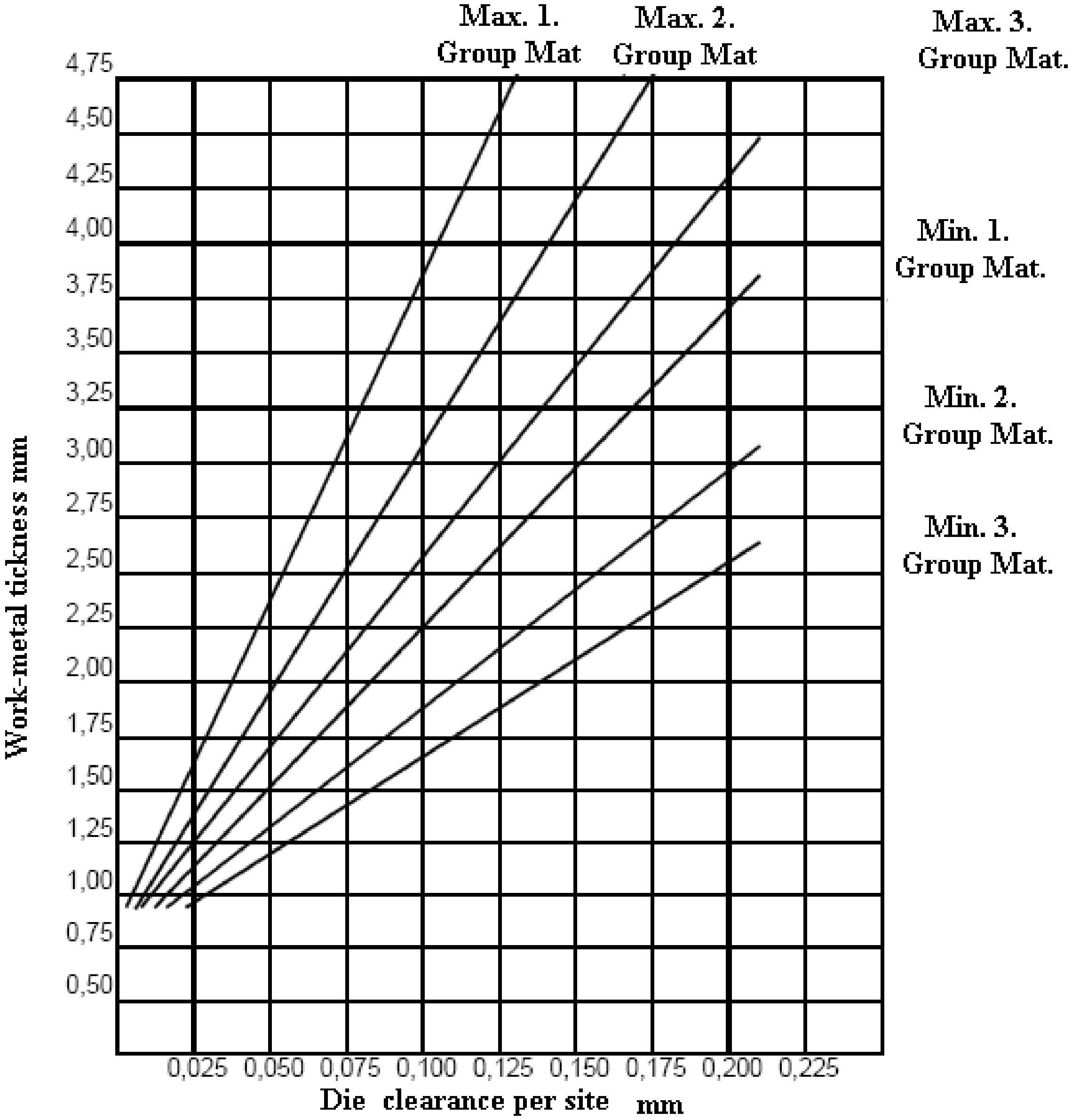

Group	Clearance per side, % of stock thickness[(a)]	
	Average	Range
1. Aluminum alloys 1100 and 5052, all tempers	2.25	**1.7-3.4**
2. Aluminum alloys 2024 and 6061, T4 and T6 tempers; brass, all tempers; cold-rolled steel, dead soft	3.0	**2.25-4.5**
3. Cold-rolled steel, half hard	**3.75**	**2.8-5.6**

Figure 3.30 Ranges of punch-to-die clearance per side recommended by one manufacturer for piercing and blanking of various metals up to 3.18 mm thick **(Semiatin, 1988).**

3.6.5 Quality of Sheared Edges

The quality of the cut surface is greatly influenced by the clearance between the two shearing edges. If the sidewall of a pierced hole is not smooth or straight enough for the intended application, it can be improved by shaving in a die or by reaming. When done in quantity, shaving is the least expensive method of improving the sidewall of a pierced hole. Shaving in one or two operations generally makes the sidewall of a hole uniform and smooth through 75 to 90% of the stock thickness.

Burr height is an important element in hole quality, and a maximum burr height is usually specified. For most applications, the limit on burr height is between 5 and 10% of stock thickness. Burr height in piercing a given workpiece is primarily governed by punch-to-die clearance and tool sharpness. Burr condition and limits usually determine the length of run before the punch and die are re-sharpened. With good practice, burr height generally ranges from 0.013 to 0.076 mm (0.0005 to 0.003 in.), but may be much greater, depending on workpiece material and thickness, clearance, and tool condition. The cutting surfaces at the different clearances are shown in Figure 3.31.

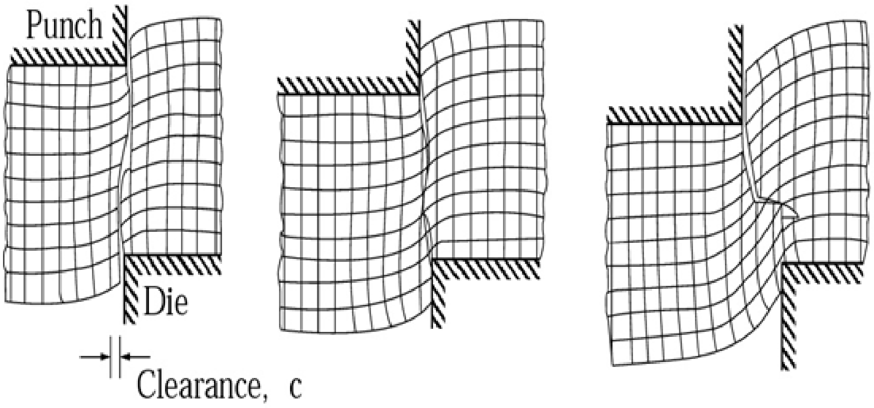

Figure 3.31 Cutting surfaces at the different clearances

The clearance between the punch and the die plays an important role in the blanking process. The selection of the clearance will influence the life of the die or punch, the blanking force, the unloading force and the dimensional precision. In the blanking process, some factors such as the punch–die clearance, the punch velocity, the tool geometry, lubrication and the mechanical properties of the materials influence the final part edge quality (ratio of the different zones). Selecting some different process factors, a work piece can be obtained with different quality. The clearance changes according to thickness, material and tensile strength of sheet metal. The clearance between the punch and the die will affect the precision of the shape and dimensions dramatically (ratio of the different zones) **(Semiatin, 1988).**

3.6.6 Cutting Forces

Calculation of the forces and the work involved in blanking gives average figures that are applicable only when the correct shear strength for the material is used and when the die is sharp and the punch is in good condition, has correct clearance, and is functioning properly. The total load on the press, or the press capacity required to do a particular job, is the sum of the cutting force and other forces acting at the same time, such as the blank holding force exerted by a die cushion. When punch and die surfaces are flat and at right angles to the motion of the punch, the cutting force can be found by multiplying the area of the cut section by the shear strength of the work material:

$$L = S_s * t * l \tag{3.20}$$

where L is the load on the press (N) (cutting force), S_s is the shear strength of the stock (MPa), t is the stock thickness (mm), and l is the length or perimeter of the cut (mm). The shear strengths of various steels and nonferrous metals are given in Table 3.6. The cutting force for a die with shear can be calculated after first finding the work done (energy used) in blanking. The work done in blanking equals the force required in blanking (load on the press) multiplied by the distance that the force acted:

$$W = L * s \tag{3.21}$$

where W is the work done in blanking (in mm-N), L is the load (in N), and s is the distance the load acts (thickness multiplied by percentage of penetration before fracture) (in mm). To obtain accurate work values, the percentage penetration must be known accurately.

Table 3.6 Shear strengths of various steels and nonferrous metals at room temperature

Carbon steels	**S_s(MPa)**	**Nonferrous metals**	**S_s(MPa)**
0.10% C	241-296	Aluminum alloys	48-317
0.20% C	303-379	Copper and bronze	152-483
0.30% C	358-462	Lead alloys	13-40
High-strength low-alloy steels	310-439	Nickel alloys	242-800
Silicon steels	414-483	Tin alloys	20-77
Stainless steels	393-827	Titanium alloys	414-483

Cutting or blanking force is reduced by the use of angular shear in the die; the amount of reduction in force depends on the depth of the angular shear. The reduced average cutting force on the press is:

$$L_{sh} = \frac{W}{s_1 + s} \tag{3.22}$$

where L_{sh} is the average cutting force (N), with angular shear, W is the work done in blanking (mm-N), s is the distance (mm) that the load acts (thickness multiplied by percentage of penetration before fracture), and s_1 is the depth of angular shear (inches). In simplified practice, some plants ignore partial shear in calculating cutting force for blanking. When full shear is used, force is calculated as without shear and then reduced by 30%.

Stripping force is the force needed (when drop-through is not used) to free the blank from the die or the strip from the punch when they stick or jam because of spring back. Stripping force can be calculated using:

$$L_{st} = k * A \tag{3.23}$$

where L_{st} is the stripping force (N), k is a stripping constant (N per square mm), and A is the area of the cut surface (mm^2) (stock thickness t multiplied by length or perimeter of cut l) **(Semiatin, 1988).**

CHAPTER 4

DESIGN AND CONSTRUCTION OF HIGH ENERGY RATE FORMING (HERF) HAMMER

4.1 INTRODUCTION

The principle of internal combustion engine to obtain high energy rate was used to achieve the aim of this thesis. In the high energy rate forming (HERF) hammer, re-cocking mechanism works mechanically. As a result of moving triggered unit, compressed air-fuel mixture burns in cylinder. The HERF hammer may be accepted as a new classification in the HERF hammer literature. A lot of machine elements were used to the transfer explosion energy from the power unit to the forged workpiece. These machine elements were produced or bought so as they withstand the applied stresses.

Design and construction of Prototype HERF hammer is divided into five main units, namely:

- Frame,
- Power unit,
- Ignition unit,
- Injection unit,
- Re-cocking mechanism.

In the following parts of this chapter, these five main units are explained in detail.

4.2 PARTS OF HERF HAMMER

4.2.1 Frame

While the frame was being constructed, different size profiles were used. Thickness of these profiles was 2mm. The dimensions of the profiles in mm are 20x40, 40x40, and 40x60. By using aforementioned profiles the frame was constructed. Connections of the profiles, which were used for frame, were performed by using arc-welding. After constructing the frame, internal combustion engine was connected to it by using steel bars with 25 mm diameters. Connections of the internal combustion engine to the main body were portable. A 30 mm diameter ram carries the power obtained from the internal combustion engine to the upper die. It was constructed between piston and upper die. Upper die can be changed when needed. Ram was fixed from two different points to obtain the straight motion. Lower die was constructed adjustably to enable the stroke changeability. A square threaded power screw with 45 mm diameters was used to perform the lower and upper motion easily. Nut of square screw was welded to the main body to resist the power transferred from the ram. Wooden-based adjustable screws were used to decrease the vibration. The view of the frame can be seen in Figure 4.1.

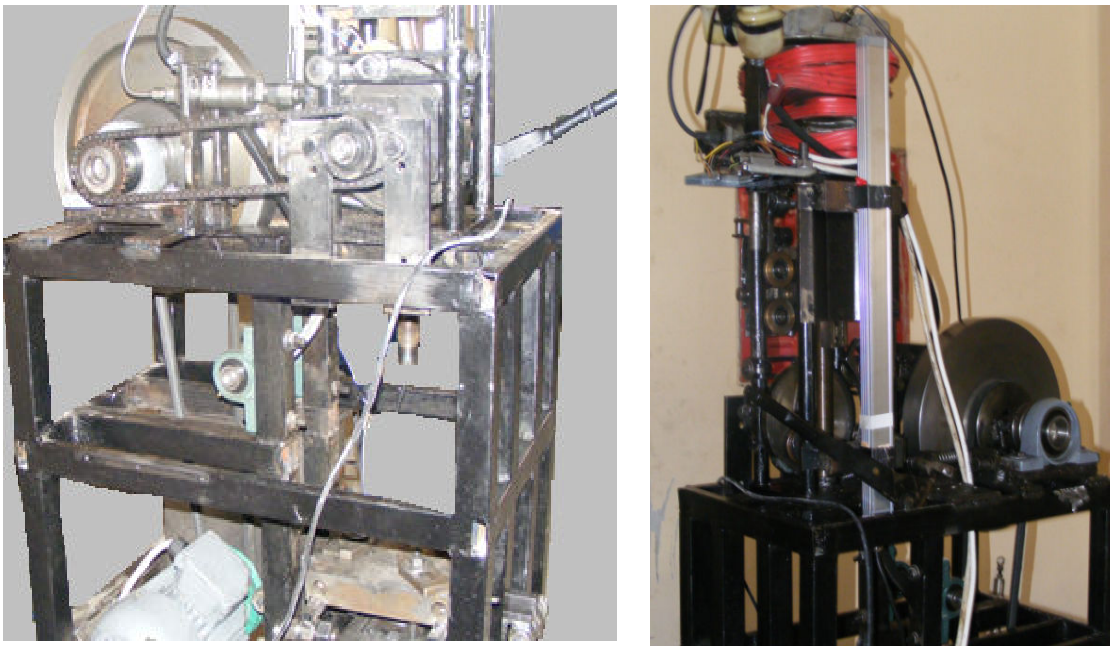

Figure 4.1 Frame of the hammer

4.2.2 Power Unit

An internal combustion engine converts the energy contained in a fuel into mechanical power. Generally, this mechanical power is used to turn a shaft in the engine. A generator is attached to the internal combustion engine to convert the rotational motion into power **(Rakopoulos, 1988).**

In this thesis, an internal combustion engine is operated in two stroke cycles as seen in Figure 4.2. In the two stroke cycle engines, the ram starts driving the piston toward the spark plug for the compression stroke. While the air in the cylinder is compressed, injection unit sprays the fuel into cylinder. When the piston leads to the end of the compression stroke, the spark plug fires to generate combustion pressure and thus drives the piston. The sides of the piston are acting like valves, covering and uncovering the intake and exhaust ports communicating into the side of the cylinder wall. Two stroke engines are lighter, simpler and less expensive to manufacture. They have a greater power in proportion to weight, but they are lesser in efficiency and they require lubrication oil to be fed with fuel.

As the power unit does not work continuously during experiments, the temperature of the internal combustion engine is usually below the room temperature. Although the fuel injected into the combustion chamber of the internal combustion engine has to be atomized, some of the fuel is liquidated because of cold condition. To avoid such a condition, the internal combustion engine is heated with electrical resistance, which is demonstrated in Figure 4.2.

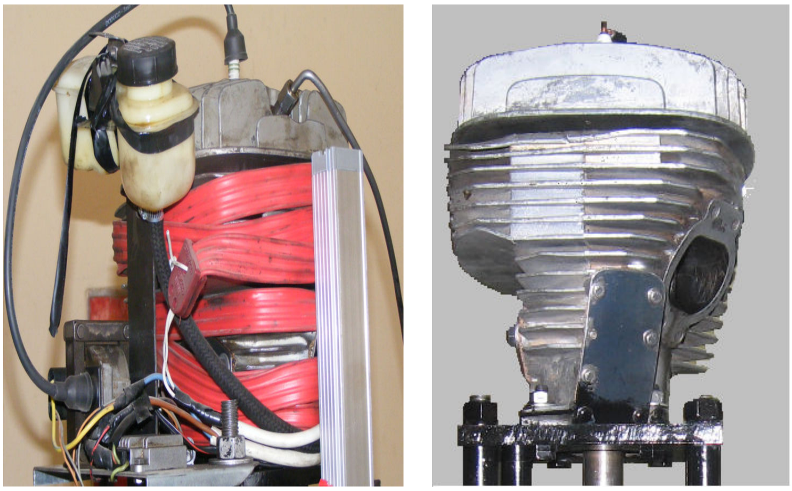

Figure 4.2 The used internal combustion engine

4.2.3 Injection Unit

The third part of the HERF hammer was the injection unit. So as for this unit to function, a cam fixed on a flywheel was used. Angular motion of flywheel was converted to direct motion by using cam. Obtained direct motion was transmitted to the fuel pump. As a result of the transmitted direct motion, 25 atm pressure was obtained when the fuel left the fuel pump. This high pressure fuel was conveyed to injector by using a steel pipe. Expansion coefficient of used steel pipe must be very low. Injector was constructed to the upper part of the used engine head. High pressure fuel was atomized by the injector, and then it was sprayed into the cylinder.

In locating the fuel pump, the time of injecting the fuel into the combustion chamber of internal combustion engine was flexible. It was necessary for determining the effect of injection time on burning quality. The mechanism, different views of which are given in Figure 4.3, was designed and constructed. This mechanism enables the injection operation to take place at the right time. Thus, this brings about burning quality and enables the forming energy, which is transferred to the workpiece being formed, to be variable. The working principle of this mechanism is shown schematically in Figure 4.4.

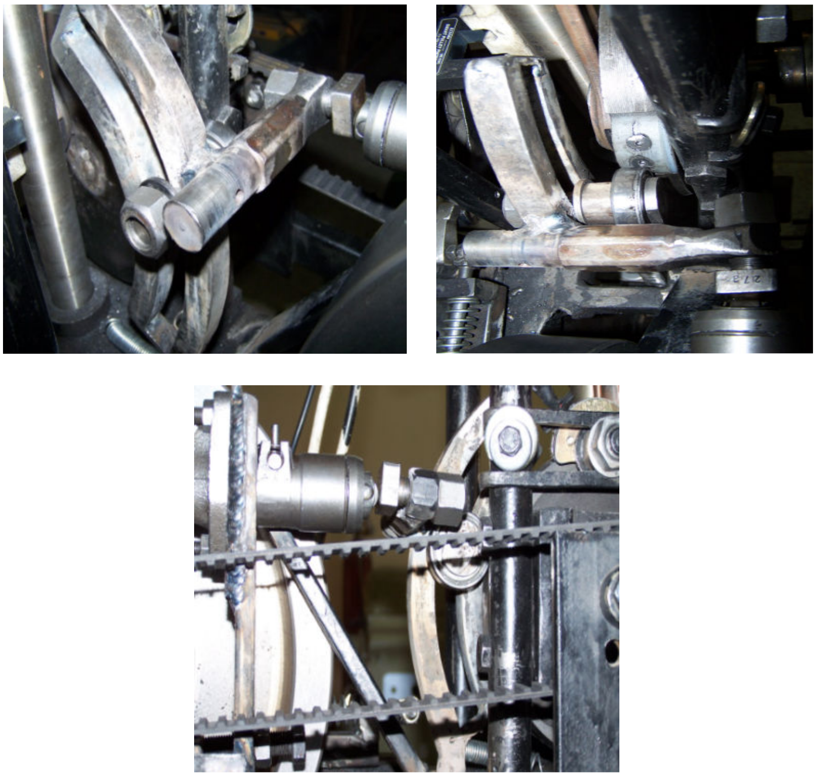

Figure 4.3 Different views of injection unit and pump location

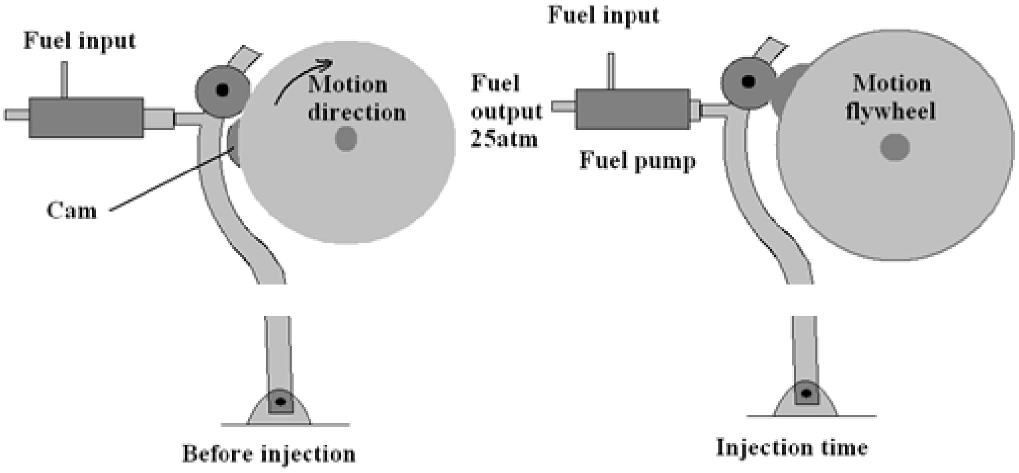
Fuel input
Motion direction
Cam
Before injection
Fuel input
Fuel output 25atm
Fuel pump
Motion flywheel
Injection time

Figure 4.4 The working principle of injection mechanism

4.2.4 Ignition Unit

220V network voltage is used for working of ignition unit. A transformer is used for the conversion of 220V to 12V. A bobbin is used to raise the 12V, which is received from the transformer, to 20.000V. A signal of trigger circuit is necessary for ignition of spark plug. A cam is constructed on the flywheel for the working of trigger circuit. While cam passed under the trigger circuit, it is perceived magnetically and then the signal of trigger circuit is produced. Produced signal is transmitted to the electronic unit. At the same time, electronic unit permits the high voltage to reach the spark plug. High voltage makes an arc in the cylinder to burn the compressed air-fuel mix. Pictures and schematic view of the ignition unit is given in Figure 4.5a and Figure 4.5b, respectively.

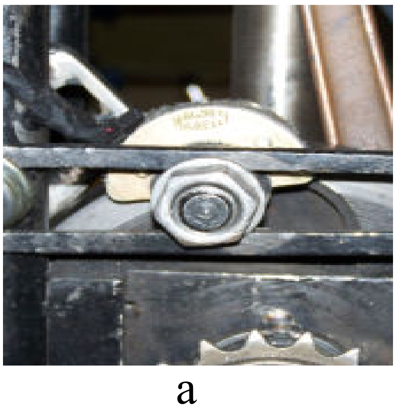

a

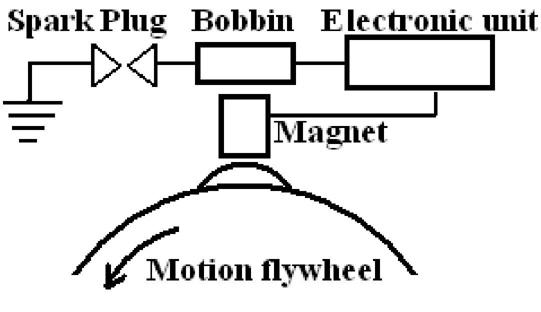
Spark Plug
Bobbin
Electronic unit
Magnet
Motion flywheel

b

Figure 4.5 Ignition unit

4.2.5 Re-cocking Mechanism

Compression of air-fuel mixture in cylinder is the main duty of re-cocking mechanism. Design and construction of Prototype HERF hammer's re-cocking mechanism is divided into six main units, namely;

- AC servo motor, driver unit and energy flywheel,
- Trigger mechanism,
- Locking mechanism,
- Chain-gear mechanism,
- Motion flywheel and compression car,
- Release cam and spring locking mechanism

In the following parts of this section, these six main units will be explained in detail.

4.2.5.1 AC Servo Motor, Driver Unit and Energy Flywheel

An AC servomotor was installed to regulate the piston compression rate. AC servo motor driver unit, AC servo motor and energy flywheel are demonstrated in the Figure 4.6a and 4.6b. The flywheel is charged by AC servo motor and the obtained kinetic energy is used to adjust the piston compression rate.

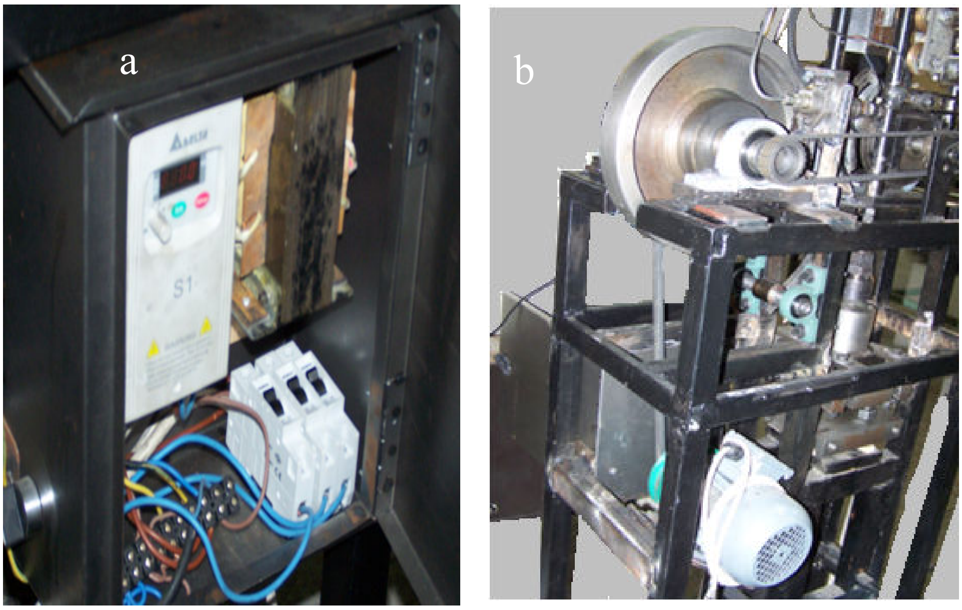

Figure 4.6 a) AC servo motor driver unit b) Energy flywheel and AC servo motor

4.2.5.2 Trigger Mechanism

At the end of each full rotation of energy flywheel, a work piece is deformed. Thus, to provide possibility for forming a new workpiece, a trigger mechanism was installed on the main body of the prototype high rate energy forming machine. With the aid of this mechanism, rotational energy of flywheel can be transferred to the shaft with only one cycle. When the trigger arm is pulled, latch turns to the open position. Then, energy flywheel drives its energy to the shaft. Then, towards the end of the motion of trigger arm, cam mechanism on the trigger arm turns the latch to the closed position. Thus, it serves to complete the rotation of energy flywheel at the 360 degrees. Trigger arm and its latch are presented in Figure 4.7 and the functioning principle is presented schematically in Figure 4.8.

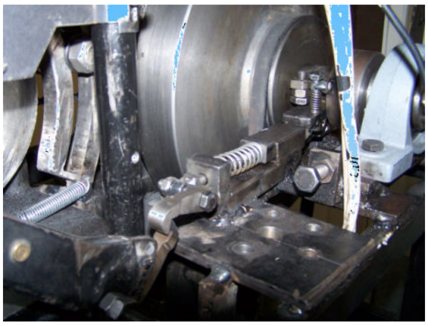

Figure 4.7 Trigger arm and its latch

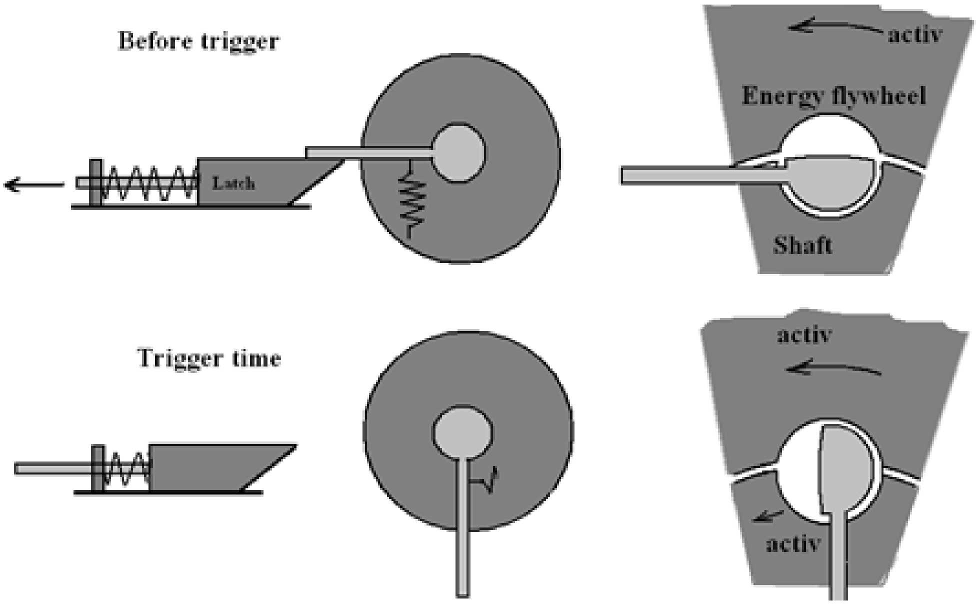

Figure 4.8 Functioning principle of trigger mechanism

4.2.5.3 Locking Mechanism

The kinetic energy of the energy flywheel must be transferred to its shaft to compress the piston. With the aid of a locking mechanism, rotational energy of flywheel is transferred to the flywheel shaft. Figure 4.9 illustrates the working principle of the above mentioned process.

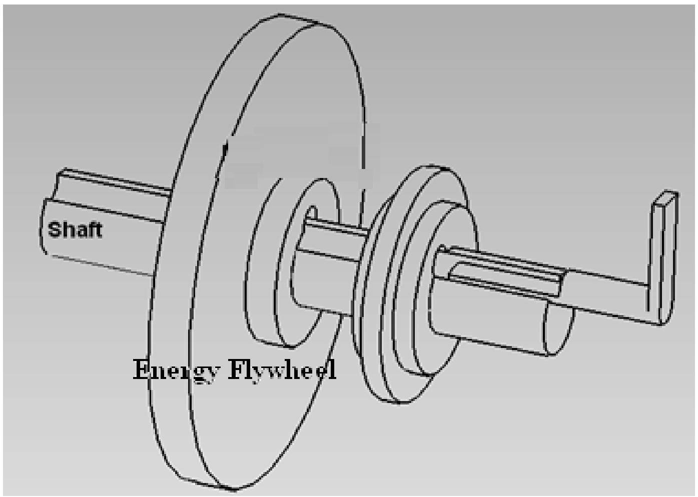

Figure 4.9 Locking mechanism

4.2.5.4 Chain-gear Mechanism

A gear chain mechanism of one to one ratio is used to transfer the energy from the main shaft to the motion flywheel (Figure 4.10).

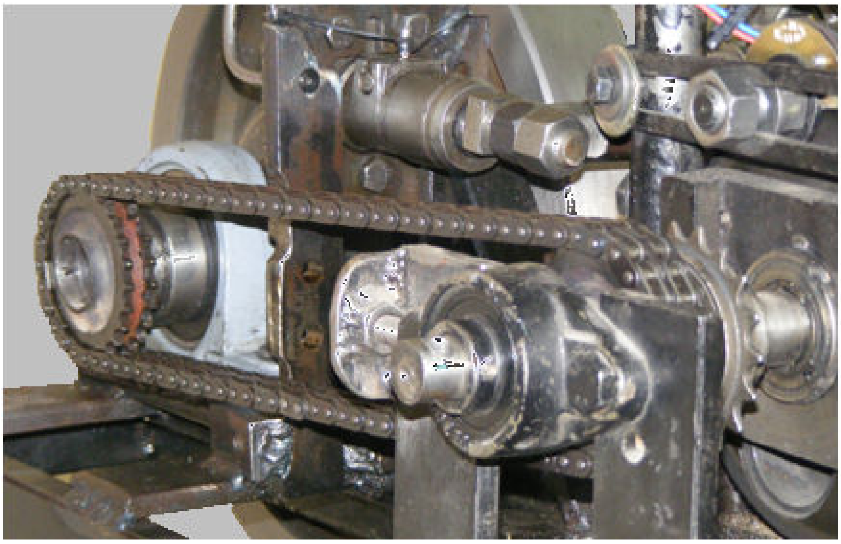

Figure 4.10 Chain-gear-mechanisms

4.2.5.5 Motion Flywheel and Compression Car

The rotational motion of the flywheel is linearly transferred to the compression car. The process is performed via a connecting rod, various views of which are shown in Figure 4.11. Figure 4.12 gives a schematic view of the compression car. The compression latch is in the open position during the first motion of the compression car. The upward motion of compression car contacts to the adjustable nut on the ram connecting the piston and upper die and compresses the piston towards the top dead center.

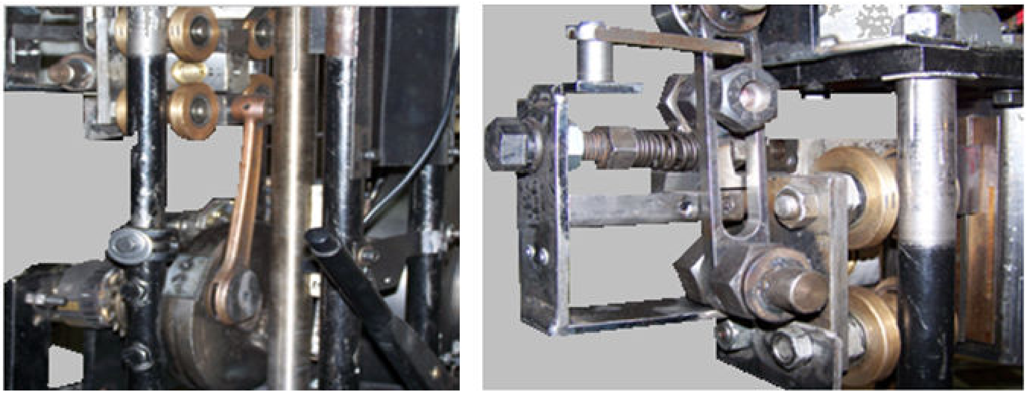

Figure 4.11 Different views of compression car

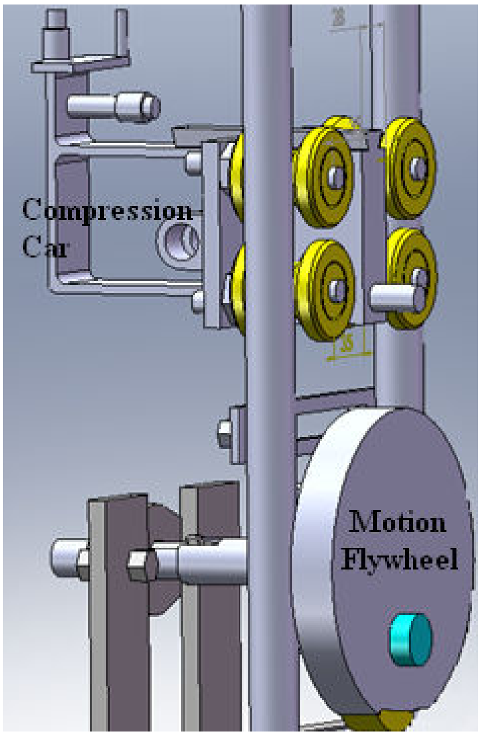

Figure 4.12 Schematic view of the compression car and motion flywheel

4.2.5.6 Release Cam and Spring Locking Mechanism

When the piston reaches the top dead center (TDC), the compression latch is turned to the close position by using cam mechanism is shown in Figure 4.13a. After compression car reaches the top dead center, it continues its motion in reverse direction. This motion of the compression car causes the compression latch to turn to open position. Thus, it causes the energy released during the explosion to apply pressure on the compression latch instead of the workpiece. In order to avoid this situation, the latch must keep its open position until the completion of the forming process. The spring locking mechanism constructed on the compression car (Figure 4.13 b) makes the compression latch stay in the open position till the end of the process. A schematic view of release cam and spring locking mechanism is given in Figure 4.14.

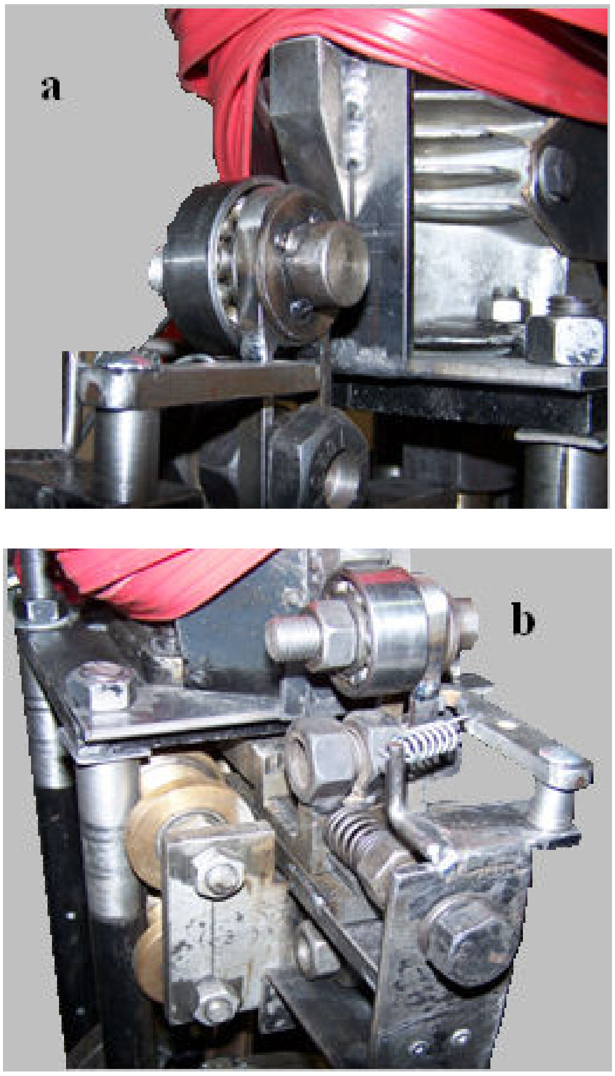

Figure 4.13 a) Freilassen cam mechanism b) Spring locking mechanism

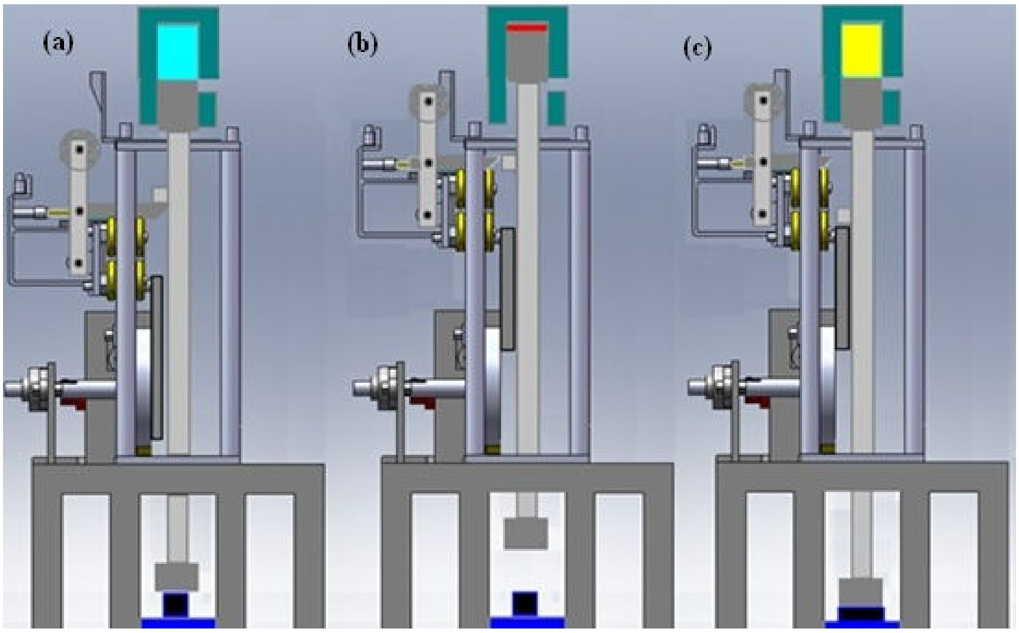

Figure 4.14 Schematic views of release cam and spring locking mechanism

4.3 DETERMINATION OF THE GENERATED FORMING ENERGY

4.3.1 Otto Cycle

An ideal cycle has no irreversibility. Air is assumed to behave as an ideal gas; all processes are considered to be reversible and heat losses do not occur. It is well known in practice that the air standard analysis of a cycle is useful for illustrating the thermodynamic aspects of engine performance. However, for a real Otto cycle, heat transfer irreversibility between the working fluid and the cylinder wall is not negligible. Heat loss strongly affects the overall performance of the engine. If it is omitted, the analysis will just depend on the ideal air standard cycle. The air standard Otto cycles are significant tools, as they explain the actual processes and the behavior of internal combustion engines.

The cycles differ from each other according to the type of energy input process. An air standard Otto cycle is shown in Figure 4.15. The heat addition is a reversible constant volume shown as a process between 2 and 3 in Figure 4.15 in an ideal air standard Otto cycle. Assuming constant specific heats, the energy added to the working fluid can be defined from the first law of thermodynamics as: **(Ozsoysal, 2006)**

$$Q_{in} = m_a c_{vo}(T_3 - T_2) \tag{4.1}$$

where C_{vo} is the specific heat coefficient at constant volume and m_a is the amount of air mass, which is the working fluid. The combustion energy is obviously not adiabatic since the maximum temperature in the cycle is far below the adiabatic combustion temperature.

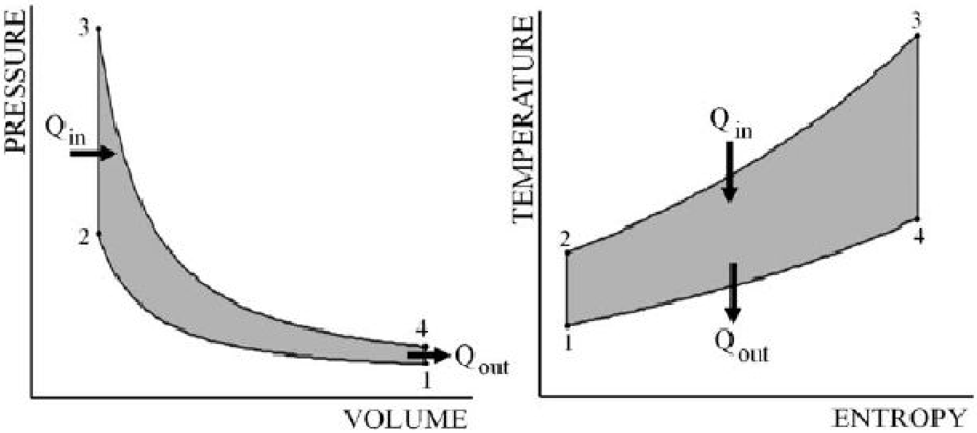

Figure 4.15 Pressure–volume and temperature–entropy diagrams for an air standard Otto cycle

The spark ignited internal combustion engine is modeled as an Otto cycle. The four stroke ideal Otto cycle models the intake of fuel–air mixture as the piston moves from (TDC) to (BDC) position with the intake valve open. Then the mixture is compressed (isentropic process 1–2) as the piston moves back to TDC with the intake valve closed. At TDC, the spark instantaneously ignites the fuel–air mixture (isochoric process 2–3) providing a heat input. The mixture is expanded (isentropic process 3–4) as the piston moves from TDC to BDC. At BDC the exhaust valve opens and pressure drops so that the exhaust process (isochoric process 4–1) followed by positive displacement pumping out of the products of combustion as the piston moves from BDC to TDC with the exhaust valve open. At TDC the exhaust valve closes and the intake valve opens so the cycle can repeat as shown in Figure 6. The areas underneath the processes represent work (w) done or added. The net output work for one cycle is represented by ((W_{34})-(W_{12})). Notice that the length of the compression stroke (isentropic process 1–2) and that of the expansion stroke (isentropic process 3–4) are equal in the Otto cycle. The major four functions (process 1–2, process 2–3, process 3–4, and process 4–1) described above are executed in just two strokes: the power stroke and the compression stroke. The traditional thermodynamic analysis of the four-stroke Otto cycle is the same as that of a two-stroke Otto cycle **(Wu et al, 2003) and (Ge et al. 2005).**

To evaluate compression ratio, displacement and combustion chamber volumes must be calculated. Figure 4.16 and 4.17 show the volumes. In volume calculation, geometrical values are used and then the compression ratio, CR, is evaluated.

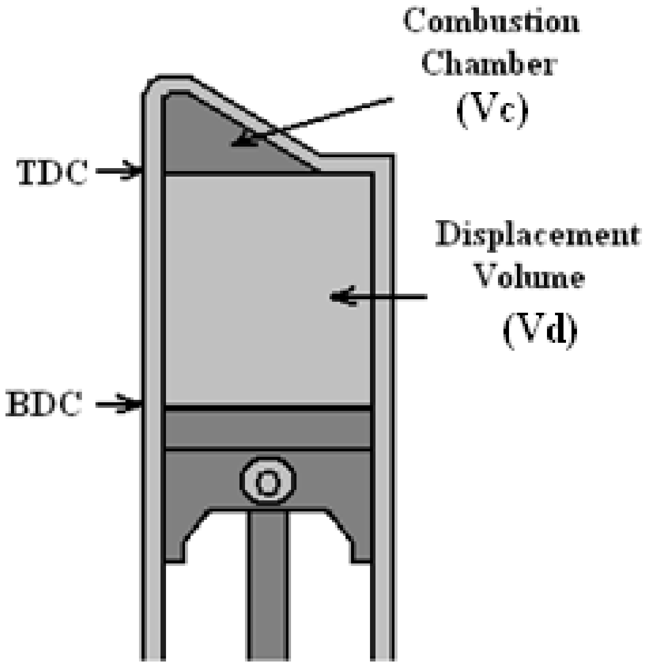
Combustion
Chamber
(Vc)
TDC
Displacement
Volume
(Vd)
BDC

Figure 4.16 Combustion chamber and Displacement volume

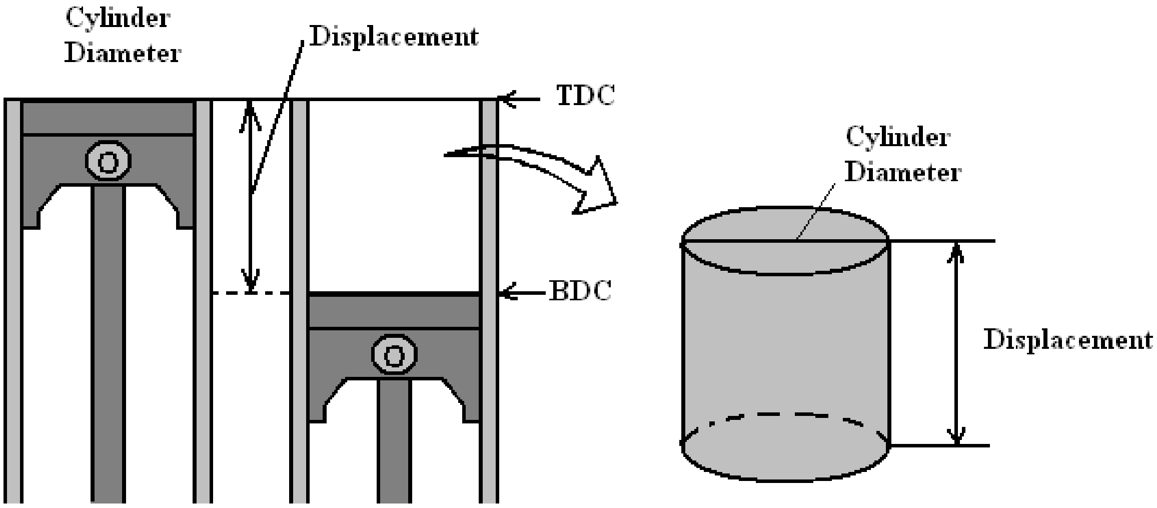
Cylinder
Diameter
Displacement
TDC
BDC
Cylinder
Diameter
Displacement

Figure 4.17 Tap dead center and Bottom dead center

$$CR = \frac{V_c + V_d}{V_c} \tag{4.2}$$

$$V_d = \frac{\pi D^2}{4} l \tag{4.3}$$

V_a = Total cylinder volume ($V_c + V_d$) (4.4)

$V_a = V_1 = V_4$, $V_c = V_2 = V_3$

$$CR = \frac{V_a}{V_c} = \frac{V_1}{V_2} \tag{4.5}$$

Determination of pressure P_2 after compression processes

$$P_1 V_1^k = P_2 V_2^k \tag{4.6}$$

$$P_2 = \frac{P_1 V_1^k}{V_2^k}$$

$$P_2 = P_1 \left(\frac{V_1}{V_2} \right)^k \tag{4.7}$$

$$P_2 = P_1 * CR^k \tag{4.8}$$

Determination of temperature after compression process

$$\frac{T_2}{T_1} = \left(\frac{V_1}{V_2} \right)^{k-1}$$

$$T_2 = T_1 * CR^{k-1} \tag{4.9}$$

Theoretically, when piston is at TDC air fuel mixture is ignited and then burning is started. The pressure and temperature of air fuel mixture increase due to the explosion of air fuel mixture. Increasing of pressure and temperature of air fuel mixture occurs instantaneously. In another word, it was assumed that the piston does not move when the explosion occurs. This situation is called as the isochoric process (constant volume) **(Ge et al. 2005).**

The value of pressure, which occurs after explosion, increases up to 45 kg/cm^2. It depends on compression ratio and quality of used fuel. As a result of pressure increase, the piston moves from TDC to BDC. The pressure (P3) after explosion is calculated as follows:

$$\frac{P_2}{P_3} = \frac{T_2}{T_3}$$

The power stroke is an isentropic expansion process. Determine pressure P_4 after expansion processes

$$P_4 = P_3 * CR^k \tag{4.10}$$

Determine temperature after compress process

$$\frac{T_3}{T_4} = \left(\frac{V_4}{V_3}\right)^{k-1}$$

$$T_4 = T_3 * CR^{k-1} \tag{4.11}$$

Calculation of thermal efficiency in theoretically

$$\eta = 1 - \frac{1}{CR^{k-1}} \tag{4.12}$$

When calculating thermal efficiency, same formula is used but instead of k, corrected n coefficient is used in practice (n=1.3).

$$\eta = 1 - \frac{1}{CR^{n-1}} \tag{4.13}$$

4.3.2 Theoretical Determination of the Generated Forming Energy

AC servo motor was used to start the motion of re-coking mechanism. Figure 4.18 illustrates working process of HERF hammer. As seen in Figure 4.19, compression in the cylinder continues until reaching 4.5 to 1 ratio. Thus, the temperature of compressed air-fuel mixture rises to 152ºC. Ignition unit starts the motion when there is 10 degrees to the upper dead center. As a result of ignition, the explosion occurs and then piston and ram assembly moves downward quickly due to pressure. The spring locking mechanism constructed on the compression car makes the compression latch stay in the open position till the end of the process. This process must be repeated to ignite each explosion.

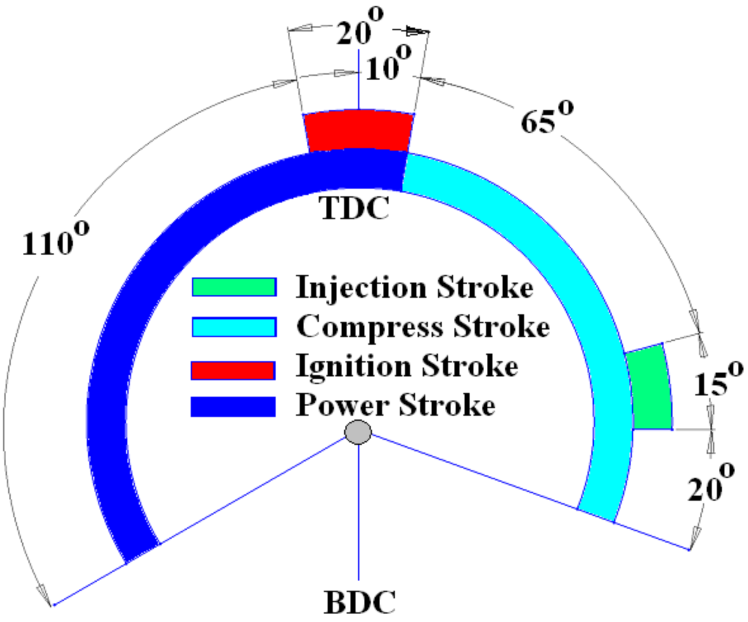
20°
10°
65°
110°
TDC
Injection Stroke
Compress Stroke
Ignition Stroke
Power Stroke
15°
20°
BDC

Figure 4.18 Diagram of working principle

Technical properties of the internal combustion engine and the fuel are given Table 4.1 and Table 4.2 respectively. These properties are used to determine thermal and mechanical efficiency of HERF hammer.

Table 4.1 Technical specifications of used engine

Number of cylinder	1
Working principle	2 stroke injection
Diameter of cylinder	7.15cm
Stroke	5.5cm
Total cylinder volume	$270cm^3$
Combustion chamber volume	$50cm^3$
Displacement volume	$220cm^3$
Compression ratio	5.4
Cooling unit	Air cooling
Initial temperature	300K
Initial pressure	$1kg/cm^2$
Compress ratio	14.6/1
Ratio of specific heats (k)	1.3

We analyzed pressure value of after compression stroke P_2 by using Motor meter in four different measures and found that P_2 pressure was 4.5 as was shown in Figure 19.

Table 4.2 Technical specifications of used gasoline

Formula	C_8H_{18}
Molecular weight(kg/mol)	114
Boiling point(ºC)	30-225
Liquid density(15ºC,kg/m^3)	735
Vapor pressure(20ºC,kg/cm^2)	0.49-0.81
Specific mass(gr/cm^3)	0.735
Flame temperature(air ºC9	1977
Thermal value(kJ/kg)	44000
Air/fuel ratio	14.6/1

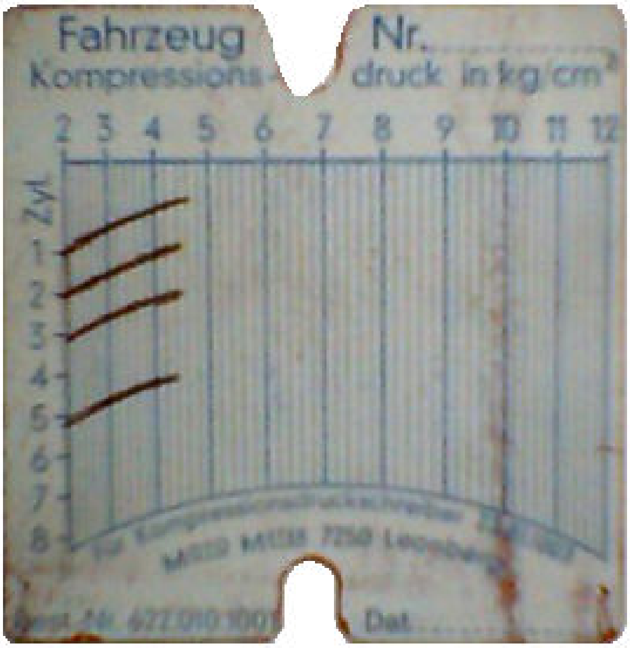
Fahrzeug
Nr.
Kompressions-
druck in kg/cm²
2 3 4 5 6 7 8 9 10 11 12
Zyl.
1
2
3
4
5
6
7
8
Dat.

Figure 4.19 Alternative measure of P2 by using Motor meter

After getting the pressure values, following calculations were performed using the formulas that were obtained through otto cycle.

P_1= 1 kg/cm^2, P_2= 4.5 kg/cm^2, k=1.4

$P_2 = P_1 * CR^k$

With correction coefficients the formula converts to $P_2 = 1 * CR_d{}^{1,3}$

$CR_d{}^n = \frac{P_2}{P_1} = 4{,}5$ $\qquad CR_d = 3.2$

$T_2 = T_1 * CR_d{}^{n-1}$ $\qquad T_2 = 300 * 3{,}2^{1,3-1} = 425$ K^o

P_3= P_2+5.1*CR_d=4.5+5.1*3.2=20.82kg/cm^2 (5.1 is a constant value of volume ratio.)

$$T_3 = \frac{P_3 T_2}{P_2} = \frac{20{,}82 * 425}{4{,}5} = 1967 K^o$$

$$\eta_t = 1 - \frac{1}{CR_d^{n-1}} = 1 - \frac{1}{3.2^{0.3}} = 1 - 0{,}7054 = 0{,}2945$$

As a result, thermal efficiency is calculated as: η_t= %29.45. Air/fuel ratio was taken as 14.6/1 and specific gravity as 1.157 kg/m^3. Total weight of air that corresponds to cylinder volume was calculated as 0.312 gr. Thus, the ideal fuel weight in the combustion chamber for one explosion can be calculated as follows:

$$m_f = \frac{m_{air}}{\left(m_{air}/m_f\right)}$$

The total fuel weight for one explosion is 0.0214 gr.

As for the amount of energy that is injected into and atomized in the cylinder:

Q_{in}= m_{fuel}(kg)* Thermal value of gasoline (kj/kg)

Q_{in}= 0.0214*10^{-3}(kg)*44000(kJ/kg)

Q_{in}= 0.9416kJ = 942J

Using thermal efficiency values, the work that is produced with the explosion is calculated

W=η_t*Q_{in} = 0.2945*942J= 277J

The obtained energy is found to be rather low. This is resulted from the low thermal efficiency. Factors such as low temperature of engine surface and intake air can be some of the reasons that decrease thermal efficiency.

4.3.3 Energy Losses

The ideal impact event is defined as a rigid accelerated ram striking a target workpiece, which is mounted on a rigid boundary (anvil). The impact event begins with an elastic loading of the workpiece and is followed by a plastic deformation for sufficiently large initial kinetic energy. Consider the experimental arrangement in Figure 4.20, where the kinetic energy of the impacting ram is available for dissipation after impacting against the specimen. At the moment of maximum compression the velocity of the ram will have been reduced to zero.

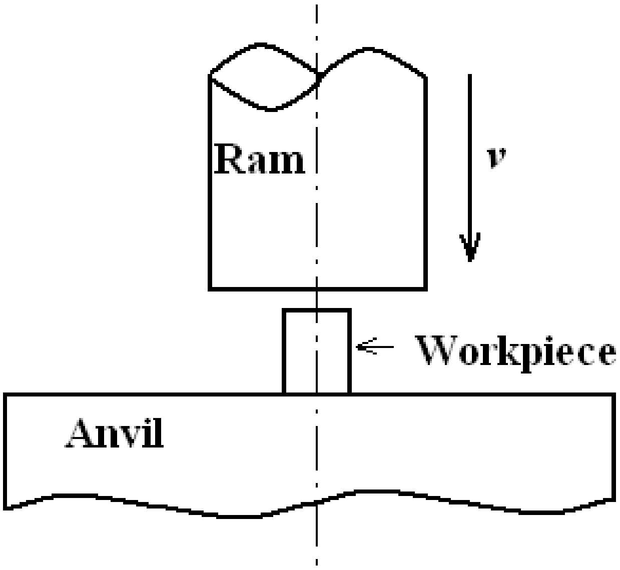

Figure 4.20 Experimental arrangement

The actual impact event is somewhat different from that described above because the boundary conditions may not be perfect. Rather than being mounted on a perfectly rigid support, the workpiece is placed on an elastic anvil, both the anvil and ram are deformed elastically during the impact, which modifies the deformation process as follows (see Figure 4.21):

- Initial impact event
- Elastic–plastic deformation of the workpiece until the velocity of the ram becomes almost zero
- Elastic recovery of the workpiece and anvil (this may not commence simultaneously)

- Projectile rebound The total energy is equal to the kinetic energy of the ram and is given by

$$E_t = \frac{1}{2} mV^2 \tag{22}$$

Where, m and v are the mass and the initial velocity of the ram, respectively.

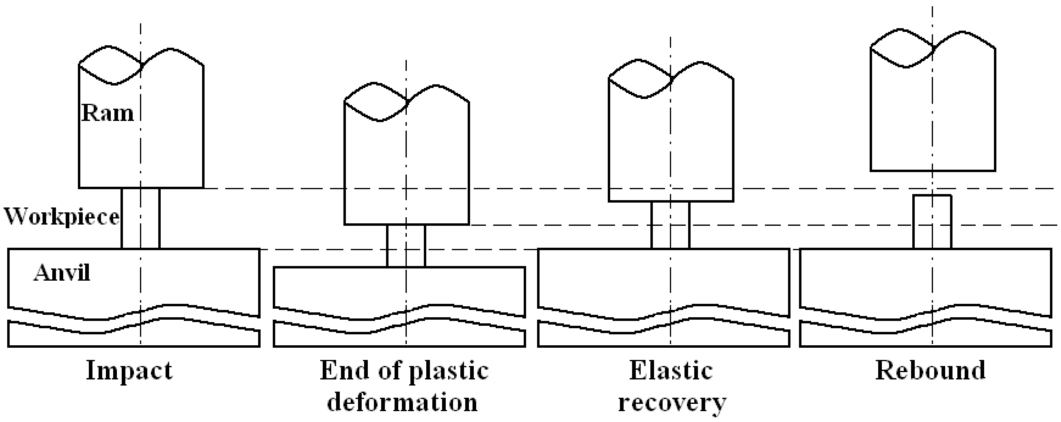

Figure 4.21 Motion of the ram and anvil for workpiece during an impact

It is likely that no further plastic deformation of the workpiece occurs after stage 2. The kinetic and elastic strain energies remain in the unit (ram, workpiece, and anvil) are not absorbed plastically by the workpiece. Therefore, the sum of these energies (E_t) may be considered. That is;

$$E_t = E_d + E_{e1} + E_f + E_{ar} + E_m + E_a \tag{23}$$

where deformation of the workpiece is E_d, elastic deformation of the dies and the machine E_{e1}, friction in die and machine guide elements E_f, for overcome of the air drag E_{ar}, for spring back of the moving parts E_m, for spring back of the anvil E_a i.e.

The impact efficiency $\acute{\eta}_i$ is

$$\acute{\eta}_i = \frac{E_d}{E} \tag{24}$$

As was calculated in previous experiments such as forging and blanking operation, the energy transferred from HERF hammer to aluminum, St37 mild steel and stainless steel test specimens was approximately 100J. Thus, the mechanical efficiency of HERF hammer can be calculated as in the following formula:

$$\acute{\eta}_i = \frac{\mathrm{E_d}}{E} = \frac{100}{277} = 0.36$$

Therefore, calculated mechanical efficiency was 36 %. The remaining energy (approximately 64 %) is absorbed by the other parts of HERF hammer.

4.3.4 Factors Affecting Generated Forging Energy

4.3.4.1 Compression Rate

Figure 22 shows a comparison of different fuel-air mixture pressure P_2 values prior to the explosion and piston compression velocity. While the piston velocity of the piston changes between 0.45 and 0.75 m/s, P_2 pressure ranges from 4.4 to 5.6 kg/cm^2. When the piston velocity reaches to 0.75 m/s, the highest P_2 pressure 5.6 kg/cm^2 is obtained. A relation in the form of second order polynomial regression function between piston velocity and P_2 was determined by curve fitting on 13 test measurements and given Figure 4.22. There is a strong relationship with the correlation coefficient of 0.947 between these two measurements.

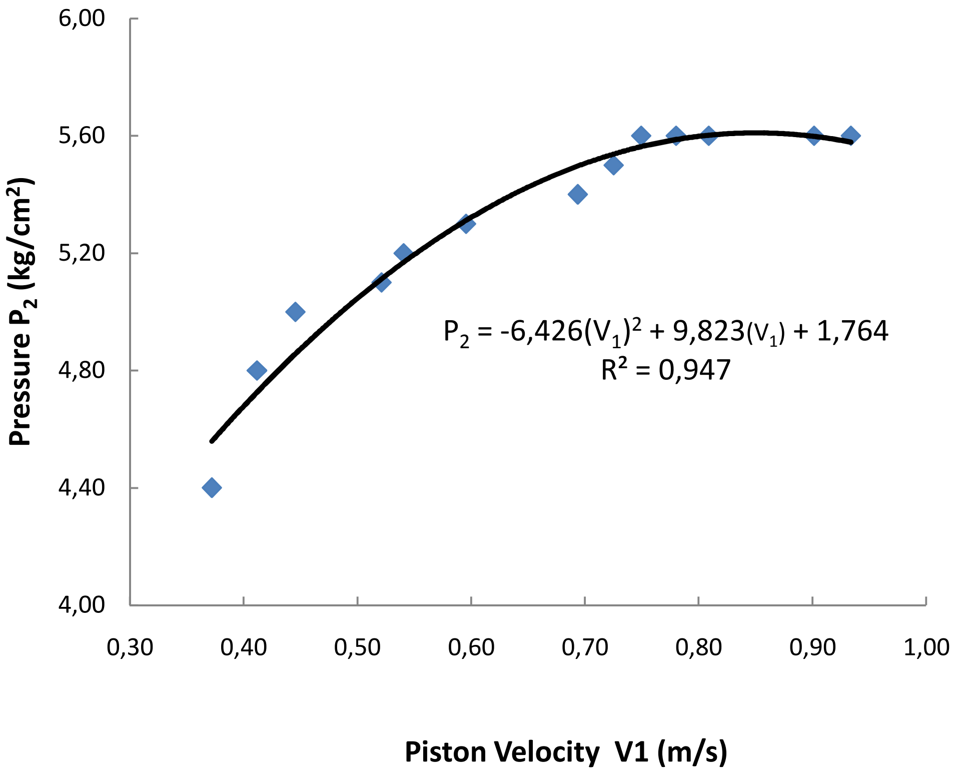

Figure 4.22 Change in pressure (P_2) with respect to piston velocity

4.3.4.2 Temperature

The effect of the change in pressure P_2 on the thermal efficiency can be calculated as follows. Figure 4.23 demonstrates the linear relation between the thermal efficiency and pressure P_2. In order to evaluate compression ratio, displacement and combustion chamber volumes must be calculated. In volume calculation, geometrical values are used and then the compression ratio, CR, is evaluated.

$$CR = \frac{V_c + V_d}{V_c}$$

Determination of pressure P_2 after compression

$$P_1 V_1^k = P_2 V_2^k$$

$$P_2 = P_1 \left(\frac{V_1}{V_2} \right)^k$$

$$P_2 = P_1 * CR^k$$

Calculation of thermal efficiency in theory

$$\eta = 1 - \frac{1}{CR^{k-1}}$$

When calculating thermal efficiency, the same formula is used but instead of k, corrected n coefficient is used in practice (n=1.3).

$$\eta = 1 - \frac{1}{CR^{n-1}}$$

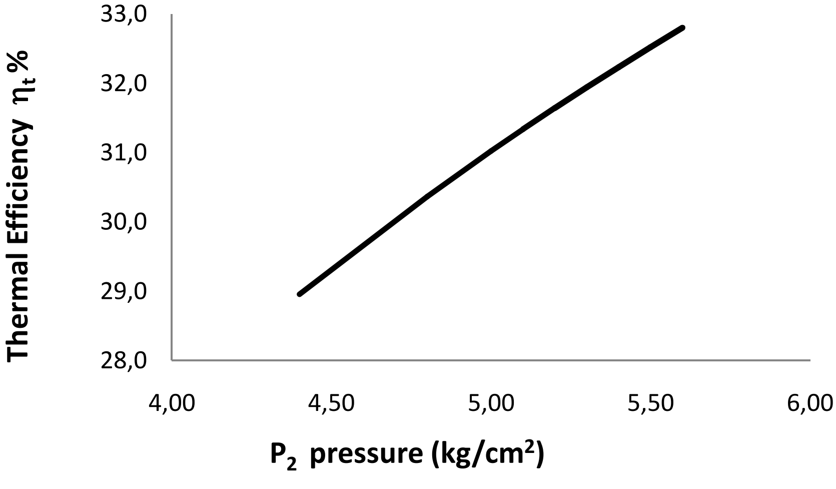

Figure 4.23 Change in pressure (P_2) with respect to thermal efficiency

4.3.4.3 Injection Time

With the newly designed unit, trials at different injection times were performed. Therefore, different piston velocities were obtained for the same amount of fuel consumption. As a result, it is understood that the injection time affects the burning quality. Trials carried out at different injection times showed that the injection time of 40 degrees before the TDC, reached a maximum velocity of 12 m/s (Figure 4.24).

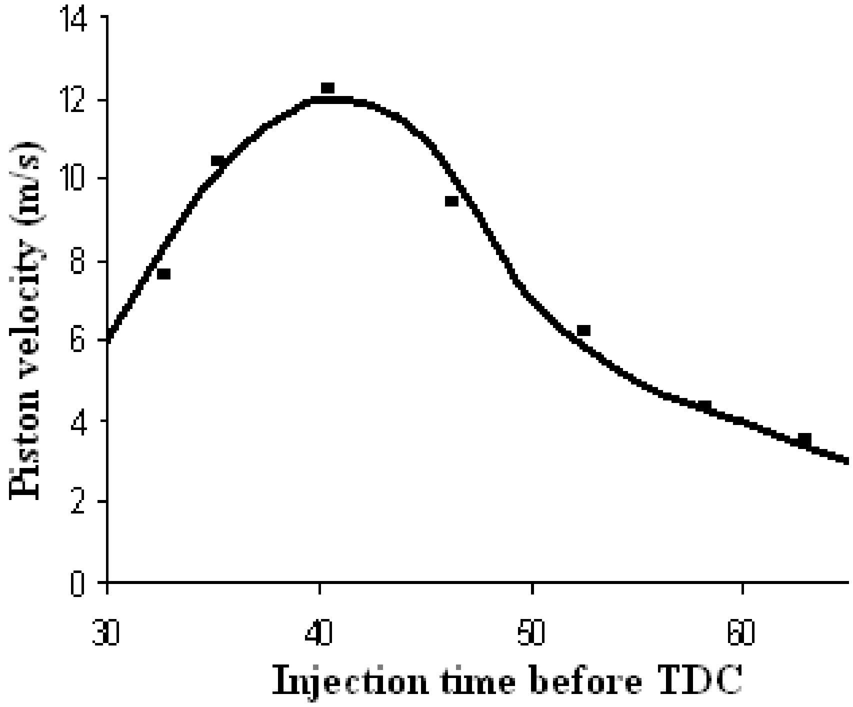

Figure 4.24 Ram velocities with respect to injection time

4.3.4.4 Fuel Rate

The amount of fuel that is injected into in the cylinder is one of the parameters that affect the amount of the energy used for forging. This can be seen in the following formula:

Q_{in}= m_{fuel}(kg)* Thermal value of gasoline (kj/kg)

As seen in the formula, the energy formed in the combustion chamber is directly proportional to the amount of fuel. The energy produced in combustion chamber decreases in ratios below and above the ideal air-fuel mixture ratio, which is 14.6/1.

4.4 MEASURMENT UNIT

4.4.1 Magnetic Ruler

In order to observe the changes in the performance of the HERF hammer, ram velocity must be measured. A magnetic piece was constructed for velocity measurement. It is attached to the ram so that they move together. Velocity measurement unit is fixed to the frame as shown in Figure 4.25.

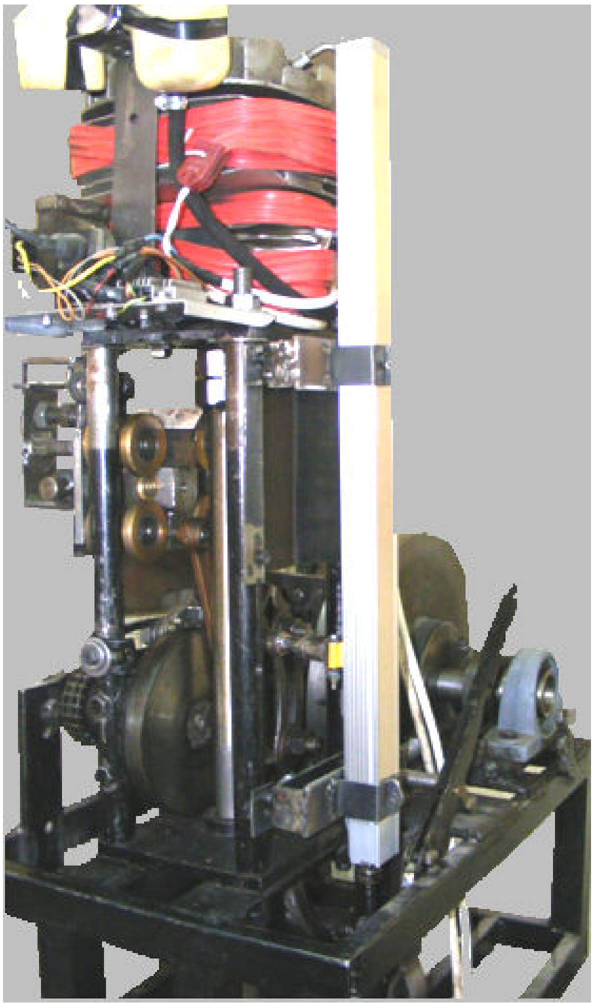

Figure 4.25 Specifically-designed magnetic piece and velocity measurement schedule

Elapsed time interval is measured with special software and hardware on the PC. Figure 4.26 visualizes a graphical view of the software used. This software also provides velocity-time and acceleration-time graphics.

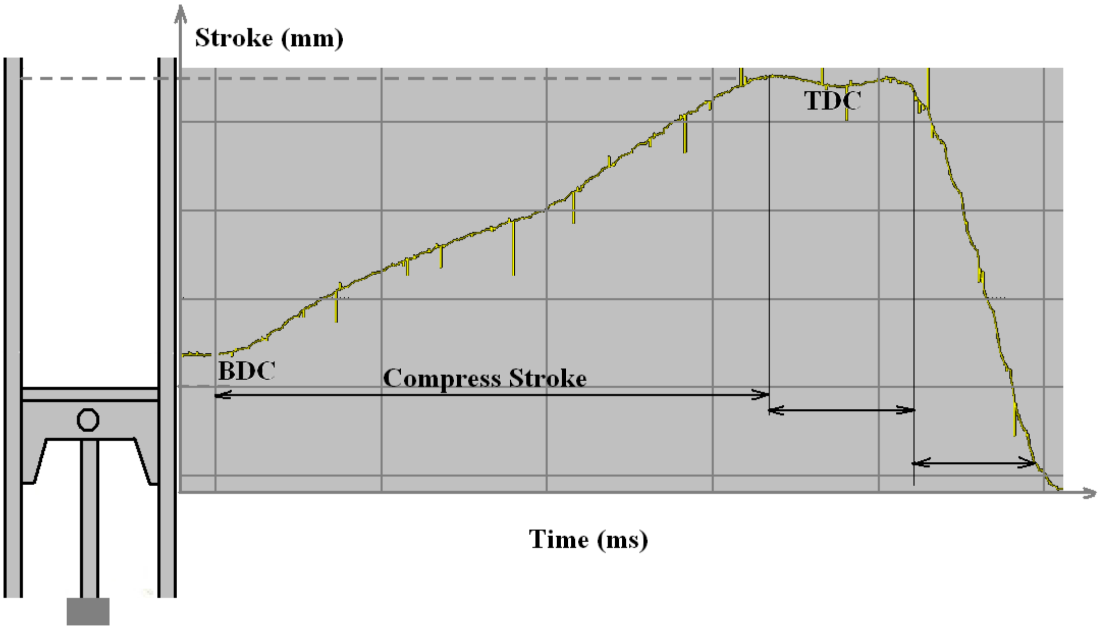

Figure 4.26 Stroke-time graph output of used software

4.4.2 Loadcell

In order to observe the changes in the performance of the HERF hammer, forming load must be measured. Load is measured with loadcell. It was attached to the main body so that they move up and down. Loadcell mounting between main body and lower die are illustrated in Figure 4.27a. Elapsed time interval is measured sensitively with special software and hardware on the PC. This software also provides load-time as shown in Figure4.27b.

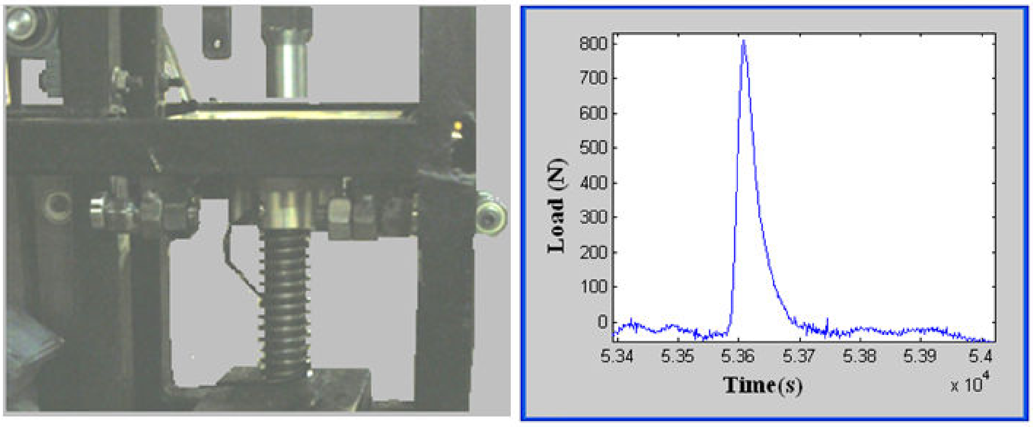

(a) (b)

Figure 4.27 (a) Loadcell mounting, (b) Load time curve

CHAPTER 5

EXPERIMENTAL STUDY

5.1 INTRODUCTION

In this chapter, experimental work carried out in this study is explained. In order to compare the performance of the designed and constructed HERF hammer with those of the Conventional and Hydraulic presses, open die forging and blanking operation were performed on the three different types of materials. When selecting the materials which were used in the experimental studies, their availability and machinability were taken into account. Aluminum, St37, and AISI304 were selected as examples of soft, medium hard and hard materials, respectively. The chemical compositions, mechanical and thermal behavior of these materials are given in the following section. Open die forging and blanking operations are the two main working processes in the press application.

5.2 MATERIALS

5.2.1 AISI 304 Stainless Steel

Ø5x10 mm cylindrical AISI 304 stainless steel billets were used for the open die forging applications. 2 mm thickness sheet samples were cut for the blanking operation. The chemical composition and mechanical properties of the examined stainless steel is presented in Table 5.1. Stress-strain curves that depend on the strain rate and temperature of AISI304 stainless steel that was used in the open die forging and piercing operations were given in Figures 5.1 and 5.2, respectively.

Table 5.1 Chemical composition of AISI 304 stainless steel

Designation	Chemical Composition						
	C	Si	Mn	P	S	Cr	Ni
AISI 304 SS	0.07	0.75	1.98	0.04	0.02	18.4	9.9

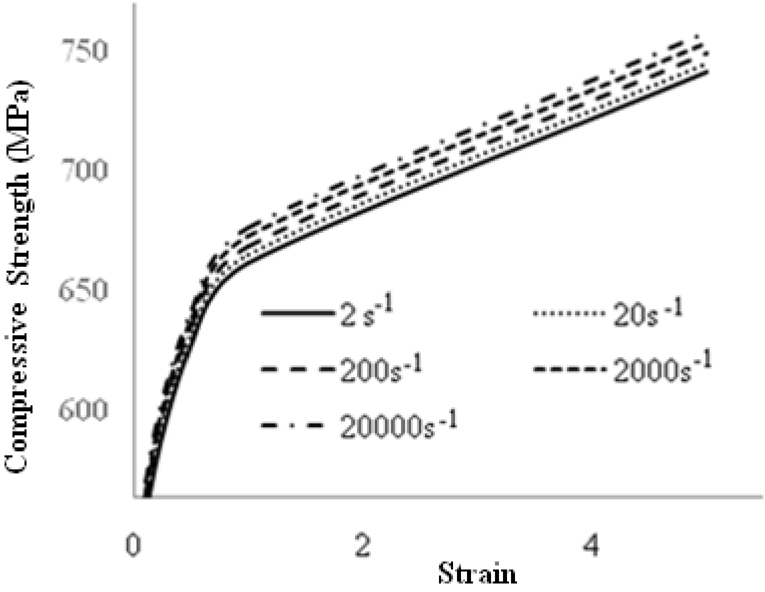

Figure 5.1 Stress-strain curve of AISI 304 depending on strain rate

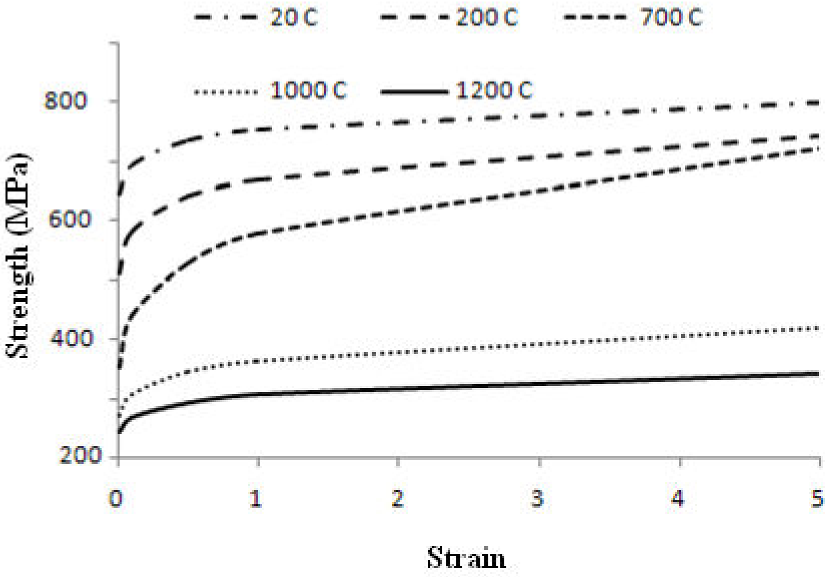

Figure 5.2 Stress-strain curve of AISI 304 depending on temperature

5.2.2 St 37 Mild Steel

Ø5x10 mm cylindrical St37 low carbon steel billets were used for the open die forging applications. 3.5 mm thickness sheet samples were cut for the blanking operation. The chemical composition and mechanical properties of the examined low carbon steel is also presented in Table 5.2, and Table 5.3, respectively.

Table 5.2 Chemical composition of St37 mild steel

Designation	Chemical Composition Wt%					
St37 Mild Steel	C	Si	Mn	P	S	Other
	0.17	0.30	0.40	0.045	0.050	0.009

Table 5.3 Mechanical properties of St37 mild steel

Designation	Mechanical Properties			
St37 Mild Steel	Hardness (HVN)	Ultimate tensile strength (MPa)	Elongation (%)	Yield strength (MPa)
	150	360	24	240

5.2.3 Aluminum

Aluminum that was an example for the soft materials is used as in the open die forging and piercing operation investigations. Ø5x10 mm cylindrical aluminum billets were used for the open die forging applications. 5mm thickness sheet samples were cut for the blanking operation. The chemical composition and mechanical properties of the aluminum is also presented in Table 5.4, and Table 5.5.

Table 5.4 Chemical composition of aluminum

Designation	Chemical Composition Wt%					
Aluminum	Al	Si	Mn	Fe	Cr	Other
	99.42	0.111	0.066	0.333	0.014	0.031

Table 5.5 Mechanical properties of aluminum

Designation	Mechanical Properties			
Aluminum	Hardness (HVN)	Ultimate tensile strength (MPa)	Elongation (%)	Yield strength (MPa)
	50	100	34	70

5.3 EQUIPMENT

In the open die forging operations, three different types of presses, namely, hydraulic (HP), conventional mechanic press (CP), and high energy rate forming (HERF) hammer were used. To compare the quality of the cutting surfaces, laser cutting machine (LCM) was also used. In the following parts of this section, details about the used presses were given. Moreover, information about the mechanical properties and chemical compositions of the used die materials and die types were presented.

5.3.1 Machines

5.3.1.1 Hydraulic Press (HP)

The hydraulic press was used in the experiments (Figure 5.3). It has a capacity of 60 tons and the upper ram is stationary. However, the lower ram and the die seat, move in upward and downward directions. The velocity of die seat is controlled by means of the velocity control handle. As the seat of the press goes upwards or downwards, the drum rotates by means of the pulleys. Force-distance graphic is obtained on the scaled (millimeters) paper rolled on the drum. Rising and lowering the press bed is carried out by the loading and unloading arm.

Hydraulic press was used for the open die forging of Ø5x10 mm cylindrical billets of aluminum, St37 mild steel, and AISI304 stainless steel. This pres is located in Materials Laboratory of Mechanical Engineering, Gaziantep University. It was also used for the blanking operations of the 5 mm thickness sheet of aluminum samples, 3.5 mm thickness sheet of St37 mild steel, and 2 mm thickness sheet of AISI304 stainless steel. Specimens were punched at the 10 mm diameters. Punching speed of the Hydraulic Presses is at nearly quasistatic (0.01m/s).

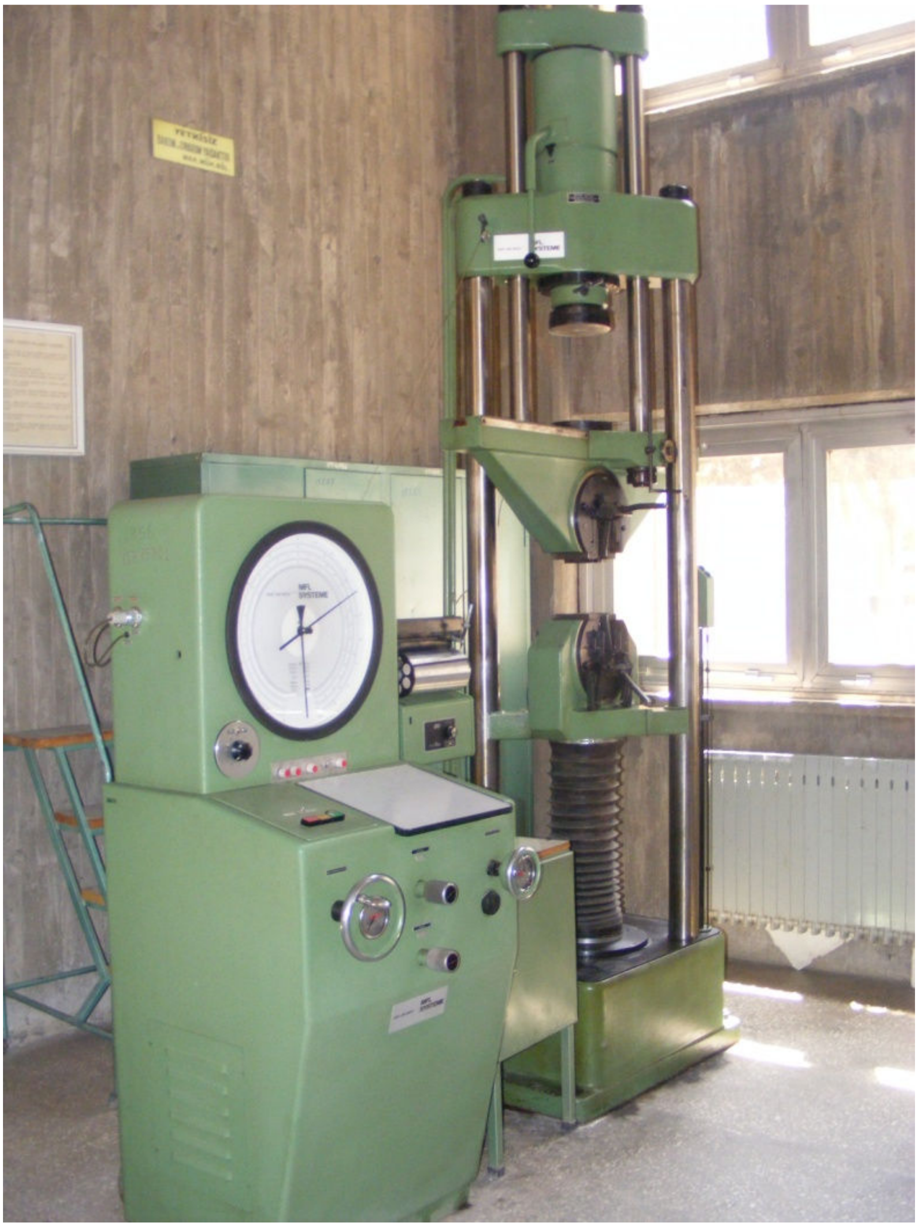

Figure 5.3 Hydraulic press used for experimental studies

5.3.1.2 Conventional Mechanical Press (CP)

A 30 tons capacity C type eccentric press (Dirinler, model CDCS 30T PY) is used as shown in Figure 5.4. This pres is located in Die Laboratory of Vocation School, Gaziantep University. Its punching speed is about 0.2 m/s. CP was used for the open die forging of Ø5x10 mm cylindrical billets of aluminum, St37 mild steel, and AISI304 stainless steel. It was also used for the blanking operations of sheet materials such as aluminum, St37 mild steel and AISI304 stainless steel samples with thickness of 5, 3.5 and 2 mm, respectively. Specimens were punched to Ø 10 mm.

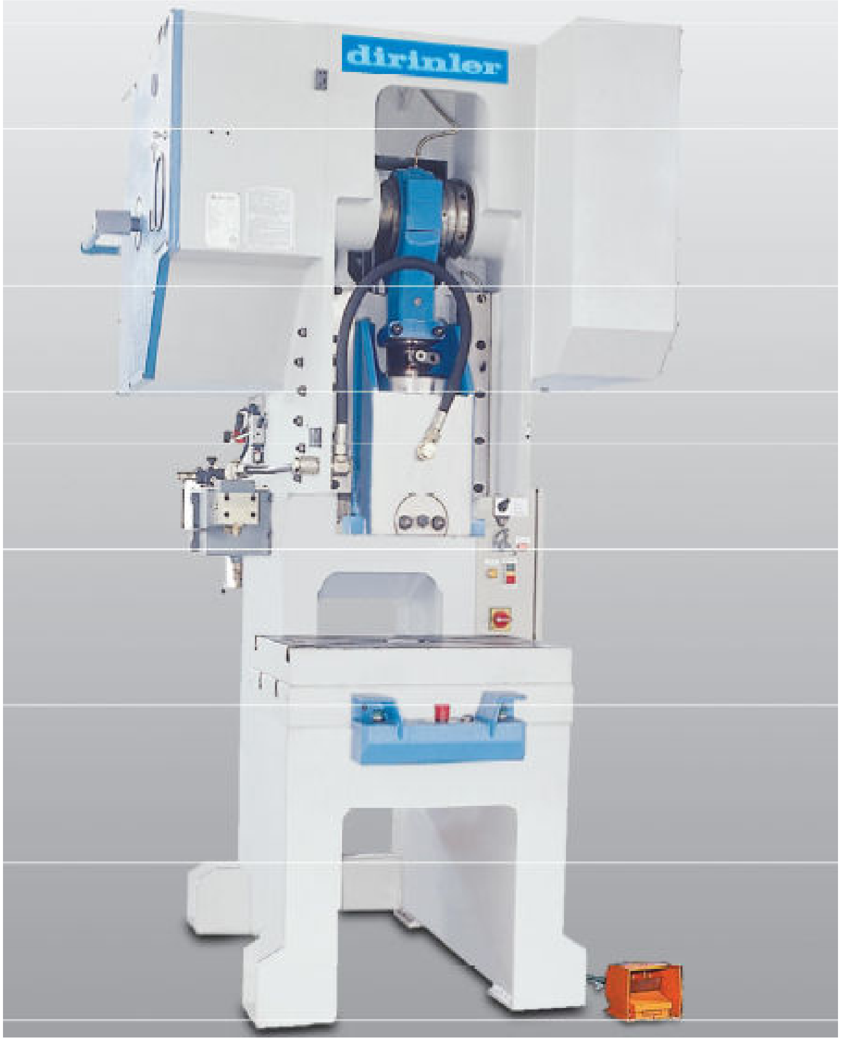

Figure 5.4 Eccentric press used for experimental studies

5.3.1.3 High Energy Rate Forming (HERF) Hammer

The HERF hammer, explained in Chapter 4, was used for high speed forging and blanking experiments. The position of the fixed magnet is detected by a magnetic ruler. The loadcell placed under the lower die provides the value of the load transferred to workpiece. A data logger (10^6 data/second) is used so as to transfer the data from the magnetic ruler and the loadcell to a computer. A schematic view of the magnetic ruler, the loadcell, and the connection of data collection devices is given in Figure 5.5. It was observed that prototype machine can reach the 12 m/s punch velocity so it can be called as high energy rate forging machine. As it is known if a machine had higher than 5 m/s punch velocity it can be called as high energy rate forging machine **(Semiatin, 1988).**

HERF was used for the open die forging of Ø5x10 mm cylindrical billets of aluminum, St37 mild steel, and AISI304 stainless steel. HERF was also used for the blanking operations of the 5 mm thick sheet of aluminum samples, 3.5 mm thick sheet of St37 mild steel, and 2 mm thick sheet of AISI304 stainless steel.

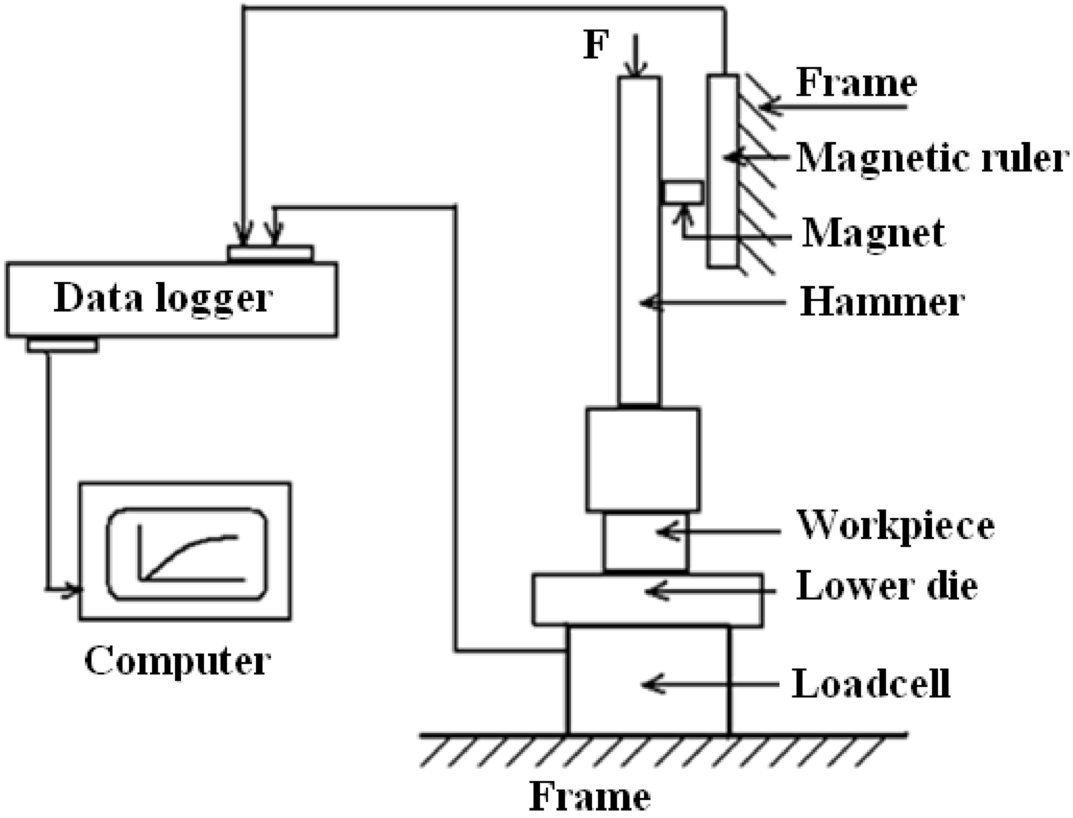

Figure 5.5 Schematic view of magnetic ruler, loadcell and data-logger

5.3.1.4 Laser Cutting Machine (LCM)

The laser cutting machine and its control unit that was used throughout experiments was presented in Figure 5.6. TRUMPF's TruLaser 3200 flat sheet laser cutter was used. This machine is located in GAP METAL, Gaziantep. It offers unparalleled mix of speed, versatility and precision, equipped with rapid changeover and setup features, and are compatible with advanced automation. This type of laser machines operates on the principle of "flying optics", the cutting head moves while the workpiece stays stationary to ensure maximum performance. AISI304 stainless steel specimens were cut by using this laser machine. When cutting the specimens, laser machine adjust and optimize the cutting parameters.

Figure 5.6 Laser cutting machine used for experimental studies

5.3.2 Dies

SAE 4140 is used for the forging and the blanking dies. Mechanical and thermal properties of the SAE 4140 die material were given in Table 5.6

Table 5.6 Mechanical and thermal properties of the specifications of the die material SAE 4140

Yield Stress	650 MPa
Maximum Elongation	12%
Hardening Temperature for Quenching in Water	820-860 ºC
Hardening Temperature for Quenching in Oil	820-860 ºC
Vickers Hardness	560 HV

5.3.2.1 Forging Die

20x40x40 mm blocks for upper and lower dies were manufactured by using SAE 4140 material. The dies were heated up to 1000 ^{o}C in an electric furnace and then they were quenched in water for the hardening to 55 Rockwell C. Forming surfaces of the dies was ground to improve the surface quality. Figure 5.7 illustrates forging dies and the forged billets.

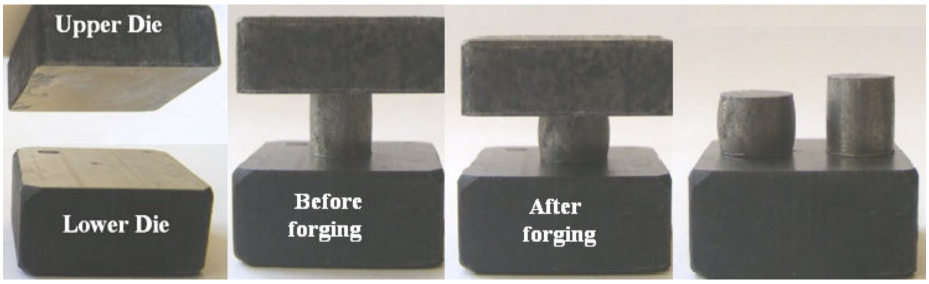
Upper Die
Lower Die
Before forging
After forging

Figure 5.7 Forging dies and the billets

5.3.2.2 Blanking Die

Figures 5.8 and 5.9 present the picture and schematic views of the blanking die, respectively. SAE 4140 is used as a blanking die material. The material stock is quenched to about 55 RC. It is manufactured using wire EDM for Ø10mm in diameter with five different clearances and then ground for sharpening.

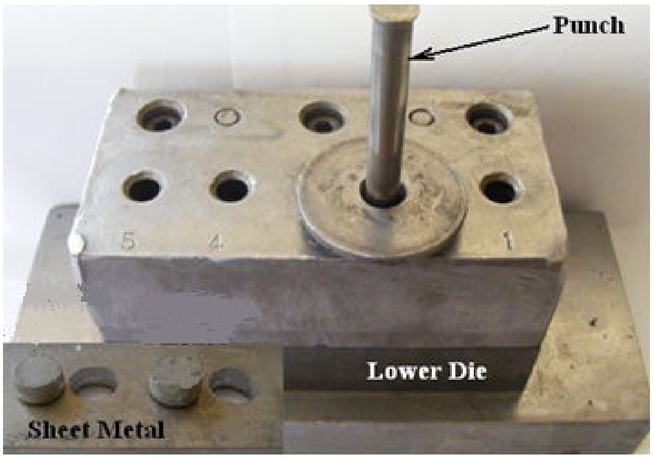
Punch
5
4
1
Lower Die
Sheet Metal

Figure 5.8 Photo of the blanking die set and the sheet.

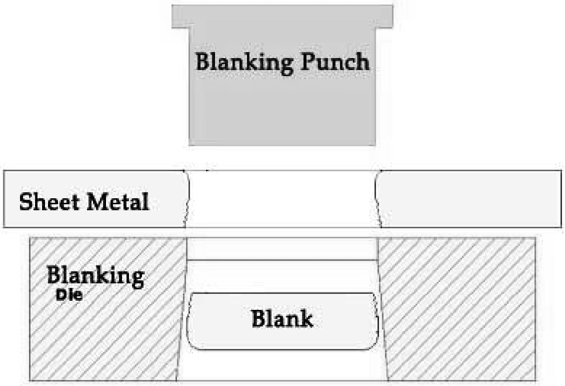
Blanking Punch
Sheet Metal
Blanking Die
Blank

Figure 5.9 Schematic view of the blanking die, sheet metal and the punch

5.4 EXPERIMENTAL PROCEDURES

Open die forging operations on the cylindrical billets and blanking operations on the sheet materials are performed to examine the performance of the designed HERF hammer.

5.4.1 Load and Energy Measurements

Loads versus strokes were measured by using a magnetic ruler and loadcell in the forging and blanking processes, respectively. Area under the load-stroke curve gives energy that is needed to the forge and cut the materials. Load stroke graphs of the each studied materials were obtained for the each press in the open die forging. In the blanking process, load stroke graphs of the each studied materials under different clearances were drawn for the each press type. In Figure 5.10, load-stroke curve and blanking surface of the 5 mm thick aluminum sheet which was blanked by the HP was given.

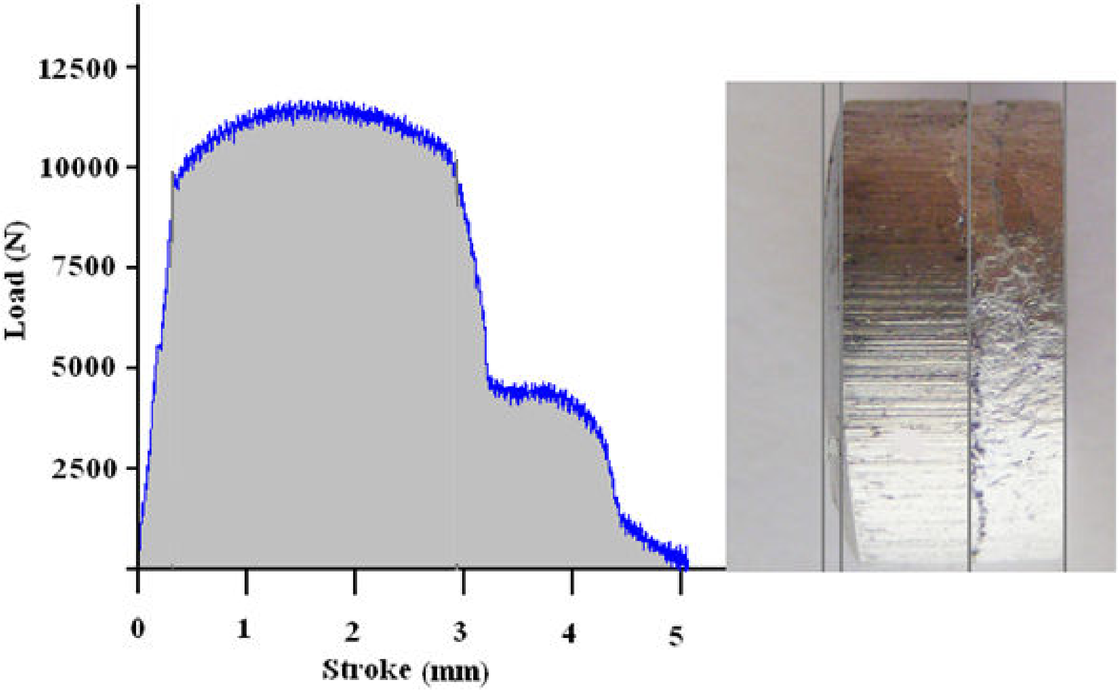

Figure 5.10 The load-stroke diagram and the surface obtained in blanking operation

Ring compression test was conducted to find out the friction coefficient of the open die surfaces. To carry out the test, the standard ring specimen ratio of 6:3:2 was used.

The outer and inner diameters of the ring are D_0 = 12.0mm and d_0 = 6.0 mm, respectively, and the height is H_0 = 4.0 mm. Figure 5.11 shows a ring specimen used in the ring compression tests.

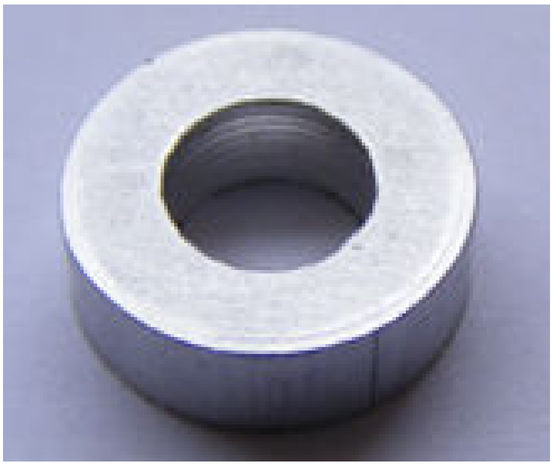

Figure 5.11 A sample ring specimen

5.4.2 Metallographic Examinations

Metallographic examinations were carried out on the blanked specimens to observe the micro-structures of the sheared surfaces. For this purpose, sheets were semi-blanked and cut into two halves through cross section. They were hot mounted using Bakelite powder and polished. Then the specimens were etched using 2% nital and microstructures were observed under light microscope.

5.4.3 Surface Roughness Measurements on the Sheared Surfaces

The surface roughness was evaluated using a Talysurf stylus-type profilometer. This machine is located in innovation center of University of Gaziantep. The surface roughness values were central-line average (Ra), and were used to evaluate the quality of the specimen surface. Each surface roughness was determined by averaging ten measurements done at various portions on the shear surface for each cutting condition. The surface roughness measuring unit is given in Figure 5.12.

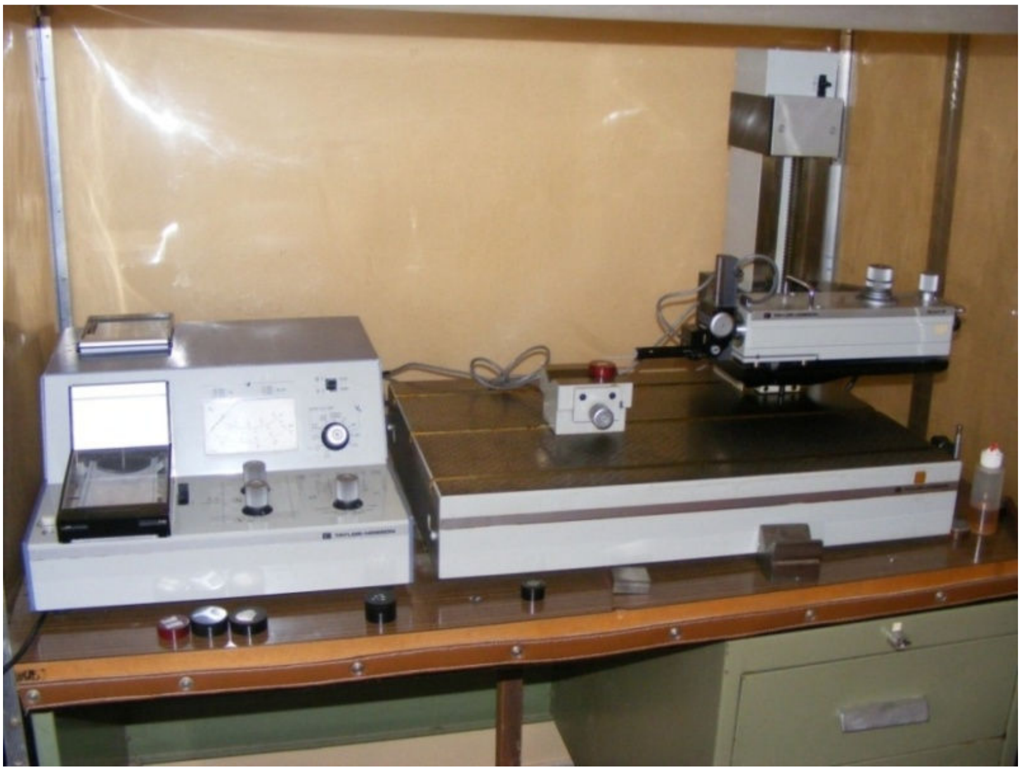

Figure 5.12 The surface roughness measuring unit.

5.4.4 Corrosion Tests on the Sheared Surfaces

Shear surface corrosion tests of the specimens that were cut under different blanking speed were performed. To perform the standard corrosion test, the working electrodes (WE) were polished with silicon carbide papers from 3 through 1 to 0.5 µm and velvet, rinsed with the twice distilled water, washed in acetone, rinsed with the twice distilled water again and then dried in the air. For cyclic voltammeter measurements, de-aerated sulphuric acid solution by bubbling argon gas for at least 45 min before each measurement as electrolyte was used. Counter electrode was a Pt gauze electrode for polarization and corrosion measurements. The reference electrode used in all experiments was a saturated calomel electrode (SCE). All the potentials are referred against SCE (**Stephen and Bernard, 2003**).

The electrochemical behaviors of the specimens were analyzed in 3 wt.% NaCl aqueous solution at room temperature in a Pyrex glass cell. The corrosion behaviors of the samples were investigated by a potentiodynamic polarization technique. Polarization measurements were performed with an electrochemical analyzer/workstation (Model 1100, CH Instruments, USA) with a three-electrode configuration. The exposed area of the specimens was about 0.5 cm^2. The specimens were covered with a cold setting resin and immersed into the solution until a steady Open Circuit Potential (OCP) was reached. After equilibration, polarization started at a rate of 1 mV/sn. Sulphuric acid solution of 0.5 M was used as electrolyte for the OCP measurements. At least four parallel measurements were done with freshly polished samples. For cyclic voltammeter measurements the cycle began at a cathodic over-potential of − 1200 mV and the scan was stopped as soon as the specimens reached the anodic over-potential of 1200 mV. Figure 5.13 shovs the setup in which the experiments were carried out, the computer used for data collection and a view of the software used for experiments. This setup is located in physic laboratory in university of Kilis 7 Aralık.

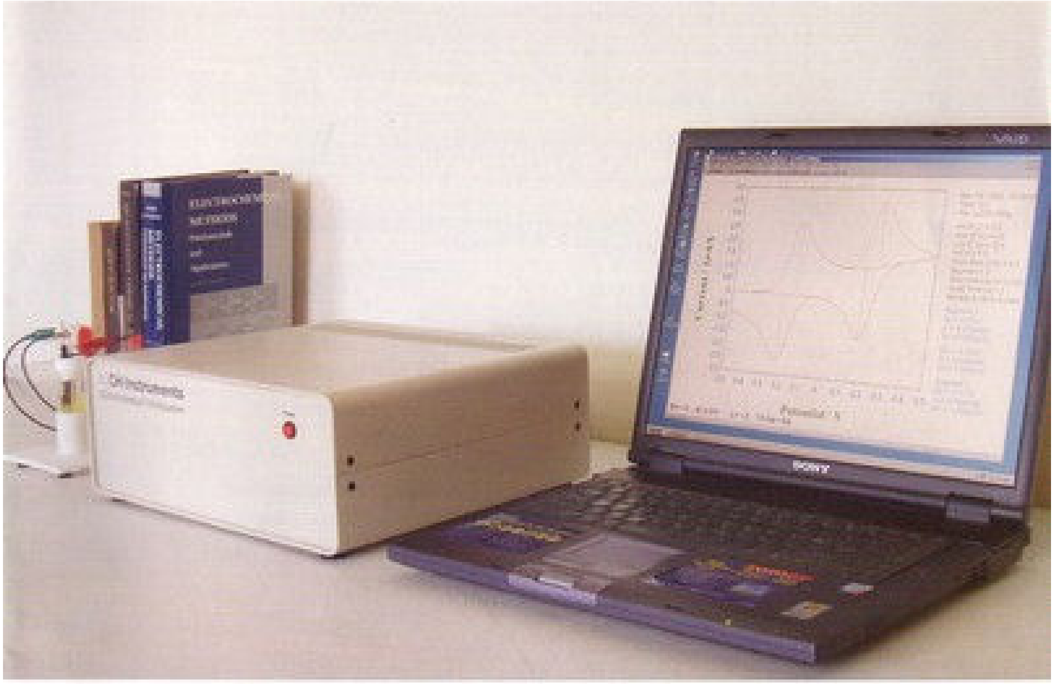

Figure 5.13 The Corrosion test equipment

5.4.5 SEM Observations

High resolution images of the morphology of a specimen and precise composition analysis are two main functions of the scanning electron microscopy (SEM), which makes it one of the most useful techniques in materials research. This machine is located in University of Gaziantep. These two functions are realized by a scanning electron probe and a moving sensor/receiver for secondary x-rays respectively. In addition, SEM can be applied to both metals and non-metals. For non-metal materials, they have to be plated with a layer of silver so that they can get a good conduction for SEM operation. The surfaces of blanked materials before and after corrosion tests were examined by SEM. Figure 5.14 provides a view of the SEM machine used for experiments.

GEMINI
SUPRA 50VP

Figure 5.14 SEM machine used for experiments

CHAPTER 6

RESULTS AND DISCUSSIONS

6.1 INTRODUCTION

The results and discussion of the experimental studies are given in this chapter. Details of the load and energy measurement of the forging and blanking and amount of barreling in forging process are presented in section 6.2. Based on the results obtained from blanking studies, work-metal thickness, a new die clearance per site graphic is proposed and also presented in the section 6.2. Surface quality, surface roughness and corrosion behavior of the blanking surfaces are presented in the sections 6.3, 6.4, 6.5, respectively.

6.2 LOAD AND ENERGY

6.2.1 Forging Load and Energy

6.2.1.1 Load and Energy Comparison According to Forging Speed

Ø5x10 mm cylindrical aluminum, mild steel, and stainless steel billets were forged at the hydraulic, conventional, and high energy rate forming machines. Figure 6.1 presents the load-stroke curves of the aluminum depend on the forging speed. It is clearly presented in the Figure 6.1 that the lowest required forging energy of aluminum was measured at the high energy rate forging machine. Moreover, the energy required in the high energy rate forming machine process was approximately 1.5 times lower than those of conventional and hydraulic machines. Figure 6.1 also demonstrates that the required energy for the forging of aluminum at the conventional press was a little lower than the hydraulic press. The maximum force for forging of the aluminum was measured at the hydraulic press as 7.5kN.

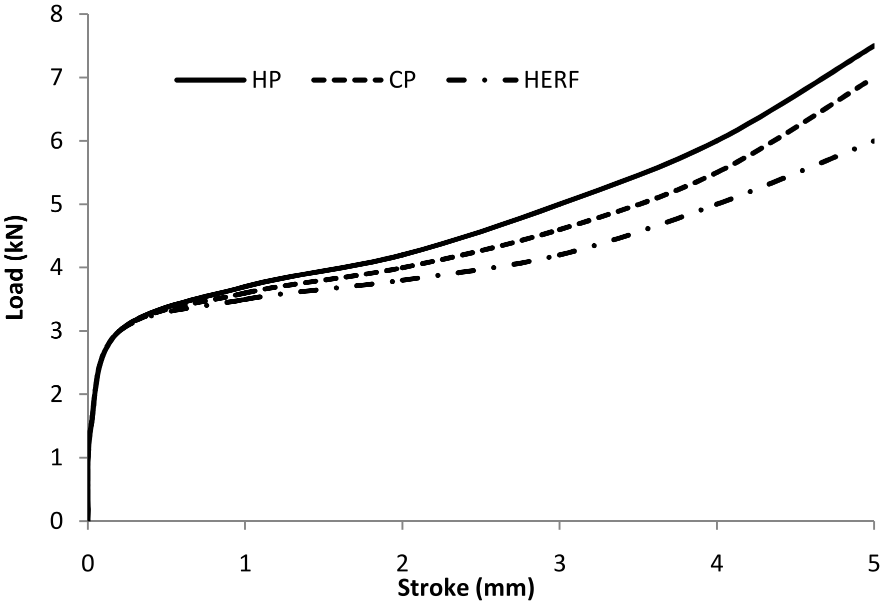

Figure 6.1 Load-stroke curves of the aluminum depending on the forging speed

Figure 6.2 illustrates the load stroke curves of the mild steel depend on the forging speed. As in the case of, the lowest required energy for forging of the mild steel was measured at the high energy rate forming machine. When the presses were ranked according to the lowest required energy for forging of the mild steel, it was listed in the order of high energy rate forging machine, conventional press, and hydraulic press. The maximum force for forging of the mild steel was measured at the hydraulic press as 13kN.

Figure 6.3 illustrates the load-stroke curves of the stainless steel depend on the forging speed. The trend of the load-stroke curve of the stainless steel was similar to the load-stroke curves of the aluminum and mild steel. The difference among the load-stroke curves of the aluminum, mild steel, and stainless steel was the value of the maximum forces which was used for the forging of the studied materials. As was expected, when the hardness of the materials increased, the required energy for forging of the material was also increased. As in the aluminum and mild steel cases, the lowest forging energy was measured at the HERF in the stainless steel. The rank of the presses according to the lowest required energy for forging of the stainless steel was same as the aluminum and mild steel. Collected data were summarized in Table 6.1 in order to explain the curves in Figures 6.1, 6.2, and 6.3 much better.

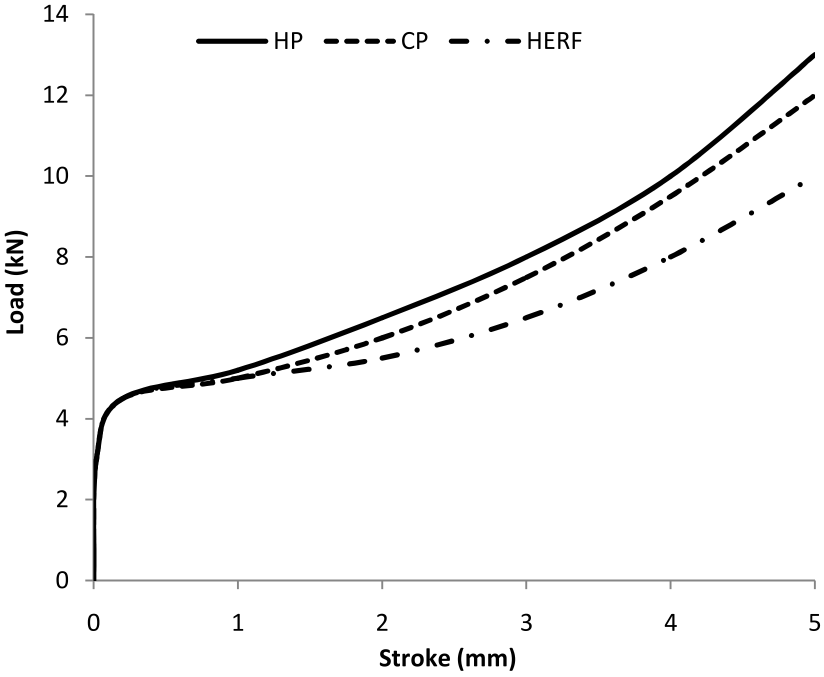

Figure 6.2 Load-stroke curves of the mild steel depending on the forging speed

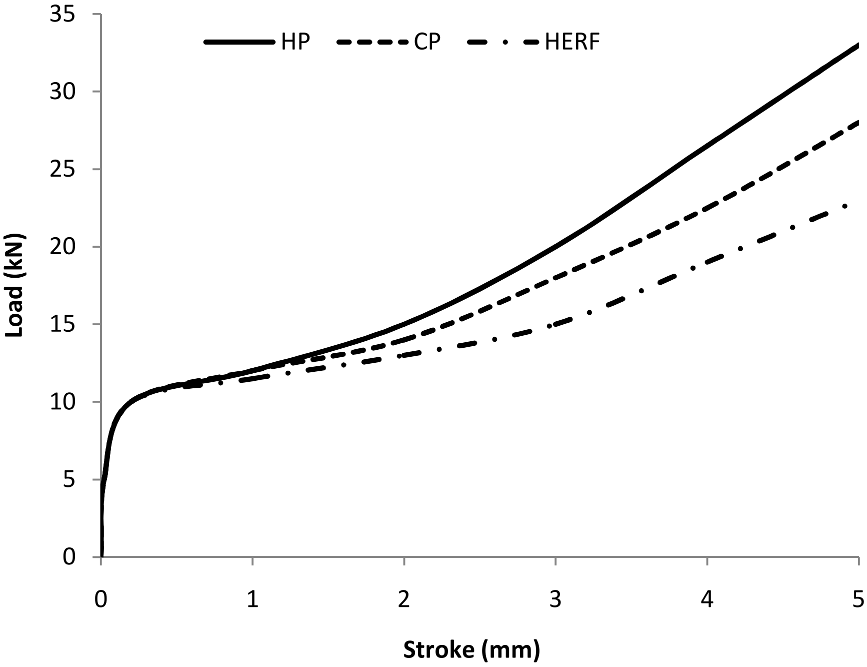

Figure 6.3 Load-stroke curves of the stainless steel depending on the forging speed

Table 6.1 Maximum load and energy of forging processes

Materials	Used Forging Machine					
	HP		CP		HERF	
	Max. Load(kN)	Max. Energy(J)	Max. Load(kN)	Max. Energy(J)	Max. Load(kN)	Max. Energy(J)
Aluminum	7,5	24	7	22	6	18
Mild Steel	13	40	12	35	10	30
Stainless Steel	33	88	28	83	23	70

6.2.1.2 Amount of Barreling in Forging

It is well known that the less the barreling the less required energy for the closed die forging. Figure 6.4 shows the main forging stages of a workpiece during the closed die forging operations. Figure 6.4a illustrates the first stage of a forging operation. Workpiece placed in the closed die and force applied on the workpiece. Figure 6.4b demonstrates second stage where the plastic region and barreling starts. Third stage is illustrated in Figure 6.4c in which central portion of the workpiece contacts the sides of the die surfaces. Because of that contact, required energy for the forging of the workpiece increases drastically. The stage illustrates complete filling, thus, as shown in Figure 6.4d, workpiece gained the shape of the die.

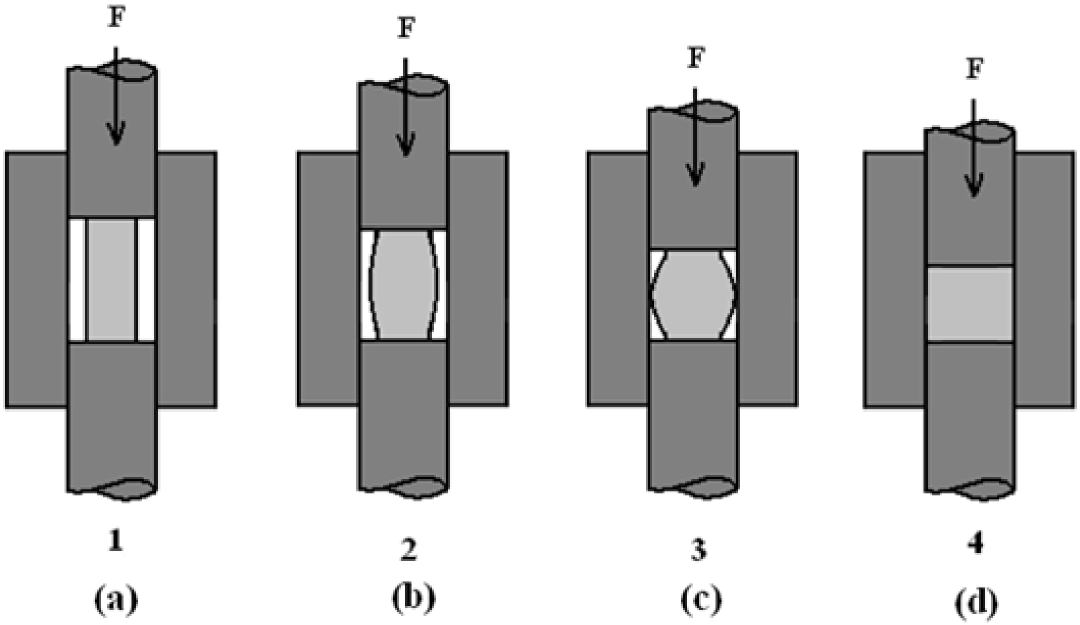

Figure 6.4 Main stages at the closed die forging operations

In Figure 6.5, trend 1-2-3-4 presents typical load-stroke curve for closed-die forging. In the typical closed die forging, because of the barreling effect, workpiece needs more forging energy. However, the later the formation of the barreling is, the less the required energy for forging of the workpiece. The reason behind this fact is that central points of the workpieces contacts with the sides of the die surfaces so required energy for forging of the workpieces increases drastically. The trend 1-2-3'-4' in Figure 6.5 illustrates load-stroke curve of a workpiece in that the formation of barreling in the forging operation was late. The difference between two aforementioned load-stroke trends illustrates an energy gain as a result of the late formation of barreling.

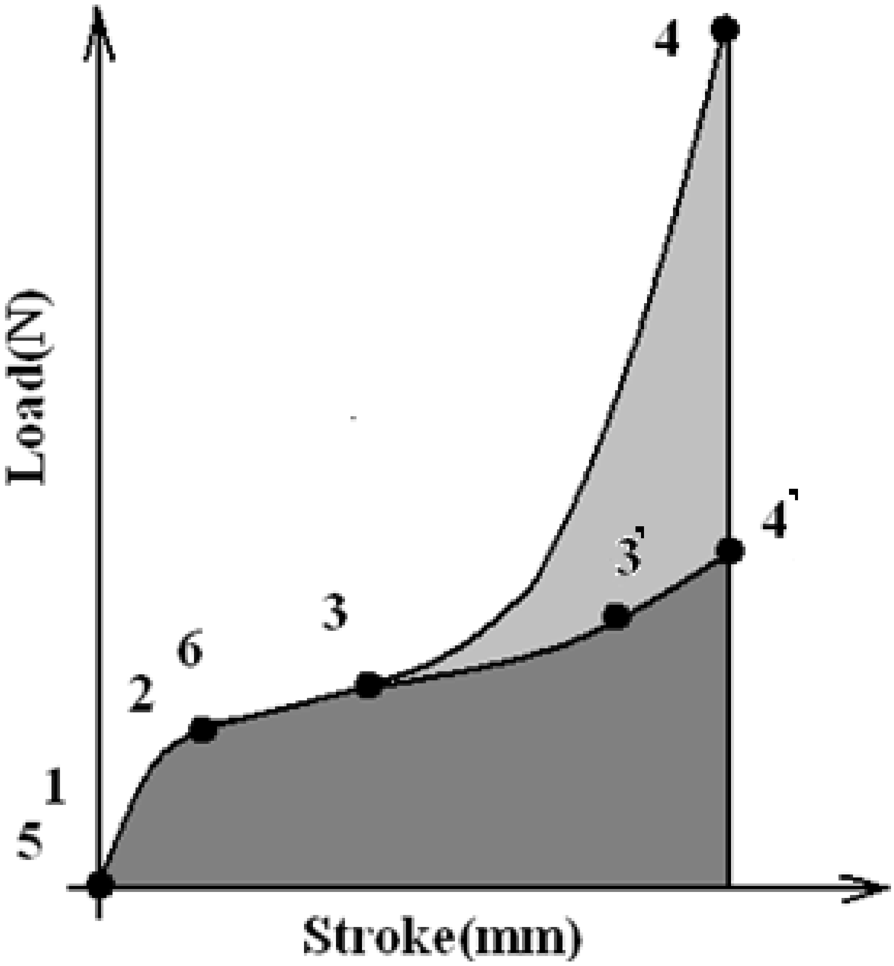

Figure 6.5 Schematic view of load-stroke curve of different forging speed

Figure 6.6a shows the shape of cylindrical material before the forging. The diameter and height of the cylinder before forging are shown as d_o, h_o, respectively. Figure

6.6b gives a schematic view of the shape of cylindrical material after the forging. D_a is the diameter of surface of workpiece that contacts the upper die, while D_c is the diameter of surface of workpiece that contacts the lower die, and D_b is the diameter of the central point of the workpiece after the forging operation.

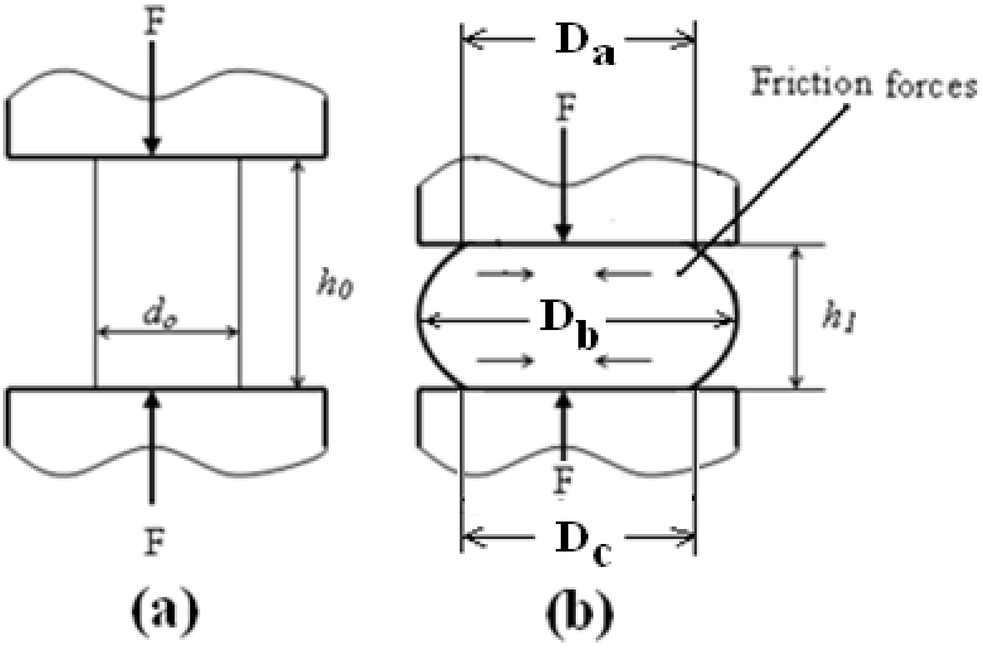

Figure 6.6 Dimensions of workpiece with barreling

Figure 6.7 provides the views of Aluminum, St 37, AISI 304 before forging in open die operation and after forging with presses that have different forging speeds. The height of the billets were reduced 50% to observe the barreling effect. D_a, D_c and D_b values of each sample is given in Table 6.2.

The difference between D_a and D_c is due to unidirectional forging (punch is moving while anvil is stationary). Amount of barreling is the difference between D_b and D_a (or D_b and D_c). The results show that barreling is getting smaller with increasing speed. This is due to change in friction condition at the contact surface of the workpiece and the die (punch and anvil).

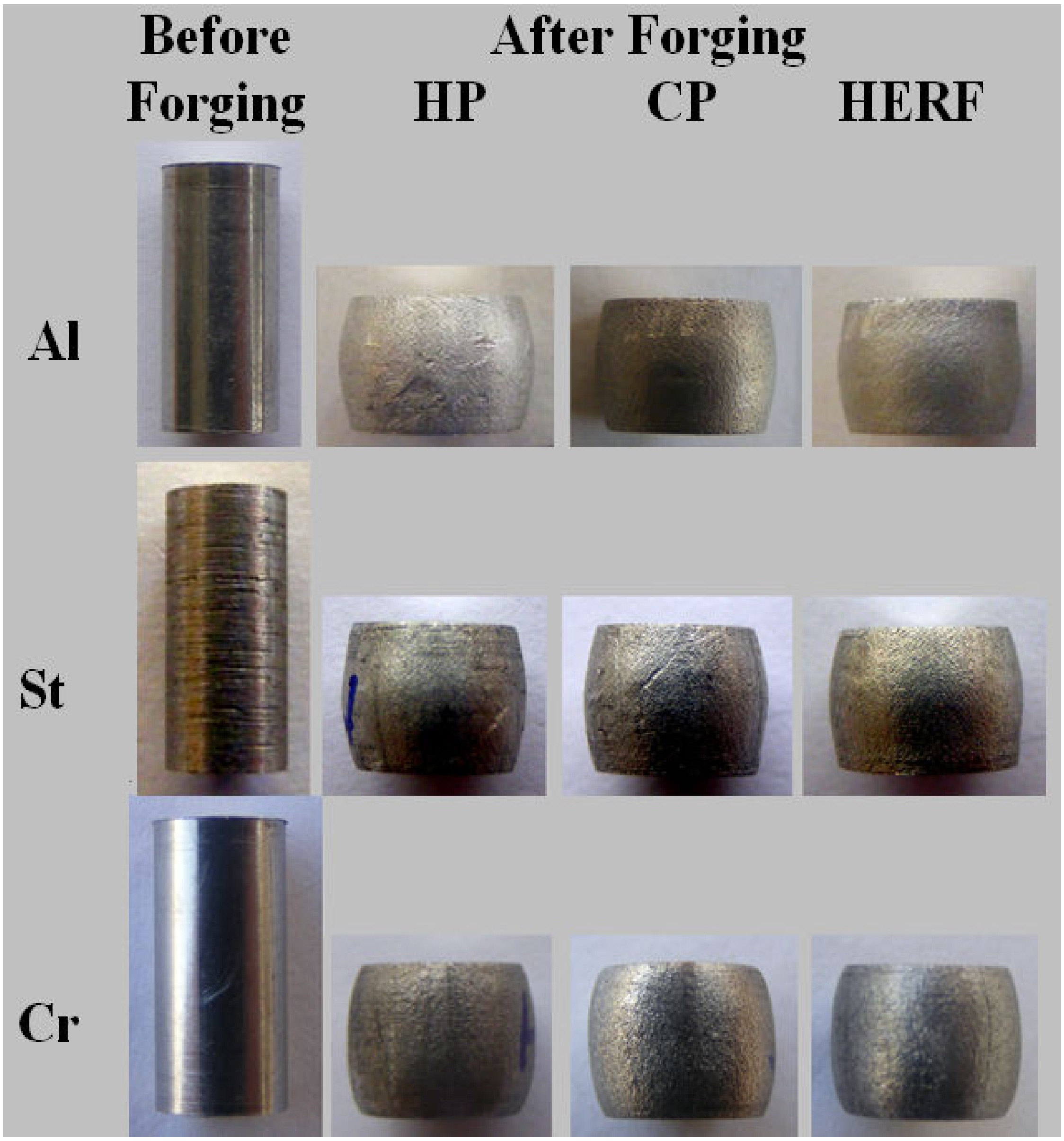
Before Forging
After Forging
HP
CP
HERF
Al
St
Cr

Figure 6.7 Before and after open die forging views

Table 6.2 Geometric values obtained from forging at different speeds

Materials	Used Forging Machine								
	HP			CP			HERF		
	D_a (mm)	D_b (mm)	D_c (mm)	D_a (mm)	D_b (mm)	D_c (mm)	D_a (mm)	D_b (mm)	D_c (mm)
Aluminum	6.75	7.85	6.50	6.90	7.60	6.60	7.05	7.30	6.80
Mild Steel	6.50	7.60	6.40	6.55	7.55	6.53	6.65	7.40	6.60
Stainless S.	6.40	7.70	6.38	6.55	7.58	6.55	6.60	7.40	6.65

6.2.1.3 Friction Measurement

Figure 6.8 presents the appearance of the ring the test specimen before and after the ring compression test. Ring compression test was performed with the hydraulic and high energy rate forming hammers. Same dies without lubrication (dry condition) were used at the both of the hydraulic and HERF hammers. Table 6.3 gives the geometrical values of compressed samples formed with the hydraulic, conventional mecanic and HERF hammers. By using the geometrical values of the compressed samples, friction coefficients of the samples were determined using the standard a ring compression test friction coefficient chart **(Male and Cockroft, 1965)** as shown in Figure 6.9. As seen in the figure, friction coefficient of the samples compressed with the hydraulic press, conventional press and HERF determined as μ= 0.3, μ= 0.27 and μ=0.09, respectively. The reason behind this situation can be that when the samples are compressed with HERF hammer, friction between the die and billet changes from the static to dynamic behavior. With the aid of this behavior, friction between the surfaces reduces significantly.

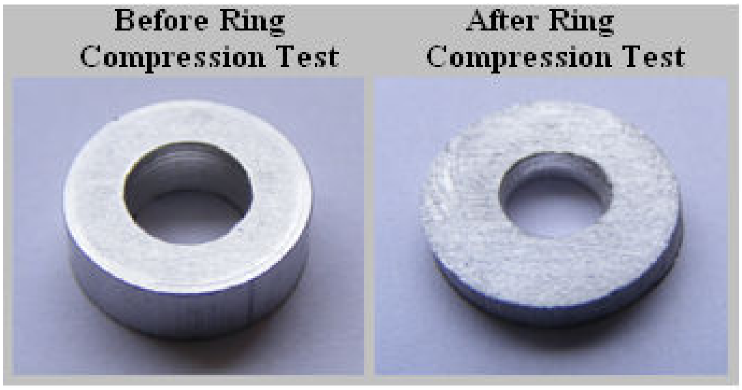

Figure 6. 8 Views of before and after ring compression test

Table 6. 3Geometric values of before and after ring compression test

Material	: Aluminum	Outside Diameter (d_{oi}):12mm	
Inside Diameter (d_{ii}) : 6mm		Height (h_i): 4mm	
After Ring Compression Test	HP	CP	HERF
Inside Diameter (d_{if})	4.7	4.5	5.4
Height h_i	2.8	2.6	2.4
Red. Int. Dia. %	21	25	10
Reduc. Height %	30	35	40

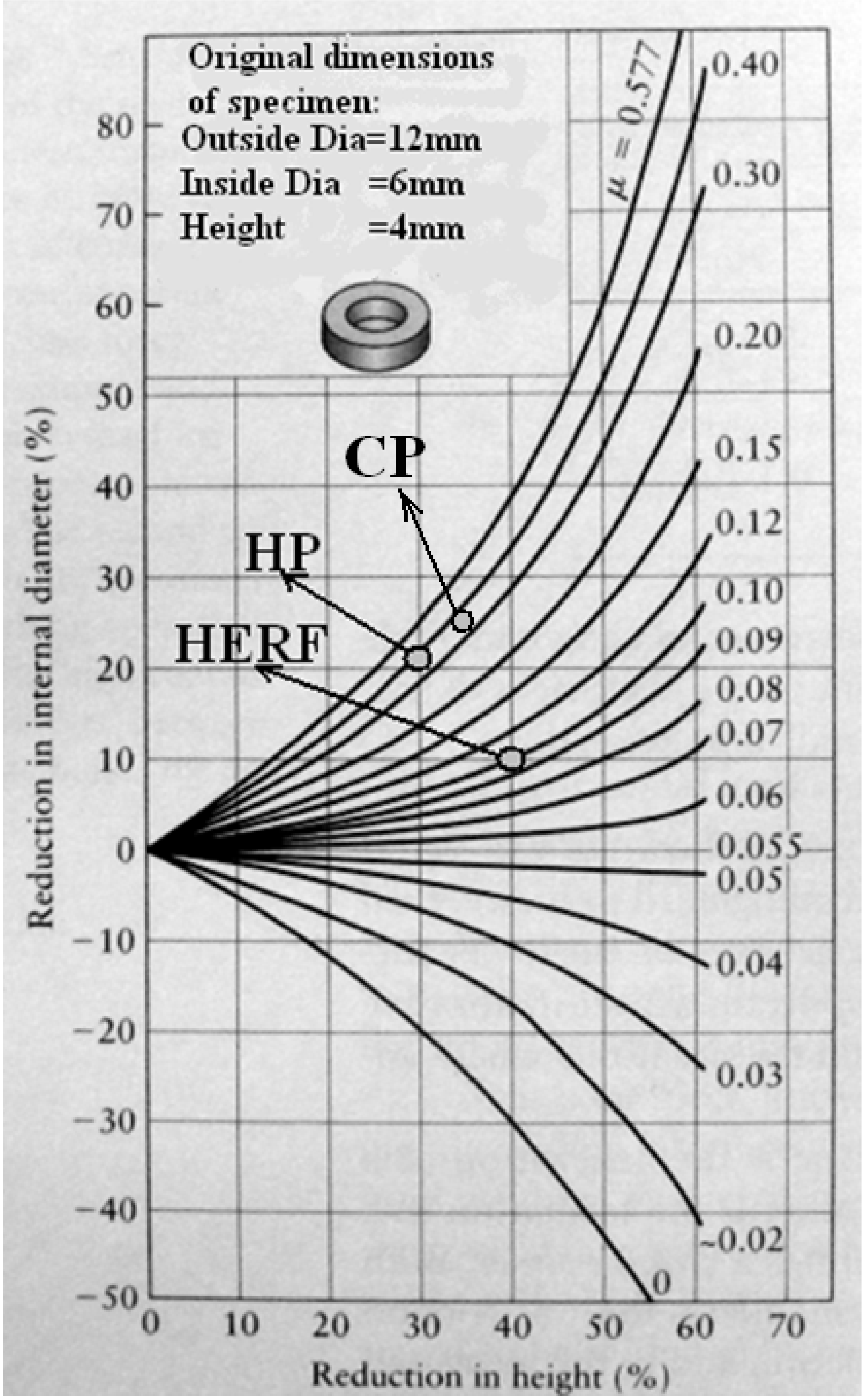

Figure 6. 9 The standard a ring compression test friction coefficient chart

Figure 6.10 and 6.11 show compared ideal and measured forging load for aluminum on HERF hammer and HP, respectively. The ideal loads of forging operation were calculated through the formula in section 3.3.4. The fact that ideal forging load and experimental forging results were parallel verifies the accuracy of load measurements in experiments. Also, it is apparent in these two graphics that there is a decrease in required forging energy and maximum load value due to the decrease in friction coefficient, which is a result of high speed forging. In forging with HERF hammer, where the friction coefficient is low, the barreling effect seems to be low.

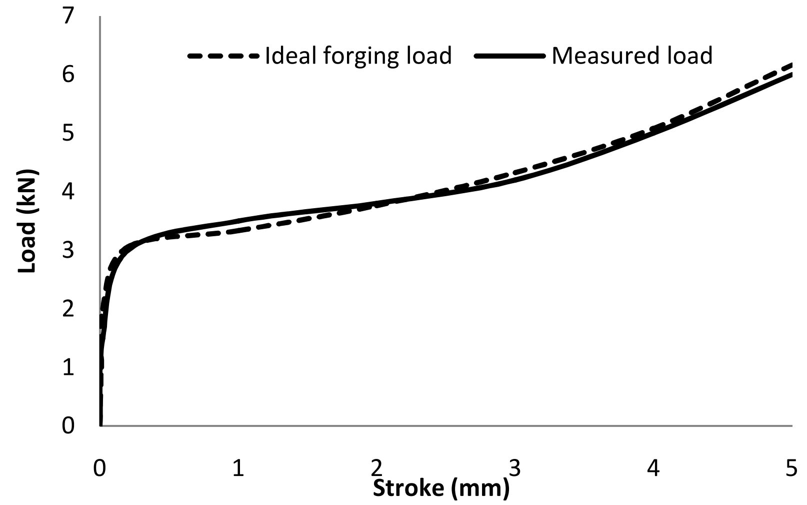

Figure 6. 10 Comparison of ideal and measured forging loads for aluminum on HERF hammer

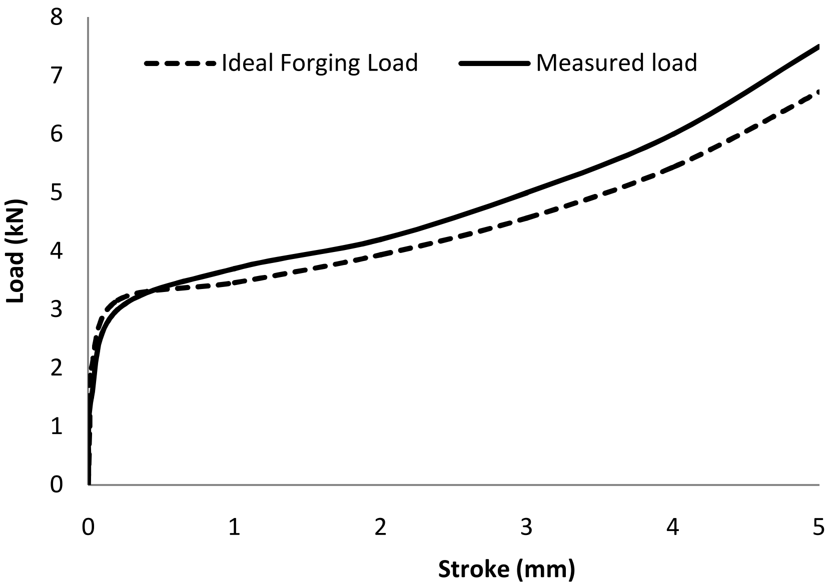

Figure 6. 11 Comparison of ideal and measured forging loads for aluminum on HP

6.2.2 Blanking Load and Energy

6.2.2.1 Effect of Blanking Speed on Aluminum

Figure 6.12 presents the load-stroke curves of the 5 mm thick aluminum sheet for different die clearances at the hydraulic press. Load-stroke measurements performed at the five (2.0, 2.5, 3.0, 3.5, and 4.0%) different clearances. It is clearly seen in Figure 6.12 that when the die clearances increased, required energy for blanking of aluminum material decreased remarkably. For instance, required energy was approximately 30% decreased when the die clearances increased from 2% to 4%. Moreover, the lowest required energy for blanking the aluminum material was observed at the 4% die clearance for the given range. However, maximum forces to blanking of the aluminum did not significantly alter and its value is about 12kN. For higher clearance (more than 4%), decreasing in energy may not be observed as given in the other blanking speeds (CP and HERF).

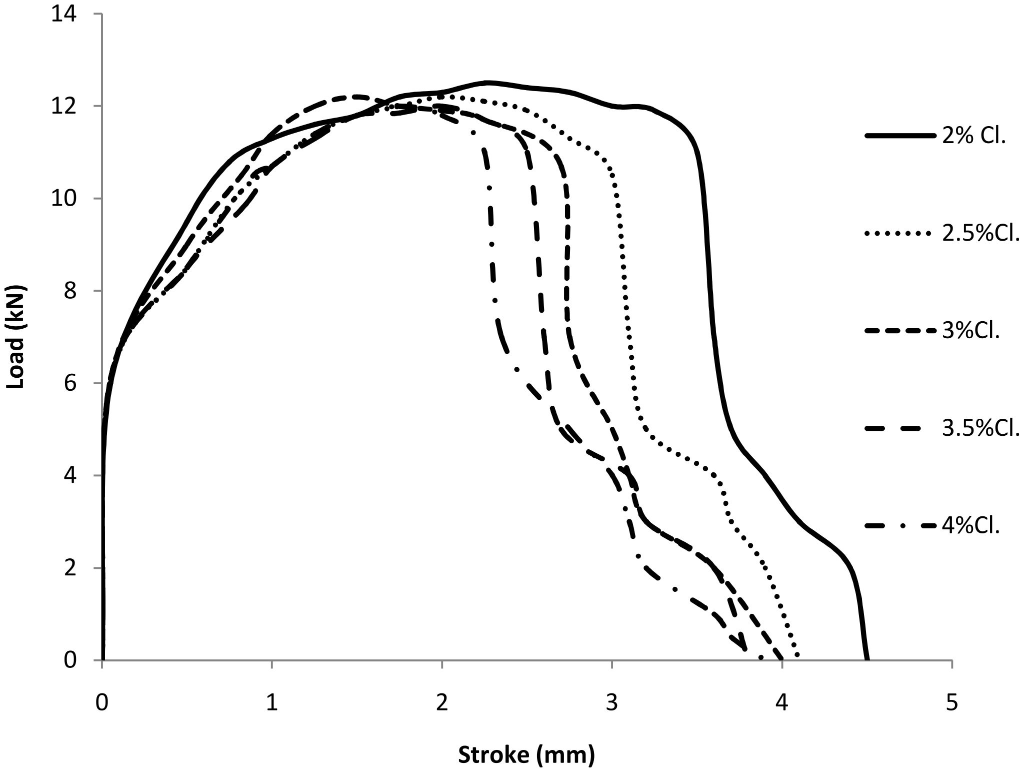

Figure 6.12 Load-stroke curves of aluminum for different clearances at HP

Load-stroke alterations of the aluminum material at the conventional press depend on the die clearances was demonstrated at the Figure 6.13. Same clearances which were implemented at the hydraulic press were also studied at the conventional press. The lowest required energy for blanking the aluminum at conventional press was measured at 3.5% die clearance, however, that energy was obtained at the 4.0% die clearances at the hydraulic press. This result demonstrates that punching speed affecting amount of die clearance for lower blanking energy. As in the hydraulic press, increasing the die clearances from 2% to 3.5% decreased the required energy significantly at the conventional press, but more clearance (4%) results in increasing energy. Maximum load for blanking did not changed with clearance significantly similar to hydraulic press, but its value is reduced to 11kN.

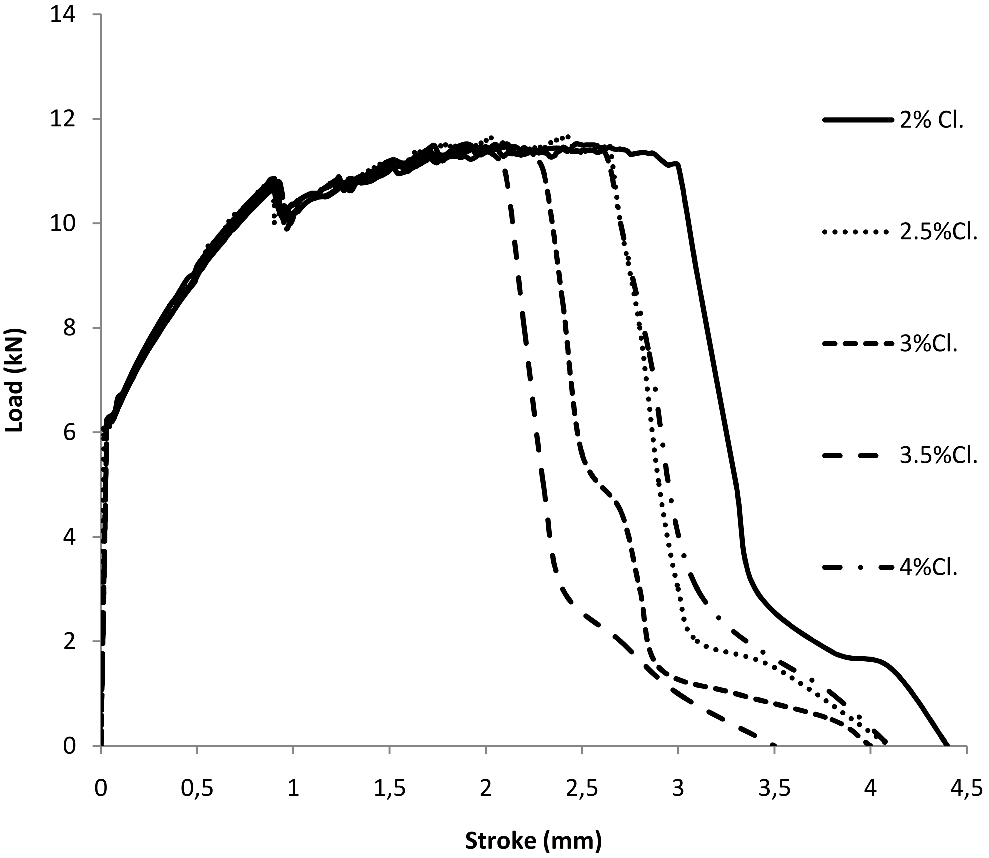

Figure 6.13 Load-stroke curves of aluminum depending on the clearances at CP

A general load-stroke diagram obtained in our HERF hammer is shown in Figure 6.14. As the HERF hammer is a type of energy restricted machines, all of the energy produced by the machine is directly transferred to the work piece. In this figure, the dark area shows the energy used for blanking and the grey area shows the remaining energy. This remaining energy is transferred to the press body through punch stopper. For comparison of the results, only the first portion (dark area) of the load stroke diagram is taken in the following sections for blanking at the HERF hammer.

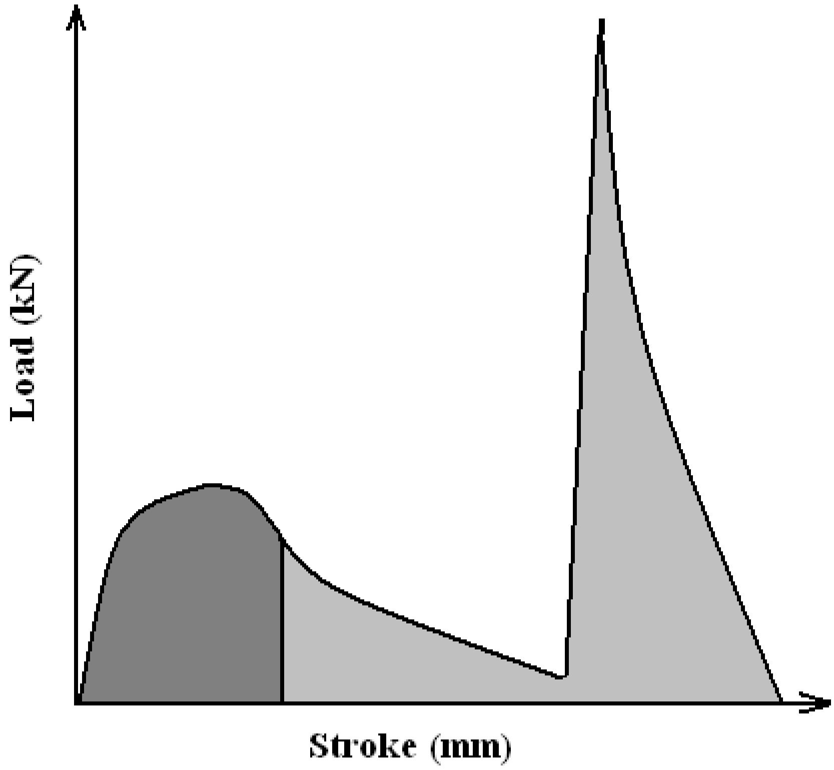

Figure 6.14 General load-stroke diagram obtained in our HERF hammer

Effect of die clearances on the load-stroke diagram of the aluminum at the high energy rate forming machine was illustrated in Figure 6.15. The trend which was observed at the conventional and hydraulic presses was also measured at the high energy rate forming machine. However, the lowest required energy for blanking the aluminum was measured at the 3% die clearance. Moreover, the maximum force that is used to blanking the aluminum decreased to 2.5kN at the high energy rate forming machine, however, that value was 12kN and 11kN at the hydraulic and conventional presses, respectively. At the high energy rate forming machine, it was also observed that as the maximum forces decreased, the die clearances increased. This situation is not observed for the conventional and hydraulic presses.

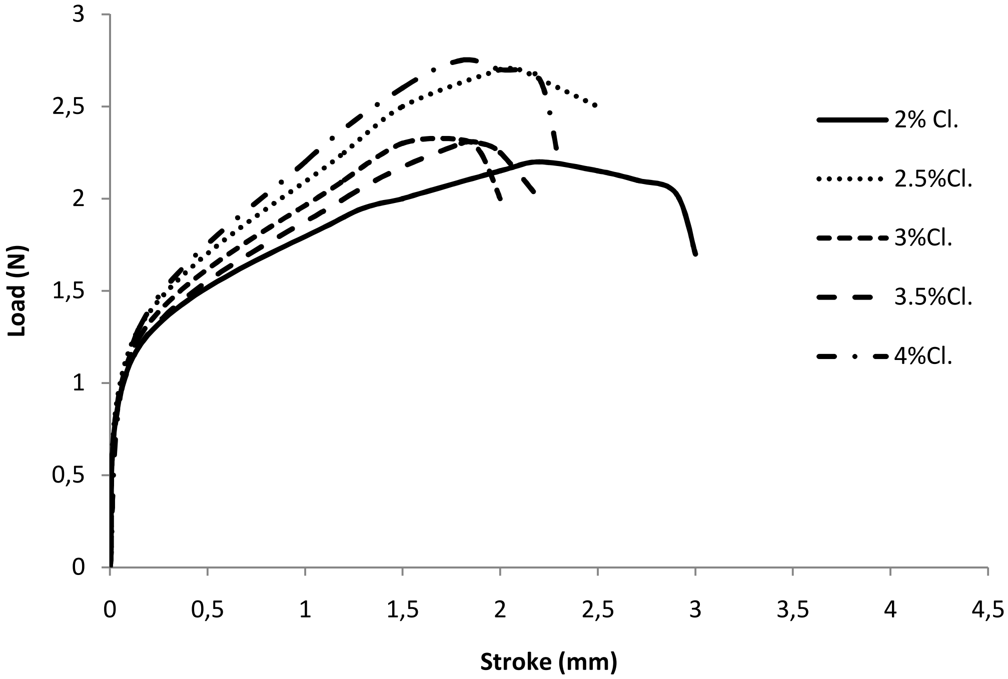

Figure 6.15 Load-stroke curves of aluminum depending on the clearances at HERF

Maximum load and used energy values of the Figures 6.12, 6.13, and 6.15 are given in Table 6.4 in order to assess better the load stroke curves given separately for 5 different clearance values (2%, 2.5%, 3%, 3.5%, 4%) using HP, CP, HERF hammers respectively in the blanking process of aluminum sheet with a thickness of 5mm. Analyzing the maximum load and used energy values, a significant decrease is apparent in the blanking process carried out in HERF hammer in comparison with blanking with other machines.

Table 6.4 Maximum load and energy of blanking processes

	Used Blanking Machine					
	HP		CP		HERF	
Clearance	Max. Load(kN)	Max. Energy(J)	Max. Load(kN)	Max. Energy(J)	Max. Load(kN)	Max. Energy(J)
2%	12.20	48.0	11.60	40.0	2.20	7.0
2.5%	12.10	43.0	11.50	35.0	2.50	8.0
3%	12.00	40.0	11.40	30.0	2.30	6.0
3.5%	12.00	35.0	11.30	28.5	2.30	7.0
4%	11.90	30.0	11.30	35.0	2.60	7.0

Comparison of the ideal clearances with respect to the punching speeds for the aluminum was shown at the Figure 6.16. It was observed in Figure 6.16 that conventional press at 3.5% die clearance and hydraulic press at 4.0% die clearances had almost the same load and energy. On the other hand, when the high energy rate forming machine was used, it was seen that the load and energy were decreased drastically at the 3.0% die clearances.

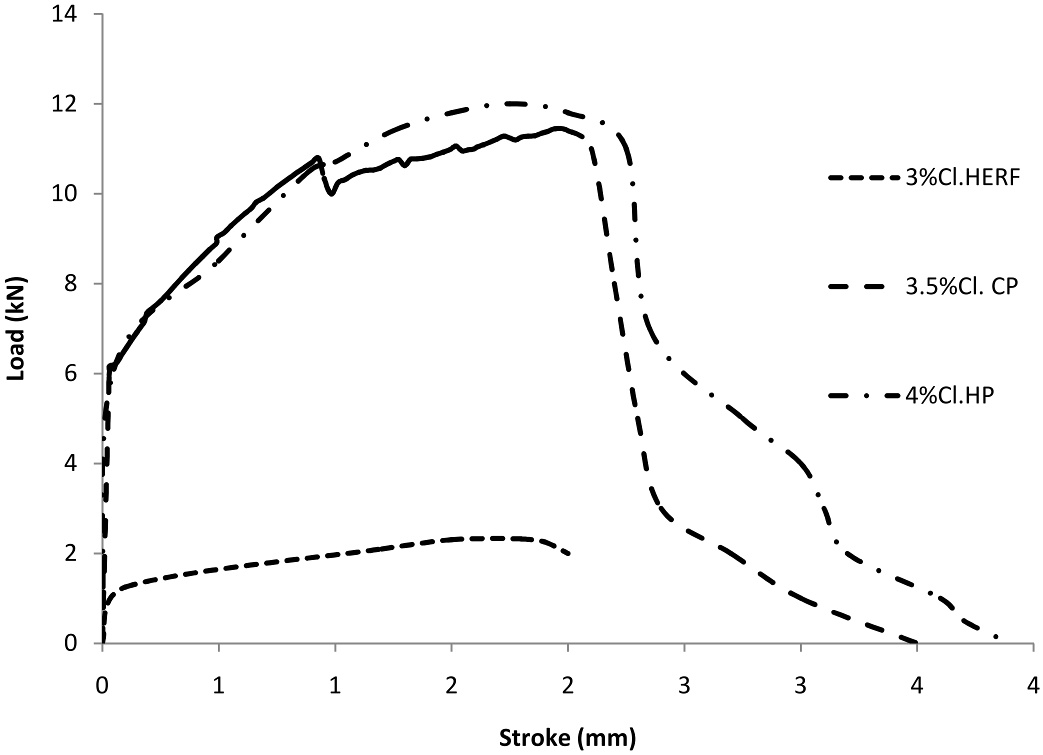

Figure 6.16 Comparison of the ideal die clearances with respect to the blanking speed

Die clearance selection diagram in blanking according to sheet thickness for the first group materials that are called “soft materials” is given in Figure 6.17. This figure gives the maximum and minimum clearance values (lines) for mechanic presses. Proper clearance is determined by approximation to the ideal cutting condition (less blanking energy and 30% penetration in depth). For different sheet thickness (5, 4 and 3mm) aluminum sheet were blanked using HP, CP and HERF. The results show that as the blanking speed increases, the proper clearance value decreases.

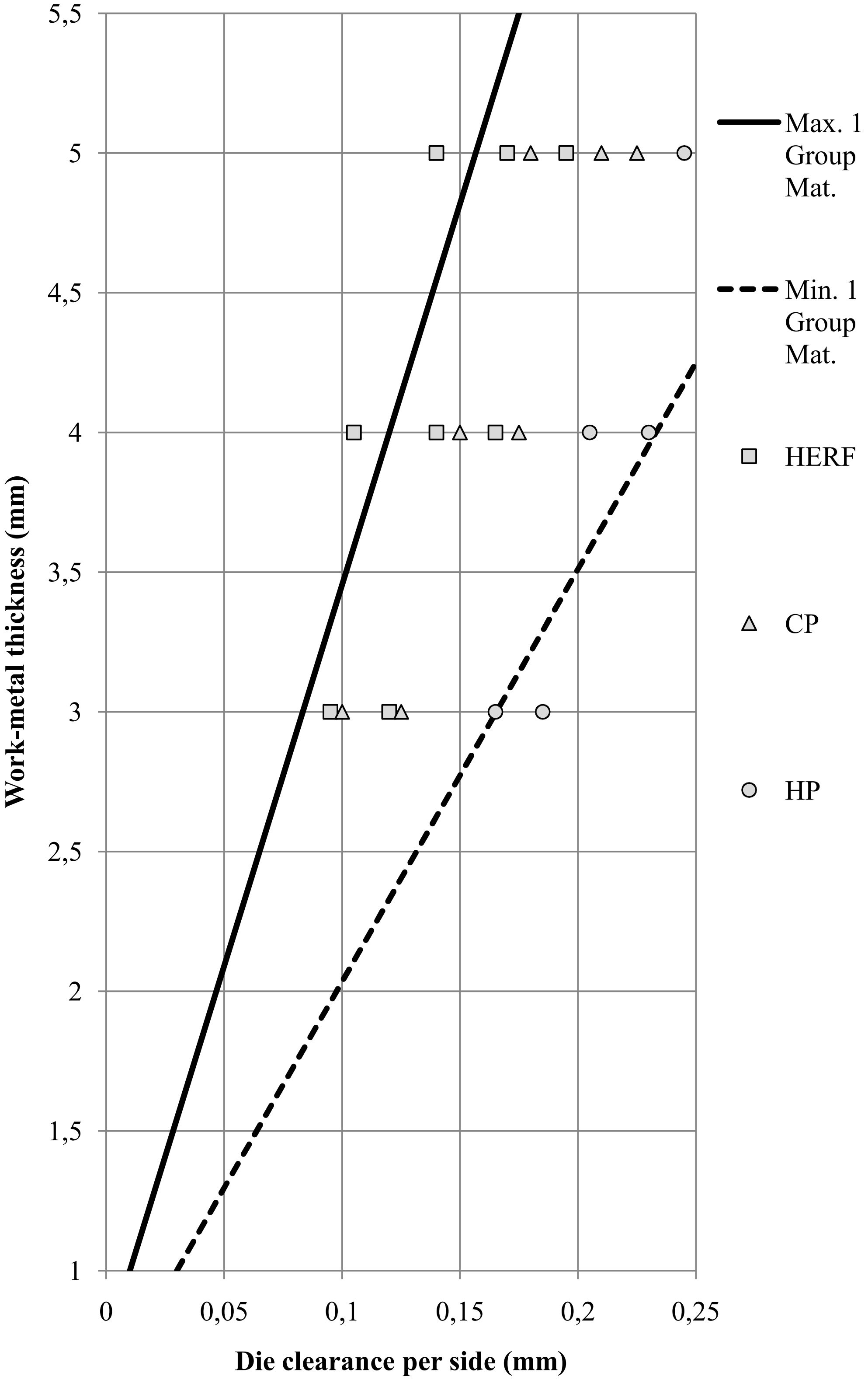

Figure 6.17 Effects of the blanking speed on the die clearance per side for the first group (soft) materials.

6.2.2.2 Effect of Blanking Speed on Mild Steel

Figure 6.18 presents the load-stroke curves of the 3.5 mm thickness mild steel material for different die clearances (2.8, 3.6, 4.3, 5.0, and 5.5%) at the hydraulic press. The maximum load for the blanking of the mild steel was roughly the same for all studied clearances (about 35kN) as seen in Figure 6.18. It was obviously observed in Figure 6.18 that increasing of the die clearances decreased the required blanking energy considerably. As explained earlier, this situation was valid for the blanking of the aluminum materials. The lowest required energy was measured at the die clearance 5.5%.

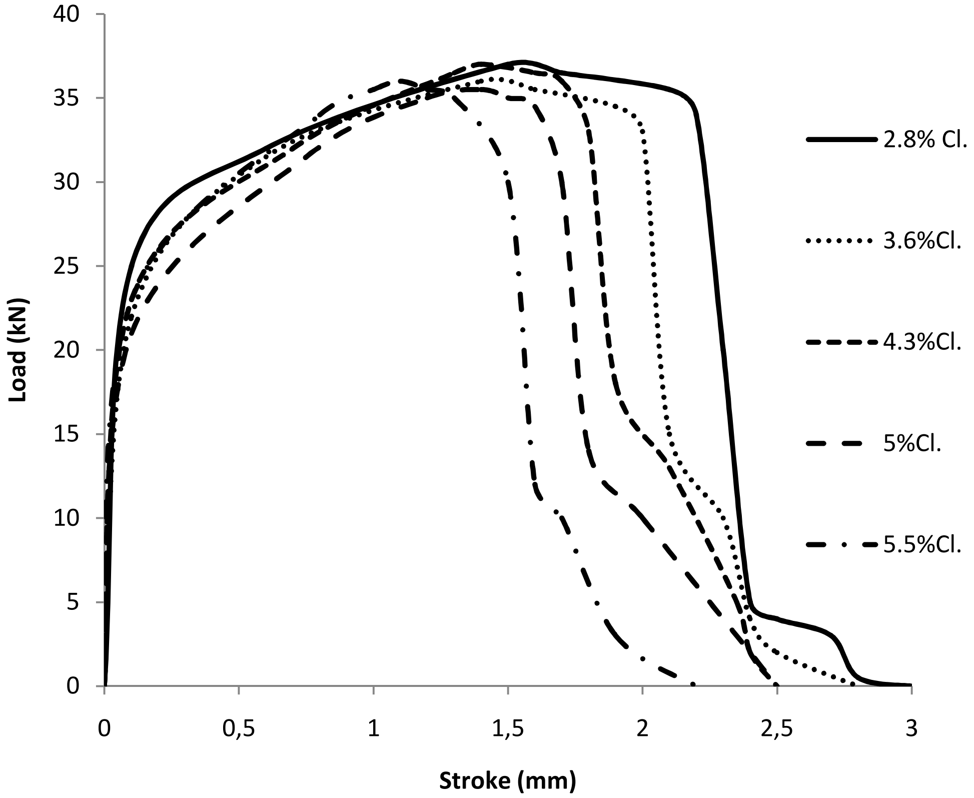

Figure 6.18 Load-stroke curves of mild steel material depending on the die clearances at HP

Effects of the die clearances on the load-stroke diagram of the mild steel at the conventional press were illustrated in Figure 6.19. As in the hydraulic press case, when the clearances increased from 2.8% to 5.5% linearly, required blanking energy was decreased. Moreover, the lowest required energy was observed at the 5.5% die clearances. The maximum load for blanking of the mild steel at conventional press was somewhat lower than that of the hydraulic press. A variation at the maximum load did not observed with the increasing of the die clearances.

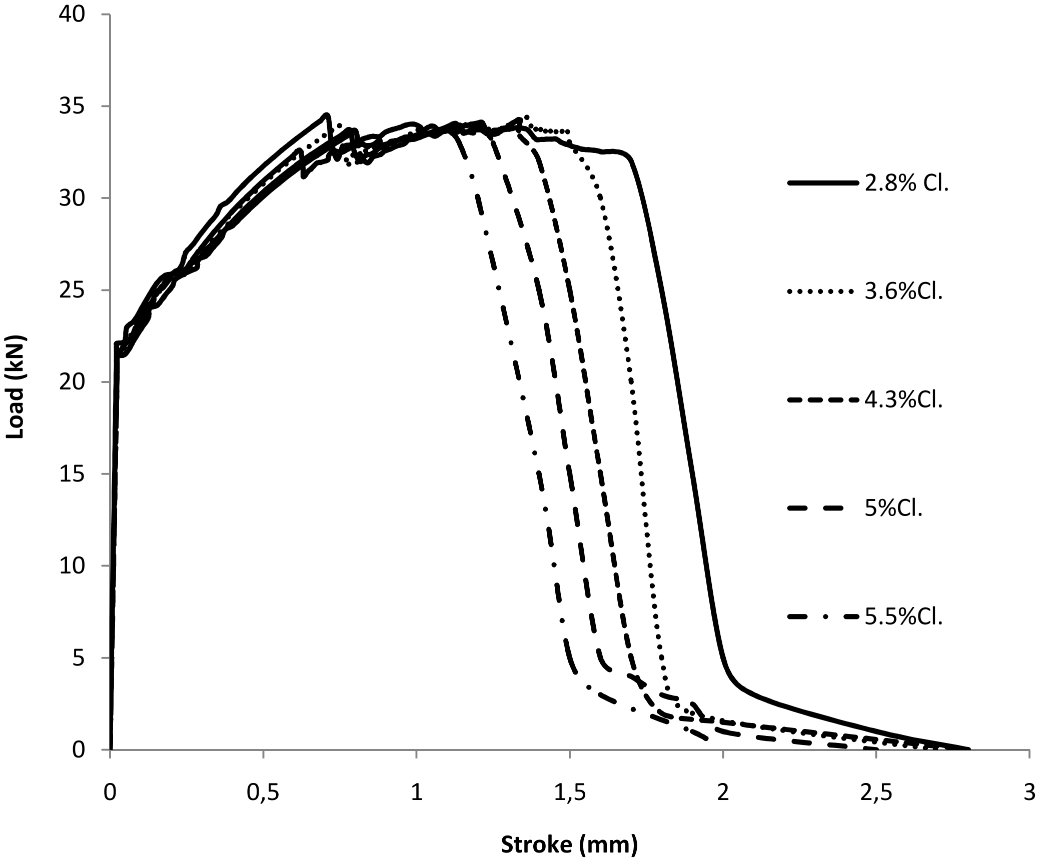

Figure 6.19 Load-stroke curves of mild steel material depending on the clearances at CP

Figure 6.20 presents the load-stroke diagram of the mild steel depend on the die clearances at HERF hammer. The lowest required energy for blanking of the mild steel was measured at the 5.0% die clearances. The required energy for blanking of mild steel at the 2.8, 3.6, 4.3, and 5.5% die clearances were higher than that of the 5.0% die clearances. Although, the lowest required blanking energy were observed at the highest die clearances at the conventional and hydraulic presses, the lowest blanking energy was measured at the 5.0% die clearances in the HERF hammer. The maximum force that is used to blanking of the mild steel material decreased to 3.5kN at the high energy rate forming machine, however, that value was 35kN and 33kN at the hydraulic and conventional presses, respectively.

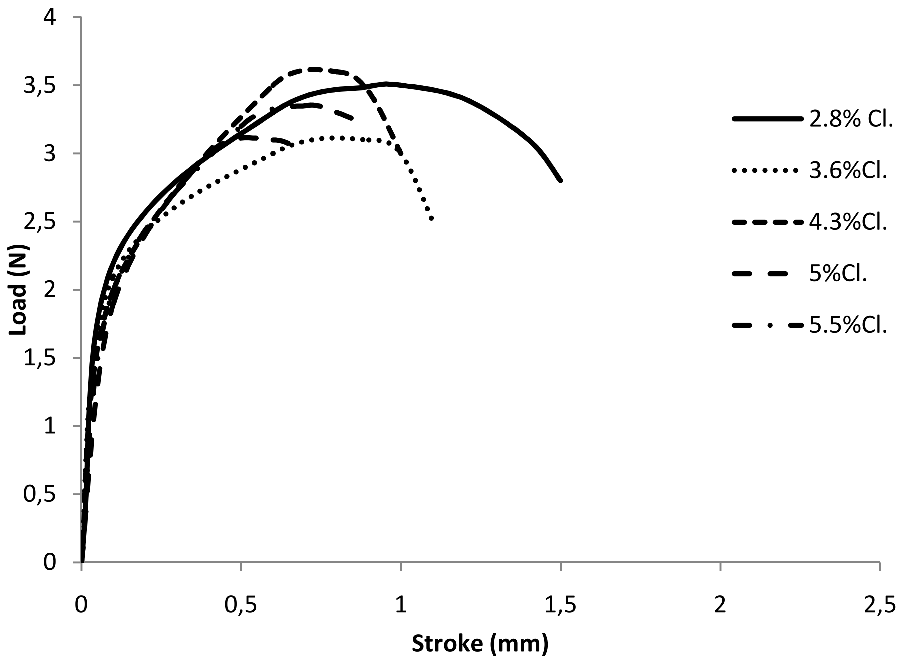

Figure 6.20 Load-stroke curves of mild steel material depending on the clearances at HERF

Blanking energy values and maximum load of the Figures 6.18, 6.19, and 6.20 are given in Table 6.5 so as to assess better the load stroke curves given separately for 5 different clearance values (2.8%, 3.6%, 4.3%, 5%, 5.8%) using HP, CP, HERF hammers respectively in the blanking process of St 37 sheet material with a thickness of 3.5 mm. Examining the maximum load and the energy values, a significant decrease is apparent in the blanking process carried out in HERF hammers in comparison with blanking with other machines.

Table 6.5 Maximum load and energy of blanking processes

Clearance	Used Blanking Machine					
	HP		CP		HERF	
	Max. Load(kN)	Max. Energy(J)	Max. Load(kN)	Max. Energy(J)	Max. Load(kN)	Max. Energy(J)
2.8%	36.00	80.0	34.50	65.00	3.60	8.0
3.6%	35.00	70.0	34.40	60.00	3.10	7.5
4.3%	35.00	65.0	34.30	55.00	3.40	7.0
5%	34.00	60.0	34.30	50.00	3.10	7.0
5.8%	33.00	50.0	34.20	45.50	3.40	7.5

Load stroke diagram of the mild steel according to the ideal die clearances depend on the punching speed in presented in Figure 6.21. It was observed in Figure 6.21 that conventional and hydraulic presses at 5.5% die clearance had almost the same load and energy. On the other hand, when the high energy rate forming machine was evaluated, it was seen that the load and energy were decreased drastically at the 5.0% die clearances.

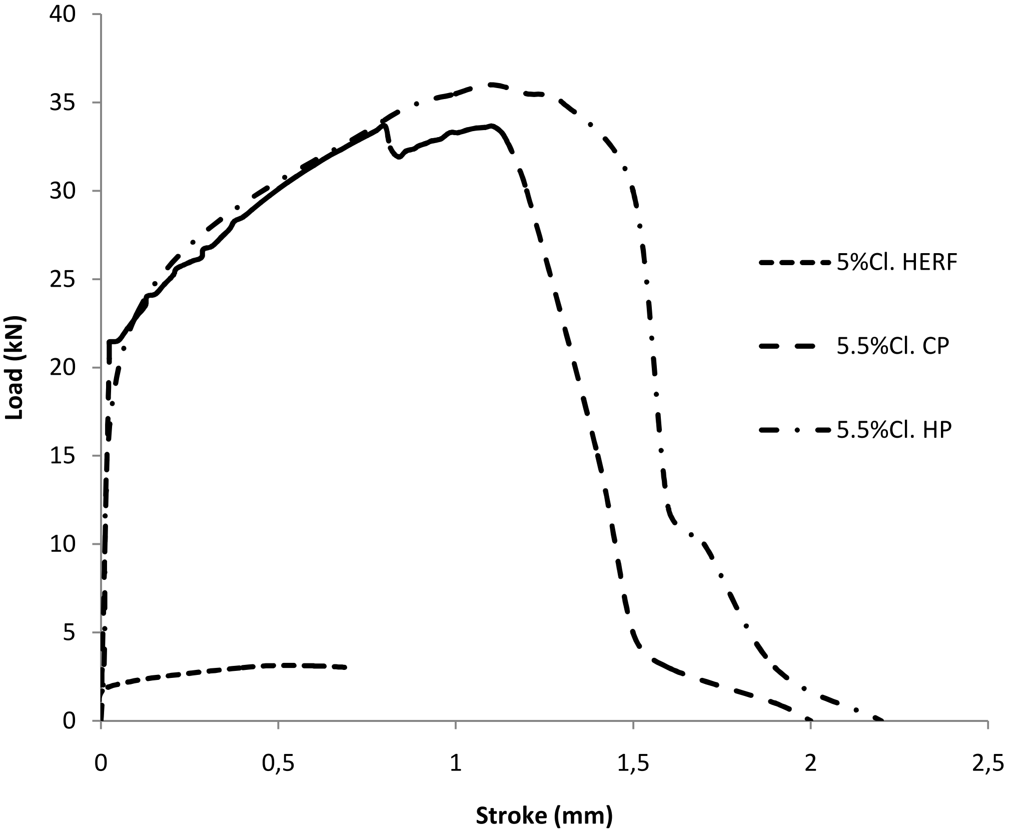

Figure 6.21 Comparison of the ideal die clearances with respect to the blanking speed at mild steel

Die clearance selection diagram for "semi-hard materials" is presented in Figure 6.22. This maximum and minimum clearance values for mechanic presses according to the thickness of the sheet material are shown by a visible and a hidden line; respectively. 3.5, 2.5 and 2mm thick St37 sheet were blanked and proper clearances were chosen according to the blanking energy and the amount of penetration. Figure 6.22 show that as the blanking speed increases, the clearance degreases.

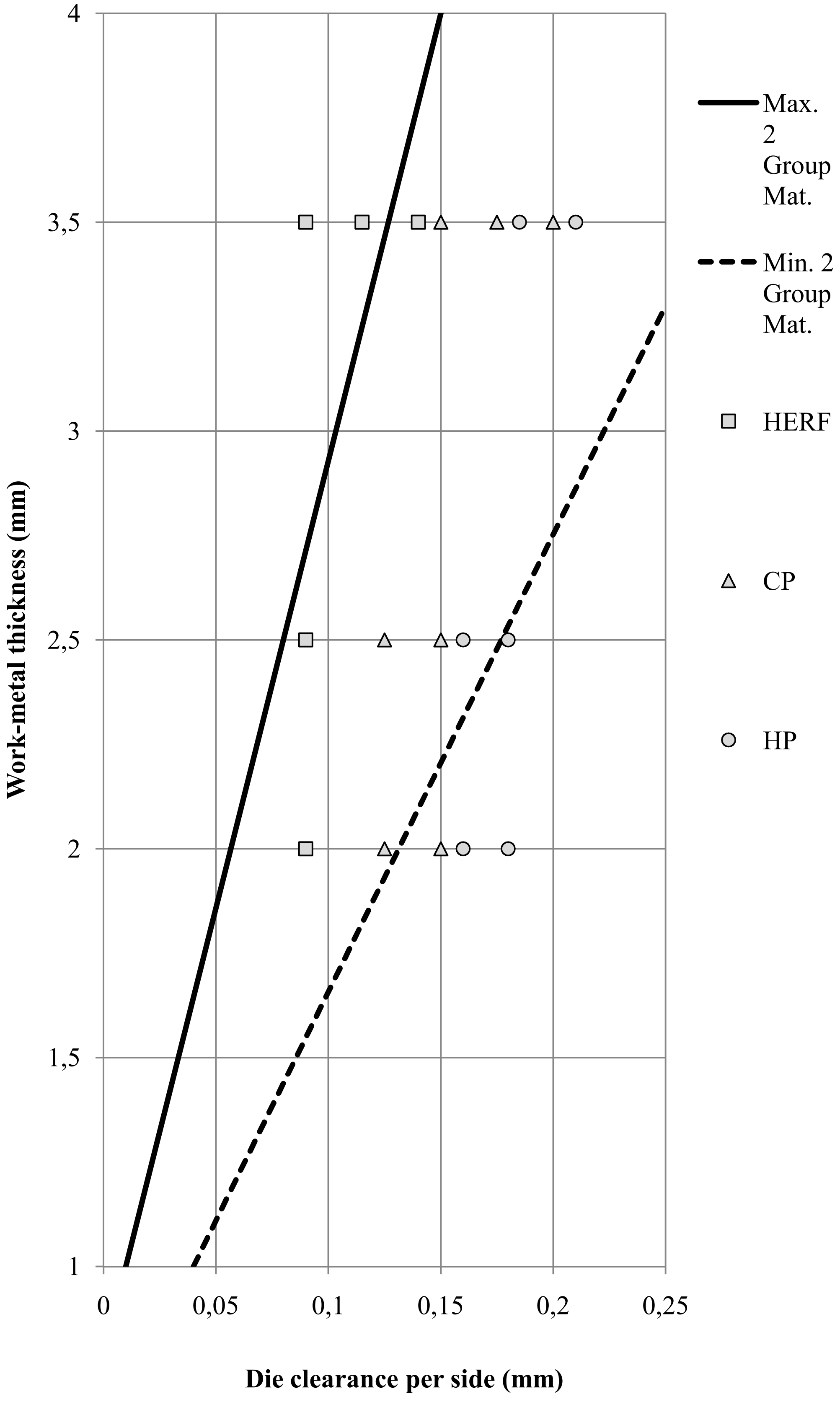

Figure 6.22 Effects of the blanking speed on the die clearance per site at the second group (medium-hard) materials.

6.2.2.3 Effect of Blanking Speed on Stainless Steel

Figure 6.23 presents the load-stroke diagrams of the 2.0 mm thickness stainless steel depend on the die clearances at the hydraulic press. Load-stroke measurement performed at the five (5.0, 6.25, 7.5, 8.75, and 10.0%) different clearances. Load-stroke curve of the stainless steel had the same trend as in the aluminum and mild steel, but the maximum blanking load is about 40kN. Increasing of the die clearances decreases the required blanking energy of the stainless steel. This situation was similar at the aluminum and mild steel. The lowest blanking energy was measured at the 10.0% die clearance.

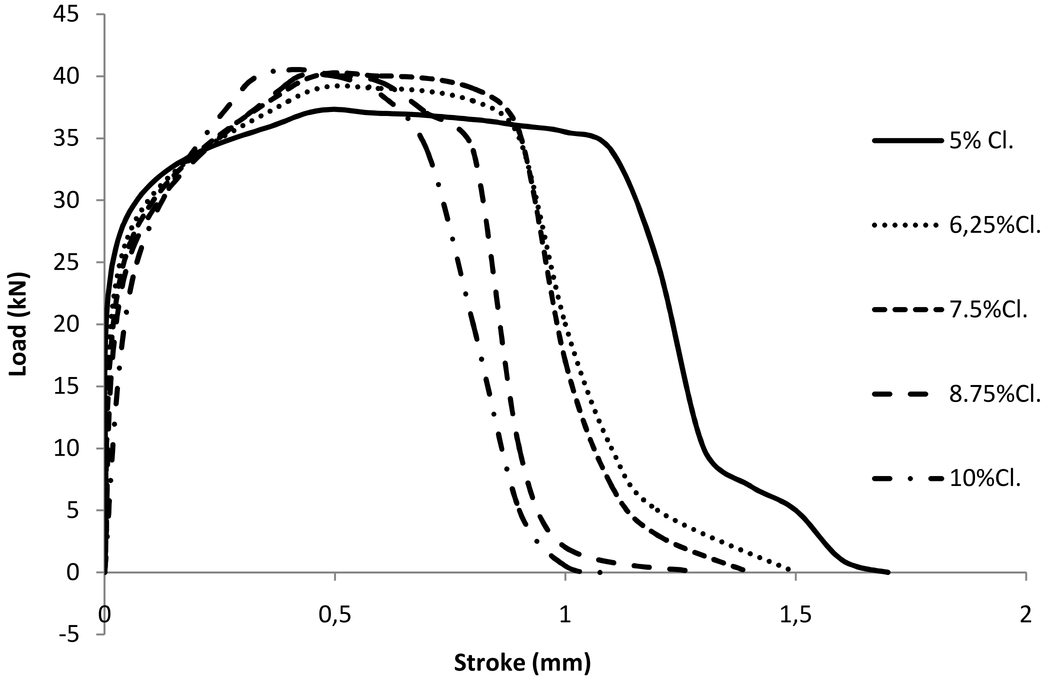

Figure 6.23 Load-stroke curves of stainless steel depending on the die clearances at HP

Load measurements for stainless steel with respect to the stroke and die clearance at the conventional press was presented in Figure 6.24. When the blanking speed was increased with the changing of the press types from hydraulic to conventional, maximum forces decreased from 40kN to 35kN. As expected, increasing the die clearances decreased the required energy for the blanking of the stainless steel. Moreover, the lowest required blanking energy was measured at the 10.0% die clearances.

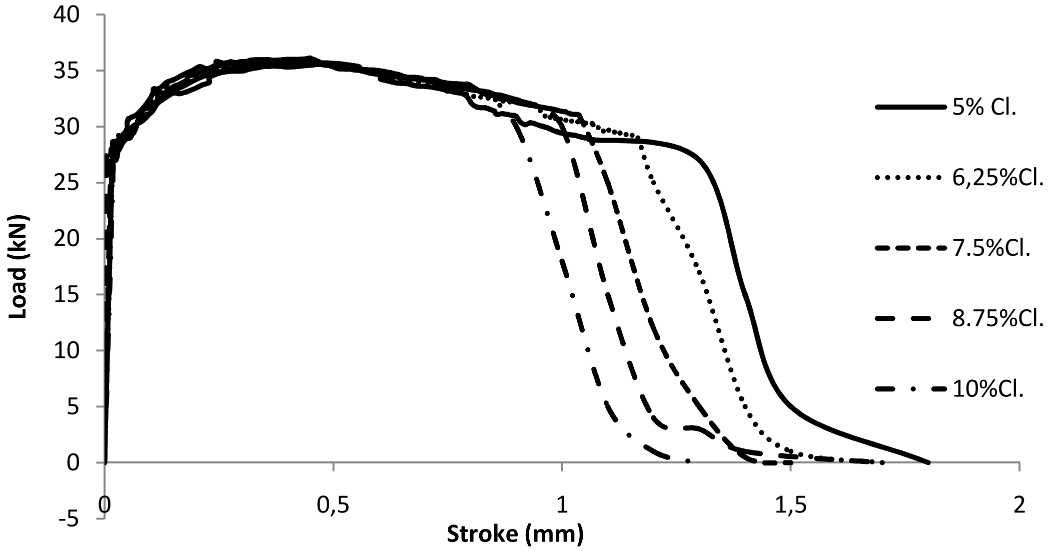

Figure 6.24 Load-stroke curve variation of stainless steel depending on the die clearances at CP

Figure 6.25 illustrates load-stroke curves of stainless steel depend on the die clearances at HERF hammer. When the stainless steel was blanked with HERF hammer, maximum load was decreased approximately 12 times than the conventional and hydraulic presses. The lowest required energy which was used for the blanking of the stainless steel was observed at the 8.75% die clearance at HERF hammer.

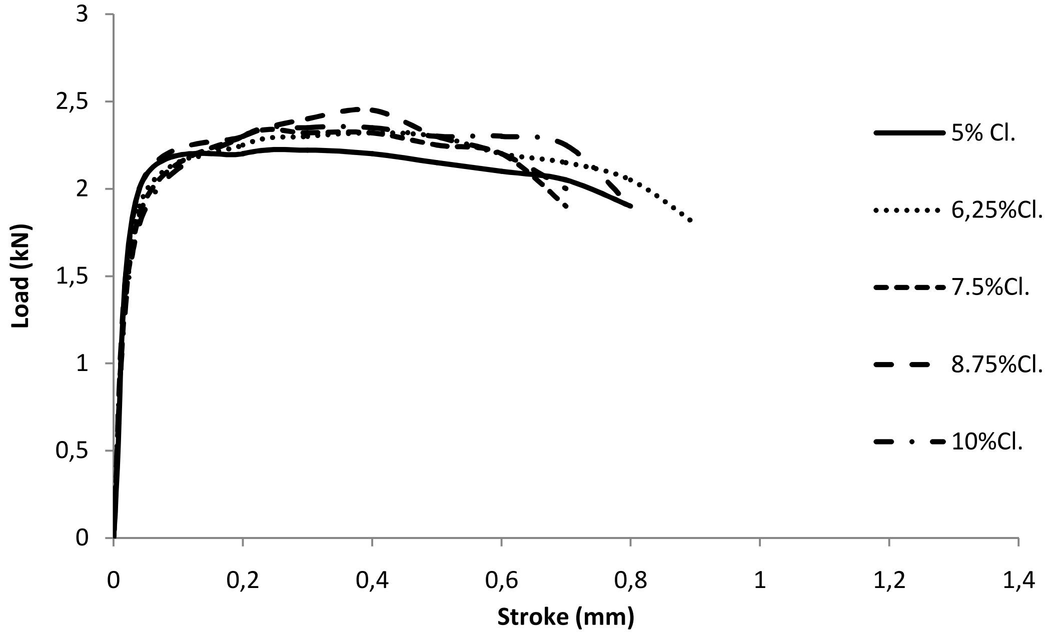

Figure 6.25 Load-stroke curve variation of stainless steel depending on the die clearances at HERF

Maximum load and energy values of the Figures 6.23, 6.24, and 6.25 are presented in Table 6.6 for 5 different clearance values (5%, 6.25%, 7.5%, 8.75%, 10%) and HP, CP, HERF hammers respectively in the blanking process of stainless steel sheet material with a thickness of 2 mm. Probing the maximum load and energy, a significant decrease is apparent in the blanking process carried out in HERF hammer in comparison with the other machines.

Table 6.6 Maximum load and energy of blanking processes

Clearance	Used Blanking Machine					
	HP		CP		HERF	
	Max. Load(kN)	Max. Energy(J)	Max. Load(kN)	Max. Energy(J)	Max. Load(kN)	Max. Energy(J)
2.8%	37.50	42.0	36.0	40.0	2.2	2
3.6%	40.50	40.0	36.0	39.0	2.2	1.9
4.3%	41.00	41.0	36.0	38.0	2.3	1.5
5%	41.5	38.0	36.0	37.0	2.5	1.6
5.8%	42.00	37.5	36.0	36.0	2.4	1.9

Load stroke diagram of the stainless steel according to the ideal die clearances depending on the punching speed in presented is the Figure 6.26. It was observed in Figure 6.26 that conventional and hydraulic presses at 10.0% die clearance had almost the same load and energy. On the other hand, when the high energy rate forming machine was used, it was seen that the load and energy were decreased drastically at the 8.75% die clearances.

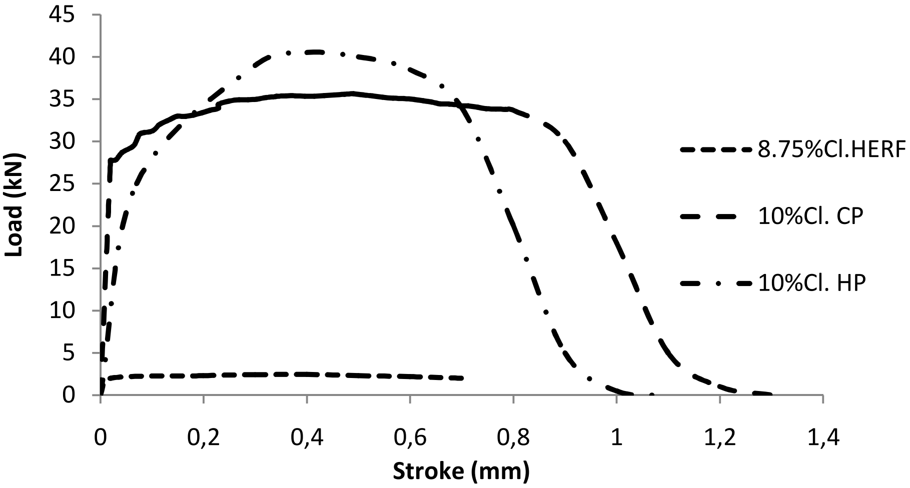

Figure 6.26 Comparison of the ideal die clearances relies on the blanking speed at SS

Die clearance selection diagram of the third group materials that are called "hard materials" is presented in Figure 6.27 for mechanical presses according to the thickness of the sheet material. Some amount of shift of the maximum and minimum limits of the clearance was observed from the results of the blanking performed on different stainless steel sheet thicknesses. The proper amount of clearance decreases with increasing blanking speed.

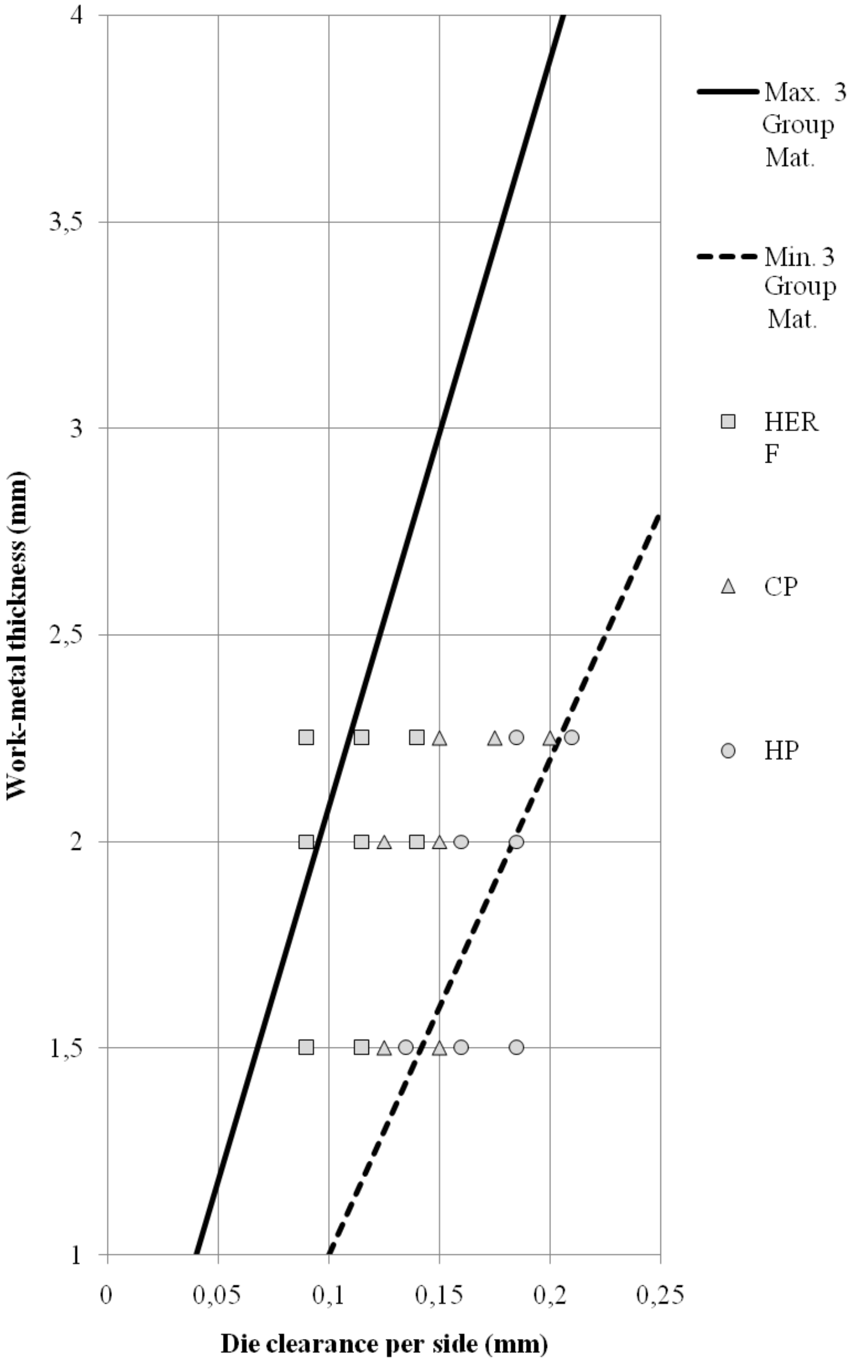

Figure 6.27 Effects of the blanking speed on the die clearance per side for the third group (hard) materials.

6.2.2.4 Effect of Blanking Speed on the Load and Energy

The load stroke graphics of St 37 with thickness values of 3.5, 5, and 6 mm are given in Figure 6.28, Figure 6.29 and Figure 6.30 respectively according to HP, CP and HERF hammers. The areas below these curves show the energy needed for blanking. Although the curves of HP and CP are almost identical, they are significantly different from the HERF ones.

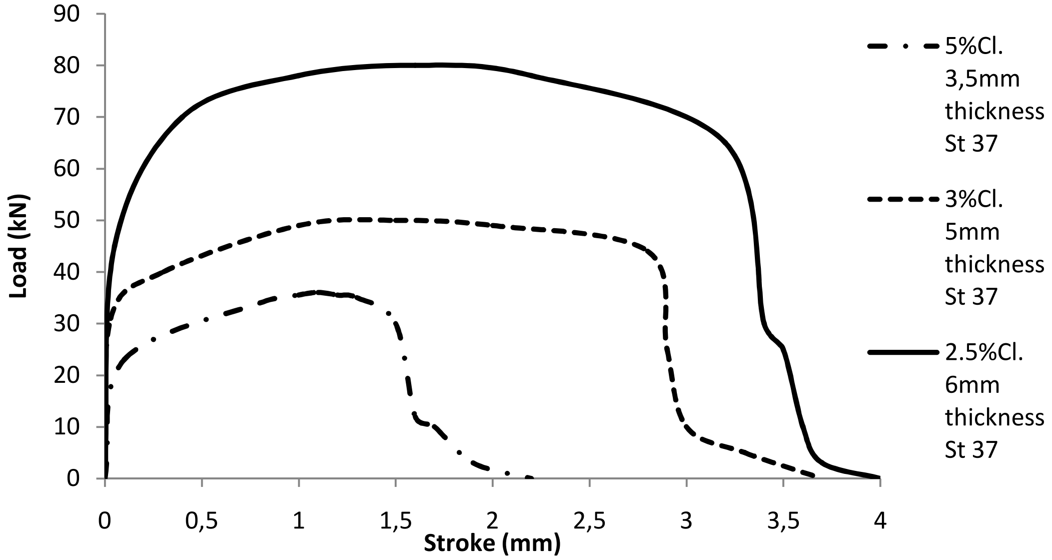

Figure 6.28 The load stroke diagram of St 37 with thickness values of 3.5, 5, and 6 mm according to HP

The curve in Figure 6.30 seems to be different from the curves in 6.28 and 6.29. As the HERF hammer is a type of energy restricted machines, all of the energy produced by the machine is directly transferred to the work piece. In this figure, before the "a" point shows the energy used for blanking and after the "a" point shows the remaining energy under the curves area. This remaining energy is transferred to the press body through punch stopper. The sum of both areas is the same in all three applications. As the thickness of the material increases, the amount energy needed for blanking increases and that the remaining energy decreases. Notifying that the prototype HERF hammer, which was designed and constructed has a maximum 100 J forming energy (see Section 4.3.3), spends 7, 30, and 45 J for blanking of 3.5, 5, and 6 mm thick St 37 sheets, respectively. In Figure 6.28, the areas a, b, and c are load stroke curves of 3.5, 5, and 6 mm St 37 material, respectively.

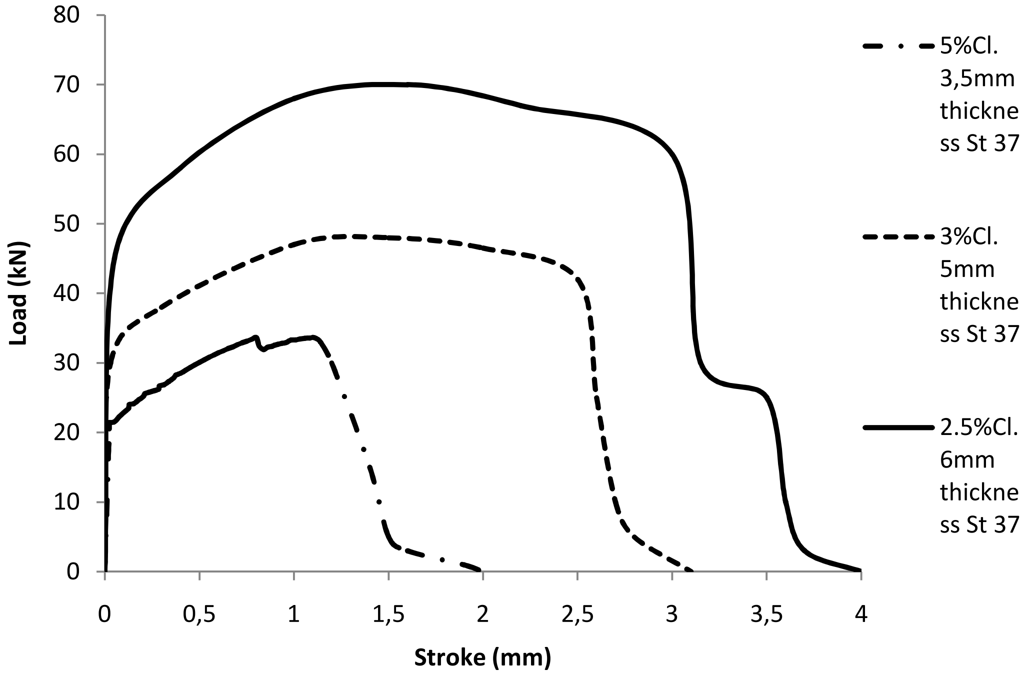

Figure 6.29 The load stroke diagram of St 37 with thickness values of 3.5, 5, and 6 mm according to CP

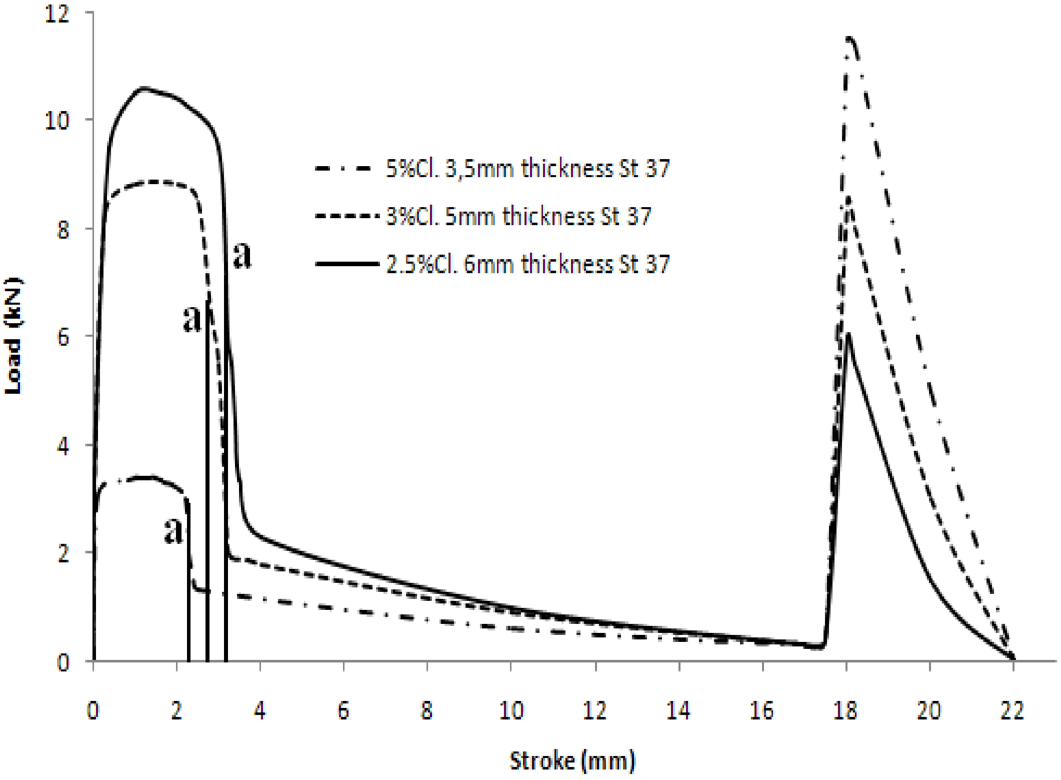

Figure 6.30 The load stroke graphics of St 37 with thickness values of 3.5, 5, and 6 mm according to HERF

Max load and used energy values of the Figures 6.28, 6.29, and 6.30 are presented in Table 6.7 to better assess the load stroke curves given for the same clearance values using HP, CP, and HERF hammer respectively in the blanking process of St 37 mild steel material with thickness values of 3.5, 5, and 6 mm. Studying the max load and used energy values, a significant decrease is apparent in the blanking process carried out in HERF hammer in comparison with blanking with other machines.

Table 6.7 Maximum load and energy of blanking processes

Materials	Used Blanking Machine					
	HP		CP		HERF	
	Max. Load(kN)	Max. Energy(J)	Max. Load(kN)	Max. Energy(J)	Max. Load(kN)	Max. Energy(J)
5%Cl. 3.5mm	33	50	34.5	45.5	3.4	7
3%Cl. 5mm	52	130	48	124	8.8	30
2.5%Cl. 6mm	80	270	70	210	10.5	45

6.2.2.5 A proposed Die Clearance Selection Diagram for the HERF Hammer

The results of blanking experiments show that there is some amount of shift in the clearance in the HERF comparing to HP and CP. For a practical purpose a new die clearance selection diagram, shown in the Figure 6.31 is proposed. The minimum and maximum limits of clearances versus sheet thickness for soft, medium-hard and hard materials are shown in the Figure 6.31.

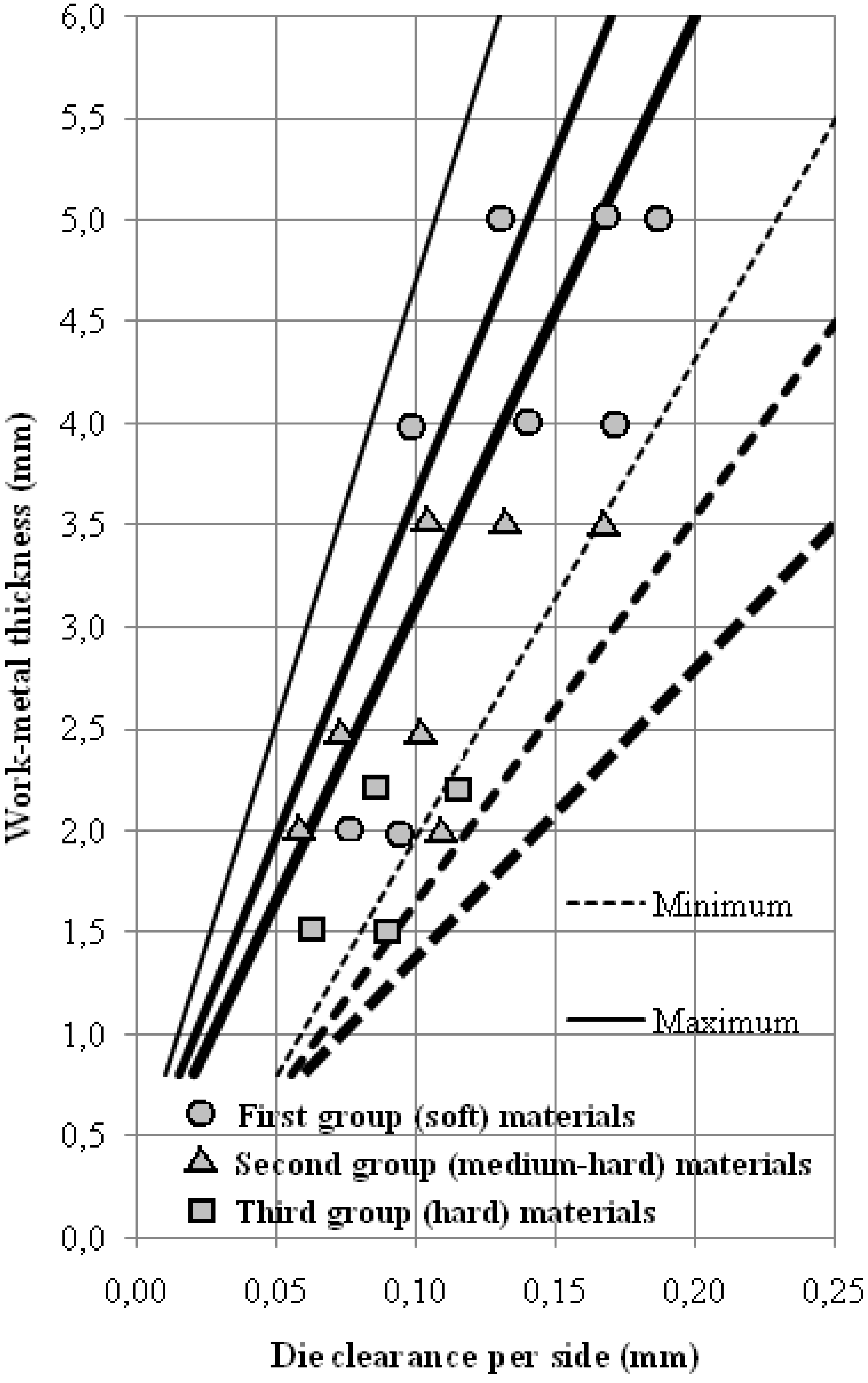

Figure 6.31 Die clearances selection diagram for the HERF hammer

6.2.3 Micro-structures of the Blanked Surfaces

Samples of 3.5mm St37 were half-blanked to analyze the effect of blanking speed in the blanking area. In Figures 6.32, 6.33 and 6.34 (x90) different views formed as a result of half-blanking at the same die clearance at different blanking speeds. Differences in grain structures, adiabatic shear band, rollover depth, plastic deformation, and flow-line views of surfaces blanked at different speeds were observed.

It was observed that shear bands of HERF samples at high speeds were drastically narrower than samples blanked at other machines. Although the flow lines of HERF samples were in the shear line, flow lines of HP and CP samples were observed to extend to outer sections of the shear line. As the expansion in the flow line demonstrates the sections affected in the blanking process, the narrowness of the shear band shows that the energy required for the blanking operation will be lower. Graphics in previous sections confirm that high speed blanking requires less energy.

It was observed that there was a decrease in rollover depth and plastic deformation in HERF blanking samples compared to HP and CP and that, therefore, there was an improvement both in the geometry of the blank and the sheet surfaces.

Figure 6.34 and 6.35 give micro-structure results of HERF blanking of St 37 mild steel at clearance values of 5 % and 2.5 %, respectively. Although the shear bands are close to each other at both blanking clearances at high speeds, the band was observed to be narrower at low clearances. Similarly, it was observed that there was a decrease in rollover depth and plastic deformation in HERF blanking samples with low clearance values compared to HERF blanking samples with high clearance and that there was an improvement both in the geometry of the blank and the sheet surfaces.

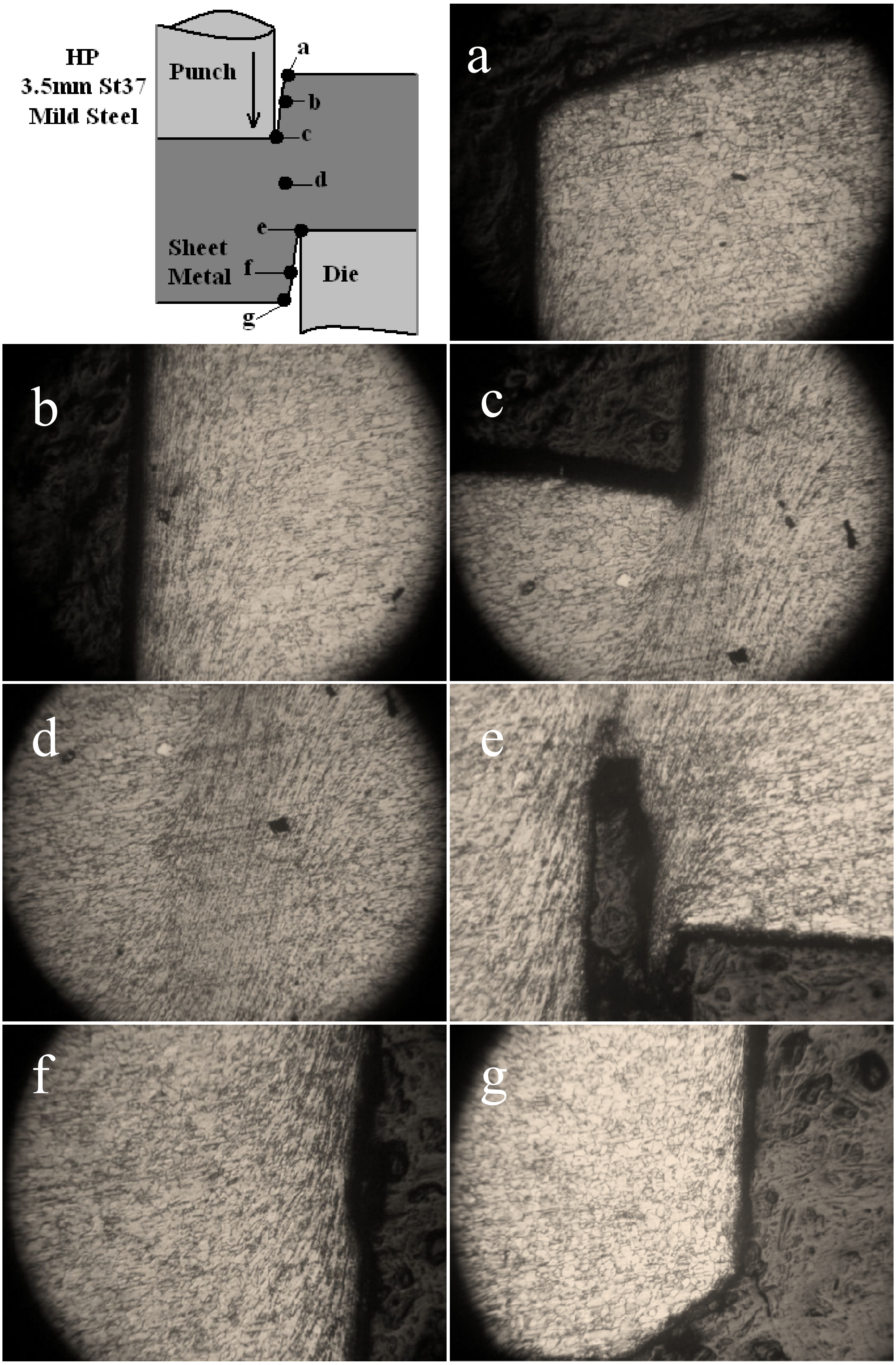
HP
3.5mm St37
Mild Steel
Punch
a
b
c
d
e
Sheet
Metal
f
g
Die
a
b
c
d
e
f
g

Figure 6.32 Micro-structure of blanking and piercing part of 3.5mm St37 at HP (x90)

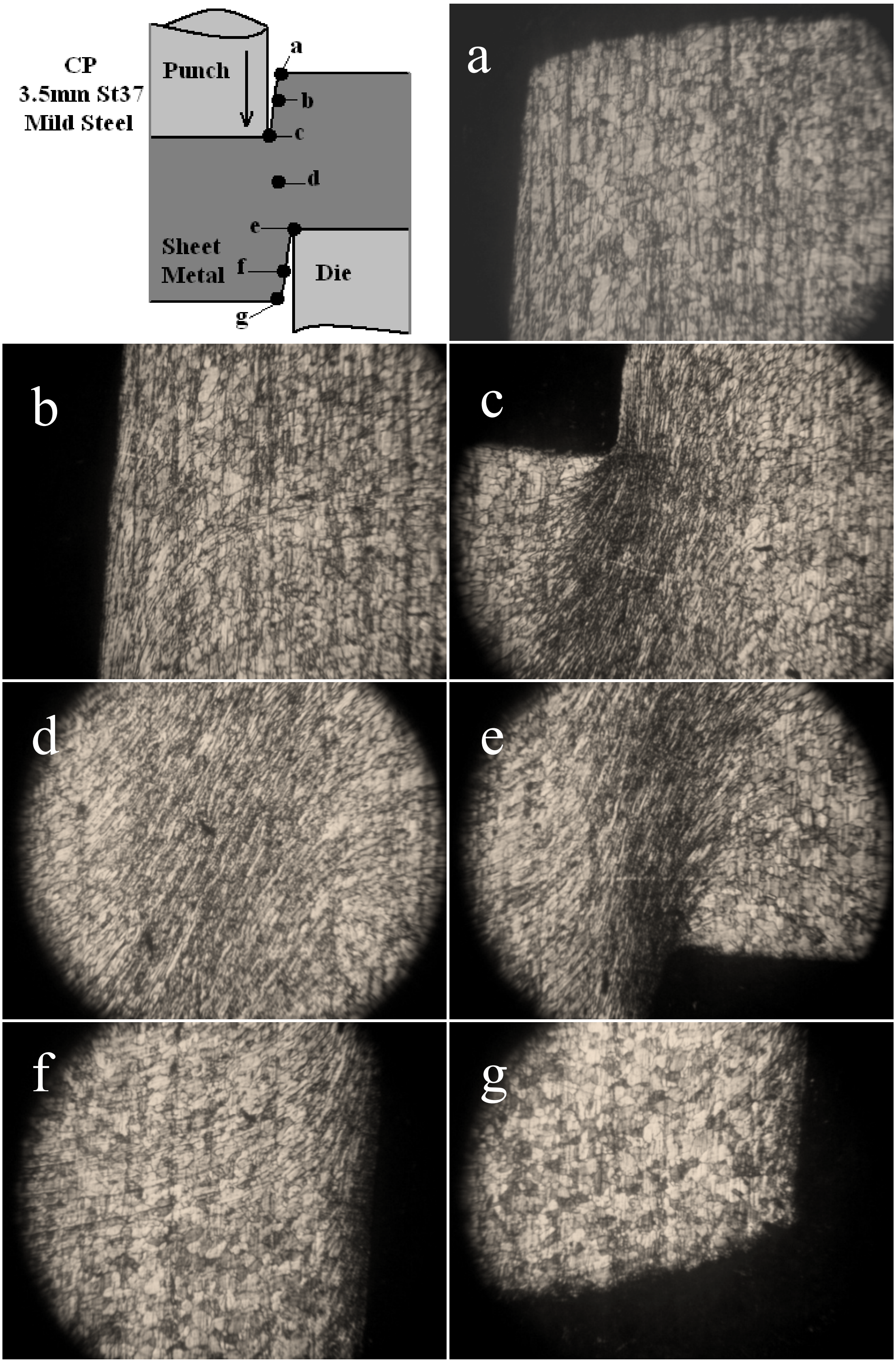
CP
3.5mm St37
Mild Steel
Punch
a
b
c
d
e
Sheet
Metal
f
Die
g
a
b
c
d
e
f
g

Figure 6.33 Micro-structure of blanking and piercing part of 3.5mm St37 at CP (x90)

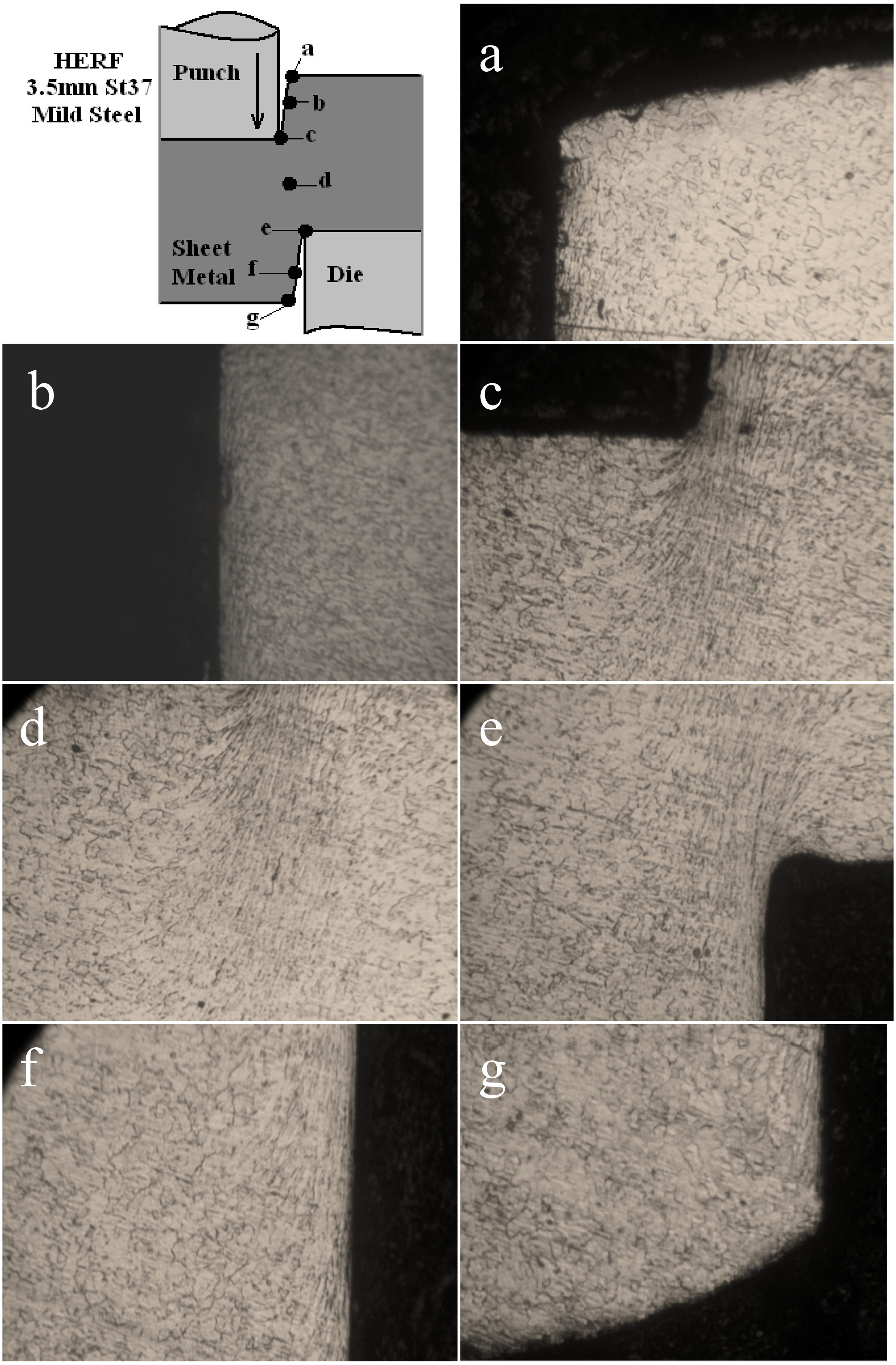
HERF
3.5mm St37
Mild Steel
Punch
Sheet
Metal
Die
a
b
c
d
e
f
g

Figure 6.34 Micro-structure of blanking and piercing part of 3.5mm St37 at HERF (x90)

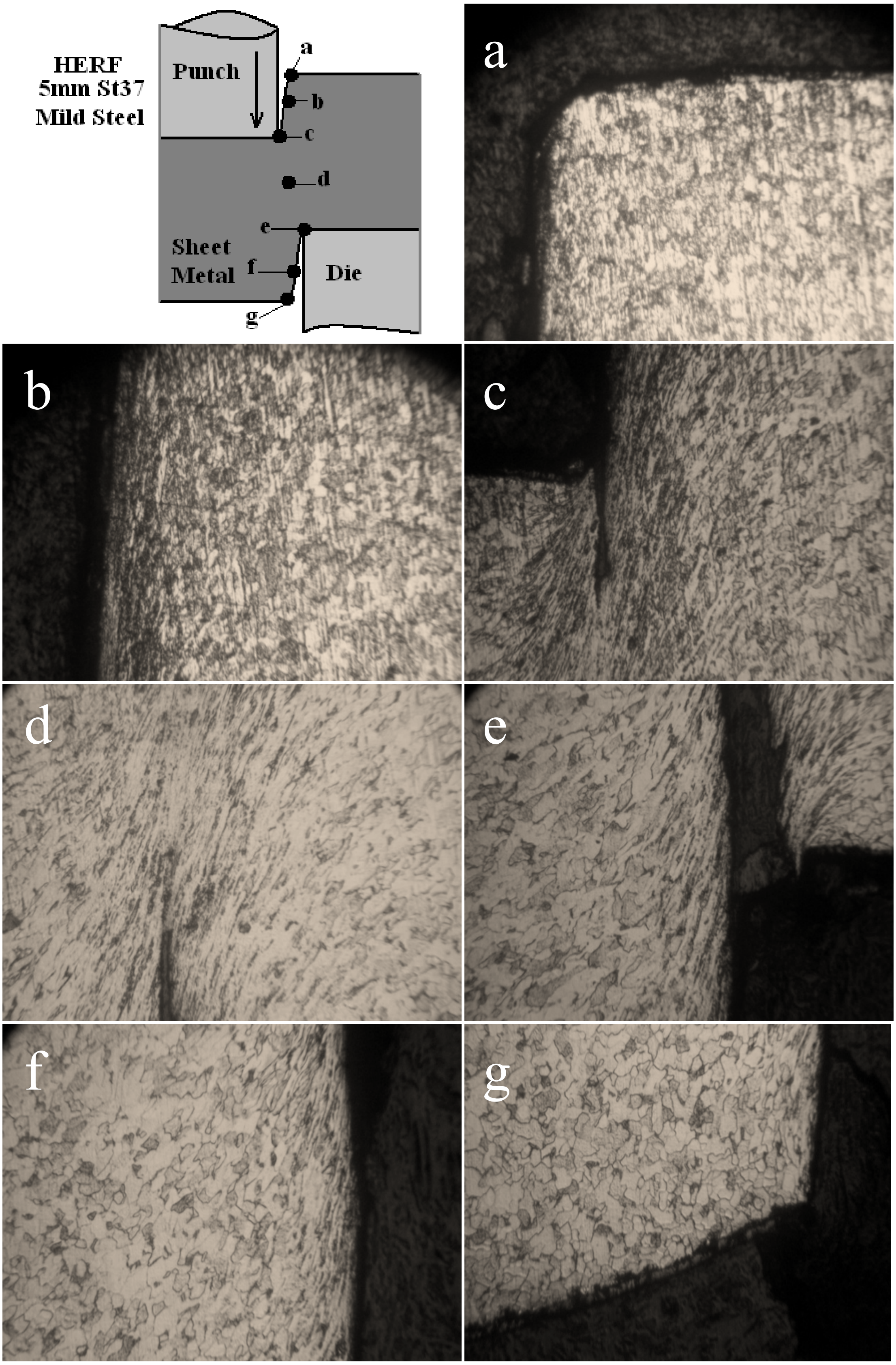
HERF
5mm St37
Mild Steel
Punch
Sheet
Metal
Die
a
b
c
d
e
f
g

Figure 6.35 Micro-structure of blanking and piercing part of 5mm St37 at HERF (x90)

6.2.3. Explanation of Blanking Load and Energy Reduction in HERF Hammer

The results of experimental studies show that there is a significant reduction in the blanking load and energy for all the materials under inspection (aluminum, mild steel, stainless steel) worked on the HERF hammer. The reason of this reduction may be explained using the adiabatic shear phenomena.

Adiabatic shear is a deformation model, which is unique to high strain rates of deformation. In metals and alloys, it is well known that at room temperature, about 95%of the work done in plastic flow is converted to heat. Adiabatic shearing is a particular situation in which the heat generated in a localized band cannot be dissipated because of the high strain rate and the thermal properties of the material **(Woodward, 1990).** In fact, a truly adiabatic deformation does not exist, some part of the heat is being lost to the surrounding, but the term adiabatic is taken here to show that large part of the heat is retained in the band **(Hamouda, 2002)**.

When the metals and alloys are deformed at large strain and very high strain rates such as in ballistic impact and penetration, machining, and high speed forging, localized shearing can occur, leading to localization of heat generation. Generally, the flow stress increases with increasing strain and strain rate. However, in localized shearing, the increased temperature reduces the flow stress.

There have been a number of attempts to measure the temperature rise associated with shear bands. **Hartney et al. (1987)** used an infrared radiation detection method to measure temperature rises across shear bands in mild steel. Temperatures of the order of 400 ^{0}C were recorded, and there was a variation in temperature across the bands.

Altan et al (2006) studied one of the benefits of high-speed blanking is that temperatures up to 980^{o}C may be generated in the shearing zone, creating a stress-release effect within the material.

Dixon and Parry (1991) studied the effect of temperature rise during deformation in carbon steel type 224. They reported that for strain rate of less than$(10^{-2}\ s^{-1})$, the compression test on this type of steel can be regarded as isothermal. However, when the strain rate exceeds about $(4\ s^{-1})$, the tests have definitely shown to be adiabatic.

Because of the fact that the speed of HERF hammer is 12m/s and that the average strain rate is 3500 s^{-1}, adiabatic shear band forms in blanking process. Micro-structures of samples from literature (a), those obtained with the prototype HERF hammer (b) and CP (c) are given in Figure 6.36. The fact the shear bands in Figure 6.36a and Figure 6.36b are narrow and parallel to each other shows that they are adiabatic shear bands. On the other hand, the fact the shear band in Figure 6.36c is wide proves that it is not adiabatic shear band.

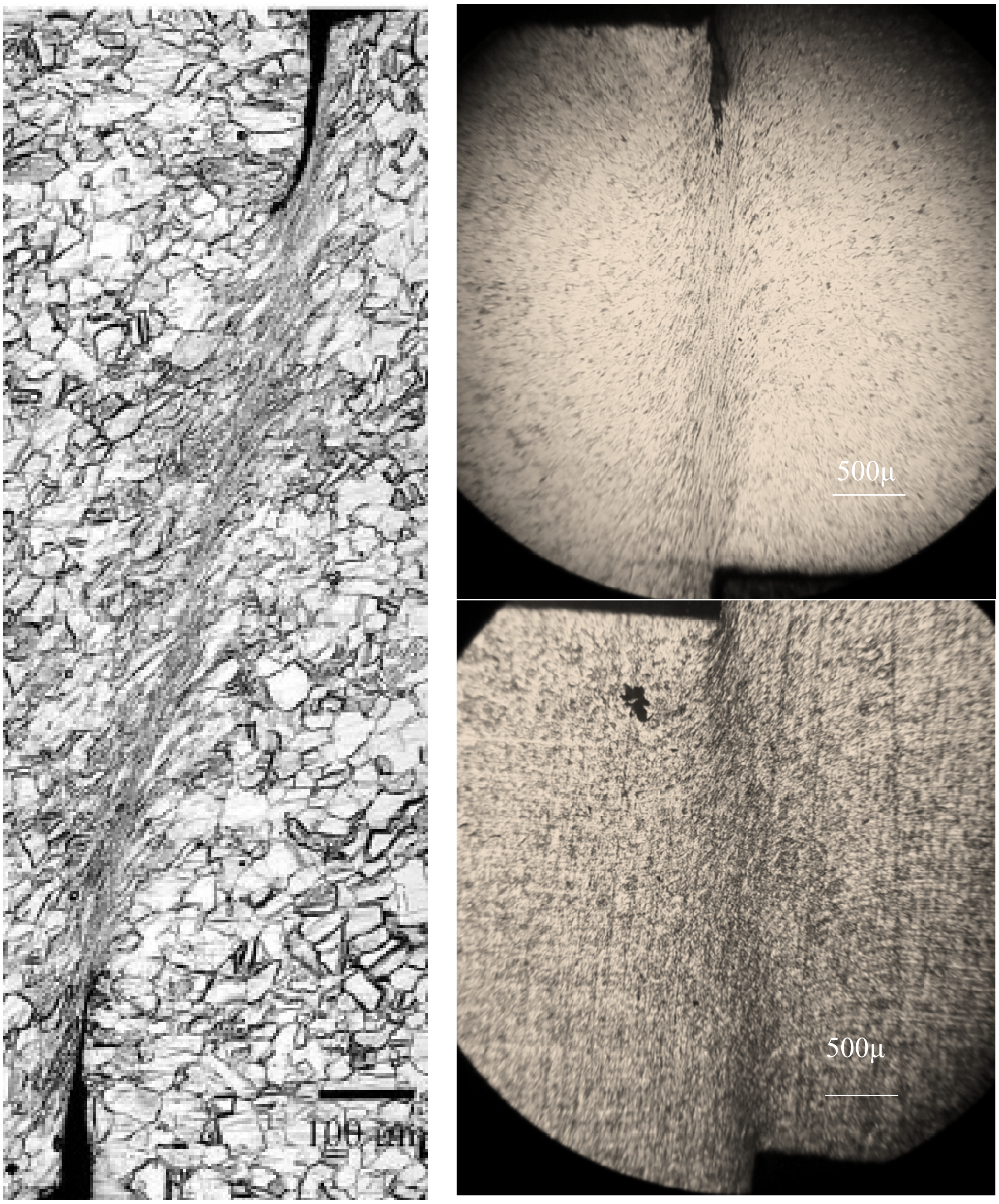

Figure 6. 36 a) Adiabatic shear band Ref (Bronkhorst, 2006) b) adiabatic shear band result of the HERF hammer c) non-adiabatic shear band result of the CP

6.3 SHEAR SURFACE QUALITY

6.3.1 Shear Surface Geometry

Figure 6.37 presents the effects of die clearances and punching speeds on the shear and fracture surfaces of the aluminum materials. As it is obviously seen in Figure 6.37, increasing the die clearances from 2% to 4% decreased the shear surface of the aluminum material significantly. The same situation was also observed at increasing of the punching speed. Increasing of the punching speed decreased the shear surface of the material and it was close to the ideal rate. The ideal shear to the whole surface rate was defined as 30% **(Semiatin, 1988)** for increasing the surface quality and for decreasing of the required energy.

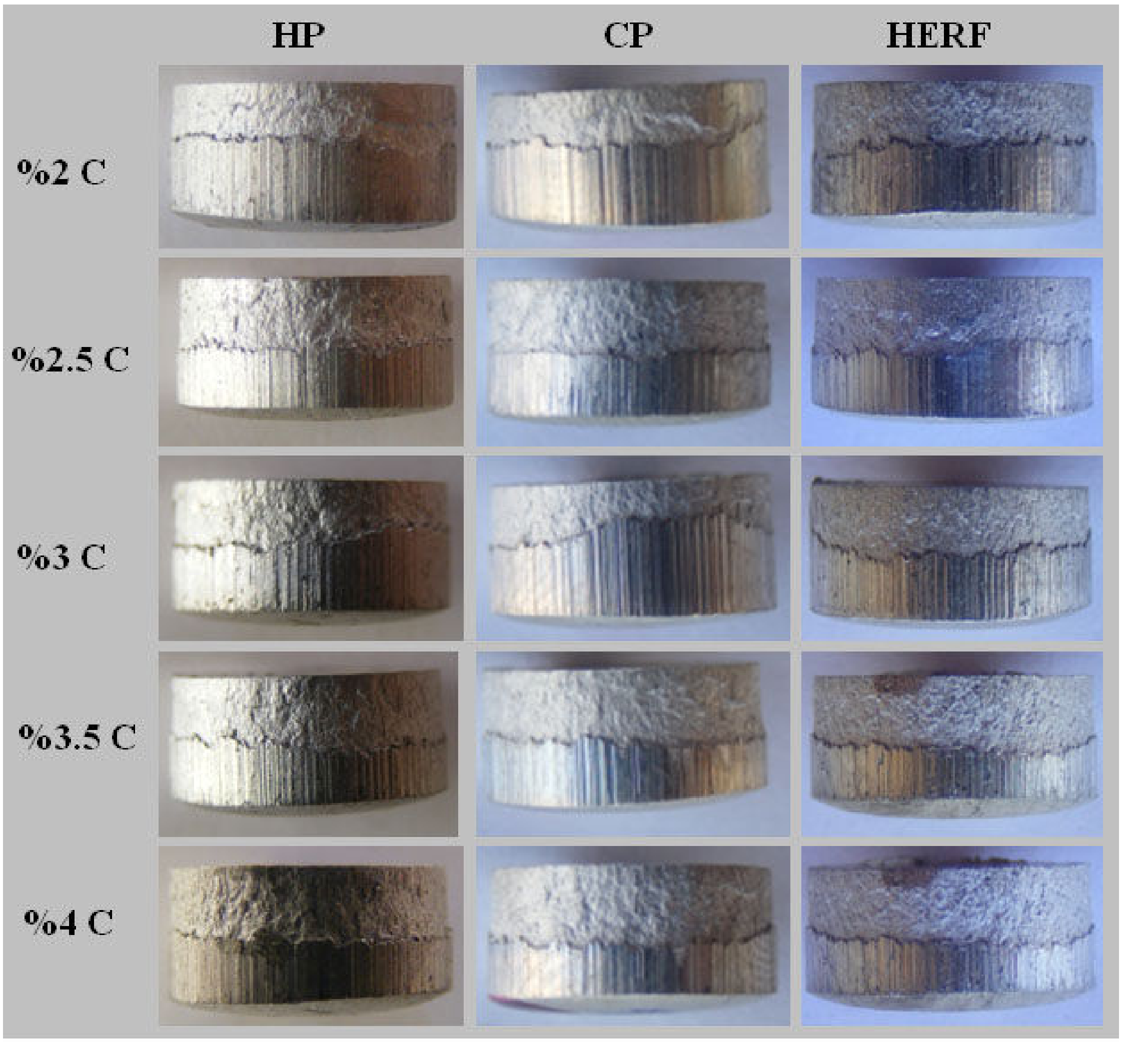

Figure 6.37 Shear and fracture surfaces of the aluminum materials according to the press type and die clearances

Certain geometric values of aluminum samples which were obtained at different clearance and speed levels and illustrated in Figure 6.37 are given in Table 6.8. In order to obtain accurate values, at least three samples verifying each other were taken for each situation and their mean value was recorded as the result. Data in the table confirm that the geometric quality of blank pieces at high speed punching was quite high.

Table 6. 8 Geometric values of 5mm Aluminum at different blanked speed

Aluminum	Geometric Value				
Machine	Clearance %	Shear Surf. %	Fracture Surf. %	Roll. Depth %	Dishing (μm)
HP	2	70	20	10	131
	2.5	60	29	11	137
	3	50	38	12	140
	3.5	42	44	14	156
	4	40	45	15	170
CP	2	60	31	9	120
	2.5	48	41	11	126
	3	44	44	12	130
	3.5	40	48	12	140
	4	34	53	13	145
HERF	2	45	48	7	83
	2.5	40	52	8	86
	3	38	53	9	112
	3.5	33	56	9	122
	4	32	58	10	126

Figure 6.38 presents the shear and fracture surfaces of the mild steel according to the die clearances and press types. As in the aluminum case, shear surfaces of the mild steel decreased with both of the die clearances and punching speed increased. The best surface quality of the mild steel was observed at the 5.5% die clearances at the conventional and hydraulic presses, while at the HERF hammer it was observed at the 5.0% die clearances.

Table 6.9 gives certain geometric values of St 37 mild steel samples which were obtained at different clearance and speed levels and illustrated in Figure 6.38. Data in the table confirm that the geometric quality of blank pieces at high speed punching was quite high.

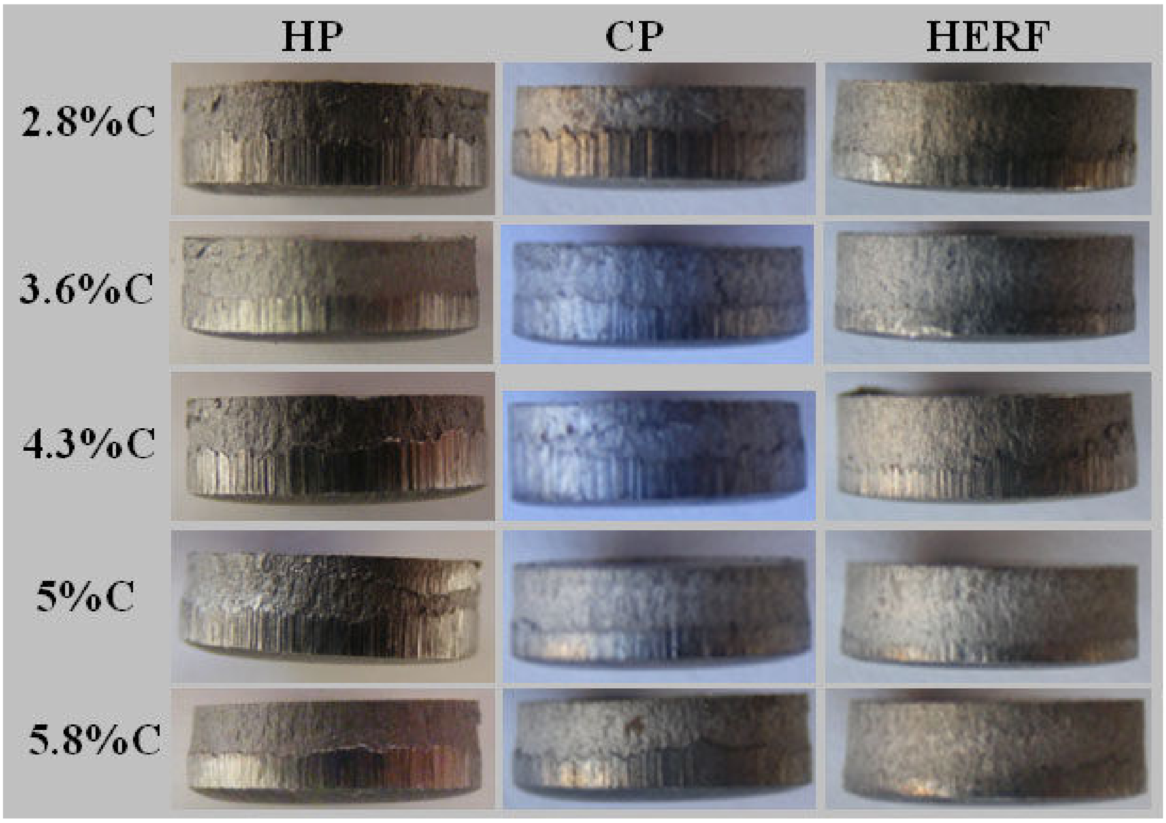

Figure 6. 38 Shear and fracture surfaces of the mild steel material according to the press type and die clearances

Table 6.9 Geometric values of 3.5mm St37 mild steel at different blanked speed

St 37 Mild Steel	Geometric Value				
Machine	Clearance %	Shear Surf. %	Fracture Surf. %	Roll. Depth %	Dishing (µm)
HP	2.8	60	28	12	68
	3.6	50	37	13	75
	4.3	45	41	14	85
	5	40	45	15	98
	5.8	32	52	16	103
CP	2.8	51	39	10	50
	3.6	45	45	10	65
	4.3	39	49	12	78
	5	34	53	13	85
	5.8	30	57	13	90
HERF	2.8	35	59	6	46
	3.6	30	64	6	55
	4.3	28	65	7	67
	5	22	71	7	70
	5.8	20	72	8	79

Figure 6.39 presents the shear and fracture surfaces of the stainless steel according to the die clearances and press types. As in the aluminum and mild steel cases, shear surfaces of the stainless steel decreased with both of the die clearances and the punching speed increased. The best surface quality of the mild steel was observed at the 10.0% die clearances at the conventional and hydraulic presses, while at the HERF hammer it was observed at the 8.75% die clearances.

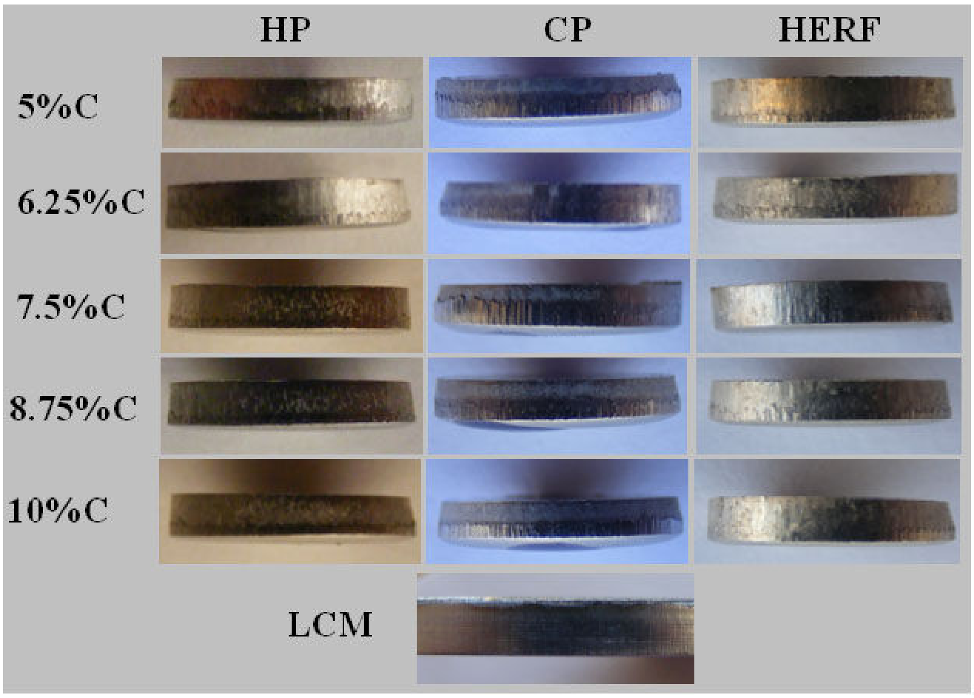

Figure 6. 39 Shear and fracture surfaces of the stainless steel materials according to the press type and die clearances

Certain geometric values of AISI 304 stainless steel samples which were obtained at different clearance and speed levels and illustrated in Figure 6.39 (see Table 6.10). Data in the table confirm that the geometric quality of blank pieces at high speed punching was quite high.

Surface views of St 37 mild steel with thickness values of 3.5, 5, and 6 mm obtained at three different speeds are presented in Figure 6.40. These samples blanked at the same die clearance show that samples blanked at high speeds have better surfaces. Secondary crack formation is observed in this figure for HP and CP blanks due to lower clearances as explained in section 3.6.4.

Table 6.10 Geometric values of 2mm AISI 304stainless steel at different blanked speed

AISI 304 Stainless Steel			Geometric Value		
Machine	Clearance %	Shear Surf. %	Fracture Surf. %	Roll. Depth %	Dishing (μm)
HP	5	50	42	8	108
	6.25	45	45	10	125
	7.5	40	50	10	145
	8.75	35	53	12	163
	10	30	58	12	177
CP	5	65	27	8	150
	6.25	50	37	13	185
	7.5	45	38	17	228
	8.75	35	47	18	285
	10	30	50	20	390
HERF	5	33	63	4	35
	6.25	28	68	4	45
	7.5	25	70	5	52
	8.75	20	74	6	60
	10	15	79	6	63

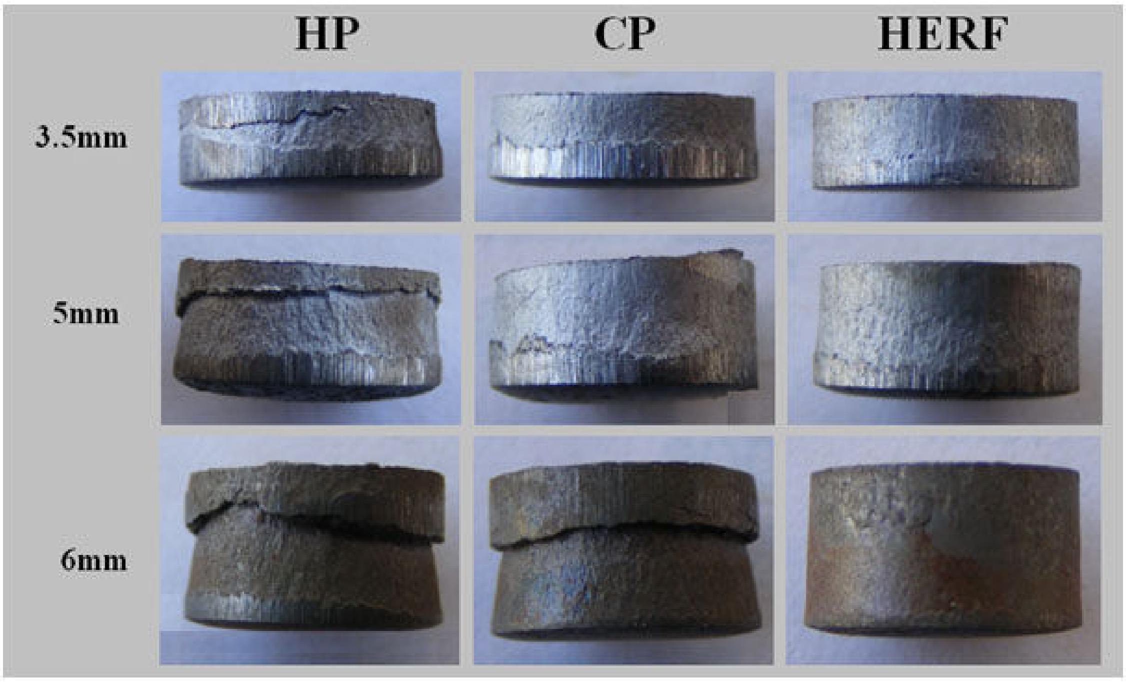

Figure 6. 40 Views of St 37 blanked material with thickness values of 3.5, 5, and 6 mm at HP, CP, and HERF hammers

6.3.2 Surface Roughness

6.3.2.1 Effects of High Speed Blanking on the Shear Surface Roughness of St 37 Mild Steel

The micro-geometrical quality of the shear and fracture surfaces were characterized by the average (Ra) roughness parameter. Figure 6.41 presents the roughness of shear and fracture surfaces of the three different types of cutting machines with using four different die clearances for 3.5mm thick mild steel specimens. It is clear in Figure 6.41 that the increase in cutting speed has a tendency of improving both cutting and fracture surfaces. The best cutting and fracture surfaces were obtained at the 5, 5.5, and 6% clearance by using HERF, CP, and HP, respectively. However, fracture surface roughness values of the HERF hammer were comparable to the shear surface roughness values CP and HP.

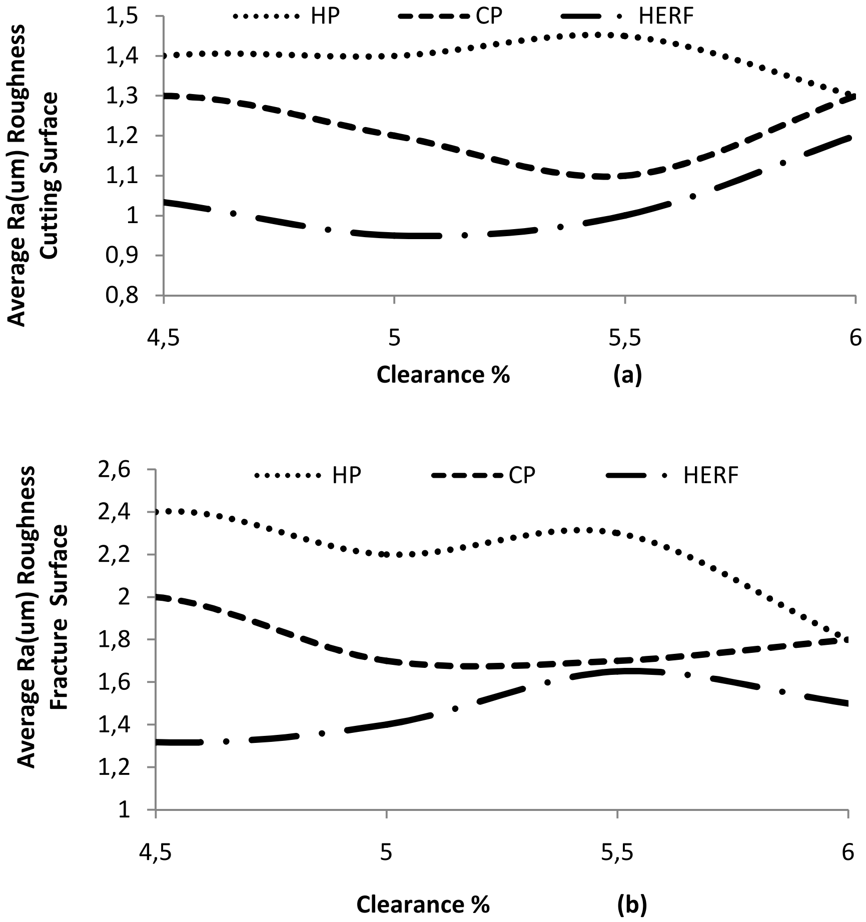

Figure 6. 41 Relationship among the three different types of cutting machines with using four different die clearances a) cutting surface b) fracture surface

Surface and detailed SEM views of the shear and fracture region of the blanks obtained from machines with different punching speeds are given in Figure 6.42. The best roughness values depend on the clearance for the each machine type is presented in the figure. As the punch speed increases, a decrease in roughness value in the shear and fracture region appears.

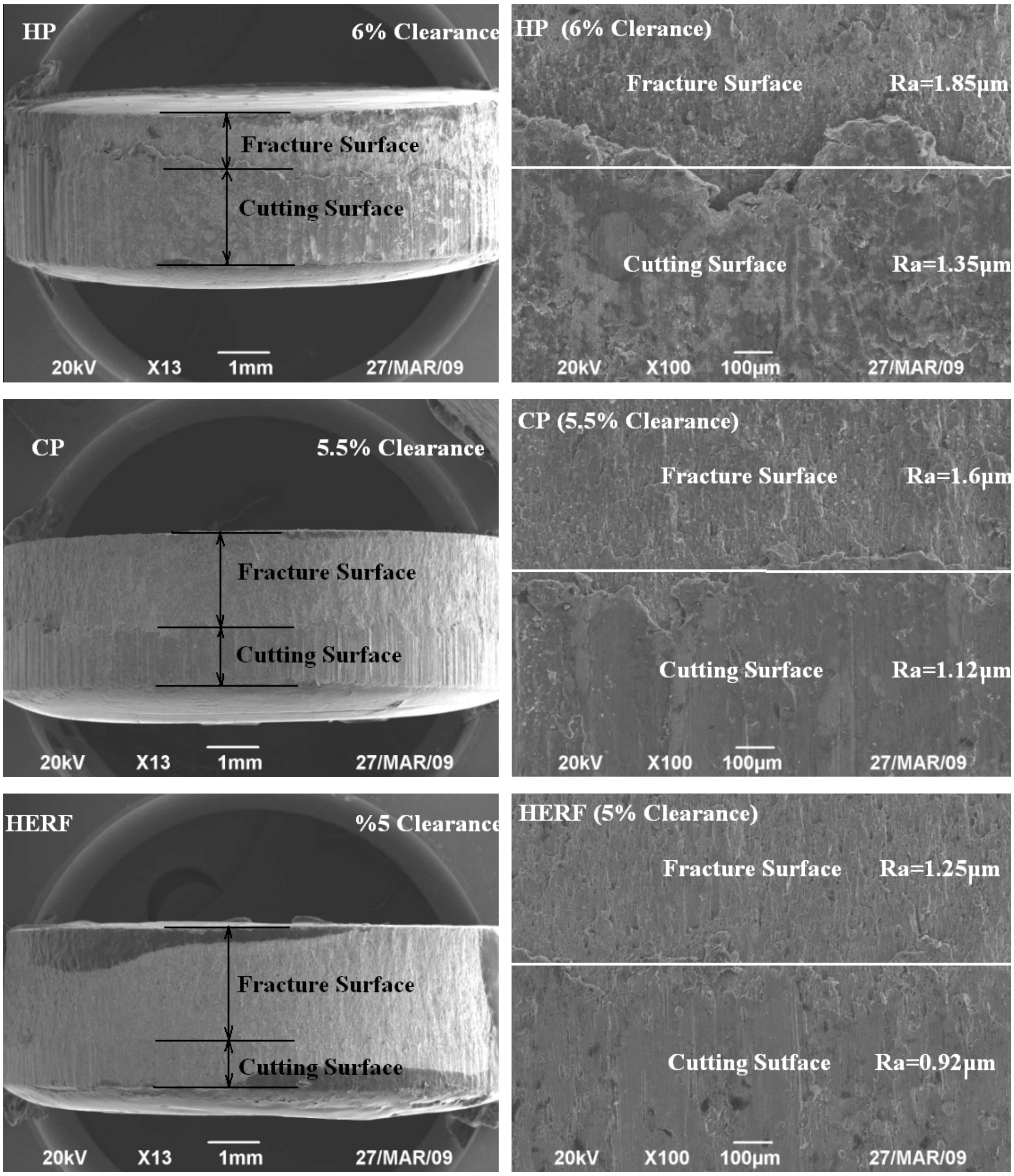
HP
6% Clearance
Fracture Surface
Cutting Surface
20kV X13 1mm 27/MAR/09
HP (6% Clerance)
Fracture Surface Ra=1.85μm
Cutting Surface Ra=1.35μm
20kV X100 100μm 27/MAR/09
CP
5.5% Clearance
Fracture Surface
Cutting Surface
20kV X13 1mm 27/MAR/09
CP (5.5% Clearance)
Fracture Surface Ra=1.6μm
Cutting Surface Ra=1.12μm
20kV X100 100μm 27/MAR/09
HERF
%5 Clearanc
Fracture Surface
Cutting Surface
20kV X13 1mm 27/MAR/09
HERF (5% Clearance)
Fracture Surface Ra=1.25μm
Cutting Sutface Ra=0.92μm
20kV X100 100μm 27/MAR/09

Figure 6. 42 SEM views the shear and fracture region of the St 37 blanks obtained from machines with different punching speeds

Altan et al (2006) state that average surface roughness values were between 0.3 – 1.2 µm and that high speed blanking gives good results comparable to fine blanking. Values within this range are achieved even in fracture surface of blanks at HERF hammer.

6.3.2.2 Effects of High Speed Blanking on the Shear Surface Roughness of AISI 304 Stainless Steel

Figure 6.43 presents the relationship between four different types of cutting machines which cut AISI 304 Stainless Steel specimens and their shear surface roughness. The average surface roughness (Ra) values of the specimens were about 0.32µm, 0.65 µm, 0.7µm and 0.72µm for HERF, HP, CP, and LCM (laser cutting machine), respectively. Increase in cutting speed has a tendency of improving the surface finish and thus reducing the Ra parameter as indicated in Ref **(Gurnel ,2006) and (Boothroyd, 1989**). Upper and lower limits of average surface roughness are stated for different cutting machines.

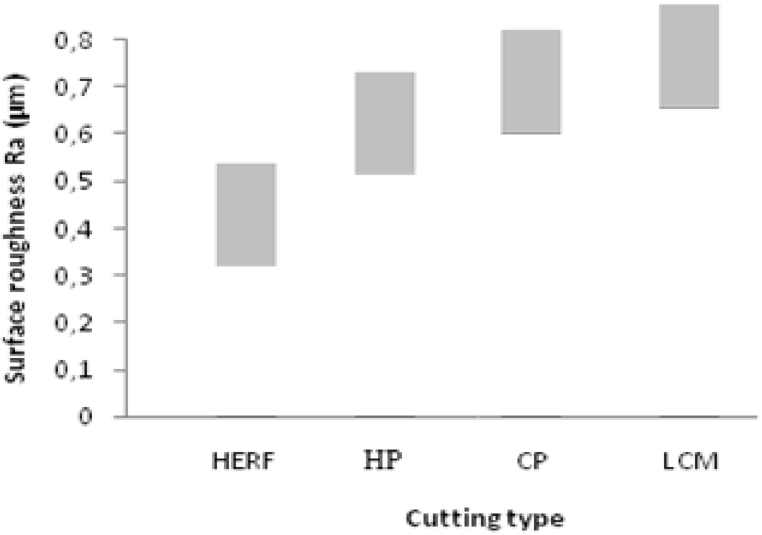

Figure 6. 43 Surface roughness (Ra) for different cutting conditions

Figure 6.44 shows AISI 304 Stainless Steels were cut with three different types of cutting machines, namely Laser Cutting Machine, Conventional Presses and HERF hammer.

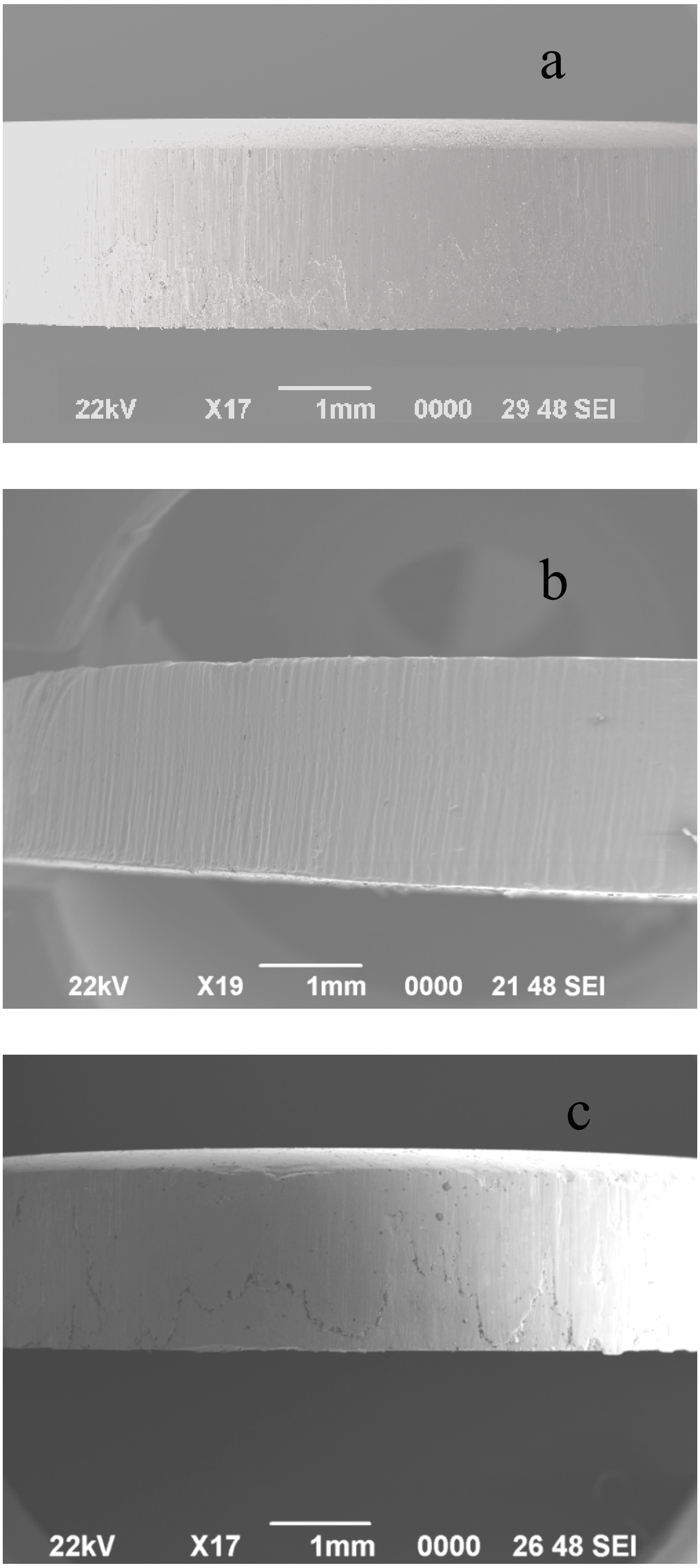
a
22kV X17 1mm 0000 29 48 SEI
b
22kV X19 1mm 0000 21 48 SEI
c
22kV X17 1mm 0000 26 48 SEI

Figure 6. 44 SEM views of the blanks cut by a)CP b)LCM c)HERF

6.4 CORROSION BEHAVIOUR

6.4.1 Effects of High Speed Blanking on the Shear Surface Corrosion of St 37 Mild Steel

The sheared surface of the blanks were subjected to corrosion in 3.5% NaCl solution and potential corrosion graphics are given in Figure 6.45. The corrosion resistance in shearing with Hydraulic Press (a) increased in direct proportion with clearance and the shear performed in 6% die clearance reflected the best corrosion properties. In other shears, too, the clearance proportion of 4.5% showed poor corrosion properties; while the shear performed with a die clearance of 5.5% in mechanical presses (b) and 5% in HERF (c) reflected the best corrosion properties.

The corrosion potential in shear with hydraulic press (E_{corr}) is -0.615 V (SCE) for the blank with a clearance of 6%, while it is -0,730 V for the blank with a die clearance of 4.5%. Compared to the blank with a die clearance of 4.5%, the blank with a die clearance of 6% is 18% more corrosion resistant. In blanks formed with eccentric press, the lowest corrosion potential was observed in the blank with a die clearance of 4.5% (-0.790 V), whereas the highest potential was recorded for the blank with 5.5% die clearance (-0.643 V). There is a 23% improvement between the two blanks. In blanks shaped with high energy, the lowest corrosion potential is -0.689 V for blanks of 4.5% die clearance, while the highest resistance (-0.594) was observed in the blank with a die clearance of 5%, and thus a corrosion potential difference of 16% occurred.

The corrosion potential of all blanks is given in Table 6.11. The comparison of the blanks that give the best corrosion rate for each shearing technique is given in Figure 6.46. In all the die clearances that were tested, the corrosion potential of the blanks that were formed with HERF hammer was found to be favorable.

Post-experiment SEM views of the shear and fracture surface of blanks after corrosion test are given a magnification of x1000 in Figure 6.47. In punching with eccentric press, the shear and fracture surface of the blank is more vulnerable to corrosion when compared to other punching techniques. The surface of blanks produced with HERF hammer is observed to be less influenced by corrosion experiments. The SEM views of the blanks verify the graphics in Figures 6.45, 6.46.

When mild steels are put into natural aqueous solution, this leads to defects in oxide layer on the steel. This corrosion defects appear in dislocation networks or grain boundaries on steel surface as mechanical damage such as erosion and roughness.

Literature **(Pardo et al,2006),(Chen et al,200) and (El-Hossary et al,2008)** verifies that material's resistance to shear increases at high speeds and strain rates, and that at the same time temperature on sheared surface of soft steels increases to approximately 600 ºC. Temperature of the blanks produced with HERF increases to stress relief annealing levels immediately after shearing and then cools to room temperature again. This eliminates substantially the residual stresses that form on the shear and fracture surfaces in blanking. Therefore, the corrosion potential of blanks produced with HERF appears to be higher. Strain rates (s^{-1}) of blanks produced eccentric press are not high enough to increase the shear surface temperature to treatment temperature. At the same time, it is high enough to increase resistance against shear. Hence, compared to other blanks, the shear and fracture surface corrosion potential of the blanks produced with eccentric press seems to be low.

Table 6.11 The corrosion potential of all blanks

Type of Presses	Clearance			
	%4,5 (V)	%5 (V)	%5,5 (V)	%6 (V)
HP	-0,7307	-0,6784	-0,6235	-0,6157
CP	-0,7908	-0,7268	-0,6432	-0,7164
HERF	-0,6889	-0,5935	-0,6052	-0,6150

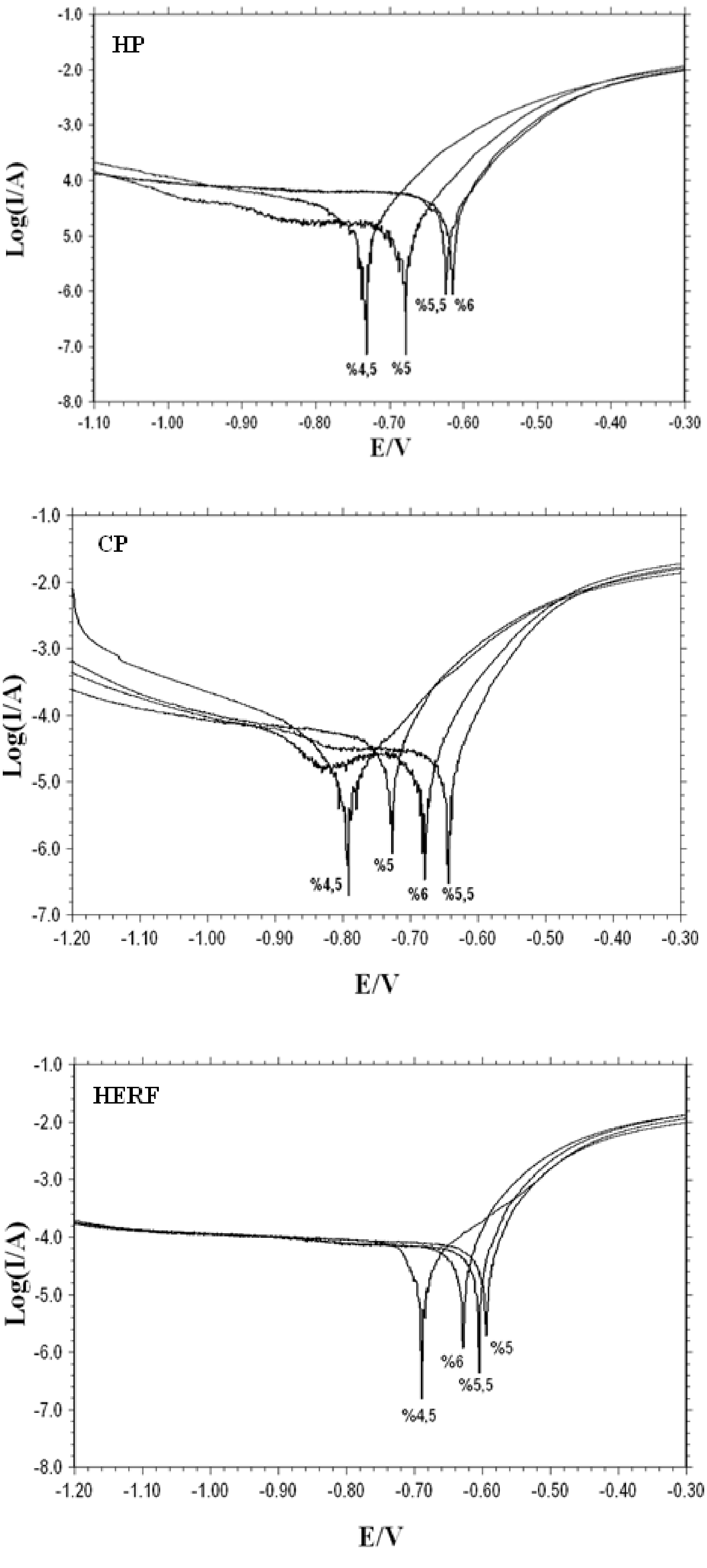

Figure 6. 45 Potential corrosion graphics of the blanks produced in different clearances for a) Hydraulic b) Conventional c) HERF

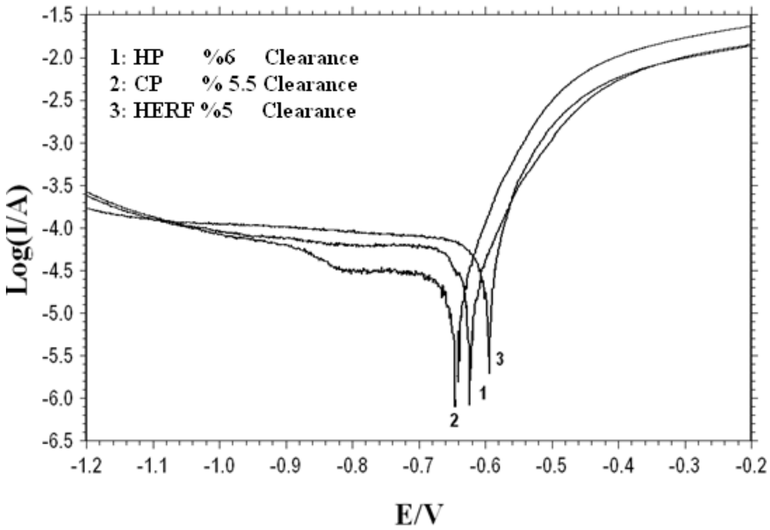

Figure 6. 46 The comparison of the blanks with the best corrosion rate for each shearing technique

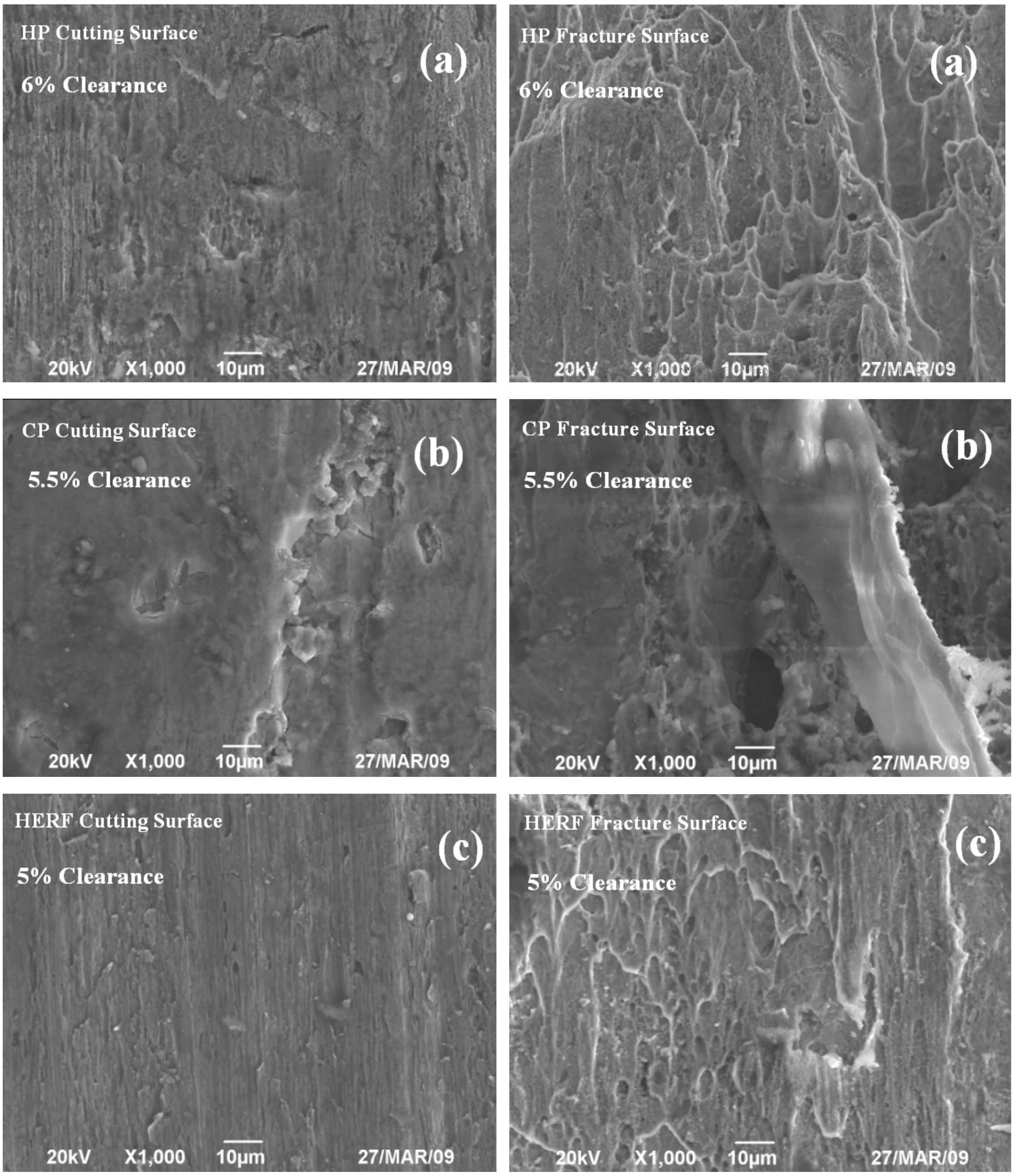
HP Cutting Surface
6% Clearance
(a)
20kV X1,000 10μm 27/MAR/09
HP Fracture Surface
6% Clearance
(a)
20kV X1,000 10μm 27/MAR/09
CP Cutting Surface
5.5% Clearance
(b)
20kV X1,000 10μm 27/MAR/09
CP Fracture Surface
5.5% Clearance
(b)
20kV X1,000 10μm 27/MAR/09
HERF Cutting Surface
5% Clearance
(c)
20kV X1,000 10μm 27/MAR/09
HERF Fracture Surface
5% Clearance
(c)
20kV X1,000 10μm 27/MAR/09

Figure 6. 47 SEM views of the shear and fracture surface of the blanks after corrosion test for a) Hydraulic b) Conventional c) HERF

6.4.2 Effects of high speed blanking on the shear surface corrosion of AISI 304

In Table 6.12, the average values and their standard deviations are given. The Open Circuit Potential (OCP) is the most negative for the CP punched AISI 304 steel followed by the steel cut with LCM, while it is the least negative for the HERF punched steel. The series are CP< LCM< HERF in the OCP holds.

Table 6.12 Open circuit potentials in 0.5 mol/dm^3 in de-aerated sulphuric acid solution vs. SCE

Cutting Type	Number of experiments	OCP (mV)
Conventional Press	10	-482±8
Laser Cutting Machine	10	-467±6
HERF Hammer	10	-440±5

Potentiodynamic polarization curves of the Conventional specimens cut with Laser and HERF are given in Figure 6.48. It can be clearly seen that the highest corrosion resistance is exhibited by the HERF punched specimen. It is evident that fast cutting can significantly improve the corrosion characteristics of AISI 304 steel. When compared with other cutting speeds, the corrosion resistance has generally been worse because of the increasing surface energy after low punching speed.

Compared to E_{corr} values obtained in this figure, E_{corr} value of the HERF punched specimen is ~ 925 mV higher than that of the Conventional punched specimen and 788 mV higher than the one cut with laser. (− 587 mV, -450 mV and 338 mV for conventional, laser and HERF- cut specimens, respectively). Moreover, anodic current values (I_{corr}) of the samples after both conventional and laser cutting are so close to each other and lower than the one cut with HERF. The improved corrosion behavior of the HERF-cut sample is related to the fast cutting of the surface.

The specimen cut in a conventional way shows active behavior evidencing a low corrosion potential (−587 mV) and very high anodic currents. HERF-cut specimen is more resistant to general corrosion in comparison with conventional and Laser-cut specimens, but is subjected to pitting corrosion. After the potentiodynamic polarization tests, the corroded specimens exhibit the presence of many pits distributed on the surface as a typical results of chloride attack.

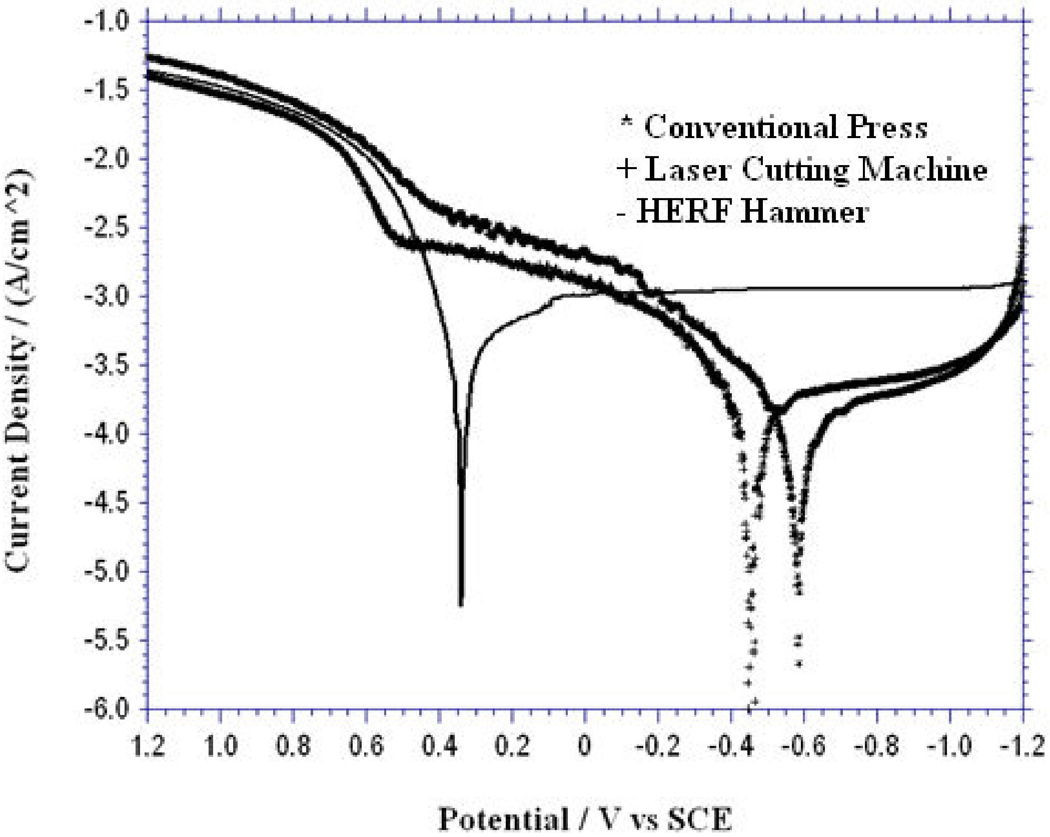

Figure 6. 48 Potentiodynamic polarization curves of specimens at different blanking speeds.

To give an overall view of the electrochemical processes cyclic voltammetry is used. Figure 6.49 shows the cyclic voltammograms (CV) of AISI 304 steels. The passivation peak for the conventional and laser cutting samples were very clear, while it is very small for the HERF cutting steel.

A smaller passivation peak means an originally existing protective surface oxide layer. This argument leads to the conclusion that the protective oxide layer on the HERF cutting steel is so stable that it is only slightly reduced during the negative scan. In case of the AISI 304 steel, however, the oxide layer was considerably reduced during the negative scan, since the passivation peak exists (Kerner et al, 2007).

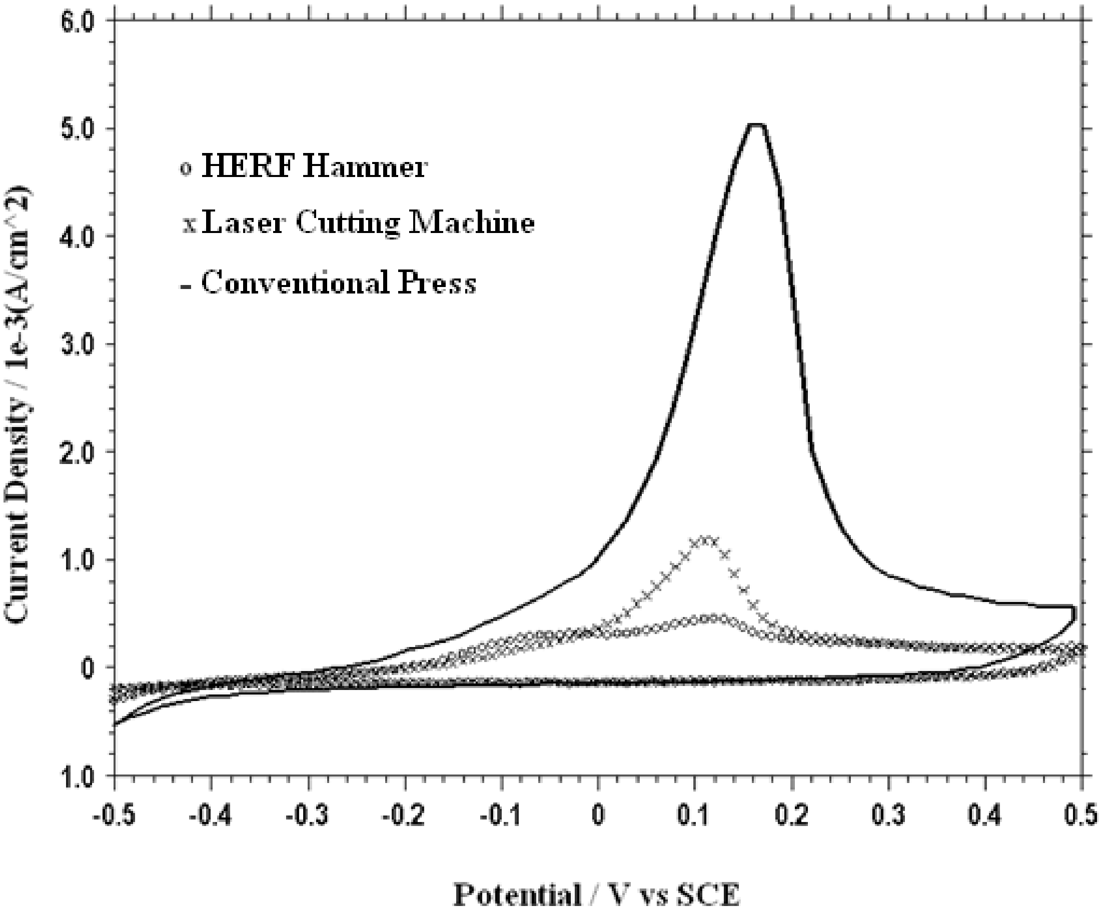

Figure 6. 49 Cyclic voltammograms of HERF cutting (frame cycle line), laser cutting (diagonal cross line), and conventional cutting (solid black line) AISI 304 steels in 0.5 mol/dm^3 sulphuric acid solution with 0.1 V/s scan rate, start potential −0.5 V,and negative first scan direction.

Thus, cyclic voltammetry allowed us to draw the same conclusion as we obtained from the OCP measurements; this supports the observation that the HERF cutting sample is the most corrosion resistive of the steels. The results obtained from the cyclic voltammetry and open circuit potentials are consistent with the work in Ref. (Kerner et al, 2007). Figure 6.50 and 6.51 show the SEM micrographs of before and after corrosion test. The reason of the pits is the local breakdown of the passivity occurred during the corrosion tests.

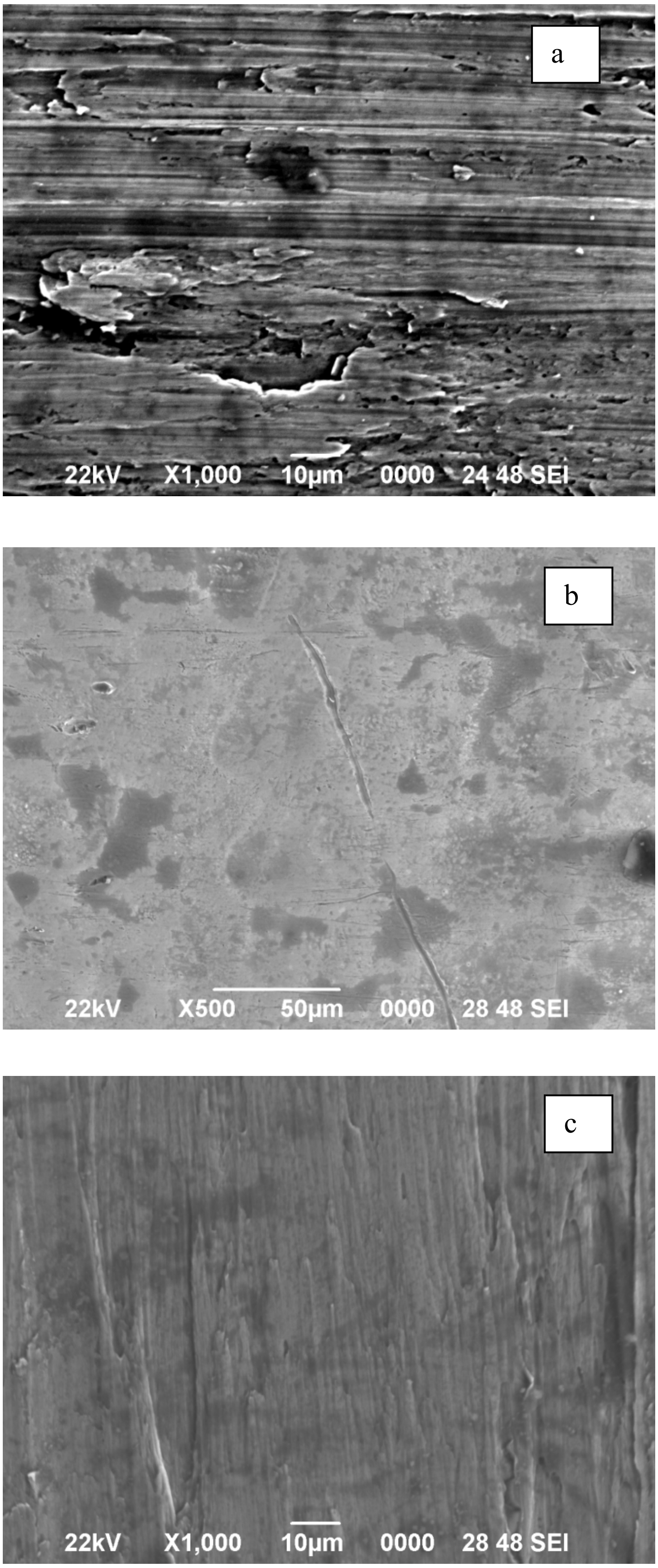
a
22kV X1,000 10µm 0000 24 48 SEI
b
22kV X500 50µm 0000 28 48 SEI
c
22kV X1,000 10µm 0000 28 48 SEI

Figure 6. 50 SEM micrographs of the samples before corrosion test a) CP b)LCM c)HERF

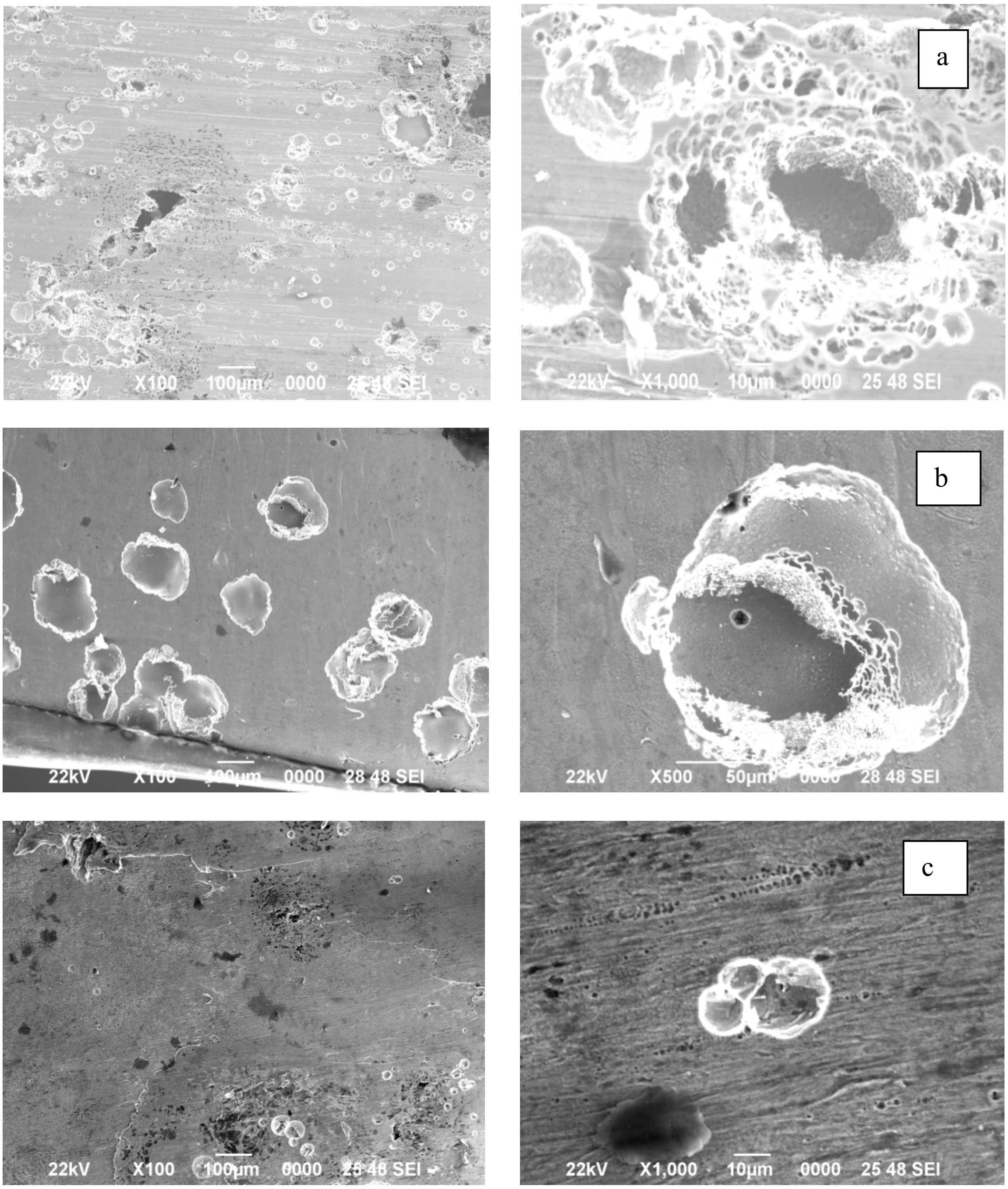
22kV X100 100µm 0000 25 48 SEI
a
22kV X1,000 10µm 0000 25 48 SEI
22kV X100 100µm 0000 28 48 SEI
b
22kV X500 50µm 0000 28 48 SEI
22kV X100 100µm 0000 25 48 SEI
c
22kV X1,000 10µm 0000 25 48 SEI

Figure 6. 51 Corrosion micrographs of specimens before corrosion test, a) CP b) LCM c) HERF.

Figure 6.51 shows SEM micrographic of the specimens that were cut with three different types of cutting machines. The metallographic investigations have showed that the effective corrosion formed on all specimens is pitting. The surface of the corroded sample of HERF-cut sample appeared almost untouched, and no severe corrosion damage at the end of corrosion tests was observed. It is well known that pitting corrosion forms holes and pits on the metal surfaces and these pits may be at rather different shapes and dimensions. The pits are oval in shape and average dimensions of the pits are 40 to 90 μm. The pit cell sizes have been found to be in the range of ∼ 20–35 μm, ∼ 170–195 μm and ∼ 120–180 μm for HERF-cut, conventional-cut and laser- cut, respectively. As a result of the corrosion tests, it is found that the HERF-cut specimens have smaller pit dimensions and exhibit better corrosion resistance when compared with the laser-cut and conventional-cut specimens, since smoother surface formed on the surface after the HERF cutting. However, the corrosion resistance is worse in the laser and conventional cutting because of the slow cutting of the surfaces.

CHAPTER 7

CONCLUSIONS AND FUTURE STUDIES

7.1 INTRODUCTION

The results of the study are concluded in this chapter. Suggestions for future studies are also given.

7.2 CONCLUSIONS

7.2.1 The HERF Hammer

The designed and constructed HERF hammer can be used in experimental purposes and its advanced versions can be constructed and used in metal forming industry.

The principle of two-stroke internal combustion engine to obtain high energy rate was used to achieve the aim of this thesis. In the high energy rate forming (HERF) hammer, re-cocking mechanism works mechanically. As a result of moving triggered unit, compressed air-fuel mixture burns in cylinder. Compression of air-fuel mixture in cylinder is the main duty of re-cocking mechanism.

This hammer is in small size when compared with conventional forming machines. Thus it takes small amount place in workshop. By using designed HERF hammer, the products can be manufactured advantageously at higher production rate.

Characteristics of the prototype HERF hammer were identified. The prototype HERF hammer has a maximum forming energy of 100 J and a ram velocity of 12m/s.

7.2.2 Forging using the HERF Hammer

The difference among the load-stroke curves of the aluminum, mild steel, and stainless steel was the value of the maximum forces, as was expected, when the hardness of the materials increased, the required energy for forging of the material was also increased.

When the presses were ranked according to the lowest required energy for forging of the billets of the same material, it was listed in the order of high energy rate forging machine, conventional press, and hydraulic press.

Moreover, the forging energy at the high energy rate forming machine was approximately 1.5 times lower than those of conventional and hydraulic machines for the same billets.

The results show that barreling is getting smaller with increasing the forging speed. This is due to change in friction condition at the contact surface of the workpiece and the die (punch and anvil).

Friction coefficient (μ) of the samples compressed with the hydraulic press, conventional press and HERF determined using the ring compression tests as 0.3, 0.27 and 0.09, respectively. The reason behind this situation can be that when the samples compressed with HERF hammer, friction between the die and billet changes from the static to dynamic behaviour. With the aid of this behaviour, friction between the surfaces and forging load were reduced significantly.

The fact that ideal forging load and experimental forging results were identical verifies the accuracy of load measurements in experiments.

7.2.3 Blanking using the HERF Hammer

The results of experimental studies show that there is a significant reduction in the blanking load and energy for all the materials under inspection (aluminum, mild steel, stainless steel) worked on the HERF hammer. The reason of this reduction may be explained using the adiabatic shear phenomena. As the speed of HERF hammer is

12m/s and that the average strain rate is 3500 s^{-1}, adiabatic shear band forms in blanking process. Micro-structures of the samples proved this situation.

The results show that as the blanking speed increases, the proper die clearance value decreases. For a practical purpose, a new die clearance selection diagram is proposed. The minimum and maximum limits of clearances versus sheet thickness for soft, medium-hard and hard materials were presented in this study.

It was observed that shear bands of HERF samples at high speeds were drastically narrower than other samples blanked at other machines. Although the flow lines of HERF samples were in the shear line, flow lines of HP and CP samples were observed to extend to outer sections of the shear line. As the expansion in the flow line demonstrates the sections affected in the blanking process, the narrowness of the shear band shows that the energy required for the blanking operation will be lower. Graphics in previous sections confirm that high speed blanking requires less energy.

The results also show that there was a decrease in rollover depth and plastic deformation in HERF blanking samples compared to HP and CP and that, therefore, there was an improvement in the geometry of blank and the sheet surfaces.

Even the same die clearance used, samples blanked at high speeds have better surfaces. Secondary crack formation is observed on the HP and CP blanks due to insufficient clearances.

It was observed that punching speed is very effective on the shear surface roughness values of the samples. When the punching speed increased, shear surface roughness values of the samples decreased drastically. Also, the corrosion resistance of the HERF-cut specimens was better than that of the laser-cut and conventional-cut specimens, since the cutting speed formed the least roughness on the surface.

7.3 FUTURE STUDIES

The following areas that required further investigation have become evident during the course of this study;

More rigid anvil and body can be designed in order to increase the efficiency of the mechanical re-cocking and combustion actuated HERF hammer.

A higher capacity HERF hammer can be designed to meet the requirements of the metal-working industry.

Following the improvements about internal combustion engines in literature and utilizing efficiency-raising innovations, the efficiency of the HERF hammer can be improved.

Studies that probe the use of natural gas, Liquid Petrol Gas (LPG), and diesel or any type of explosives as energy resource instead of gasoline can be carried out.

The HERF hammer can be used for material testing at high speeds by adjusting the compression ratio, i.e. forming speed.

Aerospace alloys and smart materials will be formed with different ram velocity and then the effect of forming speed on the properties of the forged product can be investigated.

REFERENCES

Abachi, S. (2004). Wear Analysis of Hot Forgings Dies. M. Sc. Thesis, Middle East Technical University, Ankara, Turkey

Aktakka, G. (2006). Analysis of Warm Forgings Process. M. Sc. Thesis, Middle East Technical University, Ankara, Turkey

Altan, T.(1998). Metal Forming Handbook. Schuler (c) Springer-Verlag Berlin Heidelberg

Altan, T., Boulger, F, W., Becker, J, R., Akgerman, N., and Henning, H, J. (1973). Forging Equipment, Materials and Practices, Batelle Columbus Laboratories Metalworking Division, Ohio

Astakhov, V. P. and Shvets, S. V. (2001). A novel approach to operating force evaluation in high strain rate metal-deforming technological processes, Journal of Materials Processing Technology 117 (2) 226-237

Banerjee, B. (2005). An evaluation of plastic flow stress models for the simulation of high- temperature and high-strain-rate deformation of metals, *Department of Mechanical Engineering, University of Utah, 50 SCentralCampusDr., MEB 2110, Salt Lake City, UT 84112, USA*

Batra, R.C. and Lear, M.H. (2005) Adiabatic shear banding in plane strain tensile deformations of 11 thermoelastoviscoplastic materials with finite thermal wave speed, International Journal of Plasticity 21 1521-1545

Berg, J.M., Adams, R.J., Malas, J.C. and Banda, S.S. (1995). Nonlinear Optimization-Based Design of Ram Velocity Profiles for Isothermal Forging IEEE Transactions on control systems technology. VOL 3, NO 3

Bhattacharyya A., Rittel, D. and Ravichandran G. (2005) Effect of strain rate on deformation texture in OFHC copper Scripta Materialia 52 657-661

Bing, G.J.A, and Wallbank J., (2008) The effect of using a sprung stripper in sheet metal cutting, Journal of Materials Processing Technology 200 176-184

Bishop, J.F.W. (1956) An approximation method for determining the temperatures reached in steady motion problems of plane plastic strain, Quart. J. Mech. Appl. Mater. 9 236.

Bodurov P. and Penchev T. (2005) Industrial rocket engine and its application for propelling of forging hammers Journal of Materials Processing Technology 161 504-508

Boothroyd G. (1989). Fundamentals of Machine and Machine Tools, Marcel Dekker, New York, USA

Bronkhorst, C.A., Cerreta, E.K., Xue, Q., Maudlin, P.J., Mason, T.A. and Gray, G.T, (2006). An experimental and numerical study of the localization behavior of tantalum and stainless steel, International Journal of Plasticity **22** 1304-1335

Brokken, D. Brekelmans W.A.M., and Baaijens F.P.T., (1998). Numerical modelling of the metal blanking process, Journal of Materials Processing Technology 83 192-199

Carrecker, R. P. and Hibbard Jr., W. R. (1957).Trans. TMS-AIME, Vol. 209
Chan, L.T,. Bakhtar, F., Tobias S.A., (1966) Design and development of Petro Forge high energy rate forming machines. Proc. Inst. Mech. Eng. 180

Chen J. Y., Yu G. P., Huang J. H., (2000) Corrosion behavior and adhesion of ion-plated TiN films on AISI 304 steel, Materials Chemistry and Physics 65 310-315

Chen, Y., Lee, J.D., Eskandarian, A., and Bedewi, N.E. (2000). Adibatic Shear Localization in Impact problems, International Conference of Crashworthiness, London, September 2000

Choi J.C.,and Kim C., (2001) A compact and practical CAD/CAM system for the blanking or piercing of irregular shaped-sheet metal products for progressive working, Journal of Materials Processing Technology 110 36-46

Chou, P. C, Hashemi, J., Chou, A., and H. C. Rodgers, (1991). Experimentation and Finite Element Simulation of Adiabatic Shear Bands in Controlled Penetration, Impact, International Journal of Impact Engineering, 11 305-321

Clous, R., Schreppel, U., and Veit, P., (2000). Experimental Study of Shear Band Formation in Various Steels, Advances in Mechanical Behavior, Plasticity and Damage; Proceedings of Euromat 2000, 463-468

Cora, O.N. (2004). Friction analysis in cold forging., A MSc thesis submitted to the graduate school of natural and applied sciences of METU, pp 23

Costin L.S., et al (1984) On the localisation of plastic flow in mild steel tubes dynamic torsional loading, in: J. Harding (Ed.), Mechanical Properties at High Rates of Strain, Inst. Phys. Conf. Ser. No. 70, 90

Dabboussi, W. and J.A. Nemes (2005). Modeling of ductile fracture using the dynamic punch test, International Journal of Mechanical Sciences 47 1282-1299

Davies, R. and Austin, E.R. (1970). Developments in high speed metal forming. New York: Industrial Press Inc.

Davies, R. and Dhawan, S.M. (1966). Further developments in high speed blanking of metals. In: Proceedings of 7th International machine tools design research conference, University of Birmingham

Dieter, G. E. (1976). Mechanical Metallurgy, McGraw Hill Kogakusha, Ltd., Tokyo

Dixon, P.R. and Parry, D.J. (1991). Thermal softening effects in type 224 carbon steel, in: Dymat'91, Strasbourg, France, p. 85

Doege, E. and Bohnsack, R. (2000). Close Die Technology for Hot Forging. Journal of Material Processing Technology, 98 165-170

Dougherty, L.M., Cerreta, E.K. Pfeif, E.A. Trujillo, C.P. and Gray III G.T. (2007). The impact of peak shock stress on the microstructure and shear behavior of 1018 steel, Acta Materialia 55 6356-6364

El-Hossary F.M., Negm, N.Z. Abd El-Rahman A.M., Hammad M., Templier C., (2008). Duplex treatment of AISI 304 austenitic stainless steel using rf nitriding and dc reactive magnetron sputtering of titanium, Surface & Coatings Technology 202 1392-1400

Farren, W.S. and Taylor, G.I. (1925). The heat developed during plastic extension of metals, Proc. R. Soc. London 107a 422

Faura F., Garcı, A. and Estrems M. (1998). Finite element analysis of optimum clearance in the blanking process, Journal of Materials Processing Technology 80-81 121-125

Ge, Y., Chen, L., Sun, F. and Wu, C. (2005). Thermodynamic simulation of performance of an Otto cycle with heat transfer and variable specific heats of working fluid, International Journal of Thermal Sciences 44 506-511

Groover, M. P. (1996). Fundamentals of Modern Manufacturing. Prentice-Hall Int. Inc.

Guohe, L., Minjie, W. and Chunzheng D. (2009). Adiabatic shear critical condition in the high-speed cutting, journal of materials processing technology 209 1362-1367

Gupta, N.K. Mohamed Sheriff, N. and Velmurugan, R. (2007). Experimental and numerical investigations into collapse behavior of thin spherical shells under drop hammer impact, International Journal of Solids and Structures 44 3136-3155

Gurnel A.G., (2006). An element-free Galerkin method approach for estimating sensitivity of machined surface parameters, International Journal of Machine Tools & Manufacture, 46 1637-1642

Hallstroöm, J. (2000). Influence of friction on die Rolling in counterblow hammer forging, Journal of Materials Processing Technology 108 21-25

Hambli R., (2001). Finite element model fracture prediction during sheet-metal blanking processes, Engineering Fracture Mechanics 68 365-378

Hambli, R. and Guerin F., (2003). Application of a neural network for optimum clearance prediction in sheet metal blanking processes, Finite Elements in Analysis and Design 39 1039-1052

Hamouda, A.M.S. (2002). Effect of energy losses during an impact event on the dynamic flow stress, Journal of Materials Processing Technology 124 209-215

Hartley, P. and Pillinger, I. (2006). Numerical simulation of the forging process. Computer methods in applied mechanics and engineering, 195, 7776-6690

Hartney K.A. et al., (1987). Measurement of the temperature profile during shear band formation in steels deforming at high strain-rates, J. Mech. Phys. Solids 35 283

Hatanaka, N., Yamaguchi, K. and Takakura N., (2003). Finite element simulation of the shearing mechanism in the blanking of sheet metal, Journal of Materials Processing Technology 139 64-70

Hosford W. F. and Caddell, R.M (1983). Metal Forming: Mechanics and Metallurgy, Prentice-Hall

Hosford, W. F. (2005). Mechanical Behavior of Materials. Cambridge University Press The Edinburgh Building, Cambridge CB2 8RU, UK

Hsu R.Q., Chang J.R.,and Liang D.L., (2008). Prediction of slug carry-up by the punch in blanking by air-blow of the slug, Journal of Materials Processing Technology 201 252-255

http://www.forging.org

Husson, C. Correia, J.P.M. Daridon, L.and Ahzi, S. (2008). Finite elements simulations of thin copper sheets blanking: Study of blanking parameters on sheared edge quality, Journal of Materials Processing Technology 199 74-83

Kalpakjian, S. and Schmind, S.R. (2006). Manufacturing Engineering and Technology. Pearson Education Inc.

Kerner Z., Horvath A., Nagy G., (2007). Comparative electrochemical study of 08H18N10T, AISI 304 and AISI 316L stainless steels, Electrochimica Acta 52 7529-7537

Kim, Y.H. and Wagoner, R.H. (1987). A analytical investigation of induced heating in tensile testing, Int. J. Mech. Sci. 29 179

Klepaczko, J.R. (2005). Review on critical impact velocities in tension and shear, International Journal of Impact Engineering 32 188-209

Klepaczko, J.R. and Klosak, M. (1999). Numerical study of the critical impact velocity in shear, Eur. J. Mech. A/Solids 18 93-113

Kobayashi, S. and Lee, C.H., (1973). Deformation Mechanics and Workability in Upsetting Solid Circular Cylinders, in Proceedings of the First North American Manufacturing Research Conference, Vol 1, Society of Manufacturing Engineers, 185

Lange, K., (1985). Handbook of Metal Forming, McGraw-Hill, New York

Lee, W. S., and Lin C. F., (1998). Plastic Deformation and Fracture Behavior of Ti-6A1-4V Alloy Loaded With High Strain Rate Under Various Temperatures, Materials Science and Engineering. A Structural Materials, 41, 48-59

Lee, W.S., Sue, W.C. and Lin, C.F. (2000). The effects of temperature and strain rate on the properties of carbon-fiber-reinforced 7075 aluminum alloy metal-matrix composite Composites Science and Technology 60 1975-1983

Lee, S.W. and Pourboghrat, F. (2005). Finite element simulation of the punchless piercingprocess with Lemaitre damage model, International Journal of Mechanical Sciences 47 1756-1768

Li, Z. and Wu, D. (2007). Study of the high strength and low yield ratio cold forging steel Materials Science and Engineering A 452-453 (142-148)

Luo, G.W. (2006). Dynamics of an impact-forming machine, International Journal of Mechanical Sciences 48 1295-1313

Makelt, H. (1960). Mechanical Presses, Edward Arnold (Publisher) Ltd.

Male, A.T. and Cockroft, M.G. (1964-1965). J Inst. Metals, 93: 38-46

Mamalis, A.G., Szalay, A., Giibl, N., Vajda, I. and Raveau, B. (1998). Near net-shape manufacturing of metal sheathed superconductors by high energy rate forming techniques Materials Science and Engineering B53 119- 124

Marouani, H., Ben Ismail, A., Hug, E. and Rachik, M. (2009). Numerical investigations on sheet metal blanking with high speed deformation, Materials and Design, 30 3566-3571

Meyers, M. A., Xu, Y. B., Xue, Q., Perez-Prado, M. T., and McNelley, T. R., (2003). Microstmctural Evolution in Adiabatic Shear Localization in Stainless Steel, Acta Materialia, 51, 1307-1325

Navinsek, B., Panjan, P. and Gorenjak, F. (2001). Improvement of hot forging manufacturing with PVD and DUPLEX coatings. Surface and Coatings Technology 137 255-264

Odeshi, A.G., Al-ameeri, S. and Bassim M.N. (2005). Effect of high strain rate on plastic deformation of a low alloy steel subjected to ballistic impact, Journal of Materials Processing Technology 162-163 385-391

Odeshi, A.G., Al-ameeri, S., Mirfakhraei, S., Yazdani, F. and Bassim M.N. (2006). Deformation and failure mechanism in AISI 4340 steel under ballistic impact Theoretical and Applied Fracture Mechanics 45 18-24

Ozsoysal, O.A. (2006) Heat loss as a percentage of fuels energy in air standard Otto and Diesel cycles, Energy Conversion and Management 47 1051-1062

Pardo A., Merino M.C., Carboneras M., Viejo F., Arrabal R., Munoz J., (2006) Influence of Cu and Sn content in the corrosion of AISI 304 and 316 stainless steels in H2SO4, Corrosion Science 48 1075-1092

Poullikkas, A. (2007). Implementation of distributed generation technologies in isolated power systems, REVIEW ARTICLE *Renewable and Sustainable Energy Reviews*, *Volume 11, Issue 1*, *January 2007*, *Pages 30-56*

Rakopoulos, C.D. (1988). Ambient temperature and humidity effects on the performance and nitric oxide emission of spark ignition engine vehicles in Athens/Greece, Solar Wind Technology 5 315-320

Rittel, D., Landau, P. and Venkert A., (2009). Dynamic Recrystallization as a potential cause for adiabatic shear failure, To appear in Physical Review Letters

Rusinek, A., Rodríguez-Martínez J.A., Klepaczko J.R. and Pecherski R.B. (2009). Analysis of thermo-visco-plastic behaviour of six high strength steels, Materials and Design 30 1748-1761

Sandor, B.I., Roloft, R., Birn, S.M. and brown, M.L(2005). Mechanics of Solids, CRC Press LLC Bela I

Semiatin S.L., (1993). Forming and Forging was published in 1988 as Volume 14 of the 9th Edition Metals Handbook. With the third printing the series title was changed to ASM Handbook

Seth, M., Vohnout, V.J. and Daehn, G.S. (2005) Formability of steel sheet in high velocity impact Journal of Materials Processing Technology 168 390-400

Sheljaskov, S., (1994) Current Level of Development of Warm Forging Technology, Journal of Materials Processing Technology, 46 3-18

Shima K.H., Lee S.K., Kang B.S.,and Hwang S.M., (2004). Investigation on blanking of thin sheet metal using the ductile fracture criterion and its experimental verification, Journal of Materials Processing Technology 155-156 1935-1942

Singh, S. and Jha, A.K. (2001). Analysis of dynamic effects during high-speed forging of sintered preforms, Journal of Materials Processing Technology 112 53-62

Souther, T.G., (2003). Study of shear localization using a novel test specimen loaded in a split-hopkinson compression bar, B.S.M.E. A THESIS Submitted to the Graduate Faculty of Texas Tech University

Stegeman Y.W, Goijaerts, A.M, Brokken, D, Brekelmans VAM, Govaert LE and Baaijents (1997). An experimental and numerical study of a planer blanking process, J. Materials and Processing Technology. 87 266-267

Stephen D. Cramer and Bernard S. Covino, Jr.P. (2003) Marcus, Introduction to the Fundamentals of Corrosion, Corrosion: Fundamentals, Testing, and Protection, Vol 13A, ASM Handbook, ASM International, p 209-219

Stock, T. A. C, and Wingrove, A. L., (1971). The energy Required for High-Speed Shearing of Steel," Journal of Mechanical Engineering Science, Vol. 13 No. 2, 11O-121

Taylor, G.I. and Quinney, H. (1933). The latent energy remaining in a metal after cold working, Proc. R. Soc. London 143a 307

Tekiner Z., Nalbant M., and Gürün H., (2006) An experimental study for the effect of different clearances on burr, smooth-sheared and blanking force on aluminium sheet metal, Materials and Design 27 1134-1138

Tobias, S.A. (1985). Survey of the development of Petro-Forge forming machine, Machine Tool Design Research 105-197

Tschaetsch, H.(2006). Metal Forming Practise. (A. Koth, Trans.). Springer-Verlag Berlin Heidelberg

Wick, C. H. (1961). Chipless Machining, The Industrial Press, 93 worth st. New York

Woodward R.L. et al., (1987). Direct measurement of temperature in high speed torsion tests, J. Eng. Mater. Tech. 109 140

Woodward R.L., (1990) Materials failure at high strain-rates, in: J. Zukas (Ed.), High Velocity Impact Dynamics, Wiley, New York, 76

Wu, C., Puzinauskas, P.V. and Tsai J.S. (2003) Performance analysis and optimization of a supercharged Miller cycle Otto engine, Applied Thermal Engineering 23 511-521

Xue, Q., Meyers, M.A. and Nesterenko, V.F. (2004). Self organization of shear bands in stainless steel, Materials Science and Engineering A 384 35-46

Yaldız, S., Saglam, H., Unsacar, F. and Isık, H. (2007). Design and applications of a pneumatic accelerator for high speed punching. Materials and Design, 28 889-896

Yoo, Y. H. and Yang, D. Y. (1997) Finite element modelling of the high-velocity impact forging process by the explicit time integration method Yang Journal of Materials Processing Technology 63 718-723

CIRRICULAM VITAE

PERSONAL INFORMATION

Surname, Name: KANCA, Erdoğan

Nationality: Turkish (TC)

Date and Place of Birth: 13 March 1972, Samsun

Marital Status: Married

Phone: +90 542 4328184

Fax: +90 348 814 26 69

E-mail: kanca@gantep.edu.tr

EDUCATION

Degree	**Institution**	**Year of Graduation**
MS	Department of Mechanical Engineering University of Gaziantep	2001
BS	Department of Mechanical Engineering University of Gaziantep	1996
High School	Samsun Vocational High School	1990

WORKING EXPERIENCE

Year	Place	Enrollment
1999-	Kilis Vocational High School in Higher Education	Instructor

HOBBIES

Visiting his friends and neighbors

PUBLICATIONS

1. Ahmet Öztaş, Murat Pala, Erdoğan Özbay, **Erdoğan Kanca.** Naci Çağlar, M.Asghar Bhatti (2006). Predicting the compressive strength and slump of high strength concrete using neural network. Journal of Construction and Building Materials, 20(9), 769-775.

2. Omer Eyercioglu, **Erdogan Kanca**, Murat Pala, Erdogan Ozbay, (2008). Prediction of martensite and austenite start temperatures of the Fe-based shape memory alloys by artificial neural networks. journal of materials processing technology 2 0 0 146–152

3. Murat Eskil, **Erdogan Kanca**, (2008). A new formulation for martensite start temperature of Fe–Mn–Si shape memory alloys using genetic programming Computational Materials Science 43 774–784

4. **Erdoğan Kanca**, İ. Hakkı Karahan, Ö. Eyercioğlu (2008). Shear-surface improvement of the austenitic stainless steel AISI 304 using high-speed punching. Optoelectronics and Advanced Materials-Rapid Communications Vol. 2, No. 12, December p. 822 – 827

5. **Erdoğan Kanca**, Necip Fazıl Yılmaz, Ömer Eyercioğlu,(2007). Yüksek Enerjili Şekillendirme (YEŞ) Presinin Tasarım ve İmalatı, IV. Makine Tasarımı ve İmalatı Teknolojileri Kongresi,75-82, Konya

6. **Erdoğan Kanca**, Necip Fazıl Yılmaz, Ömer Eyercioğlu, (2008). Yüksek Enerjili Şekillendirme (YEŞ) Presleri, Metal Makina Dergisi, Sayı 171, 420-423

7. **Erdoğan Kanca**, Ömer Eyercioğlu, Kürşad Göv (2009). Düşük Karbonlu Çelik Levhalarda Zımba Hızının Kesme Yüzeyi Geometrisine Etkisinin İncelenmesi, 11. Otomotiv Sempozyumu, Kalıpçılık ve Tasarım, 317-324, Bursa 2009

8. **Erdoğan Kanca**, Ömer Eyercioğlu, Kürşad Göv ve İsmail Hakkı Karahan (2009) Siyah Saç Levhalarda Kesme Yüzey Kalitesine Zımba Hızının Etkisinin İncelenmesi, V. Makine Tasarımı ve İmalatı Teknolojileri Kongresi, (Accepted for pub.), Konya

FOREIGN LANGUAGES

Turkish (Native Language), English